DETERMINATION OF THE KINETIC MODELS AND ASSOCIATED PARAMETERS FOR THE LOW TEMPERATURE COMBUSTION AND GASIFICATION OF HIGH-ASH COAL CHARS

D. NJAPHA
M. Tech (Chemical Engineering)

Thesis submitted in fulfillment of the requirements for the degree Philosophiae Doctor in Engineering of the Potchefstroomse Universiteit vir Christelike Höer Onderwys

Promoter: **Professor R.C. Everson (PU for CHE)**
Co-promoter: **Professor H.W.J.P. Neomagus (PU for CHE)**

November 2003
Potchefstroom

DECLARATION

This thesis is presented in fulfillment of the requirements for the degree of the Philosophiae Doctor in Engineering at the School of Chemical and Minerals Engineering of the Potchefstroom University for Christian Higher Education.

Hereby I, Delani Njapha, declare that the dissertation with the title: DETERMINATION OF THE KINETIC MODELS AND ASSOCIATED PARAMETERS FOR THE LOW TEMPERATURE COMBUSTION AND GASIFICATION OF HIGH-ASH COAL CHARS is my own work and has not been submitted at any other university either in whole or in part.

Signed at Potchefstroom on the ..... day of 2003

.....

D. Njapha

LIST OF PUBLICATIONS
(Conference proceedings and accredited journals)

Everson, R.C., Neomagus, H.W.J.P., and Njapha, D. Kinetics of combustion of coal-chars using a non-isothermal thermogravimetric method: A regression procedure for evaluation of rate equations and parameters, *submitted to Fuel*

Everson, R.C., Neomagus, H.W.J.P., Njapha, D. and Kaitano, R., Coal-char combustion and gasification kinetics using thermogravimetric analyser measurements. American Institute of Chemical Engineers. Annual meeting, November 4-8, 2002, Indianapolis, (United States of America)

Njapha, D., Neomagus, H.W.J.P. and Everson, R.C., The determination of kinetics of combustion and gasification of low-ranked South African coal using a thermogravimetric analyser. Coal Indaba 2002, 8th Coal Science and Technology conference, organised by the Fossil Fuel Foundation (FFF), October 15-17, 2002, Secunda (South Africa)

Njapha, D., Neomagus, H.W.J.P. and Everson, R.C., The determination of kinetics of combustion and gasification of low-ranked South African coal using a thermogravimetric analyser, 5th European Gasification Conference, April 8-10, 2002, Noordwijk (The Netherlands)

Njapha, D., Kaitano, R., Neomagus, H.W.J.P., Everson, R.C., Evaluation of combustion kinetics on high ash-coal using a thermogravimetric analyser (TGA) and a packed bed balance reactor (PBBR), Coal Indaba 2000, 6th Coal Science and Technology Conference, organised by the Fossil Fuel Foundation (FFF), November 15-16, 2000 Johannesburg (South Africa)

ACKNOWLEDGEMENTS

I would like to express my deep appreciation to the following persons for their support during course of this project:

- Professor R.C. Everson, for his excellent supervision during the course of this study.
- Professor H.W.J.P. Neomagus, for his willingness to help.
- Professor H. Kaisani, for constructive discussions on the subject.
- Mr. Quentin Campbell, for sharing his deep experience on the subject of coal.
- Mr. Hennie van Zyl and Jan Kroeze, for helping with the laboratory apparatus.
- All the personnel of the School of Chemical and Minerals Engineering for sharing constructive ideas through good and tough times.
- Eskom, for providing financial support of this project.
- My parents, for providing me an opportunity to study.
- My sisters and my brothers, for not giving up on me.
- David Attah, for his encouragement.
- All my friends, for believing in me.

Abstract

South Africa has large coal reserves and the power generation industry produces approximately 95% of the electricity from coal. Most of the high-grade coal is exported leaving behind a discard of high ash coal. For the power generation industry to sustain itself, some means of processing the high ash coal should be implemented. A fluidised bed gasification process is seen as the best alternative to conventional pulverised coal combustion process since it can handle a wide variety of feedstocks at low temperatures. The reaction kinetics becomes important for a gasifier design that can handle high ash feedstocks. This study is concerned with the determination of reaction kinetics of high ash South African chars suitable for the development of fluidised bed combustors and gasifiers.

Combustion and gasification studies of two South African high ash chars (48% ash of 70 μm and 67% ash of 20 μm diameter) were carried out isothermally and non-isothermally in an atmospheric thermogravimetric analyser. In modelling the combustion experiments, it was found that the reaction mechanism follows the shrinking unreacted core model with surface reaction. This was attributed to the low porosities of both chars. Despite the high ash contents, the kinetics of the two samples were found to match well those of low ash chars. This was explained in terms of the mineral-carbon association in chars observed during detailed characterisation. A two-step regression method capable of evaluating parameters under non-isothermal experiments has also been developed. This method gave plausible results when compared with another non-isothermal method and was capable of predicting reaction kinetics under isothermal conditions.

Gasification experiments conducted on the same chars with carbon dioxide and steam were described using a reaction controlled Langmuir-Hinshelwood rate equation. Reactivity profiles have been obtained in the temperature range from 800 to 950 °C at different steam and CO_2 partial pressures. The shrinking unreacted core model with surface reaction was also found to provide the best fits for both chars. The obtained parameters match well with those of other chars with lower ash contents indicating that most of the carbon occurs with no mineral association for both chars investigated. Finally experiments were carried out under synthesis mixtures of $CO/CO_2/H_2/H_2O$ at equilibrium

conditions and showed that the overall rate of reaction with CO_2 and H_2O proceed over different carbon sites.

Uittreksel

Suid Afrika het 'n groot aantal steenkool reserwes en die krag generering industrie is heeltemal afhanklik van steenkool. Ongeveer 95% van die elektrisiteit produseer deur Eskom is hoofsaaklik vanaf steenkool. Meeste van die hoë graad steenkool word uitgevoer en sodoende bly 'n hoë as steenkool oor. Vir die krag generasie industrie om dit self te onderhou moet 'n manier gevind word om hoë as steenkool te prosesseer. 'n Gevloeidiseerde bed verbrandings prosesse word gesien as die beste alternatief na gewone fyn steenkool verbranders proses aangesien dit 'n groot variasie voer by laë temperature kan hanteer. Die kinetika word belangrik vir 'n vergasser ontwerp wat hoë as voerstroom kan hanteer. Hierdie studie is gefokus op die bepaling van kinetika van hoë as Suid-Afrikaanse verkoolsels geskik vir die ontwikkeling van gevloeidiseerde bed verbrander en vergasser.

Verbranding en vergassings studies van twee Suid-Afrikaanse hoë as verkoolsels (48% as van 70μm en 67% van 20μm diameter) was uitgevoer isotermies en nie-isotermies in 'n atmosferiese termograwimetriese analiseerder. Deur die verbrandings eksperimente te modelleer is daar gevind dat die reaksie meganisme die krimpende kern model met oppervlak reaksie volg. Dit is toegeskryf aan die laë porositeit vir beide verkoolsels. Ten spyte van die hoë as hoeveelhede, is gevind dat die die kinetika van die twee monsters goed vergelyk met laë as verkoolsels. Dit was verduidelik in terme van die mineraal-koolstof assosiasie in die verkoolsels geobserweer gedurende detail karakterisering. 'n Twee stap regressie metode wat in staat is om parameters te bepaal onder nie-isotermiese eksperimente was gebruik. Die metode het goeie resultate gegee wanneer vergelyk word met 'n ander nie-isotermiese metode en was ook gebruik om die kinetika te voorspel onder isotermiese kondisies.

Vergasings studies met koolstof dioksied en stoom was ook ondersoek met die selfde verkoolsels deur gebruik te maak van 'n atmosferiese TGA. Reaktiewiteits profiele was gevind in die temperatuur reeks vanaf 800 to 950 °C by verskillende stoom en CO_2 parsiële drukke. 'n Kinetiese uitdrukking gebaseer op die Langmuir-Hinshelwood kinetics beskryf die reaksie(s) redelik goed. Daar is ook gevind dat die krimpende onreageerende kern model met oppervlak reaksie beide die verkoolsels goed beskryf. Die gevinde parameters stem goed ooreen met ander laë as verkoolsel. Finaal is eksperimente

uitgevoer met mengsels van $CO/CO_2/H_2/H_2O$ by ewewig kondisies en het gewys dat die algemene reaksie tempo met CO_2 en H_2O oor verskillende koolstof aktiewe punte plaas vind.

TABLE OF CONTENTS

PAGE

DECLARATION II

LIST OF PUBLICATIONS III

ACKNOWLEDGEMENTS IV

Abstract v

Uittreksel vii

TABLE OF CONTENTS IX

LIST OF FIGURES XVI

LIST OF TABLES XIX

GLOSSARY XXI

1. GENERAL INTRODUCTION 1

1.1 COAL AS AN ENERGY SOURCE 1

1.2 CURRRENT TECHNOLOGY IN THE ELECTRICITY GENERATION FROM COAL 9

1.3 COAL AND THE ENVIRONMENT 10

1.4 CLEAN COAL TECHNOLOGIES 12

1.5 SCOPE AND OBJECTIVES 13

REFERENCES 16

2. COAL AND CHAR CHARACTERISATION 17

2.1 INTRODUCTION 17

2.2 ORIGIN OF COAL SAMPLES 18

2.3 PROPERTIES DETERMINED 18

2.5 PARTICLE SIZE DISTRIBUTION 22

2.6 POROSITY 23

2.7 MINERALS IN ASH 24

2.8 CHAR CHARACTERISATION SCANNING ELECTRON MICROSCOPE RESULTS 25

2.8.1 Minerals present in the char 26

2.8.2 Distribution of carbon and minerals in a char sample 27

2.9 PETROGRAPHY ANALYSIS 30

2.10 CONCLUSIONS 32

NOMENCLATURE 33

REFERENCES 34

3. COMBUSTION REACTION KINETICS 36

3.1 INTRODUCTION 36

3.2 LITERATURE SURVEY 37

3.2.1 Introduction 37

3.2.2 Combustion reactions of coal chars 37

3.2.3 Factors affecting the reaction rates of coal chars 38
3.2.3.1 Char preparation 38
3.2.3.2 Char composition 39
3.2.3.3 Particle size effect 40
3.2.3.4 Effect of pore size 41
3.2.3.5 Effect of temperature 41

3.2.4 Combustion models 42

3.3 DERIVATIONS OF FUNDAMENTAL REACTION RATE MODELS 44

3.3.1 Introduction 44

3.3.2 Shrinking unreacted core model (SUCM) 44
3.3.2.1 Description 44
3.3.2.2 Derivation of equations 45

3.3.3 Shrinking reacted core model (SRCM) 49
3.3.3.1 Description 49
3.3.3.2 Derivation of equations 49

3.3.4 Homogeneous Model 54

3.4 EXPERIMENTAL 55

3.4.1 Description of the experimental apparatus 55

3.4.2 Experimental procedure 58
3.4.2.1 Char preparation 58
3.4.2.2 Char combustion 59
3.4.2.3 Reagent gases 60
3.4.2.4 Char properties 60

3.4.3 Experimental results confirming absence of diffusional effects 60
3.4.3.1 External diffusion 60
3.4.3.2 Intra-particle diffusion 61
3.4.4 Error calculation 62

3.5 RESULTS AND DISCUSSION: ISOTHERMAL OPERATION 63

3.5.1 Introduction 63

3.5.2 Experimental results 63

3.5.3 Validation of models: Shrinking Unreacted Core Models 65

3.5.4 Validation of models: Shrinking Reacted Core/Homogeneous Model 67

3.6 RESULTS AND DISCUSSION: NON-ISOTHERMAL OPERATION 70

3.6.1 Introduction 70

3.6.2 Experimental results 70

3.6.3 Methods used for evaluation 72
3.6.3.1 The method of Flynn and Wall 73

3.6.3.2 Regression method 75

3.6.4 Determination of kinetic parameters 76
3.6.4.1 Method proposed by Flynn and Wall 77
3.6.4.2 Regression method 86

3.6.5 Comparison of methods 91

3.7 CONCLUSIONS 94

NOMENCLATURE 96

REFERENCES 99

4. GASIFICATION REACTION KINETICS 106

4.1 INTRODUCTION 106

4.2 LITERATURE SURVEY 107

4.2.1 Introduction 107

4.2.2 Gasification reactions 107

4.2.3 Factors affecting the reaction rates of coal chars 107

4.2.4 Gasification models 108

4.3 FUNDAMENTAL REACTION RATE EQUATIONS 110

4.3.1 Introduction 110

4.3.2 Langmuir-Hinshelwood rate equations 111
4.3.2.1 Carbon dioxide gasification mechanism and rate equations 111
4.3.2.2 Steam gasification mechanism and rate equations 113
4.3.2.3 Overall reaction rates of char with product gases 114

4.4 EXPERIMENTAL 115

4.4.1 Introduction 115

4.4.2 Description of the experimental apparatus 115

4.4.3 Char preparation 116

4.4.4 Char gasification 116

4.4.5 Char properties 117

4.5 RESULTS AND DISCUSSION 117

4.5.1 Introduction 117

4.5.2 Reactivities of different gases 117

4.5.3 Reaction of chars with carbon dioxide 118
4.5.3.1 Experimental results 118

4.5.4 Carbon dioxide/Carbon monoxide mixture 127

4.5.5 Steam/Nitrogen mixture 128
4.5.5.1 Experimental results 128
4.5.6 Steam/Hydrogen mixture 137

4.5.7 (CO_2/CO/H_2/H_2O) Mixtures 139

4.5.8 Comparison of reactions with carbon dioxide and steam 140

4.5.9 Discussion of results with respect to characteristics 141

4.6 CONCLUSIONS 143

NOMENCLATURE 145

REFERENCES 147

5. GENERAL CONCLUSIONS AND RECOMMENDATIONS 153

5.1 CONCLUSIONS 153

5.2 RECOMMENDATIONS 154

RESULTS OF THE NON-ISOTHERMAL COMBUSTION EXPERIMENTS 156

APPENDIX B 159

EVALUATION OF ACTIVATION ENERGY FROM NON-ISOTHERMAL DATA-METHOD OF FLYNN AND WALL 159

APPENDIX C 162

EVALUATION OF THE CONVERSION MODEL 162

APPENDIX D 165

EVALUATION OF THE OVERALL KINETIC RATE EQUATION FROM NON-ISOTHERMAL DATA 165

APPENDIX E 168

EVALUATION OF THE OVERALL KINETIC RATE EQUATION FROM NON-ISOTHERMAL REGRESSION DATA 168

APPENDIX F 171

CHAR CONVERSION BEHAVIOR UNDER CARBON DIOXIDE GASIFICATION 171

APPENDIX G 174

VALIDATION OF THE SHRINKING UNREACTED-CORE REACTION MODEL FOR CARBON DIOXIDE GASIFICATION 174

APPENDIX H 177

THE SHRINKING UNREACTED-CORE REACTION MODEL FOR CARBON DIOXIDE GASIFICATION 177

APPENDIX I 180

VALIDATION OF CARBON DIOXIDE GASIFICATION KINETICS 180

APPENDIX J 189

BURNOFF CURVES FOR STEAM GASIFICATION 189

APPENDIX K 192

VALIDATION OF THE SHRINKING UNREACTED-CORE REACTION MODEL FOR STEAM GASIFICATION 192

APPENDIX L 195

THE REACTION CONTROLLED SHRINKING UNREACTED CORE MODEL FOR STEAM GASIFICATION 195

APPENDIX M 198

VALIDATION OF STEAM GASIFICATION KINETICS 198

LIST OF FIGURES

PAGE

Figure 1.1: The world's primary energy shares, past and expected future (WCI, 2002)..... 2
Figure 1.2: International trading of coal 3
Figure 1.3: Total world energy consumption by source in 2002 (WCI, 2002)..... 3
Figure 1.4: Total world electricity generation (WCI, 2002)..... 5
Figure 1.5: General coal reserves worldwide 6
Figure 1.6: Electricity generation from coal..... 9
Figure 1.7: Contribution to the enhanced greenhouse effect 11
Figure 1.8: Contribution of coal industry to greenhouse effects 12
Figure 2.1: Particle size distribution for char A..... 22
Figure 2.2: Particle size distribution for char B 22
Figure 2.3: Association characteristics of char A 28
Figure 2.4: Association characteristics of char B 28
Figure 2.5: Fine included kaolinite and quartz in char A rich particles (back-scatter)..... 29
Figure 2.6: A variety of extraneous mineral matter particles in char A (back-scatter)..... 30
Figure 3.1: Effect of Thiele modulus for a shrinking reacted core particle..... 53
Figure 3.2: Photograph of the horizontal 951-thermogravimetric analyser..... 56
Figure 3.3: Schematic presentation of 2050 Thermogravimetric analyser..... 56
Figure 3.4: Preparation of char from a parent coal 59
Figure 3.5: Combustion of char A using different flow rates..... 61
Figure 3.6: Combustion of char A using different particle sizes 61
Figure 3.7: Typical isothermal combustion for char A in air 64
Figure 3.8: Conversion of char A in air for different temperatures..... 65
Figure 3.9: Conversion of char B in air for different temperatures 65
Figure 3.10: Conversion of char A as a function of the normalised time, $t/t_{0.9}$..... 67
Figure 3.11: Conversion of char B as a function of the normalised time, $t/t_{0.9}$ 67

Figure 3.12: Shrinking reacted core model for char A in air 68
Figure 3.13: Shrinking reacted core model for char B in air 68
Figure 3.14: Description of the homogeneous model for char A 69
Figure 3.15: Description of the homogeneous model for char B 69
Figure3.16: Non-isothermal combustion of char A in oxygen 70
Figure 3.17: Non-isothermal combustion of char A in air 71
Figure 3.18: Non-isothermal combustion of char B in air 72
Figure 3.19: Activation energy calculation for char A in air 77
Figure 3.20: Activation energy calculation for char B in air 77
Figure 3.21: Reaction controlled SUCM for char A combustion in air 81
Figure 3.22: Reaction controlled SUCM for char B combustion in air 81
Figure 3.23: Estimation of pre-exponential factor and reaction order for both chars using Flynn and Wall method 84
Figure 3.24: Prediction of the burnoff curve for char A in air 85
Figure 3.25: Prediction of burnoff curve for char B in air 86
Figure 3.26: Evaluation of activation energy for char A in air using the regression method 87
Figure 3.27: Evaluation of activation energy for char B in air using the regression method 87
Figure 3.28: Evaluation of reaction order and pre-exponential factors for both chars using the regression method 88
Figure 3.29: Model validation and parameter evaluation for char A using the regression method 89
Figure 3.30: Model validation and parameter evaluation for char B using the regression method 90
Figure 3.31: Burnoff curves (char A) from regression parameters 90
Figure 3.32: Burnoff curves (char B) from regression parameters 91
Figure 3.33: Prediction of isothermal burnoff curve (char A) 93
Figure 3.34: Prediction of isothermal burnoff curve (char B) 93
Figure 4.1: Char gasification with various gasifying agents 117
Figure 4.2: Typical raw data for char A CO_2 gasification at 900 °C 118

Figure 4.3: Conversion rate as a function of time at 900 °C (char A) 119
Figure 4.4: Conversion rate as a function of time at 900 °C (char B) 119
Figure 4.5: Conversion models for char A gasification at 900 °C 120
Figure 4.6: Conversion models for char B gasification at 900°C 120
Figure 4.7: Char conversion model for char A gasification at 900 °C 121
Figure 4.8: Char conversion model for char B gasification at 900 °C 121
Figure 4.9: Linearised form of the Langmuir results for char A 122
Figure 4.10: Determination of activation energy for both chars 124
Figure 4.11: Determination of adsorption enthalpy for CO_2 gasification 125
Figure 4.12: Prediction of burnoff curves for char A CO_2 gasification 126
Figure 4.13: Prediction of burnoff curves for char B CO_2 gasification 126
Figure 4.14: Inhibition effect of CO during CO_2 gasification at 900 °C 127
Figure 4.15: Typical steam gasification at 900 °C 128
Figure 4.16: Conversion rate as function of time at 900 °C (char A) 129
Figure 4.17: Conversion rate as function of time at 900 °C (char B) 129
Figure 4.18: Conversion models for char A gasification in steam at 900 °C 130
Figure 4.19: Conversion models for char B gasification in steam at 900 °C 131
Figure 4.20: Unreacted-core shrinking model for char A steam gasification 131
Figure 4.21: Unreacted-core shrinking model for char B steam gasification 132
Figure 4.22: Linearised Langmuir-Hinshelwood plot for char A at 900 °C 133
Figure 4.23: Activation Energy calculation for char A and B in steam 134
Figure 4.24: Determination of adsorption enthalpy for steam gasification 136
Figure 4.25: Burnoff behaviour for H_2O/N_2 (char A) at 900 °C 137
Figure 4.26: Burnoff behaviour for H_2O/N_2 (char B) at 900 °C 137
Figure 4.27: Effect of hydrogen during steam gasification at 900 °C (char A) 138
Figure 4.28: Char gasification under synthetic mixtures for char A 139
Figure 4.29: CO_2 gasification for char A and char B at 900 °C 140
Figure 4.30: Steam gasification for char A and char B at 900 °C 141

LIST OF TABLES

PAGE

Table 1.1: Major producers of hard coal in 1999 (WCI, 2000) 4
Table 1.2: Major coal exporters (WCI, 2000) 5
Table 1.3: Coal in electricity generation (WCI, 2000) 6
Table1.4: Advantages and disadvantages of energy sources in South Africa (Eskom, 2002) 7
Table 2.1: Properties of coal and chars determined 18
Table 2.2: Proximate and ultimate analysis of the coals 20
Table 2.3: Proximate analysis of coals from different South African coal mines 20
Table 2.4: Ultimate analysis from different South African coal mines 21
Table 2.5: Proximate analysis from some international coals 21
Table 2.6: Ultimate analysis from some international coals/chars 21
Table 2.7: Properties of coal and char samples 23
Table 2.8: Porosities of different coals as presented in literature 24
Table 2.9: Mineral oxides found in ash for samples investigated 24
Table 2.10: Mineral oxides found in ash for other South African coals 25
Table 2.11: Mineral oxides for non South African coals 25
Table 2.12: Compositions of mineral abundance 26
Table 2.13: Mineral distribution of char samples compared to typical power station pulverised fuel 27
Table 2.14: Petrographic (Maceral composition) characteristics of coal A and coal B 31
Table 3.1: Summary of particle conversion models 43
Table 3.2: Specifications of the 951-thermogravimetric analyser 57
Table 3.3: Specifications of the 2050 thermogravimetric analyser 57
Table 3.4: Activation energies (kJ mol^{-1}) for char A as a function of conversion and oxygen fraction 78
Table 3.5: Activation energies (kJ mol^{-1}) for char B as a function of conversion and oxygen fraction 79
Table 3.6: Literature values for activation energy 80

Table 3.7: Slopes (dimensionless) derived for the calculation of pre-exponential factor for char A 82
Table 3.8: Slopes (dimensionless) derived for the calculation of pre-exponential factor for char B 82
Table 3.9: Calculated values of Z (s^{-1}) for char A 83
Table 3.10: Calculated values of Z (s^{-1}) for char B 83
Table 3.11: Averaged kinetic parameters for the reaction controlled shrinking unreacted core model according to the Flynn and Wall method 84
Table 3.12: Values of Z (s^{-1}) obtained from the regression method 88
Table 3.13: Summary of results from the regression method 89
Table 3.14: Comparison for char A 92
Table 3.15: Comparison for char B 92
Table 4.1: Values derived from the slopes (s^{-1}) of F(X) against time for char A ... 122
Table 4.2: Values derived from the slopes (s^{-1}) of SUCM against time for char B 122
Table 4.3: Kinetic constants for carbon dioxide gasification (char A) 123
Table 4.4: Kinetic constants for carbon dioxide gasification (char B) 123
Table 4.5: Activation energy values reported from literature 124
Table 4.6: Averaged kinetic parameters for carbon dioxide gasification 125
Table 4.7: Kinetic parameters for carbon monoxide for both chars 127
Table 4.8: Slopes (s^{-1}) derived for char A steam gasification 132
Table 4.9: Slopes (s^{-1}) derived for char B steam gasification 133
Table 4.10: Kinetic parameters for char A steam gasification 134
Table 4.11: Kinetic parameters for char B steam gasification 134
Table 4.12: Values of activation energies for steam gasification 135
Table 4.13: Values of pre-exponential factor for steam gasification 135
Table 4.14: Kinetic parameters of hydrogen for both chars 138
Table 4.15: Water gas shift reaction conditions 139
Table 4.16: Adsorption enthalpies for steam and carbon dioxide 142
Carbon dioxide 142

GLOSSARY

In this thesis, specific terminology is used for certain aspects. For clarity, this terminology is defined in this section:

Char

The term char refers to a mixture of carbon and ash (minerals).

Conversion model:

This model gives the conversion of the carbon as a function of time; the conversion is denoted as: X.

Homogeneous model:

This model is an extreme of the SRCM, in which the reaction rate is completely determined by the chemical reaction rate and not by mass transport of the gases in and out the particle.

Intrinsic reaction rate:

This is the rate of the chemical reaction between the carbon and the gas, not taking into account the degree of conversion of the carbon (X).

Overall reaction rate:

This is defined as the product of the particle conversion model and the intrinsic reaction rate.

Particle conversion model:

This model describes the relative conversion rate (ratio of reaction rate to initial reaction rate) of the char as conversion progresses and is denoted as: $f(X)$.

Shrinking unreacted core model (SUCM):

This model assumes that the reaction takes place on the surface of the char and that there is negligible penetration of the reactant gases into the core of the char particle.

Shrinking reacted core model (SRCM):

This model assumes that the reaction takes place inside the core of the porous char particle.

CCSEM (Coal Characterisation Scanning Microscopy)

CHAPTER 1

GENERAL INTRODUCTION

This chapter gives a brief introduction of this investigation. In Section 1.1, the importance of coal in the present and future society is discussed. Section 1.2 deals with the current technology of converting coal into energy and the impact of coal on the environment is given in Section 1.3. The necessity of clean coal technology is discussed in Section 1.4. Finally, the scope and objectives of this study are presented in Section 1.5.

1.1 COAL AS AN ENERGY SOURCE

Coal is a combustible, sedimentary, organic rock composed primarily of carbon, hydrogen and oxygen from vegetation, which has been consolidated between other rock strata to form coal seams, and altered by the combined effects of microbial action, pressure and heat over a considerable time period (WCI, 2002).

Coal is the world's most abundant fossil fuel and has been used as an energy source for hundreds of years. There was international trade in coal as long ago as the Roman Empire. Coal not only provided the energy that fuelled the industrial Revolution of the 19^{th} Century, but it also launched the electric era in the 20^{th} Century. Until the 1960s, coal was the single most important source of world's primary energy, (see Figure 1.1). In the late 1960s it was overtaken by oil; but it is forecast that coal, apart from its importance in the generation of electricity, could again become the primary energy source at some stage during the first half of this century, (see Figure 1.1). It can also be seen from this figure that currently, 27% of the total energy consumption worldwide is produced from coal.

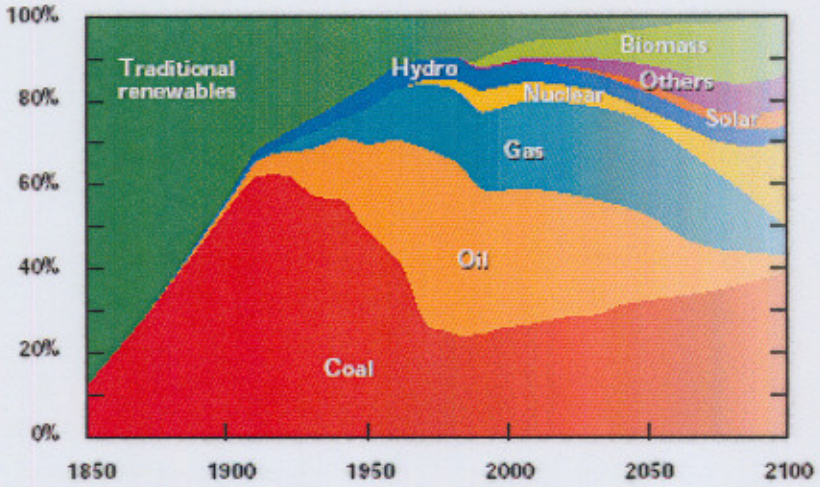

Figure 1.1: The world's primary energy shares, past and expected future (WCI, 2002)

The importance of other fossil fuels (like oil and gas) and alternative energy sources (such as nuclear) cannot be ignored. Renewable energy sources, like hydro, wind, solar, biomass and wave and tidal energy, do provide alternative sources for power generation, and are also expected to play a more important role in the 21st century.

All fossil fuel reserves are finite and need to be used as efficiently as commercially possible in order to conserve valuable resources. As the global population grows and as living standards improve in the developing world, international demand for energy increases, often at a dramatic rate. In Indonesia, for example, power generation has increased by 13% per annum during the period 1980 to 1997, and is forecast to continue growing at or above this rate.

During the period 1997 to 2010, the International Energy Association (IEA) forecasts that energy demand will rise by more than 30% equivalent to 2% per annum (WCI, 2002). Fossil fuels are expected to meet 95% of this energy demand. Adequate energy supplies are essential if the world's nations are to sustain their industrial and economic expansion.

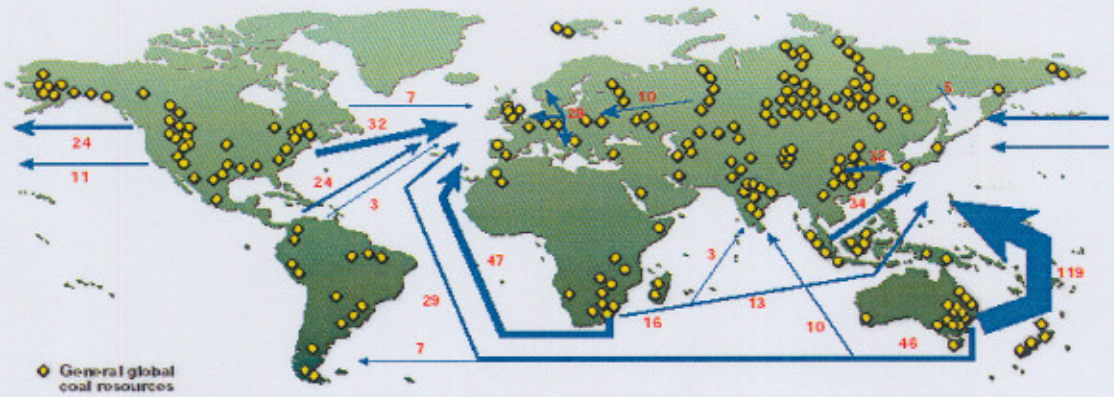

Figure 1.2: International trading of coal

Coal is still seen as the most abundant, widely distributed, safeand economical fossil fuel available to meet this escalating demand and will therefore be indispensable for the economic sustainability, as is also illustrated in Figure 1.2, showing the international trade in coal worldwide.

Nowadays, coal provides around 27% of the world's total primary energy consumption, whereas oil and gas are responsible for 39% and 24% respectively. Smaller energy sources are nuclear energy (7%) and hydro electricity (3%) as presented in Figure 1.3.

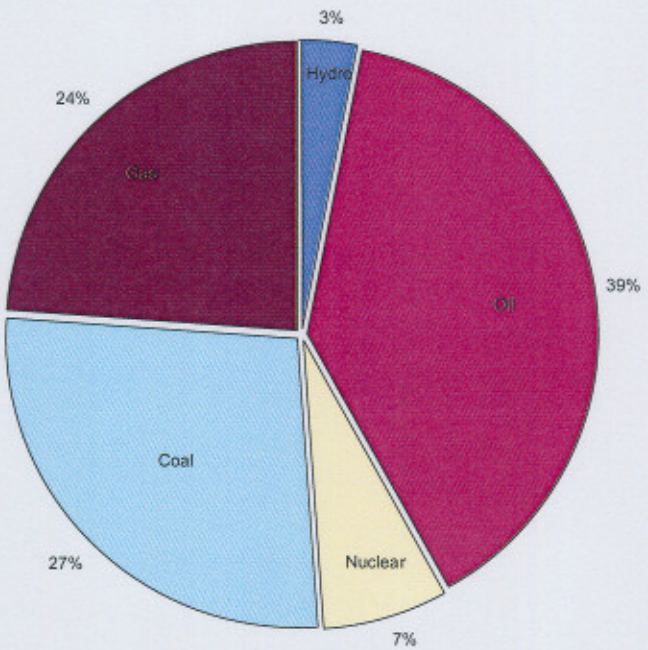

Figure 1.3: Total world energy consumption by source in 2002 (WCI, 2002)

The total global hard coal (all coal mined) production in 1975 was 2429 million tonnes (Mt) and increased by 43% to 3.466 Mt in 1999. Major hard coal producers are China and USA. South Africa is the 5th largest coal producer in the world with 225 million tons in 2001. South Africa produces over 95% of the total coal produced in Africa. Table 1.1 shows the regional shares of the world hard coal production.

Table 1.1: Major producers of hard coal in 1999 (WCI, 2000)

Country	**Amount (Mt)**	**Country**	**Amount (Mt)**
PR China	1.171	Russia	169
USA	899	Poland	102
India	310	Ukraine	81
Australia	238	Indonesia	79
South Africa	225	Kazakhstan	71

Considering the international trade of coal, Australia is the largest exporter followed by South Africa and Indonesia. Coal is traded both for electricity generation (steam coal) and for steel production (coking coal). An overview of major coal exporters is given in Table 1.2.

Table 1.2: Major coal exporters (WCI, 2000)

Country	Steam coal (Mt)	Coking coal (Mt)	Country	Steam coal (Mt)	Coking coal (Mt)
Australia	87.8	99.0	Canada	34.0	0.5
South Africa	67.5	2.5	Colombia	27.0	7.3
Indonesia	48.1	8.7	Russia	4.6	27.2
USA	48.2	6.9	Poland	18.0	5.8
China	24.6	28.4			

Coal is abundantly used for electricity generation, and about 37% of the world electricity production is dependant on this source. Other fossil fuels used for electricity generation include oil (9%), gas (16%). Alternative power generation methods include nuclear electricity (17%) and electricity derived from hydro energy (21%) as depicted in Figure 1.4.

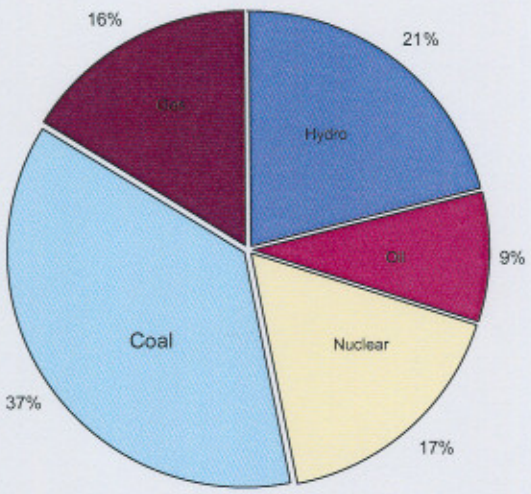

Figure 1.4: Total world electricity generation (WCI, 2002)

A lot of countries generate their electricity mainly from coal. Countries like Poland and South Africa depend extreme heavily on coal (96% and 95%) while countries like Australia (84%) and China (80%) also derive their electricity mainly from coal. The generation of electricity from coal is illustrated in Table 1.3.

Table 1.3: Coal in electricity generation (WCI, 2000)

Country	Electricity generation	Country	Electricity generation
Poland	96%	India	66%
South Africa	95%	USA	56%
Australia	84%	Denmark	52%
PR China	80%	Germany	51%
Czech Republic	71%	Netherlands	42%
Greece	69%	EU15 (1999)	25%

The (proven) reserves of coals are spread in a number of countries; see Figure 1.5 (www.gasification.org., 2001). It is estimated that around one thousand billion tones of total coal reserves are economically accessible using current mining technology, of which approximately half of it is hard coal.

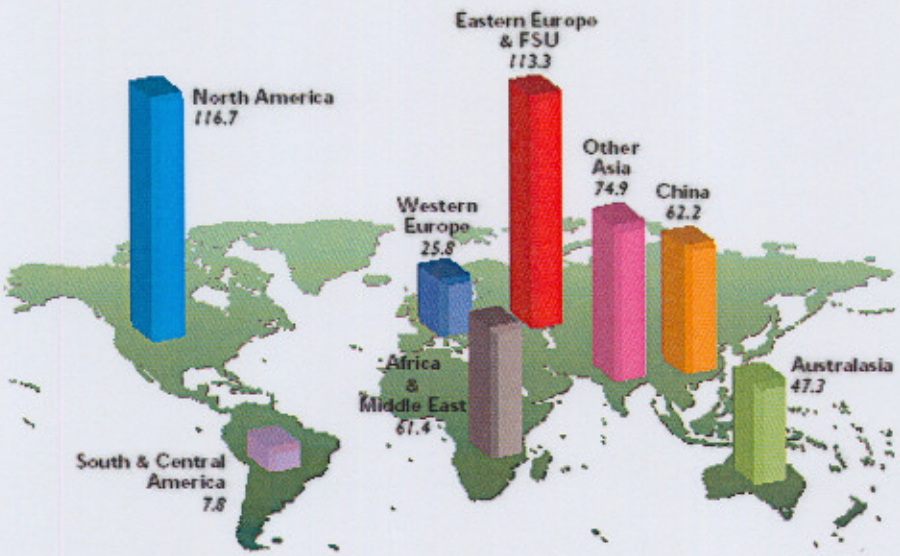

Figure 1.5: General coal reserves worldwide

At 1998 levels of production, coal reserves are sufficient to last over two hundred years. In addition, significant advances continue to be made in improving utilization efficiencies so that more useful energy is recovered from every tonne of coal. Current reserves of coal are approximately six times the reserves of oil (45 years) and four times that of gas (65

years). Due to the large amount of reserves, coal is expected to play a more and more important role as an energy source in the near future (see also Figure 1.1).

Next to energy source, coal is also increasingly used for the production of chemicals (e.g. SASOL, South Africa). In these chemical processes, coal is used as a raw material for the production of synthesis gas, from which a number of chemicals can be produced. Due to the large reserves of coal (i.e. with respect to crude oil), it is also expected that coal will play a key role in the production of chemicals in the 21st century. This investigation, however, is focussed on the use of coal in energy generation.

A survey, carried out by Eskom (2002), around the different forms of energy sources is summarised in Table 1.4. In this table, the advantages and disadvantages of different energy sources, relevant to South Africa relevant are listed. Although a lot of alternative sources (e.g. solar energy and hydro energy) have economic potential in South Africa, coal will be the most important energy source in the near future.

Table1.4: Advantages and disadvantages of energy sources in South Africa (Eskom, 2002)

Energy source	**Advantages**	**Disadvantages**
Coal	-Proven technology for large-scale electricity production. -Reliable power stations. -Very competitive economically. -Provides SA with the cheapest electricity production.	-Expensive to transport. -Worst waste problem of any energy source, i.e. sulphur, organic compounds, heavy metals and greenhouse gases.
Nuclear	-Proven technology for large-scale electricity production. -No technical problems for waste disposal. -Economical competitive. -Huge uranium reserves. -Fuel very cheap to transport.	-High capital costs of current designs. -Poor public opinion because of association with nuclear weapons and perceived problems with safety.

Hydro	-Proven technology for large-scale electricity. -Renewable -No emissions. -Economically competitive. -Enormous potential in Central Africa.	-Little potential since SA is dry with few suitable rivers. -Environmental problems with dams. -High capital costs.
Biomass	-Wood, bagasse (from spent cane) and dung are renewable. -Households use biomass for energy.	-Cutting down trees from firewood can cause land grow and gather for large-scale productions. -Large land use.
Gas	-Proven technology for large-scale electricity. -Low capital costs. -Fairly clean.	-Emissions of greenhouse gas and nitrogen oxides. -South Africa has very little gas of its own. -Uncertainty about future gas prices.
Solar	-Renewable -Clean -No emissions. -Free energy. -Northern Cape has very good conditions for solar power.	-The energy is dilute. -High capital costs. -Expensive electricity.
Wind	-Renewable -Clean -No emissions. -Free energy. -Good conditions for wind power in coastal regions.	-The energy is dilute and intermittent. -High capital costs. -Expensive electricity. -Environmental objections that it defaces the countryside.

Oil	-Proven technology. -Unrivalled for use in transport such as in cars, lorries, ships and airplanes.	-South Africa has almost no oil reserves. -Emissions including sulphur and nitrogen oxides, organic compounds and greenhouse gases. -Expensive.

1.2 CURRRENT TECHNOLOGY IN THE ELECTRICITY GENERATION FROM COAL

The earliest conventional method for generating electricity was burning lump coal on a grate in boilers to raise steam. In modern, highly efficient, versions of this system, the coal is milled to a fine powder in a pulveriser. This increases the surface area of the coal and hence the rate of combustion. The powdered coal is blown in a combustion chamber of a boiler where it is burnt at around 1600 °C. The hot gases from the boiler and radiant heat energy produced convert water in tubes lining the boiler into steam, see Figure 1.6.

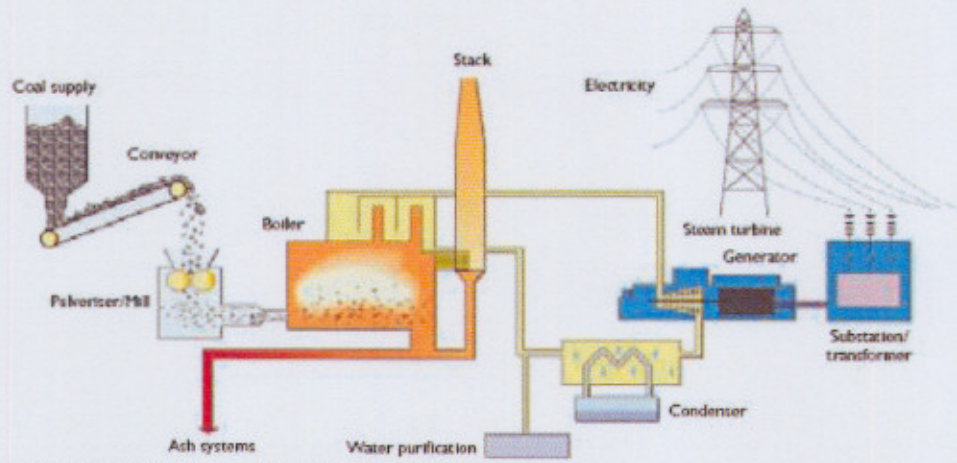

Figure 1.6: Electricity generation from coal

The high-pressure steam is passed into a turbine containing thousands of propeller-like blades. The expanding steam hits these blades causing the turbine shaft to rotate at high

speed. Mounted at the end of the turbine shaft is the generator, consisting of carefully wound wire coils. Electricity is generated when these are rapidly rotated in a strong magnetic field. After passing through the turbine chamber, the steam is condensed and recycled to the boiler to be heated once again. The electricity is transformed into the higher voltages used for economic transmission via power line grids (40,000 volts and above). Near the point of consumption, the electricity is transformed down to the safer 100 to 250-voltage system used in domestic market.

1.3 COAL AND THE ENVIRONMENT

Although cleaner, efficient and environmentally aware, the coal industry of today is still working to escape the false image of coal that lingers from the past. Coal bears the unjustifiable stigma of being a 'dirty', polluting fuel, bringing to mind pictures of black smoke rising from chimneystacks. There may once have been reason to feel this way about coal; the industrial revolution saw industrial areas covered in a dark haze, although the smoke was viewed as a symbol of economic progress. London and other European cities suffered from fogs aggravated by the inefficient combustion of coal in the countless domestic hearths. Today, however, this view needs to be left in history books. Coal can be burnt cleanly and effectively throughout the world, using constantly improving technologies.

The development of the modern world is based on the availability of industrial energy, electricity and improved modes of transport. However, in recent decades both industry and the public have recognized the increasing need for the preservation of the environment from some of the potentially detrimental effects of unregulated economic growth. Technologies have been developed to improve the environmental performance of coal to energy processes, for example electrostatic precipitators and/or bag filters have been introduced in coal power stations to avoid the emission of black smoke and dust.

The greenhouse effect has received mounting attention since the early 1980s. It is in fact a natural phenomenon referring to the warming of the surface earth, caused by the effect water vapour, CO_2 and certain trace gases in the atmosphere have on the earth's radiation balance. Without the greenhouse effect, or atmospheric re-radiation, the average surface temperature of the earth would be about 33 ^{o}C cooler than it is today and the world would

be inhabitable. The change in composition of the atmosphere, due to the emission of several greenhouse gases from industrial activities are said to have an impact on the average temperature on the earth. An increase of the average temperature on earth can have drastic effects on the life on earth. This suggests that the emissions contributing towards the greenhouse effect should be controlled. The greenhouse gases (GHGs) include water vapour (the predominant one), carbon dioxide (CO_2), methane (CH_4), nitrous oxide (N_2O) and, in recent years, halocarbons (CFCs and their substitutes) and sulphur hexafluoride (SF_6).

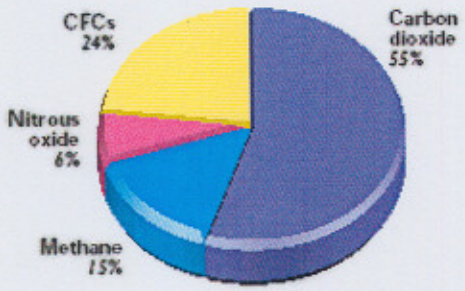

Figure 1.7: Contributionto the enhanced greenhouse effect

Arrhenius (WCI, 2002) already predicted that doubling the level of CO_2 in the atmosphere would lead to 5 to 6 °C rise in global surface temperature. Water vapour is the most active component in the atmosphere, responsible for about 67% of the natural greenhouse effect. The role of water in the climate system is crucial and extremely complex; its concentration in the atmosphere and cloud distributions is largely determined by climatic conditions. More recent scientific theories suggest this temperature rise might lie in the range of 1 to 3 °C. Increased levels of CO_2 in the atmosphere can partly be attributed to fossil fuel combustion, cement manufacture and changes in agricultural activities. However CO_2 (see Figure 1.7) is not the only gas contributing to the enhanced greenhouse effect. The atmospheric concentration of methane has more than doubled over the past 200 years.

Consumption/combustion of all fossil fuels (oil, gas and coal) creates greenhouse gas

emissions. GHGs from the coal industry are estimated to contribute less than 20% to the enhanced greenhouse effect, see Figure 1.8. Around half of the coal's GHGs emissions arise from power generation.

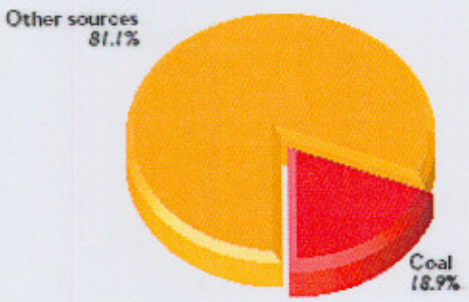

Figure 1.8: Contributionof coal industry to greenhouse effects

From the 18.9% shown in Figure 1.8, CO_2 contributes 17.5%, methane 1.1% and nitrous oxide 0.3%. Although the coal industry is not completely responsible for the greenhouse effect, the coal industry is obliged to invest in clean coal technology

1.4 CLEAN COAL TECHNOLOGIES

Clean Coal Technologies (CCT) are defined as technologies designed to enhance both the efficiency and environmental acceptability of coal extraction and use. These technologies reduce emissions, reduce waste, and increase the amount of energy gained from each ton of coal. Most CCTs concentrate on power generation from coal, as more than 50% of coal produced is used to generate electricity. An impressive array of technologies is already commercially viable, and a large number of others will become available in the near future.

A promising alternative in power generation, compared to pulverised coal combustion, is the use of gasification technology. In gasification, coal is converted to synthesis gas, which is sent to a gas turbine. The overall efficiency in an integrated coal gasification combined cycle (ICGCC) is over 45% Gururajan *et al.* (1992), while conventional pulverised coal combustion processes have only an overall efficiency of about 30% (Bermenjo *et al.*, 2003). Gururajan *et al.* (1992) also concluded that this gasification

process is attractive for high ash coals, since the processing of these types of coal in a combustion process is uneconomical and is associated with large damages to the environment. A major problem in the use of high ash coals is the extensive melting and agglomeration of the ash that takes place in the reactor. To avoid this slagging, operation at sufficient low temperatures is essential. A fluidised bed gasification process is therefore recommended above the moving bed or entrained flow gasification process, because the good temperature control in a fluidised bed. Although gasification processes are more attractive than combustion processes for high ash coals, fluidised bed combustion can have significant advantages compared to pulverised coal combustion. This is mainly because of the relative lower temperature in fluidised bed processes, making sulphur capture inside the reactor possible and reducing NO_x production simultaneously.

Résumé, a fluidised gasification process seems to be the most promising process in the use of high ash coal for energy purposes. The conversion of coal to gas takes place at relative low temperatures (< 1000 °C) with high efficiencies (> 45%) and little impact on the environment.

For the design of a large-scale gasification process, it is essential to have detailed information about the (intrinsic) kinetics and mechanisms associated with the conversion of high ash coal. This forms the basis of this project.

1.5 SCOPE AND OBJECTIVES

In this investigation, the reaction kinetics of two high-ash chars (48% and 67%), obtained from coal samples from the Witbank region (Mpumalanga) in South Africa, is studied. Both coals are obtained as a discard from the processing of coal to produce high-grade coal feedstocks.

In this study, both the combustion and the gasification has been studied. The combustion reaction is studied at low temperatures (370-560 °C) and low pressure (atmospheric pressure), using small particles (20 – 70 μm) in order to ensure operation within the chemical controlled regime (surface or volume reactions). The combustion experiments are carried out both isothermal and non-isothermal, in order to study the mechanisms of

conversion (overall reaction) that are associated with high ash chars. The gasification reactions are studied at temperatures between 800 and 950 °C at atmospheric pressure using the same coal as used in the combustion study and attention is given to the evaluation of Langmuir-Hinshelwood type reaction rate equations. Both combustion and gasification reactions are studied in the region of 10 to 90 % carbon conversion with experimentation carried out with Thermogravimetric analysers (TGA).
The overall objective of the study is to investigate the chemical reactivity of selected high-ash chars in terms of its unique physical properties, suitable for the development of fluidised bed combustors and gasifiers. The specific objectives are the following:

1. Determination of the morphological and structural properties of the high-ash coals and corresponding chars. For this purpose, advanced characterisation techniques need to be used.
2. Determination of the combustion kinetics of two pulverized coal chars. The kinetic evaluation includes the determination of the overall reaction rate model and the activation energy, pre-exponential factor and order with respect to oxygen associated with the intrinsic reaction rate. The appropriate experimental procedures and data processing methods need to be developed.
3. Determination of the kinetics of gasification for both the reaction of chars with steam and with carbon dioxide, and the effects of the reaction products on the conversion rate. The kinetic evaluation includes the determination of the overall reaction rate model, the adsorption model and relevant parameters associated with the intrinsic reaction rate (Langmuir-Hinshelwood). The appropriate experimental procedures and data processing methods need also to be developed.

In Chapter 2, a thorough characterisation is given for the used coals and resulting chars. The proximate, ultimate and petrographic analyses of the coal are presented in this chapter as well as a detailed inspection of the minerals present in the ash using CCSEM (Coal Characterisation Scanning Electron Microscopy). Additionally, some structural parameters of the coals (particle size distribution and porosity) are also given in this chapter.

The experimental results, together with a discussion on the possible reaction models with associated parameters where applicable, are reported in Chapter 3 for the combustion reaction and in Chapter 4 for the gasification reaction. Finally, Chapter 5 gives the general conclusions of this study and the recommendations for further studies.

REFERENCES

BERMENJO, M.D., COCERO, M.J. AND FERNANDEZ-POLANCO, F. 2003. Process for generating power from the oxidation of coal in supercritical water. *Fuel*, **83**: 195-204.

ESKOM. 2002. Generation and transmission. http://www.eskom.co.za

GURURAJAN, V.S., AGARWAL, P.K. AND AGNEW, J.B. 1992. Mathematical modelling of fluidised-bed coal gasifiers. *Trans IchemE*, **70**: 211-237.

GASIFICATION ORG. 2001. Gasification: A growing worldwide industry. http://www.gasifcation.org

WCI (WORLD COAL INSTITUTE). 2000. Coal power for progress. http://www.wci-coal.com/home

WCI (WORLD COAL INSTITUTE). 2002. Coal power for progress. http://www.wci-coal.com/home

CHAPTER 2

COAL AND CHAR CHARACTERISATION

2.1 INTRODUCTION

In this chapter, a detailed characterisation of the coal and char samples used in this study is presented. Since this work is concerned with the evaluation of reaction kinetics of high ash chars, the coal and char characteristics have been compared with those used in current South African power stations and worldwide. The different properties of the coal and chars include the determination of proximate and ultimate analysis, particle size distribution, porosity, minerals in ash and the determination of the maceral composition. In Section 2.4, the proximate and ultimate analyses are reported for the two coal samples investigated. This is followed by the results on particle size distribution presented in Section 2.5. The results on porosity values obtained for both chars are given in Section 2.6. In Section 2.7 a study on minerals in ash was conducted and is followed by CCSEM (Coal Characterisation Scanning Electron Microscopy) results presented in Section 2.8. Finally a study on petrography analysis is presented in Section 2.9.

2.2 ORIGIN OF COAL SAMPLES

The two South African coal chars studied in this investigation are both from Mpumalanga province in the region of Witbank. Both chars have been chosen based on their high ash content with char A having an ash content of 48% and char B with 67% ash content. Most of the coal used for power generation in South Africa has an ash content of the order of 25% ash. In this investigation, the high ash char reaction kinetics, for both combustion and gasification, have been studied at ambient pressure. For a good understanding of the mechanisms involved in the reaction of coal, it is a prerequisite to characterise the coal thoroughly. The characterisation of both coals is given in this chapter.

2.3 PROPERTIES DETERMINED

A summary of the different properties that were conducted on both coal and chars is given in Table 2.1.

Table 2.1: Properties of coal and chars determined

Characterisation method	**Coal**	**Char**
Proximate analysis	Reported	Not reported
Ultimate analysis	Reported	Not reported
Particle size distribution	Not reported	Reported
Porosity measurement	Reported	Reported
Determination of minerals in ash	Not reported	Reported
CCSEM	Not reported	Reported
Petrography	Reported	

The char particle size can determine the reaction rate, and it is therefore important to determine. Most combustion and gasification models require the knowledge of the particle size (distribution) as an input parameter. In addition, the particle size plays and important role in defining the operation regime for the kinetic measurements (diffusion effects can influence the measurement of reaction kinetics, especially at large particle diameters and high temperatures).

In gas solid reactions, the porosity of the particle is another important parameter. The porosity of the solid gives information whether a particle can be modelled as a dense or porous substance. The mineral matter in the ash analyses were conducted since it is believed that some of the minerals could have a catalytic effect on the combustion and gasification reaction as well as on the structure of the resulting chars.

A CCSEM (Coal Characterisation Scanning Electron Microscope) analysis was conducted on the coal char samples. This technique provides quantitative information about the occurrence of minerals in the char particle. It can also generate a deeper insight in what forms the minerals are present in the char and how the minerals are embedded in the carbon regions. A petrographic study was conducted in order to know the origin of carbon concerned. This is necessary because the burning behaviour is set by the nature of the maceral groups found in coal. The coal porosity is also strongly related to the petrography.

2.4 PROXIMATE AND ULTIMATE ANALYSES

Proximate and ultimate analyses were carried out by the CSIR (Centre for Scientific Industrial Research) in Pretoria, South Africa. The results for both coal samples are presented in Table 2.2. For the proximate analysis different ovens corresponding to the standard methods were used for the analysis. The VARIO instrument was used for ultimate analysis. The standard methods are presented in Table 2.2.

Table 2.2: Proximate and ultimate analysis of the coals

Property	**Coal A (db)**	**Coal A (ar)**	**Coal A (daf)**	**Coal B (db)**	**Coal B (ar)**	**Coal B (daf)**
Coal proximate analysis						
% Moisture (SABS SM924)	-	2.4	-	-	2.2	-
% Ash (ISO 1171)	37.3	36.3	-	54.3	53.1	-
% Volatiles (ISO 562)	20.9	20.4	33.3	19.1	18.7	41.8
% Fixed carbon (by difference)	41.9	40.9	66.7	26.6	26	58.2
Coal ultimate analysis						
% Total sulphur (ASTM D4239)	1.7	1.7	2.8	3.1	3.0	7.0
% Carbon (ASTM D5373)	50	49.1	80.0	35	34.2	79.7
% Hydrogen (ASTM D5373)	2.7	2.6	4.2	1.7	1.7	4.0
% Oxygen (by difference)	7.1	6.9	11.2	3.4	3.3	7.7
% Nitrogen (ASTM D5373)	1.1	1.1	1.8	0.7	0.7	1.6

The amount of ash based on char was found by excluding the moisture and the volatiles and was found to be 47 % and 67 % for char A and B respectively. In Table 2.2 it can be seen that coal B has the higher ash content. It can be seen that coal B also has the higher amount sulphur than the other coal. The emissions of SO_x and H_2S from these chars can be significant from any combustion or gasification process (more in char B).

A comparative study conducted by Pretorius *et al.* (2002) on other coals obtained from the same area (Witbank mines) is given in Table (2.3 and 2.4).

Table 2.3: Proximate analysis of coals from different South African coal mines

Coal-char	Moisture (wt. %)	Ash (wt. %)	Volatile matter (wt. %)	Fixed carbon (wt. %)	Total sulphur (wt. %)
Arnot	4.6	22.0	22.1	51.3	0.56
Blackwattle	2.9	15.0	26.2	55.9	0.35
Boschmans	2.4	16.5	26.7	54.4	0.79
Dorsfontein	3.5	11.2	30.1	55.2	0.68
Delmas	3.8	23.0	23.8	49.4	1.28

Table 2.4: Ultimate analysis from different South African coal mines

Coal-char	Carbon (wt. %)	Hydrogen (wt. %)	Nitrogen (wt. %)	Sulphur (wt. %)	Oxygen (wt. %)
Arnot	59.68	2.91	1.36	0.56	8.89
Blackwattle	69.40	3.85	1.54	0.32	7.09
Boschmans	67.38	3.73	1.47	0.81	7.91
Dorsfontein	69.63	4.05	1.60	0.50	7.32
Delmas	68.11	3.71	1.63	1.07	6.28

It is seen from Table 2.3 that the ash content of the studied coals is much higher and the amount of fixed carbon is lower compared to the coals used for power generation in South Africa. The ultimate analysis also shows higher values of carbon compared to the coals investigated in this work. If the South African coals are compared with analyses of coals from USA and Sweden in particular, it can be concluded that the South African coals have a relative high ash and low carbon content (see Table 2.5 and 2.6).

Table 2.5: Proximate analysis from some international coals

Coal-char	Moisture (wt. %)	Ash (wt. %)	Volatile matter (wt %)	Fixed carbon (wt. %)
Gottelborn char[1]	1.7	9.1	36.9	54.0
Western Kentucky bituminous char[2]	4.2	7.9	36.3	51.6
Pittsburgh bituminous coal[3]	1.1	10.2	41.7	47

[1]Moors *et al.* (1999), [2]Goyal *et al.* (1989), [3]Goyal *et al.* (1990)

Table 2.6: Ultimate analysis from some international coals/chars

Coal/char	Carbon (wt. %)	Hydrogen (wt. %)	Nitrogen (wt. %)	Oxygen (wt. %)	Ash (wt. %)
Gottelborn char[1]	72.2	4.8	1.5	11	8.4
Western Kentucky bituminous char[2]	74.8	5.1	1.6	7.2	8.3
Pittsburgh bituminous coal[3]	71.8	5.2	1.1	7.1	10.3

[1]Moors *et al.* 1999, [2]Goyal *et al.* 1989, [3]Goyal *et al.* 1990

2.5 PARTICLE SIZE DISTRIBUTION

In preparing the coal samples, coal was finely pulverised using a ball mill. The pulverised coal was then sieved and the largest fraction between the screens of different sizes was used for the different combustion and gasification reactions. This was for coal A between 63 and 80 μm and for coal B the last fraction below 37 μm was taken. After sieving and fractioning, char was prepared from the coal samples. The char particle size distribution was determined using a Malvern particle size analyser (Master Sizer X 6333), see Figure 2.1 and 2.2 for char A and B respectively (volume percentage).

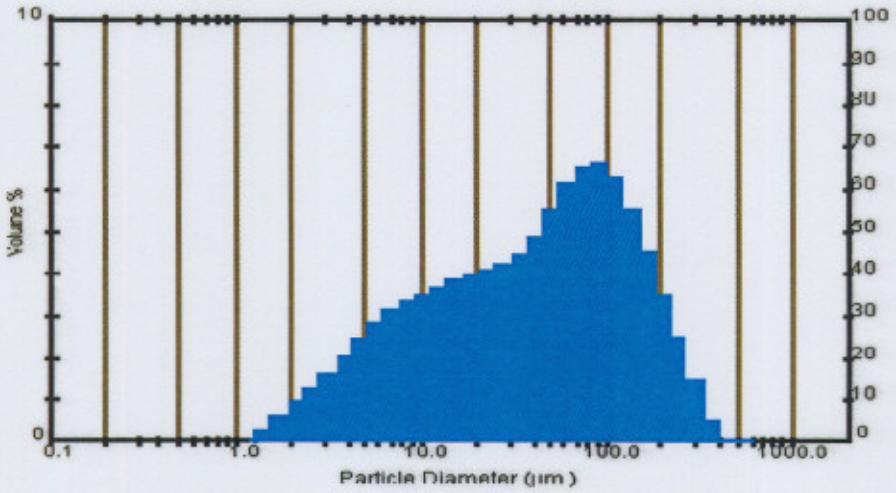

Figure 2.1: Particle size distribution for char A

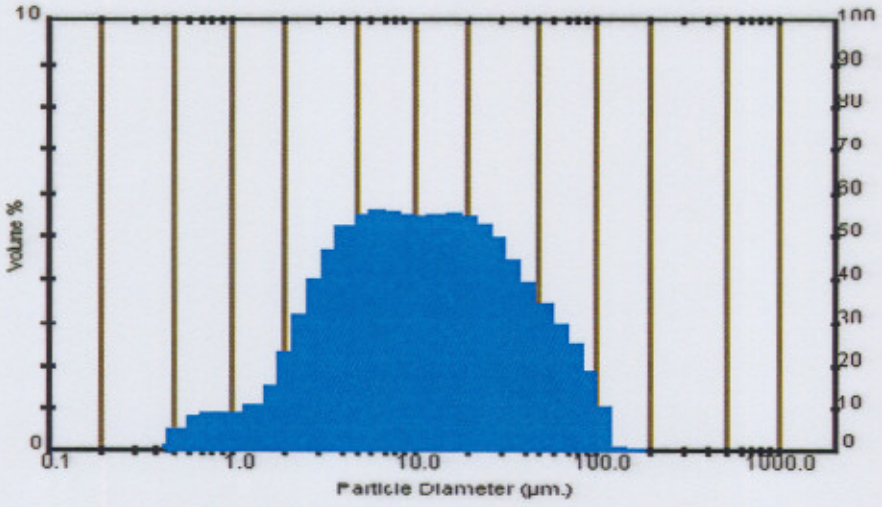

Figure 2.2: Particle size distribution for char B

The results show that the average particle size for char A is 70 μ m and for char B 20 μ m.

2.6 POROSITY

In order to gain better understanding of the particle structure, a nitrogen based BET-analysis was conducted on both coal samples using a Micromeritics ASAP 2010 analyser. The BET results give quantitative information about the porosity and pore size distribution of the coal and char particles, and the most important results are given in Table 2.7. From this table, it is concluded that the coals and chars have very low porosities. Particles with this amount of porosity could be considered as non-porous.

Table 2.7: Properties of coal and char samples

Property	Coal A	Char A	Coal B	Char B
BET surface area (m^2g^{-1})[1]	2.68	0.42	4.55	3.49
Pore volume (cm^3g^{-1})[1]	0.008	0.004	0.017	0.016
Average pore diameter (Å)[1]	113	373	150	182
Bulk density (g cm^{-3})[2]	1.936	1.945	2.5	2.58
Porosity[3]	< 2 %	< 2 %	< 5 %	< 5 %

[1]obtained from BET, [2]obtained from pycnometer, [3]calculated with Equation 2.1

The bulk density of values were measured with a pycnometer SPY-4 and the porosity was calculated from the following relationship:

$$\varepsilon = \frac{rS\rho_B}{2} \qquad \text{(Hines and Maddox, 1985)} \qquad [2.1]$$

If the porosity of the coals and chars are compared to studies that are presented in the open literature (summarised in Table 2.8), it can be concluded that the porosity of the coals and chars used in this study, is very small. This is largely attributed to the high inertinite content (see Section 2.9) of both coals (Du Cann, 2002).

Table 2.8: Porosities of different coals as presented in literature

Char origin	Ash (wt. %)	Porosity (%)	Author
Coal	16.5	50	Moors *et al.* (1999)
Coal (lignite)	6.74	22	Halder and Saha, (1991)
Coal	7	53	Gadiou *et al.* (2002)
Coal	38	28	Chen and Kojima, (1996)
Coal (sub-bituminous)	Not given	14	Tomeczek and Gil, (2003)
Coal	45	23	Senel, (1994)

2.7 MINERALS IN ASH

After the char had reacted, some of the ash was collected and a mineral analysis of this ash was carried out by CSIR, Pretoria. In Table 2.9, the results of the mineral analysis are given for both the ash obtained from char A and B.

Table 2.9: Mineral oxides found in ash for samples investigated

Samples Investigated	SiO_2 %	Al_2O_3 %	Fe_2O_3 %	CaO %	MgO %	TiO_2 %	K_2O %	Na_2O %	SO_3 %	P_2O_5 %
Char A	50.2	26.2	7.40	7.92	1.53	1.34	0.80	0.25	3.64	0.72
Char B	50.3	25.4	7.21	9.66	1.79	1.43	0.43	0.23	2.90	0.83

(All percentages are given as wt. %)

If the ash analyses are compared to the ash of coals from different South African mines (see Table 2.10), it is observed that the ash is especially rich in calcium and sulphur and in a lesser extent in iron. On the other hand, both coals have relative low titanium oxide contents.

Table 2.10: Mineral oxides found in ash for other South African coals

Colliery	SiO_2 %	Al_2O_3 %	Fe_2O_3 %	CaO %	MgO %	TiO_2 %	K_2O %	Na_2O %	SO_3 %	P_2O_5 %
Arnot	57.3	22.7	3.55	0.26	1.58	6.79	2.60	0.61	0.27	3.61
Blackwattle	58.8	29.3	1.50	0.13	1.97	4.70	0.87	0.52	0.02	2.22
Boschmans	46.7	27.6	3.36	2.75	1.31	10.9	2.54	0.62	0.24	3.78
Delmas	48.7	26.6	5.60	1.39	1.81	7.60	2.24	0.54	0.79	3.44
Dorsfontein	54.7	33.8	3.08	0.22	1.56	4.04	0.65	0.65	0.07	1.00

(All percentages are given as wt. %)

When the ashes of the coals are compared with the available literature on non South African coals (Table 2.11), it can also be concluded that the calcium content is relatively high. It is also found that the American coal is rich in iron and the East-European coal is very poor in calcium.

Table 2.11: Mineral oxides for non South African coals

Sample origin	SiO_2 %	Al_2O_3 %	Fe_2O_3 %	CaO %	MgO %	TiO_2 %	K_2O %	Na_2O %	SO_3 %	P_2O_5 %
Western Kentucky coal (Hower *et al.*, 1999)	47.61	22.26	19.41	4.35	1.44	1.06	2.52	1.13	0.75	0.23
Bulgarian coal (Vassilev *et al.*, 1999)	59.7	27.6	5.8	0.7	2.5	0.7	2.9	-	-	-

(All percentages are given as wt. %)

2.8 CHAR CHARACTERISATION SCANNING ELECTRON MICROSCOPE RESULTS

The identity, mass percentages of the minerals and the association characteristics of the mineral matter in the char samples were studied using Coal Characterisation Electron Microscope (CCSEM). This detailed mineralogical analysis as was carried out by Van Alphen, (2003) at the Technical Service Institute of Eskom is presented for both chars in Section 2.8.1 and 2.8.2.

2.8.1 Minerals present in the char

The different minerals that are present in the chars are summarised in Table 2.12. Included in Table 2.12 is the comparison between the total mineral matter composition and the % ash obtained.

Table 2.12: Compositions of mineral abundance

Mineral	Char A	Char B	Mineral source in original coal
	Mass-%	Mass-%	
Pyrite/pyrrhotite	8.0	9.5	Partial transformation of pyrite (FeS_2)
Quartz	7.5	18.1	Quartz (SiO_2)
Feldspar	1.0	1.0	Orthoclase ($KAlSi_3O_8$) feldspar
Illite	1.5	1.9	Illite $(K_{1-1.5})Al_4[Si_{7-6.5}Al_{1-1.5}O_{20}](OH)_4$
Mica	0.2	0.3	Muscovite ($KAl_3Si_3O_{10}(OH)_4$)
Kaolinite	22.3	28.5	Kaolinite ($Al_2Si_2O_5(OH)_4$) – clay
Fe-oxide	1.3	1.3	Fe-hydroxides, magnetite
Calcite	8.8	9.5	$CaCO_3$
Dolomite	2.1	2.4	$CaMg(CO_3)_2$
Ankerite/Siderite	0.4	0.4	$CaFe(CO_3)_2$/ $FeCO_3$
Apatite	0.1	0.1	$Ca_3(PO_4)_3(F,Cl,OH)$
Anatase/Rutile	0.2	0.4	TiO_2
Gypsum/Anhydrite	0.0	1.0	$CaSO_4 2H_2O/CaSO_4$
Other	0.4	2.1	Unidentified minerals
Carbon	46.2	23.5	Char
Total	100.0	100.0	
Ash-reconciliation			
Mineral Matter (MM)	53.8	76.5	MM = 100 – Mass-%Char
MM factor	1.12	1.14	MM/Ash-% (Char)
Ash-% - Carbon	48	67.0	Ash of the char after complete combustion in TGA
Ash-% - Carbon	41.3	61.3	Estimated from CCSEM analysis

It is seen from Table 2.12 that the main difference between char A and B, is the higher proportion of quartz, kaolinite and to a lesser extent calcite and pyrite. Since char B has an ash content of 67%, the proportion of carbon is significantly lower than the proportion of carbon in sample A.

In order to show the uniqueness of char A and char B, a comparison between the mineral compositions of the two char samples and mineral composition of typical power station pulverised fuel (South African) is summarised in Table 2.13.

Table 2.13: Mineral distribution of char samples compared to typical power station pulverised fuel

	Char A	Char B	Hendrina	Duhva	Kriel	Kendal
Pyrite	8.0	9.5	2.4	4.6	3.5	2.7
Quartz	7.5	18.1	9.2	3.6	3.8	4.6
Feldspar	1.0	1.0	0.7	0.2	0.3	0.7
Illite	1.5	1.9	0.8	0.7	0.2	1.8
Kaolinite	22.3	28.5	14.5	14.8	8.9	23.4
Mica	0.2	0.3	0.1	0.1	0.0	0.3
Fe-Oxide	1.3	1.3	0.6	0.8	0.1	0.7
Calcite	8.8	9.5	1.0	2.8	5.0	2.2
Dolomite	2.1	2.4	0.6	4.0	2.0	2.2
Other Carbonates	0.4	0.4	0.2	0.8	0.1	0.3
Apatite	0.1	0.1	0.0	0.2	0.2	0.2
Anatase/Rutile	0.2	0.4	0.2	0.1	0.0	0.1
Other	0.4	2.1	0.4	1.1	0.4	0.7
Carbon	46.2	23.5	69.4	66.2	75.5	60.4
Total	100.0	100.0	100.0	100.0	100.0	100.0

(All results are given as wt. %)

It is seen from Table 2.13 that the minerals in char A and B do not match well the samples obtained from different power stations. This is also another indication of how different the two chars are to those used in typical South African power generation.

2.8.2 Distribution of carbon and minerals in a char sample

Association of mineral matter with carbon can be described by classifying the particles based on the relative proportion of mineral matter and carbon in each particle. In the CCSEM analysis, the total area proportion of the particle and the area proportion of the individual mineral species and carbon in that specific particle are computed. By summing the total area proportion of the mineral matter and corresponding carbon, the particles can be classified using the relative proportion of carbon to mineral matter. The accepted standard is to classify particles into 12 area groups into intervals of 10 area-%, with the

first interval starting at 0-area% carbon and the last been 100 area-% (mineral free carbon). Thus, the particle association class of 30-40 describes a particle in which the proportion of carbon is between 30-40 area-% and the proportion of mineral matter makes up the balance. A 100-% class is carbon particle with no measured included mineral grains and the 0% class is particle with only mineral matter and no carbon present.

The % total particle distribution, % carbon distribution and % mineral matter distribution for each association class is illustrated in Figure 2.3 (char A) and Figure 2.4 (char B).

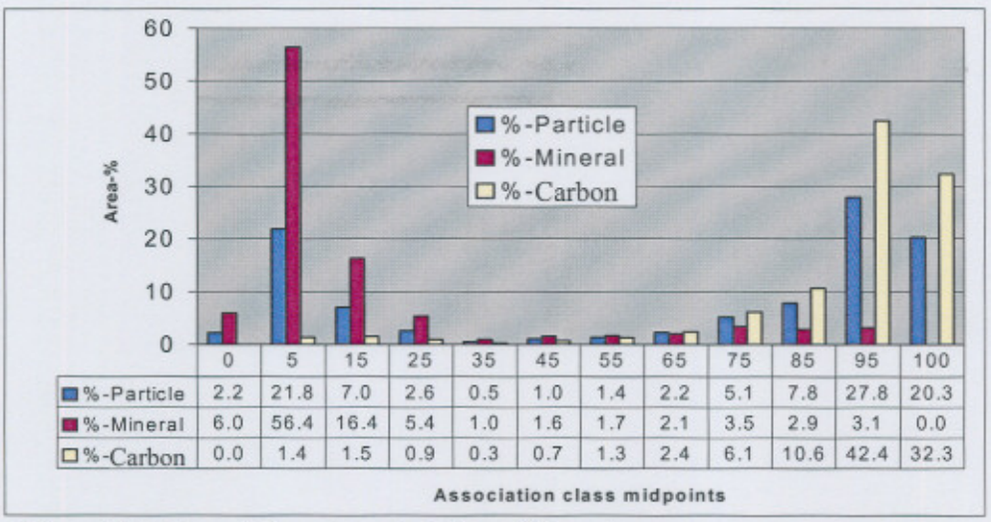

	0	5	15	25	35	45	55	65	75	85	95	100
%-Particle	2.2	21.8	7.0	2.6	0.5	1.0	1.4	2.2	5.1	7.8	27.8	20.3
%-Mineral	6.0	56.4	16.4	5.4	1.0	1.6	1.7	2.1	3.5	2.9	3.1	0.0
%-Carbon	0.0	1.4	1.5	0.9	0.3	0.7	1.3	2.4	6.1	10.6	42.4	32.3

Figure 2.3: Association characteristics of char A

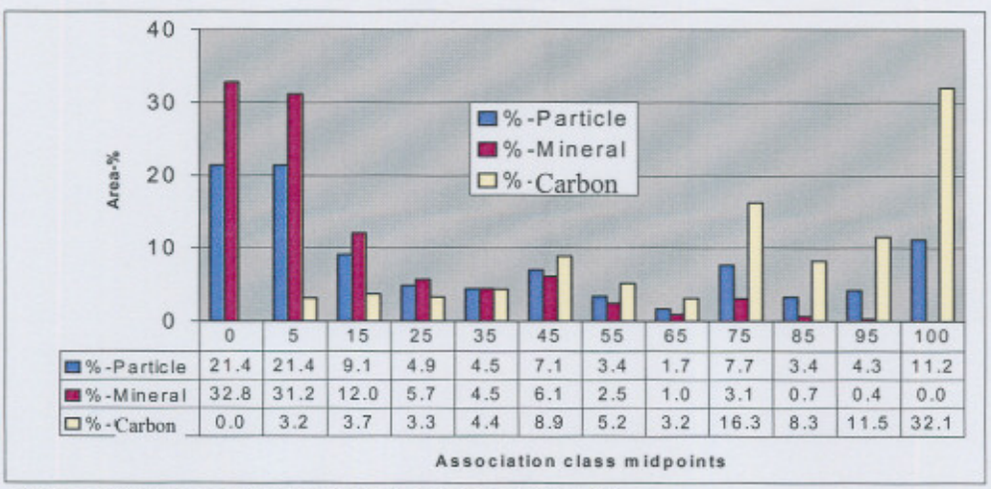

	0	5	15	25	35	45	55	65	75	85	95	100
%-Particle	21.4	21.4	9.1	4.9	4.5	7.1	3.4	1.7	7.7	3.4	4.3	11.2
%-Mineral	32.8	31.2	12.0	5.7	4.5	6.1	2.5	1.0	3.1	0.7	0.4	0.0
%-Carbon	0.0	3.2	3.7	3.3	4.4	8.9	5.2	3.2	16.3	8.3	11.5	32.1

Figure 2.4: Association characteristics of char B

It is seen from Figure 2.3 that 27.8% of the carbon particles in char A are predominantly carbon with less than 10 area % of included mineral grains (90-100 class). 21.8% are particles consisting predominantly of mineral matter with <10 area % carbon (0-10 class) and 20.3% are mineral-free carbon particles (100 class). In contrast, 21.4% of the particles in char B are 100% mineral matter with no associated carbon (0 class). 21.4% are particles consisting predominantly of mineral matter with <10 area % carbon (0-10 class) and 11.2% are mineral-free carbon particles (100 class).

About 56% of mineral matter in char A occurs as predominantly excluded minerals with minor associated carbon (<10%). In char B, the proportion of minerals occurring as excluded mineral particles with no associated carbon is 32.8% and proportion of minerals with minor associated carbon (<10%) is 31.2%. 78.8% of mineral matter in char A is associated with particles where the proportion of carbon is less than 30% (sum 0-30). In comparison, 76% of the mineral matter occurs in this group in char B. In Figure 2.3, it is seen that about 85% of carbon occurs as free char with no associations with minerals whereas in Figure 2.4 about 68% of carbon occurs with no associations with minerals. Another attractive feature of the CCSEM is that an image on how the carbon is located can be seen. In Figure 2.5 and Figure 2.6 images of char A are shown.

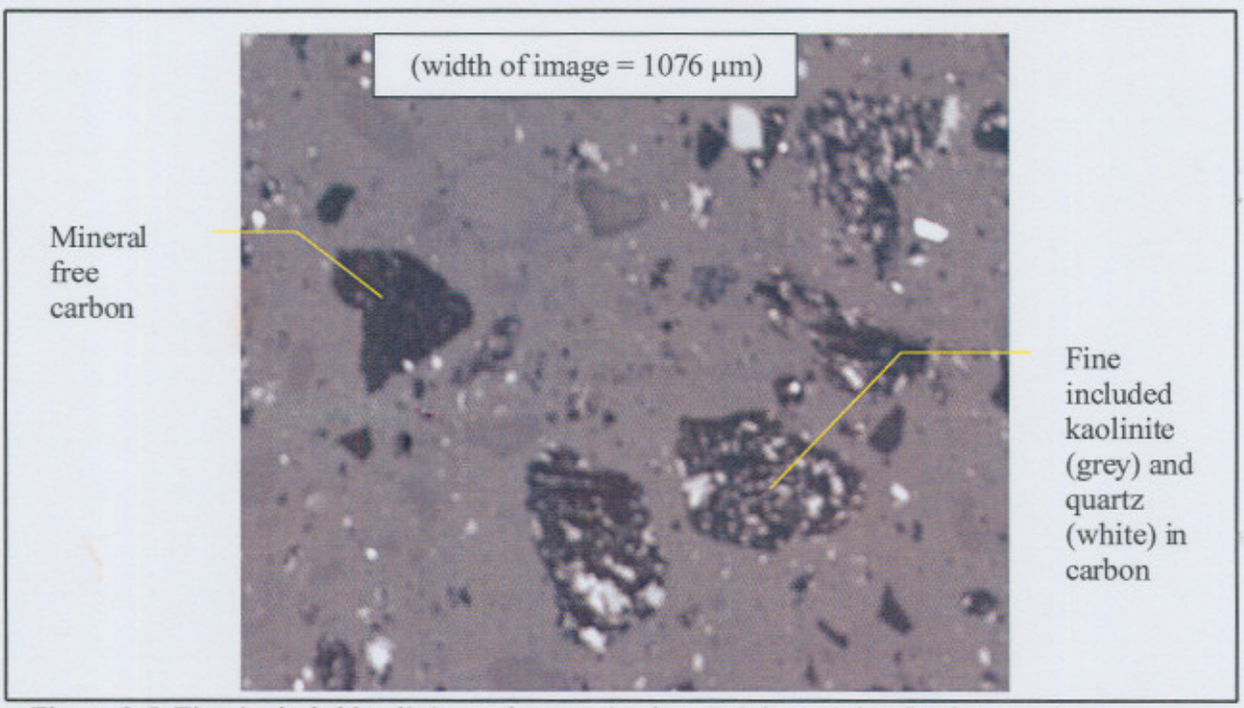

Figure 2.5: Fine included kaolinite and quartz in char A rich particles (back-scatter)

Visually, as seen in Figure 2.5, the mineral matter in the predominantly carbon rich particles (90-100) are fine isolated inclusions of predominantly kaolinite, quartz and to a less extent calcite and pyrite. In Figure 2.6 a variety of extraneous mineral matter particles is shown.

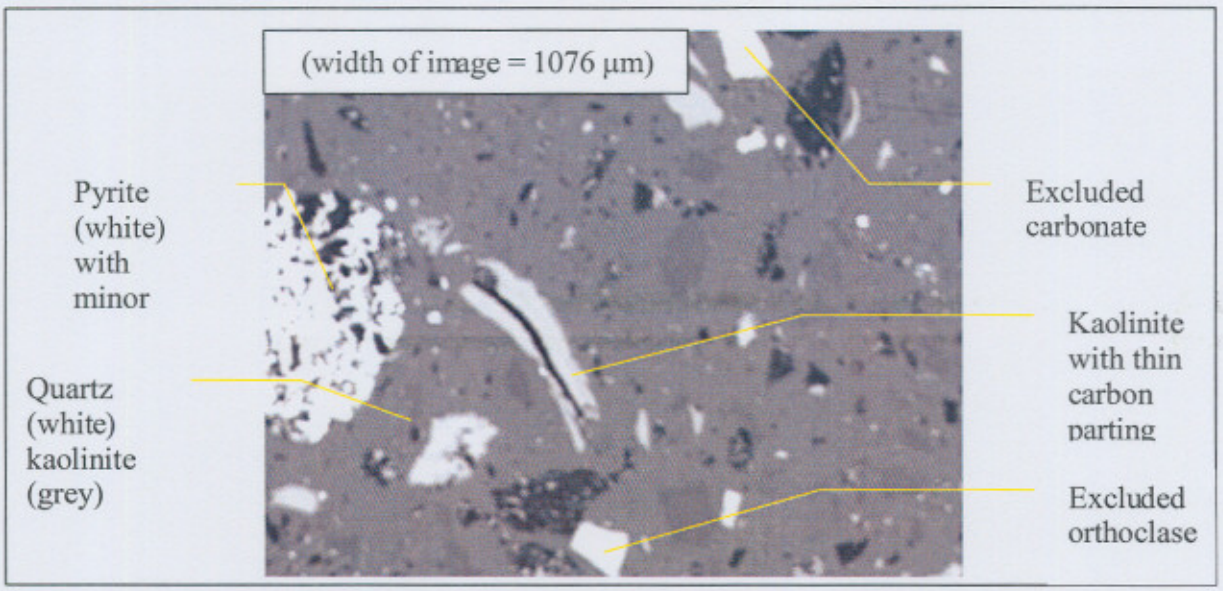

Figure 2.6: A variety of extraneous mineral matter particles in char A (back-scatter)

A higher proportion of kaolinite and quartz occur as fine included grains in carbon than pyrite and calcite/dolomite, see Figure 2.6. Pyrite (>70%) and calcite/dolomite (>60%) predominantly occur as extraneous particles (60-100 class). Excluded kaolinite/quartz particles are also common. In char B, the higher quartz content (Table 2.6) is attributed to a higher proportion of excluded quartz grains and not due to fine included quartz grains associated with carbon.

2.9 PETROGRAPHY ANALYSIS

A study on coal petrography was conducted at SABS (South African Bureau of Standards) laboratory in Pretoria. In this study, three maceral groups were identified, i.e. vitrinite, liptinites and inertinites using a petrographic microscope. Due to the much finer particle size of coal A and coal B samples, identification of the inertinite sub-macerals was not possible. The group of maceral analyses were carried out in accordance with the

ISO Standard 7404 –5, 1994. Table 2.14 shows the petrographic results obtained from the two chars investigated.

Table 2.14: Petrographic (Maceral composition) characteristics of coal A and coal B

Parent coal petrography	Coal A	Coal B
Vitrinite content (wt.%)	21	18
Liptinite content (wt.%)	3	2
Total inertinite (wt.%)	76	80

Vitrinites generally contain relatively less oxygen and more carbon than inertinites. Liptinites are relatively poor in oxygen. They are rich in hydrogen and produce the highest yield of volatile matter when heated, followed by vitrinites. Inertinites are rich in oxygen compared to vitrinites and relatively low in volatiles (Du Cann, 2002).
The major difference with petrography lies most in their behaviours during heating. Vitrinite-rich particles from bituminous coals soften, become plastic and expand to form cellular structures producing a porous char. This char then provides a greatly increased surface area for combustion to occur. The degree of expansion is affected by the heating rate. Most inertinites however, do not soften, degasify or develop into porous structures, but form dense chars, which are more difficult to ignite. They also tend to have lower burnoff rates. In terms of organic composition in bituminous coals, the inertinite group macerals generally exhibit the highest hardness, liptinites the lowest and vitrinites intermediate values. Maceral/mineral associations (in particular those where the cell cavities are filled with minerals) are characterised by increased hardness. It is seen that both coals can be classified as high inertinite bituminous coals. It is for the above reason that very low porosities were obtained with the coals investigated.

2.10 CONCLUSIONS

A detailed characterisation of the two chars and coals have been conducted. Different properties such as proximate and ultimate analysis, particle size distribution, porosity, minerals oxides in the ash, carbon-mineral association (using CCSEM technique) and petrography have been evaluated for both samples.

The following conclusions have been drawn:

- The ash content of both chars is 48 % and 67% for char A and B respectively. These values are much higher than coals normally processed in both the South African and non South African power generation industry.
- The average particle size of char A is 70 μm and that of char B was 20 μm.
- Both chars have very low porosities (< 5%) which can be attributed to the high content of inertenite (> 75 wt.%) in both coals.
- The mineral content of the ash shows large contents of calcium and sulphur and a lower iron contents compared to other South African coals. This conclusion was also confirmed by a CCSEM study on both chars.
- Microscopic inspection of the chars show that the char samples are a collection of mainly carbon rich particles (< 10% minerals) and mineral rich particles (<10% carbon), This was more pronounced for char A than for char B.

NOMENCLATURE

r	pore radius	m
S	surface area	$m^2 kg^{-1}$

Greek Letters

ε	porosity	-
ρ_B	bulk density	$kg\ m^{-3}$

Abbreviations

ar	as received
ASTM	American Society for Testing and Materials
CCSEM	Coal Characterisation Scanning Electron Microscope
CSIR	Centre for Scientific Industrial Research
daf	dry and ash free
db	dry basis
ISO	International Occupational Standards
SABS	South African Bureau of Standards

REFERENCES

CHEN, C. AND KOJIMA, T. 1996. Single char particle combustion at moderate temperature: effects of ash. *Fuel Processing Technology*, **47**: 215-232.

DU CANN, V.M. 2002. Special report: Analyses of coal product samples of South African collieries. *South African Bureau of Standards (SABS)*.

GADIOU, R., BOUZIDIDI, Y. AND PRADO, G. 2002. The devolatilisation of millimetre sized coal particles at high heating rate: the influence of pressure on the structure and reactivity of the char. *Fuel*, **81**: 2121-2130.

GOYAL, A., ZABRANSKY, R.F. AND REHMAT, A. 1989. Gasification kinetics of Western Kentucky bituminous coal char. *Industrial Engineering Chemistry*, **28**: 1767-1778.

HALDER, S. AND SAHA, R.K. 1991. Combustion kinetics of lignite char in a fluidised bed. *Journal of the Institute of Energy*, **64**: 55-61.

HINES, A.L. AND MADDOX, R.N. 1985. Mass transfer fundamentals and applications. *Prentice-Hall international series*, p46.

HOWER, C.J., RATHBONE, F.R., ROBERTSON, J.D., PETERSON, G. AND TRIMBLE, A.S. 1999. Petrology, mineralogy, and chemistry of magnetically-separated sized fly ash. *Fuel*, **78**: 197-203.

MOORS, J.H.J., BANIN, V.E., HASS, J.H.P., WEBER, R. AND VEEFKIND, A. 1999. Prediction and validation of burnout curves for Gottelborn char using reaction kinetics determined in shock tube experiments. *Fuel*, **78**: 25-29.

PRETORIUS, C.C., PINHEIRO, H.J. AND BOSHOFF, H.P. 2002. Special report: Analyses of coal product samples of South African collieries. *South African Bureau of Standards (SABS)*.

SENEL, I., 1994. Characterisation of pore structure of Turkish coals and their chars obtained by carbonisation and CO_2 activation. PhD Thesis, Ankara University, Turkey.

TOMECZEK, J. AND GIL, S. 2003. Volatiles release and porosity evolution during high pressure coal pyrolysis. *Fuel*, **82**: 285-292.

VAN ALPHEN, C. 2003. Special report: CCSEM description of selected char samples. *Van Alphen Consultancy.* Johannesburg, South Africa.

VASSILEV, S.V. AND VASSILEVA, G.C. 1996. Mineralogy of combustion wastes from coal-fired power stations, *Fuel Processing Technology*, **47**(3): 261-280.

CHAPTER 3

COMBUSTION REACTION KINETICS

3.1 INTRODUCTION

In this chapter, the kinetics of combustion of two high ash chars is determined with isothermal and non-isothermal methods using a thermogravimetric analyser. Combustion reactions have been studied with oxygen and oxygen/nitrogen mixtures at atmospheric pressure and temperatures between 370 and 560 °C. Isothermal experiments were carried out between 370 and 410 °C and the non-isothermal experiments up to 560 °C. Factors affecting the reaction rates of the char combustion have been evaluated and quantified. In Section 3.2, a literature survey is presented, in which a general background on char combustion is given. Also, the different parameters that influence the rate of combustion is presented in this section. Fundamental char combustion models, the shrinking unreacted core model, the shrinking reacted core model and the homogeneous model are discussed in Section 3.3. The experimental apparatus and the experimental procedures to determine the reaction kinetics of combustion are presented in Section 3.4. The results and discussion is given in Section 3.5 for the isothermal study and in Section 3.6 for the non-isothermal study. Finally, the conclusions of the complete study are summarised in Section 3.7.

3.2 LITERATURE SURVEY

3.2.1 Introduction

In this section, a summary of the mechanisms and particle conversion models for the combustion of char is given. The most important factors that influence the rate of combustion are also discussed.

3.2.2 Combustion reactions of coal chars

The mechanism of combustion of coal-derived char has been studied extensively in the past 50 years (e.g., Russell *et al.*, 1998, Sorenson *et al.*, 1996, Querol *et al.*, 1994 and Grovest *et al.*, 1987). It is generally accepted that chemisorption of oxygen on the char surface (Hill and Fott, 1993) is the first step in the combustion process. The resulting surface oxides decompose to form carbon dioxide (Equation 3.4) or carbon monoxide (Equation 3.1). If an excess of oxygen is present, as is the case in combustion reactions, the carbon monoxide will be oxidised to carbon dioxide very fast (Equation 3.2). The Bouduard equilibrium reaction (Equation 3.3) can also occur, especially at high temperatures (Tsai, 1982; Essenhigh, 1982).

$$2C_{(solid)} + O_{2(gas)} \rightarrow 2CO_{(gas)} \qquad [3.1]$$

$$2CO_{(gas)} + O_{2(gas)} \rightarrow 2CO_{2(gas)} \qquad [3.2]$$

$$C_{(solid)} + CO_{2(gas)} \leftrightarrow 2CO_{(gas)} \qquad [3.3]$$

$$C_{(solid)} + O_{2(gas)} \rightarrow CO_{2(gas)} \qquad [3.4]$$

The overall reaction of the combustion of char in an excess of oxygen is predominantly represented as the reaction given in Equation 3.4 (Russell, *et al.*, 1998 and Sorenson *et al.*, 1996). Therefore, this reaction is taken as the combustion reaction and forms the basis for the derivation of the different combustion models (Section 3.3).

3.2.3 Factors affecting the reaction rates of coal chars

The combustion of coal in any system, whether carried out in a fixed or fluidised bed, is primarily a matter of combustion of carbon, with primary combustion of volatiles. Under reaction conditions, the release of volatiles from the coal and the successive combustion of the volatiles is very fast compared to the combustion of char (Essenhigh, 1982; Moors *et al.*, 1999 and Tomeczek and Gil, 2003). Since the combustion of char is the rate determining step in the overall combustion process, the coal samples are devolatilised before every experiment and hence the reaction kinetics of the resulting char is studied in depth. There are several factors that influence the reaction kinetics and mechanisms of char combustion reactions. The most important factors are described in the following sections.

3.2.3.1 Char preparation

It is well known that the structure of char depends on the devolatilisation process of the coal and hence can have an influence on the char reactivity (Gonenc, 1990; Howard, 1982). As the formation of char proceeds, the porosity of the char sample increases initially. The accessibility of the pores to penetrating molecules however only increases in temperatures below 500 to 600 °C, and then severely decreases in the range of 600 to 1000 °C (Evans and Hermann, 1970). A similar conclusion was drawn by Serio *et al.* (1987) and Muhlen and van Heek (1985), who studied the reactivity of chars prepared at different temperatures and found that for chars prepared at lower temperatures (600 °C), the char exhibited a much higher reactivity than for chars prepared at higher temperatures (800 - 900 °C). This is mainly due to the degree of graphitisation of the char as the temperature increases (Howard, 1982).

One of the macroscopic changes taking place during the plastic stage in the devolatilisation process is the formation and transport of gas bubbles within the resultant viscous mass. The transport of these bubbles to the surface of the char is responsible for the formation of the char pore structure. Pore structures can be macro- or micro porous, depending on the coal and the preparation conditions (Habermehl *et al.*, 1981). These significant structural changes during devolatilisation are however not found for high

inertinite chars. For these chars, the porosity and structure of the coal is only slightly influenced by the devolatilisation process (Tomeczek and Gil, 2003).
Since the char formation process can have an effect on the reactivity of the char, it is important to carry out the devolatilisation identically before every experiment.

3.2.3.2 Char composition

The relative reactivity of chars can be quantified by studying the reaction kinetics of different chars at the same reaction conditions (Jenkins *et al.*, 1973). In this way, the reactivity of a char describes a property of the char but should therefore be reported for well-defined operating conditions (e.g. temperature and pressure). As the reactivity also varies with conversion, it should also be reported for specific conversion levels. So, the reactivity of the char is closely related to the origin of the coal.
Several researchers found that the reactivity of a char strongly depends on the composition of the char (Takarada *et al.*, 1985, Cloke and Lester, 1994 and Miura, *et al.*, 1989). According to Takarada *et al.* (1985), there are mainly three factors affecting the intrinsic reactivity of a coal derived char:

1. Chemical composition, particularly the amount of hydrogen, oxygen and sulphur that affect the imperfections of the carbon structure (active sites).
2. The coal ash, which may provide catalytic effects.
3. The rank of the coal, which determines pore size and structure.

The measurement of these char properties is therefore very important in kinetic investigations (see Chapter 2). The oxygen content of a coal is considered as a parameter indicative of the amount of free sites that will be available on the surface of a resulting char (Hashimoto *et al.*, 1986). The moisture content of a coal is considered as an indication of the porosity of a char (Takarada *et al.*, 1985).
Several investigators (e.g. Walker, 1977, Jenkins *et al.*, 1973 and Miura *et al.*, 1989) observed that the reactivity of chars increase as the grade of coal decreases. This is usually explained by a catalytic effect that the metal oxides can have on the combustion

reaction (Hill and Fott, 1993). If hydrogen, present in the carboxyl groups of the char, is exchanged by calcium and sodium, the char becomes more reactive in the reaction of chars with oxygen and other reactive gases (Hashimoto *et al.,* 1986). Other investigators (e.g. Miura *et al.*, 1989) have also observed a catalytic effect of calcium, sodium, potassium and magnesium on the reactivity of chars. Miura *et al.* (1989) found that the combustion reactivity of lower grade coals (carbon content less than 80%) is controlled by a catalytic effect of the minerals. On the other hand, the gasification rate of higher rank coals seemed to be a non-catalytic reaction of carbon, controlled mainly by the intrinsic reactivity of the char. This conclusion however, does not necessarily mean that the gasification rate of higher rank coals is not affected by catalytic activity. When alkali metals or alkali earth metals are added to these chars prior to reaction, the reactivity is greatly enhanced (Nsakala *et al.*, 1977).

To eliminate the effect of catalytic reactivity demineralised chars are often used, whereby the chars are washed in acid to remove metal constituents (Johnson, 1979; Essenhigh, 1982). Since the intrinsic reactivity of the char is of importance in this study, the chars are not demineralised before every combustion experiment.

In order to predict the combustion behaviour of chars accurately under various conditions, e.g. varying temperatures and partial pressures, it is important to develop and validate physically realistic kinetics. The availability of high-ash coal in South Africa has strongly motivated this study. Peek (2000) and Lorenz *et al.* (2000) have studied combustion of chars less than 30% ash. In literature the evaluation of kinetics of combustion of high ash coal chars greater than 48% has not been published.

3.2.3.3 Particle size effect

The reaction of porous carbons with gaseous reactants involves the transport of both reactant and product gases between the bulk gas phase and the particle surfaces, where the chemical reactions take place (Levenspiel, 1972). Under conditions where gaseous concentrations within a particle are different from the external gaseous concentrations, diffusion processes affect the overall reaction rate (Laine *et al.*, 1964). For small and relatively non-porous materials the ratio of external to internal surface area is relatively

large, and the effect of intraparticle diffusion can be neglected. External diffusion is, in these cases, the dominant diffusional resistance, which can be reduced by higher gas flow rates around the particle (Essenhigh, 1982; Hashimoto *et al.*, 1986). In contrast, with large and porous carbon particles (> 100 μm) at elevated temperatures, the reaction rate is greatly influenced by intraparticle pore diffusion (Johnson, 1979; Tsai, 1982).

3.2.3.4 Effect of pore size

The complex pore structure of coal chars, which changes during the course of combustion reactions, presents great difficulty in the analysis of diffusion behaviour. Walker *et al.* (1959) described this process in detail for the reaction of pure carbons with oxygen. Other investigators have also quantitatively considered the effect of intraparticle diffusion on the gasification rate of coal chars (Kunio and Kunii, 1969).

Walker and co-workers (1977) have indicated that coal chars have a trimodal pore structure, consisting of macropores, transitional pores and micropores. They stated that diffusion through the initial macropores and transitional pores is relatively fast. This has the result that the gaseous concentrations at the mouths of the micropores are nearly the same as the concentrations at the external particle surface.

Gaseous diffusion within the micropores can be very slow in relation to the diffusion through the macropores systems (Evans and Hermann, 1970). It has therefore been suggested that chars with a large transitional pore system will show fewer limitations to mass transport during reaction (Walker *et al.*, 1977).

3.2.3.5 Effect of temperature

High temperature favours high reaction rates (Johnson, 1979; Essenhigh, 1981). This leads to the observation that there is a transition in the controlling mechanism of gas-solid reactions from chemical reaction control to diffusion control, as the temperature increases. The reactions of a porous solid can generally be divided into three regions, and thereby is called the three-zone concept. This concept was first postulated by Wicke (1955), and was discussed in detail by Walker and co-workers (1959) for coal conversion. At low temperature (ambient-500°C), when the reaction rate is relatively low,

reactant gases can diffuse into the porous solid faster than it can be depleted by the rate of the reaction. The reaction therefore takes place uniformly throughout the particle. This is referred to as Zone 1 (Walker *et al.*, 1959).

At temperatures around (500 – 800 °C), the in-diffusing gas is consumed in a reactive zone that does not penetrate to the centre of the solid, leaving an unreacted core. This is referred to as Zone II (Walker *et al.*, 1959).

At very high temperatures (>800 °C), the reaction is so fast that no significant penetration of the gas into the solid matrix occurs. The reaction retreats to the external surface of the particle, and the rate is controlled by boundary layer (external) diffusion. This is referred to as Zone III (Walker *et al.*, 1959). It is also well established by Walker (1959) that the activation energy in Zone II is half that of the activation in Zone I (Essenhigh, 1982).

It is therefore clear that the mechanism whereby a reaction occurs, either diffusionally or chemically controlled, is dependent on a number of factors.

3.2.4 Combustion models

One of the most used empirical models to describe reaction kinetics of char oxidation at typical industrial combustion temperatures is the *n*-th order rate equation (Smith, 1982; Hurt and Mitchell, 1992; Monson *et al.*, 1995). The most common form of the *n*-th order overall reaction rate equation is:

$$\frac{dX}{dt} = k_o \exp(\frac{-E}{RT}) P_{O_2}^n . f(X) \qquad [3.5]$$

where *f(X)* is the particle conversion model, the model that describes the relative conversion rate (ratio of reaction rate to initial reaction rate) as conversion progresses. This simple equation provides a basis for estimating overall reaction rates, and has often been adequate for practical use at atmospheric pressure over small temperature ranges (Smoot and Smith, 1985) and has often been used. However, the *n*-th order rate equation does not account for pore diffusion effects on kinetics. Also, the reaction order is often observed to vary as experimental conditions vary, with limits of zero and unity

(Suurberg, 1988). Presently no theory can satisfactorily explain or predict how the reaction order of char oxidation would change with experimental conditions. Several investigators have proposed different forms of char overall reaction rate equations (Smith *et al.*, 1994). These models are presented in Table 3.1.

Table 3.1: Summary of overall reaction rate models

Researcher	Particle conversion model
Wen (1968)	$\frac{dX}{d\tau} = r_o.(1-X)^{\beta}$
Mahajan (1978)	$\frac{dX}{d\tau} = a_o + a_1\tau + a_2\tau^2$
Gardner (1979)	$\frac{dX}{d\tau} = r_o e^{-\alpha X}.(1-X)$
Johnson (1979)	$\frac{dX}{d\tau} = r_o e^{-\alpha X^2}.(1-X)^{\beta}$
Simons (1980)	$\frac{dX}{d\tau} = r_o \sqrt{X + \varepsilon_o(1-X)}.(1-X)$
Chornet (1979)	$\frac{dX}{d\tau} = r_o \sqrt{X}.(1-X)$
Bhatia and Perlmutter (1980)	$\frac{dX}{d\tau} = r_o \sqrt{1-\psi \ln(1-X)}.(1-X)$

Laurendeau (1978) and Reade (1996) state that models vary in levels of detail and can be classified into two subcategories: macroscopic and microscopic models. Macroscopic models use average properties of the particles to estimate the effective diffusivity in the porous structure, and usually do not model the evolution of pore structure with conversion. In other words, macroscopic models assume spatially uniform properties (porosity, pore size and surface reactivity) and invariant pore structures. Microscopic models involve the development of a reaction model for a single pore and then prediction of the overall particle reactivity by an appropriate statistical description of the pore size distribution (Laurendeau, 1978). Microscopic models use a pore structure model to approximate the spatial and temporal variations in local diffusivity, pore structure, and

the properties of the particles are assumed to be uniform, then the microscopic approach becomes equivalent to macroscopic approach. Microscopic models have the potential to capture the effects of burnout on reactivity. However, these models are numerically cumbersome and generally less desirable as sub-models in comprehensive combustion codes (Cope, 1995). More fundamental models are derived in the next section.

3.3 DERIVATIONS OF FUNDAMENTAL REACTION RATE MODELS

3.3.1 Introduction

In this section, different forms of the shrinking core model are described. The derivation corresponding to each model is presented. In the first part of this section a situation for a shrinking unreacted core with gas film diffusion, diffusion through the ash layer and chemical reaction controlling is considered. In the second part of this work, a situation describing the shrinking reacted core model as well as the homogeneous model is presented.

3.3.2 Shrinking unreacted core model (SUCM)

3.3.2.1 Description

This well known model consists of a nonporous char particles (at reaction conditions) with reaction occurring only on the outer surface and as the reacting surface recedes, a layer of ash can be formed around the unreacted core of char. This ash is assumed to be porous so that reaction occurs by diffusion of oxygen through this ash layer to the surface of the impervious core of char. The condition for this to occur is that the rate of movement of the reaction interface is small with respect to the velocity of diffusion of oxygen through the ash layer. The requirements for this pseudo-steady-state concept have been carefully developed and are available in many publications (Bischoff and Froment, 1963). Based on this concept there are three rates of importance and need to be investigated to determine a possible rate controlling mechanism: (1) diffusion of oxygen

through a gaseous boundary layer; gas film diffusion (2) diffusion through the ash layer, and (3) reaction at the interface between ash and unreacted core.

3.3.2.2 Derivation of equations

Consider the following reaction in a spherical particle with an initial radius R:

$$O_{2(g)} + C_{(s)} \rightarrow \text{prod} \qquad [3.6]$$

$$[\,A + S \rightarrow P + \text{ash}\,] \qquad [3.7]$$

with a reaction rate proportional to the partial pressure of oxygen only to the power n, namely:

$$r_A^s = r_s^s = k_s C_{so} P_A^n = k_s^{'} P_A^{\ n} = k_{so}^{'} e^{\frac{-E}{RT}} P_A^{\ n} \qquad [3.8]$$

The moles of carbon (denoted with subscript S) reacted at any time is:

$$N_s = \rho_s 4(R_p - r_c)^3 / 3M_s \qquad [3.9]$$

where r_c is the radius of the unreacted core.

Also the conversion X is:

$$X = 1 - (r_c/R_p)^3 = 1 - \gamma^3 \qquad [3.10]$$

Gas film diffusion control

Equating the consumption rate of carbon to the rate of mass transfer

$$\frac{1}{4\pi R_p^2}\frac{dN_s}{dt} = k_g P_{AO} = -\frac{\rho_s r_C^2}{M_s R_p^2}\frac{dr_c}{dt} \qquad [3.11]$$

Integrating for constant R_p (ash layer and core)

$$t = \frac{\rho_s R_p}{3M_s k_g P_{AO}}(1-\gamma^3) \qquad [3.12]$$

and in terms of conversion:

$$t = \frac{\rho_s R_p}{3M_s k_g P_{AO}} X = t_\infty X \qquad [3.13]$$

If the time is normalised to the time of 90% conversion, the following equation can be derived:

$$t/t_{0.9} = \frac{X}{0.9} \qquad [3.14]$$

The corresponding overall reaction rate is the following:

$$\frac{dX}{dt} = \frac{3M_s k_g P_{AO}}{\rho_s R_p} \qquad [3.15]$$

Diffusion through product ash layer control

Based on the pseudo-steady-state assumption the following differential equation is applicable:

$$\frac{d}{dr}(-D_e^{'}\frac{dC'_A}{dr}) = 0 \qquad [3.16]$$

with boundary conditions: r =R_p; $C_A^{'} = C_{AO}^{'}$, r = r_C ; $C_A^{'} = 0$. The diffusion coeffient depends on the properties of the resulting ash layer.

Equating the rate of consumption of carbon to the flux of oxygen through the ash

$$\frac{dN_s}{dt} - 4\pi r_C^2 \frac{\rho_s}{M_s}\frac{dr_C}{dt} = 4\pi R^2 D_e^{'}\frac{dC'_A}{dr}\Big|r = R_p \qquad [3.17]$$

Integrating for constant R_p (ash layer and core)

$$t = \frac{\rho_s R_p^2}{M_s D_e^{'} C_{AO}}\left(\frac{1-\gamma^2}{2} + \frac{1-\gamma^3}{3}\right) \qquad [3.18]$$

and in terms of conversion:

$$t = \frac{\rho_s R_p^2}{6 M_s D_e^{'} C_{AO}}[1 - 3(1-X)^{\frac{2}{3}} + 2(1-X)] \qquad [3.19]$$

$$t = t_\infty[1 - 3(1-X)^{\frac{2}{3}} + 2(1-X)] \qquad [3.20]$$

If the time is normalised to the time of 90% conversion, the following equation can be derived:

$$t/t_{0.9} = \frac{1 - 3(1-X)^{\frac{2}{3}} + 2(1-X)}{0.55} \qquad [3.21]$$

The corresponding overall reaction rate is the following:

$$\frac{dX}{dt} = \frac{3 M_s D_e^{'} C_{AO}}{\rho_s R_p^2}\left[\frac{1}{(1-X)^{-1/3} - 1}\right] \qquad [3.22]$$

Chemical reaction control

Equating the rate of consumption of carbon to the reaction rate at the surface:

$$\frac{1}{4\pi r_C^2}\frac{dN_s}{dt} = k_s' P_{Ao}^n = -\frac{\rho_s}{M_s}\frac{dr_C}{dt} \qquad [3.23]$$

Integrating:

$$t = \frac{\rho_s R_p}{M_s k'_s P_A^n}(1-\gamma) \qquad [3.24]$$

and in terms of conversion:

$$t = \frac{\rho_s R_p}{M_s k_s' P_{Ao}^n}[1-(1-X)^{1/3}] = t_\infty[1-(1-X)^{1/3}] \qquad [3.25]$$

If the time is normalised to the time of 90% conversion, the following equation can be derived:

$$t/t_{0.9} = \frac{1-(1-X)^{\frac{1}{3}}}{0.54} \qquad [3.26]$$

The corresponding overall reaction rate is the following

$$\frac{dX}{dt} = \frac{3M_s k_s' P_{Ao}^n}{\rho_s R_p}(1-X)^{2/3} = k_o e^{\frac{-E}{RT}} P_{O_2}^n (1-X)^{2/3} \qquad [3.27]$$

This equation is similar to the equation used by Johnson *et al.* (1979) as given in Table 3.1. If equation 3.27 is combined with Equation 3.5:

$$k_o = \frac{3M_s}{\rho_s R_p} k'_{so} \qquad [3.28]$$

3.3.3 Shrinking reacted core model (SRCM)

3.3.3.1 Description

The particles are assumed to be a homogeneous mixture of carbon (C) and minerals (ash) and with porosity such that diffusion inside the particle can affect the overall reaction rate. The reaction rate is first-order with respect to the concentration of oxygen and concentration profiles of oxygen (pseudo steady state) and carbon are generated inside the coal/char particles. As a result of the carbon being depleted inside the core a structural change (pore sizes) will be occurring during the combustion process which in turn effects the diffusion coefficient of the diffusing gases (Knudsen diffusion). Since the reaction rate is the fastest near the surface, rather than in the interior of the particle the carbon concentration will be depleted first at the surface thus forming an ash layer. This will be designated as the first period. After this period, the ash layer will increase (or will be removed) with a decreasing active porous core of the char, similar to the particle during the first period, constituting the second period. External film diffusion is not considered and the ash layer is removed as it is formed (equivalent to an ash layer with negligible diffusional resistance).

3.3.3.2 Derivation of equations

The relevant equations for this model are the following (for complete derivations see Ishida and Wen [1968]. Consider the following reaction in a spherical particle with a radius R_p:

$$O_{2(g)} + C_{(s)} \rightarrow \text{products}_{(g)}$$

with a reaction rate dependence on the concentration of oxygen (1^{st} order) only:

$$r_A^v = r_s^v = k_v C_{so} C_A = k_v^{'} C_A = k_{vo}^{'} \exp(\frac{-E}{RT}) C_A \qquad [3.29]$$

For the first period the material balance for oxygen (A) and carbon (S) is:

$$D_e(\frac{d^2 C_A}{dr^2} + \frac{2}{r}\frac{dC_A}{dr}) = -r_A^v \qquad [3.30]$$

$$\partial C_S / \partial t = -r_s^v \qquad [3.31]$$

with boundary conditions:

$$C_A = C_{A0};\ \text{at } r = R_p \qquad [3.32]$$

$$\frac{dC_A}{dr} = 0;\ \text{at } r = 0 \qquad [3.33]$$

and:

$$C_s = C_{so};\ \text{at } t = 0 \qquad [3.34]$$

The solution of these equations can be obtained as:

$$\frac{C_A}{C_{A0}} = \frac{\sinh(\phi\xi)}{\xi \sinh(\phi)} \qquad [3.35]$$

and:

$$\frac{C_s}{C_{so}} = 1 - \frac{\sinh(\phi\xi) k_v^{'} C_{A0} t}{\xi \sinh(\phi)} \qquad [3.36]$$

where:

$$\xi = \frac{r}{R_p};\ \ \phi = R_p\sqrt{\frac{k_v^{'}}{D_e}} = Thiele\ modulus \qquad [3.37]$$

The fractional conversion of carbon can be found to be:

$$X = \frac{3}{(\phi)^2}(\phi\coth\phi - 1)k_v C_{A0} t \qquad [3.38]$$

There is thus a linear relationship between X and t over the first period. The duration of the first period is determined from Equation (3.36) with $C_s = 0$ at $\xi = 1$, that is:

$$k_v^{'} C_{S0} t_1 = 1 \qquad [3.39]$$

and the fractional conversion and carbon profile at t_1 is:

$$X = \frac{3}{(\phi)^2}(\phi\coth\phi - 1) \qquad [3.40]$$

and the carbon concentration profile:

$$\frac{C_s}{C_{so}} = 1 - \frac{\sinh(\phi\xi)}{\xi\sinh(\phi)} \qquad [3.41]$$

For the second period, the material balances for oxygen (A) and carbon (S) needs to be solved for the shrinking porous particle only which are the same as for the first period except that the radius of the particle changes (with time). For a varying core radius r_m ($\xi_m = r_m / R_p$ with R_p = initial radius) the following equations are obtained:

$$\frac{C_A}{C_{A0}} = \frac{\xi_m \sinh(\phi\xi)}{\xi \sinh(\phi\xi_m)} \qquad [3.42]$$

$$\frac{C_s}{C_{so}} = 1 - \frac{\xi_m \sinh(\phi\xi)}{\xi \sinh(\phi\xi_m)} \qquad [3.43]$$

The total time duration ($t = t_1 + t_2$) is then:

$$t = \frac{1 + \ln(\xi_m \sinh(\phi)/\sinh(\phi\xi_m))}{k_v' C_{A0}} \qquad [3.44]$$

and the fraction conversion over this period is:

$$X = 1 - \xi_m{}^3 + \frac{3\xi_m}{\phi^2}[\phi\xi_m \coth(\phi\xi_m) - 1] \qquad [3.45]$$

A dimensionless time variable defined as t/t_∞ where t_∞ is the time for total combustion can be used, thus:

$$t/t_\infty = \frac{1 + \ln(\xi_m \sinh(\phi)/\sinh(\phi\xi_m))}{1 + \phi^2/6 + \ln(\sinh(\phi)/\phi)} \qquad [3.46]$$

Also a dimensionless time variable defined as $t/t_{0.9}$ where $t_{0.9}$ is the time for 90% conversion can be used, thus:

$$t/t_{0.9} = \frac{1 + \ln(\xi_m \sinh(\phi)/\sinh(\phi\xi_m))}{1 + \ln(\xi_m^{0.9} \sinh(\phi^{0.9})/\sinh(\phi^{0.9}\xi_m^{0.9}))} \qquad [3.47]$$

It should be noted that by combining Equations (3.45) and (3.46), a plot of conversion X versus t/t_∞ would result which is dependant on the Thiele modulus parameter only and

independent of the concentration of oxygen. This is also applicable to combining Equations (3.45) and (3.47)

Also the results (X versus t/t_{∞}) as shown in Figure 3.1 merge for large values of the Thiele modulus, corresponding to no penetration of oxygen into the core and is equivalent to an unreacted-core shrinking model (Ishida et al., 1968). Also applicable to X versus $t/t_{0.9}$.

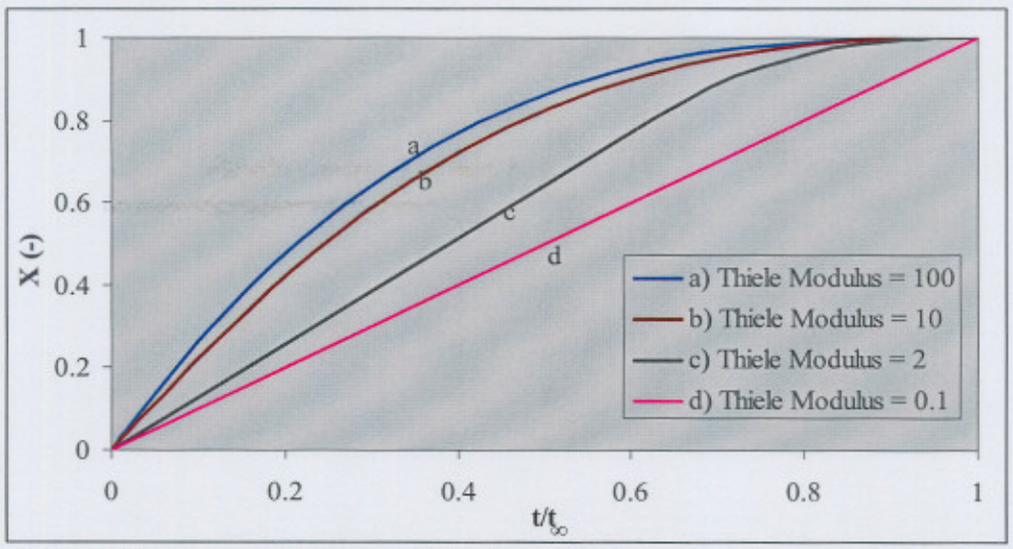

Figure 3.1: Effect of Thiele modulus for a shrinking reacted core particle

The unreacted-core shrinking model referred to corresponds to a reaction controlled surface reaction model without a product (ash) layer. The equations for conversion and dimensionless time being the following (Ishida and Wen, 1968):

$$X = 1 - \xi_c^3 \qquad [3.48]$$

$$t/t_{\infty} = 1 - \xi_c = 1 - (1 - X)^{1/3} \qquad [3.49]$$

where

$$t_{\infty} = \frac{R_p}{k_s^{sv} C_{AO}} \qquad [3.50]$$

It is well known that a plot of Equation (3.49) is good test for the validity of this model.

3.3.4 Homogeneous Model

A homogeneous model in this study is considered to describe conversion of a very porous particle (large diffusion coefficient relative to the reaction rate constant) with a constant oxygen concentration in the particle ($C_A = C_{AO}$). Consequently, the reaction is solely reaction rate controlling throughout a constant size particle (R_p) and Equation (3.31) above is applicable. Different reaction rate equations have been proposed in the literature, which give the following results.

Case 1. The rate depends on the oxygen concentration only as in Section 3.3.3 above, and substituting in Equation (3.31) above:

$$\frac{1}{\frac{4}{3}\pi R_p^3} \frac{dN_s}{dt} = \frac{dC_A}{dt} = -k_v^{'} C_{AO} \qquad [3.51]$$

Integrating over a time period t:

$$t = \frac{X C_{so}}{k_v^{'} C_{AO}} \qquad [3.52]$$

The corresponding rate equation is:

$$\frac{dX}{dt} = \frac{k'_V C_{AO}}{C_{so}} \qquad [3.53]$$

Case 2. The rate depends on both oxygen and carbon concentrations in the particle, and substituting in Equation (3.31) above:

$$\frac{1}{\frac{4}{3}\pi R_p^2}\frac{dN_s}{dt} = \frac{dC_s}{dt} = -k_v C_s C_{AO} \qquad [3.54]$$

Integrating over a time period t

$$-\ln(1-X) = k_v C_{AO} t \qquad [3.55]$$

The corresponding rate equation is:

$$\frac{dX}{dt} = k_v^{'} C_{AO}(1-X) \qquad [3.56]$$

This equation is similar to the equation used by Wen (1968) as given in Table 3.1.

3.4 EXPERIMENTAL

In this section, a brief description of the two (TGA) thermogravimetric analysers used is given. The TI 2050 vertical TGA was used for isothermal experiments while all the non-isothermal experiments were carried out using the Du pont 951 horizontal thermogravimetric analyser. The char preparation together with the combustion method followed is described. Some experimental results confirming the absence of diffusion are also presented.

3.4.1 Description of the experimental apparatus

The TGA operates on a principle whereby the sample weight change is constantly measured as a function of time and temperature. The instrument can be operated isothermally or non-isothermally. The photograph and a schematic representation of the

instruments used in this investigation are shown in Figure 3.2 and 3.3. Both instruments measure the mass and temperature at short time intervals i.e. 2-5 seconds (depending on the duration of the experiments), resulting in a semi-continuous time-temperature-mass plot (see e.g. Figure 3.4 and 3.7)

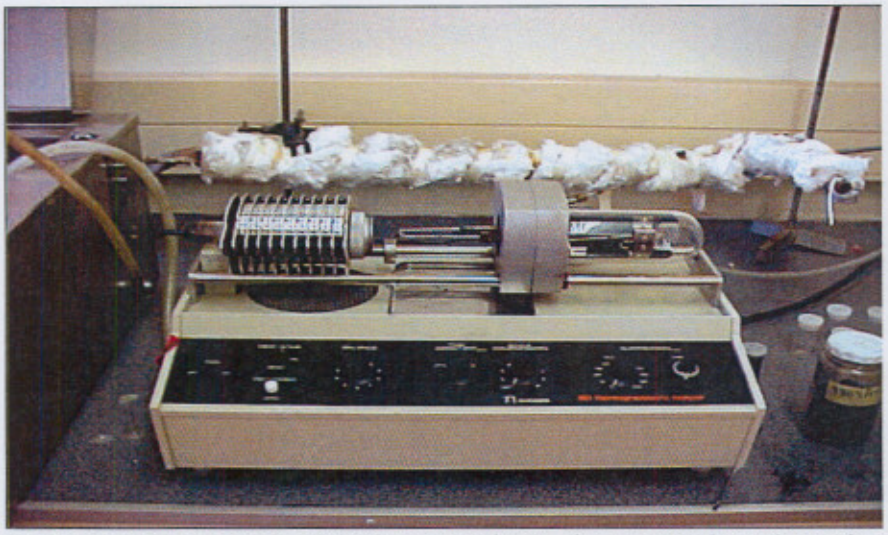

Figure 3.2: Photograph of the horizontal 951-thermogravimetric analyser

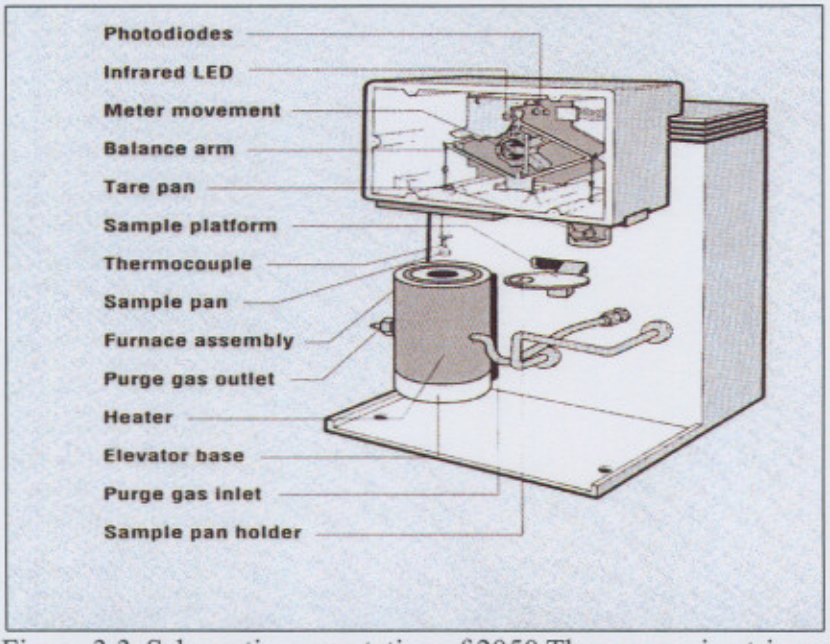

Figure 3.3: Schematic presentation of 2050 Thermogravimetric analyser

The specifications for the TGA's used in this work are given in Table 3.2 and 3.3.

Table 3.2: Specifications of the 951-thermogravimetric analyser

Capacity	500 mg including sample pan (sample mass < 110 mg)
Temperature	Ambient to 1100°C
Suppression	110 mg electronic tare
Suppression accuracy	±0.4% of suppression
Precision of weight	0.4% of full scale
Accuracy of weight	±1% full scale
Time constant	0 – 5 seconds
Pressure	Atmospheric
Purge rate	Up to 1 l/min
Control thermocouple	Platinel II
Sample thermocouple	Chromel-Alumel

Table 3.3: Specifications of the 2050 thermogravimetric analyser

Maximum weighing capacity	1.0 g
Temperature	Ambient to 1000 °C
Sensitivity/Resolution	0.2 µg
Balance accuracy	<±0.1%
Purge gas rate	Furnace 90 ml/min; Balance 10 ml/min
Temperature calibration	1 to 5 points (metal standards)
Heating rate	0.1 to 50 °C/min (0.01 °C/min increments)
Furnace cooling	Forced air
Sample pans	Platinum: 50µL, 100µL
	Alumina: 100µL, 250µL, 500µL
	Aluminum: 100µL
Thermocouple	Platinel II
Operating line voltage	115 volts, 50/60 Hz
Energy consumption	1.5 kVA
Ranges: 100 mg range	10 mg-100 mg
1000 mg range	100 mg-1000 mg
Furnace atmosphere purge gases	He, N_2, O_2, Air, Ar
Furnace atmosphere purge rates	Up to 100 cm^3/min

3.4.2 Experimental procedure

All the data used in the reaction kinetic evaluations of the combustion kinetics were obtained from combustion experiments conducted on coal-derived chars. The most common way to prepare a coal char is to heat a coal sample to a specific temperature in a nitrogen atmosphere until insignificant changes in mass sample are observed (Johnson, 1979; Tsai, 1982). The procedure followed during char preparation and char combustion is described below:

3.4.2.1 Char preparation

In all the experiments conducted, char was prepared in situ in the apparatus used for the relevant combustion. It was therefore not necessary to handle the char in any way after pyrolysis was completed, minimising contamination of the char as well as structural changes due to the breakdown of the char body with time. All cooling of the chars were conducted under flowing nitrogen, and the gas was switched directly to the combustion medium at the onset of the combustion experiments.

The coal samples were converted to char before each experiment. An internal standard procedure to prepare the char was followed in this study. Peek (2000) also made use of the same procedure. It has to be mentioned here that in industrial pulverised coal boilers and fluidised bed combustors much higher heating rates (up to 10^4 K/s) are observed. The following char preparation procedure was followed for isothermal and non-isothermal experiments:

1. The sample temperature is equilibrated at 30 °C in a nitrogen atmosphere.
2. The sample is heated at a constant heating rate of 20°C/min to 700 °C.
3. The sample is held isothermally at 700 °C for 60 minutes.
4. The char sample is then cooled down.

Figure 3.4 shows a plot obtained during the char preparation. It is seen that the volatile matter is approximately 20%, which is in agreement with results presented in Table 2.2.

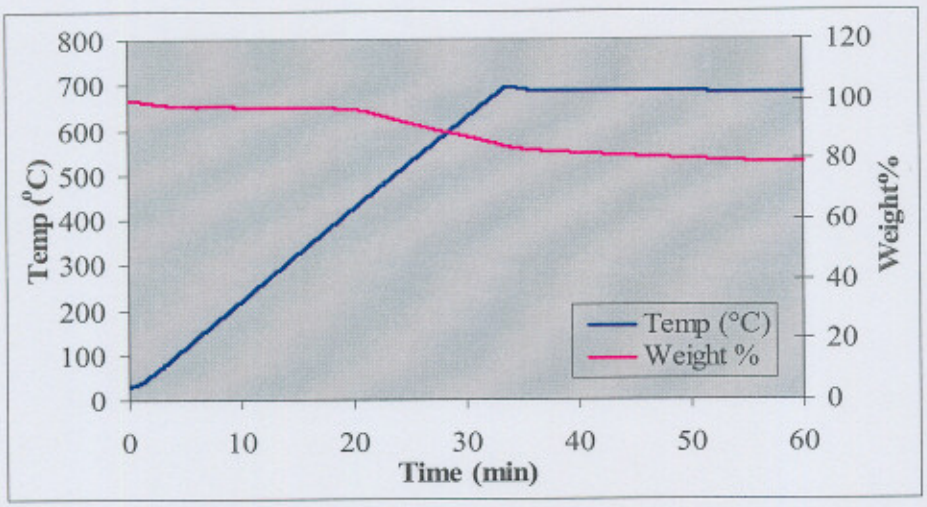

Figure 3.4: Preparation of char from a parent coal

In all experiments conducted, the sample temperature was equilibrated at 30 °C prior to the commencement of any reaction. This was done to create an identical starting point for all experimental procedures.

3.4.2.2 Char combustion

The following method was employed in all non-isothermal combustion experiments:

1. The sample temperature is equilibrated at 30 °C in a nitrogen atmosphere.
2. The sample is heated at constant heating rate of20 °C/min to 250 °C.
3. The sample is then held isothermally for 1 minute.
4. The sample is heated at a constant heating rate of B °C/min to 1000 °C.
5. The sample is then allowed to cool-down after conversion has been completed.

In the case of isothermal experiments, air was only introduced at desired operating conditions and the temperature was kept constant until the reaction attainscompletion.

3.4.2.3 Reagent gases

The following six different gases were used in this study: air, nitrogen (99.99%, oxygen (99.99%), carbon dioxide (99.99%), carbon monoxide (99.99%), hydrogen (99.99%) and distilled water. All gases were supplied by Afrox South Africa. Nitrogen was used for preparing the char. It was also used to keep the char under inert conditions until the reaction temperatures were attained. Oxygen and air were used for combustion experiments. The mixtures were made on-line using the (Brooks 5850) mass flow controllers.

3.4.2.4 Char properties

The properties of the chars are given in Chapter 2.

3.4.3 Experimental results confirming absence of diffusional effects

In this section an experimental confirmation of the absence of any diffusional limitations is presented. The effect of external and intra-particle diffusional limitations is examined. In Section 3.4.3.1 an experimental procedure followed to tests for external diffusional limitations is presented followed by Section 3.4.3.2 that describes the experimental procedure followed to test for the effect of intra-particle diffusional limitations.

3.4.3.1 External diffusion

Most researchers (*e.g.* Barrio and Hastad, 2000, Peek, 2000, Gururajan *et al.,* 1992 and Meijer, 1992) have measured kinetics without verifying the effect of diffusion resistance. Diffusion must be eliminated for proper kinetics. In order to test for the absence of external diffusion limitations the combustion experiments were conducted under identical conditions but only at different flow rates, see Figure 3.5. For all experiments, a flow rate of 80 ml min^{-1} was used.

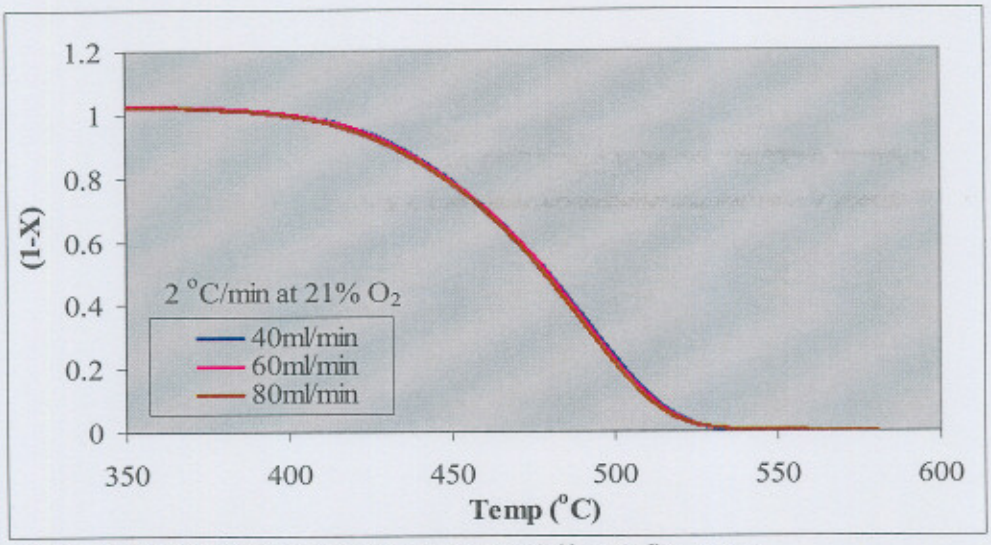

Figure 3.5: Combustion of char A using different flow rates

3.4.3.2 Intra-particle diffusion

The influence of different particle sizes during combustion was tested. Figure 3.6 shows the thermograms obtained from the combustion of different particle sizes. Char with particle sizes of approximately (40 μm – 100 μm) were combusted with air. It is seen that the thermogrammes of different particle sizes gave identical results. This is a strong confirmation that the combustion of 70 μm powder is reaction controlled.

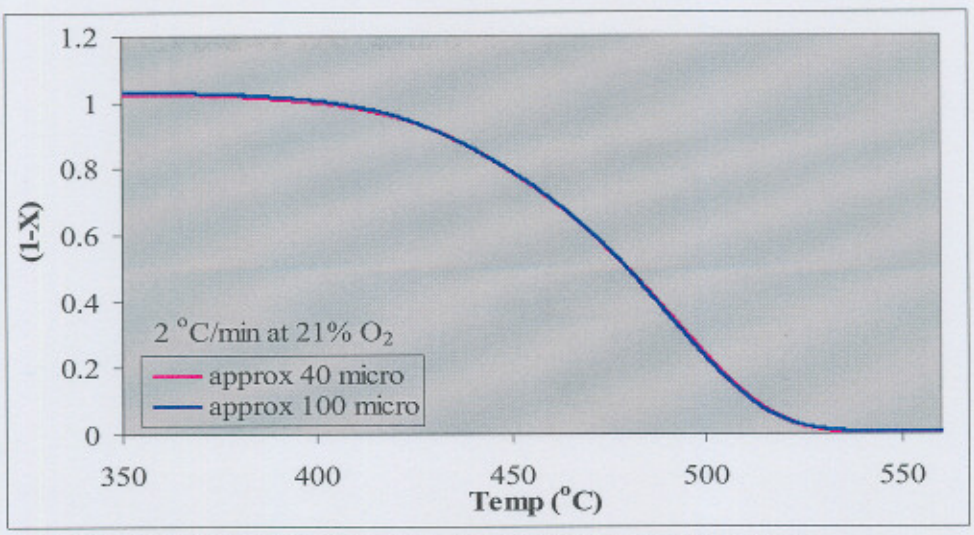

Figure 3.6: Combustion of char A using different particle sizes

3.4.4 Error calculation

The errors of the experimentally determined values in this thesis are calculated statistically. For this, a 90% confidentiality interval has been used. As an example, the average activation energy as determined in Table 3.4 is based on the mathematical average of the 45 reported values (= 133 kJ mol^{-1}). The standard deviation for this set of values is 7.5 kJ mol^{-1}, and the error is calculated as 1.65 times the standard deviation (= 12 kJ mol^{-1}), representing a 90% confidentiality interval.

3.5 RESULTS AND DISCUSSION: ISOTHERMAL OPERATION

3.5.1 Introduction

In this section, the combustion of the chars using air, carried out under isothermal conditions between 370 and 410 °C is presented. Char conversion models (as presented in Section 3.3) have been tested and the relevant reaction kinetic parameters were determined. The isothermal method is traditionally used since the results are easy to interpret (only conversion changes as the combustion proceeds). Therefore, most researchers, studying char combustion, have conducted their experiments isothermally (Guo *et al*, 2003; Olivela and Heras, 2002 and Moors *et al*., 1999). The disadvantage of an isothermal approach is that only one temperature is studied per experiment and that the temperature is restricted to low values, when using thermogravimetric methods. In this study, the particle conversion model will be determined using the isothermal approach, while the full set of reaction kinetic parameters is quantitatively determined using a non-isothermal (temperature programmed) approach (see Section 3.6). These results are used to predict the isothermal data in order to confirm the validity of a new method developed.

3.5.2 Experimental results

In Figure 3.7, a typical experimental result for the isothermal combustion of char A in air at 380 °C is presented.

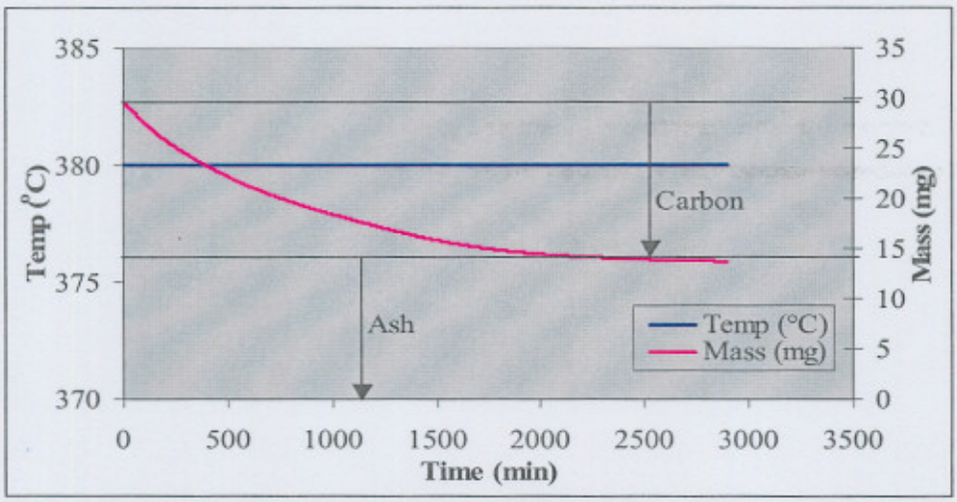

Figure 3.7: Typical isothermal combustion for char A in air

The combustion reaction commences as soon as air is supplied to the char sample (t = 0) and the temperature remains constant at ± 0.05 °C from the set temperature. The ash content is determined from each experiment and was found to be 48 (± 2) % (based on char), which is in very good agreement with the results presented in Section 2.4. If only the carbon is considered, the results can also be presented as given in Figure 3.8 and 3.9, for char A and B respectively, where the conversion of the carbon (X) is given as a function of time. The conversion is calculated by:

$$X = \frac{m_o - m_t}{m_0 - m_{ash}} \qquad [3.57]$$

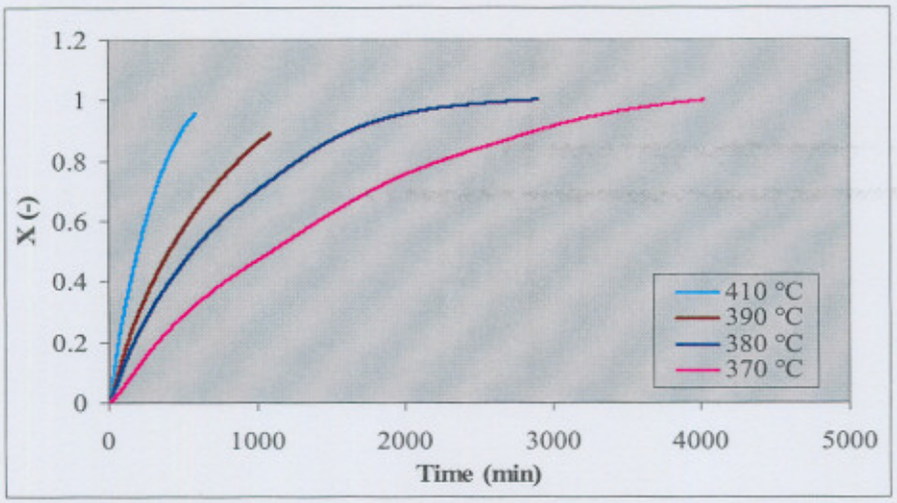

Figure 3.8: Conversion of char A in air for different temperatures

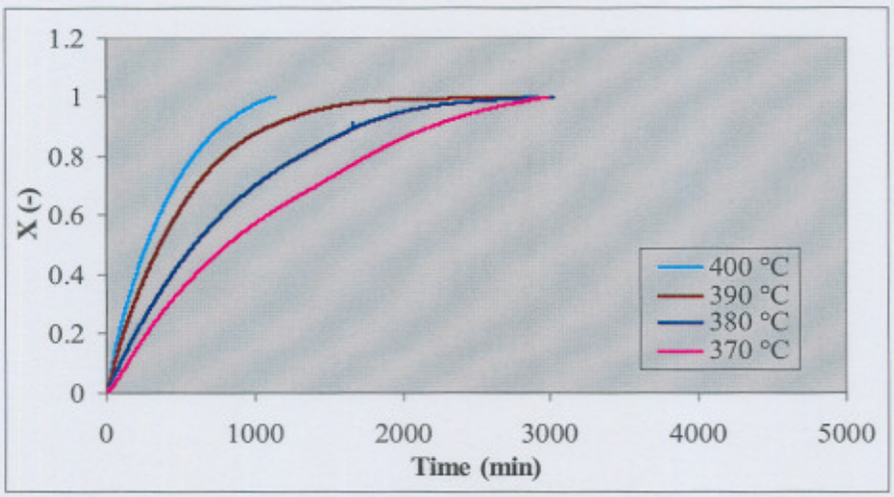

Figure 3.9: Conversion of char B in air for different temperatures

3.5.3 Validation of models: Shrinking Unreacted Core Models

The results as presented in Figure 3.8 and 3.9 are normalised with respect to time and given in Figure 3.10 and 3.11. In these figures, the char conversion is given as a function of the normalised time, $t/t_{0.9}$, which is the reaction time relative to the reaction time where 90% conversion is reached. The modelling of combustion in this investigation was confined to maximum carbon conversions of 90% because of the following reasons: The determination of the time for complete combustion, which is conveniently used for evaluating models, is very difficult to determine experimentally, because of the

asymptotic behaviour of the combustion process and inherent noise associated with measurements. The time required for a finite conversion (such as 90%) is easily obtained and more reliable and can be used for model evaluations as shown in Section 3.3.2. Some workers e.g. Liliedahl and Sjostrom, (1997) used even lower conversions as a reference state. The mechanism of combustion during the end of the combustion process (>98%) with very minute particles is very different to the combustion mechanism at lower conversions and requires very accurate measurements for accurate modeling. This was difficult to measure even with the accurate TGA's available (It was found that *F(X)* versus time (isothermal) deviated from linearity near the end of the combustion period (Equation 4.13)). Industrial processes normally do not operate at complete conversion because of the longer reaction times (larger reactor volume) required.

The results from the shrinking core model with the three different rate controlling mechanisms explained and derived in detail in Section 3.3.2 were compared with experimental results and the comparisons are shown in Figures 3.10 and 3.11. From these figures, it can be seen that the shrinking core model with a controlling surface reaction describes the conversion for both char A (Figure 3.10) and B (Figure 3.11) very well. This result when compared with the models postulated with those of Walker *et al.* (1959) indicates that as a result of the extremely low porosity of the chars, the high ash chars examined have a different behaviour at the temperature quoted by Walker *et al.* (1959). The high ash chars are not porous enough to ensure a reaction controlled homogeneous model at the low temperatures, instead a non-porous model with a controlling surface reaction is valid.

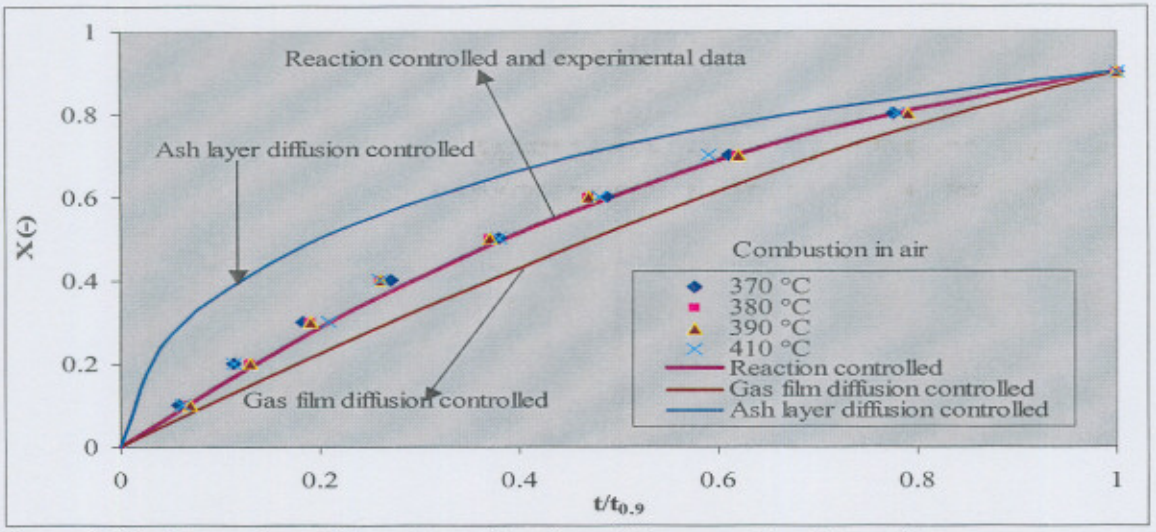

Figure 3.10: Conversion of char A as a function of the normalised time, $t/t_{0.9}$

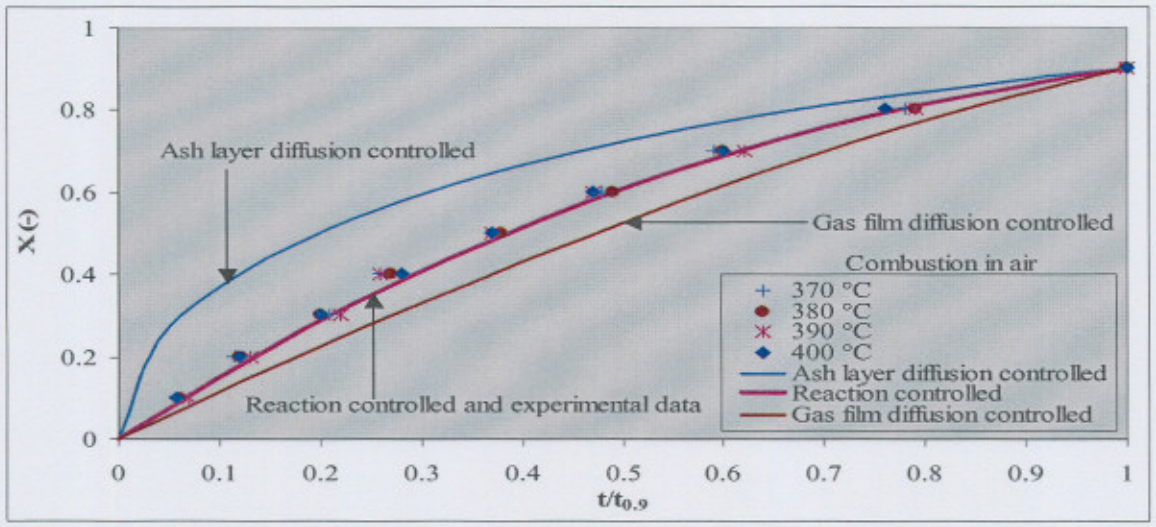

Figure 3.11: Conversion of char B as a function of the normalised time, $t/t_{0.9}$

3.5.4 Validation of models: Shrinking Reacted Core/Homogeneous Model

The shrinking reacted core model, explained in detail in Section 3.3.3 was also tested for the combustion of the chars in order to establish conclusively that the core behaviour is such that diffusion in the core is negligible under the conditions adopted in this investigation. In contrast with the shrinking unreacted model, the shrinking reacted core model has an additional parameter, the Thiele modulus, describing the combined effect of

diffusion and reaction in a porous particle. The best fits for both chars are given in Figure 3.12 (char A) and 3.13 (char B) and shows that agreement were obtained at high Thiele moduli (in the figures the SRCM is plotted using a Thiele modulus of 100). This model which uses a volume- based reaction rate becomes a diffusion controlled process for large values of the Thiele modulus and in the limit as the Thiele modulus becomes very large this model approximates a surface-based impervious core model with surface reaction control (Ishida and Wen, 1968). This being the traditional shrinking unreacted core model with surface reaction control and agrees with the result obtained above.

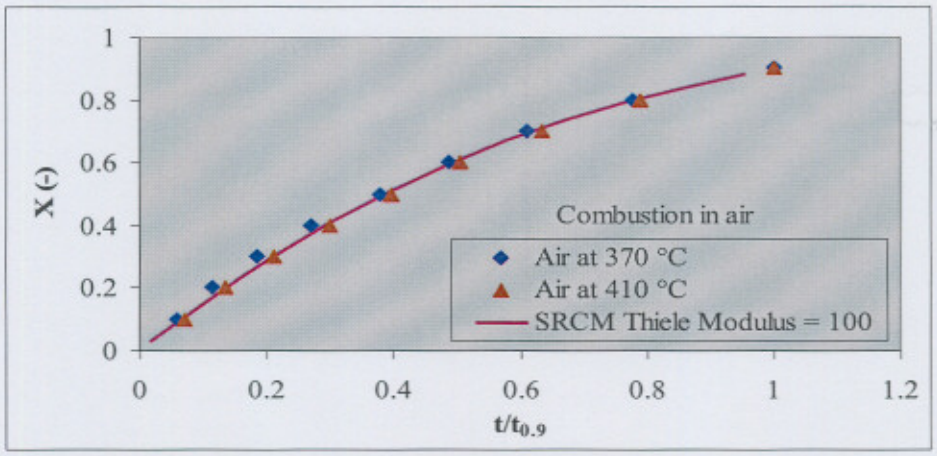

Figure 3.12: Shrinking reacted core model for char A in air

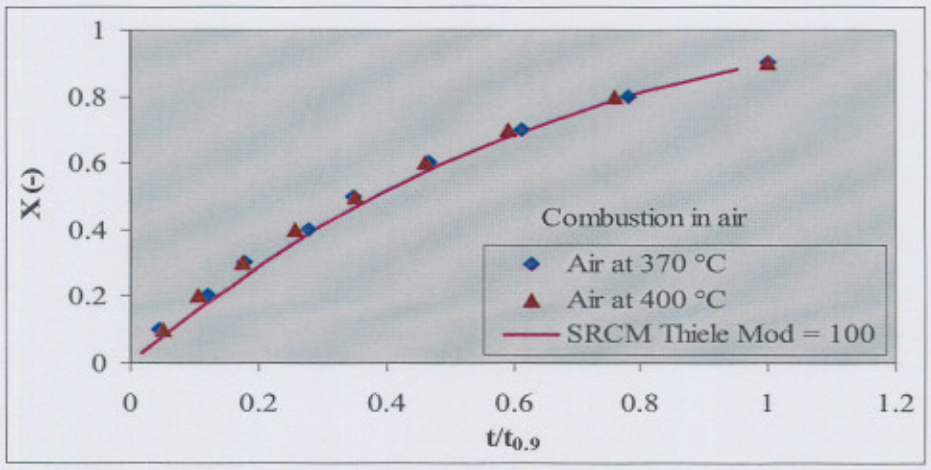

Figure 3.13: Shrinking reacted core model for char B in air

A comparison of the shrinking reacted core model for very low Thiele moduli (very porous) are also shown (Case 1, see Section 3.3.4) in Figure 3.14 and 3.15 in order to

demonstrate the magnitude of the deviation of this so-called homogeneous model (Section 3.3.4) relative to the experimental results obtained. The effect of the dependence of the reaction rate on the carbon concentration is also shown (Case 2), and it can be seen that there is also no agreement.

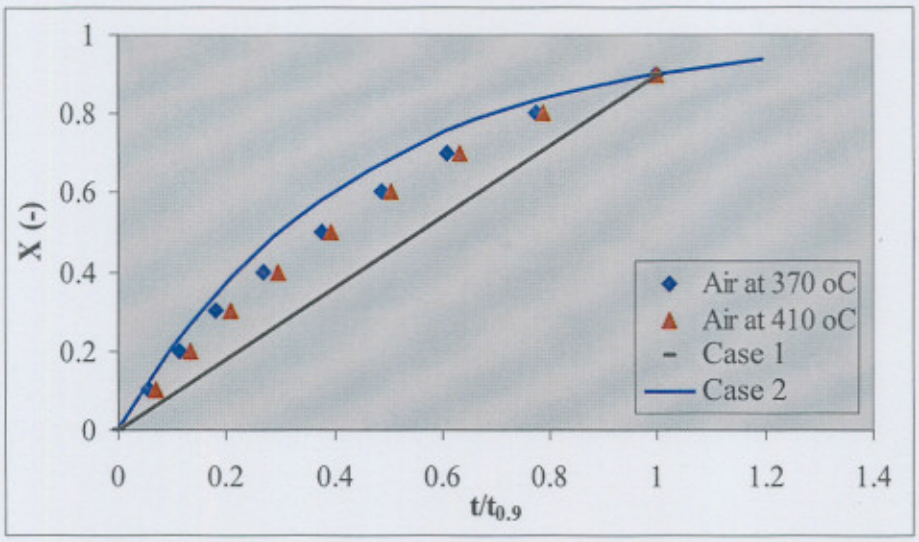

Figure 3.14: Description of the homogeneous model for char A

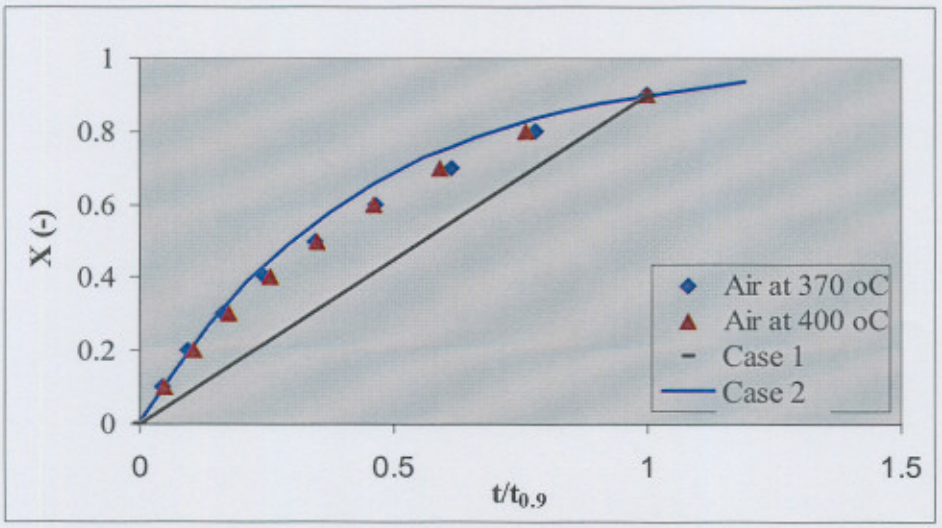

Figure 3.15: Description of the homogeneous model for char B

3.6 RESULTS AND DISCUSSION: NON-ISOTHERMAL OPERATION

3.6.1 Introduction

In this section, the char combustion results, obtained under non-isothermal conditions, are presented. The advantage of a non-isothermal method is that the change in conversion is evaluated at different temperatures within a single experiment, and the relevant kinetic parameters can therefore be determined using fewer experiments, compared to the isothermal approach. Experimentally, the non-isothermal experiments are less sensitive to thermal runaways so that a wider temperature range can be studied. In this section, the reaction kinetic parameters, for the combustion of the two chars, was determined using two different methods. The first method used is the method as presented by Flynn and Wall (1966), while the second method makes use of a two-step regression (Everson *et al.*, 2003) to quantify the kinetic parameters. The combustion was studied for 5 different oxygen fractions (0.21, 0.4, 0.6, 0.7 and 1) with the reaction temperature varying between 370 and 560 °C. For this purpose, heating rates between 1 and 4 °C/min were used.

3.6.2 Experimental results

Typical data obtained from the TGA during non-isothermal combustion is presented in the form shown in Figure 3.16.

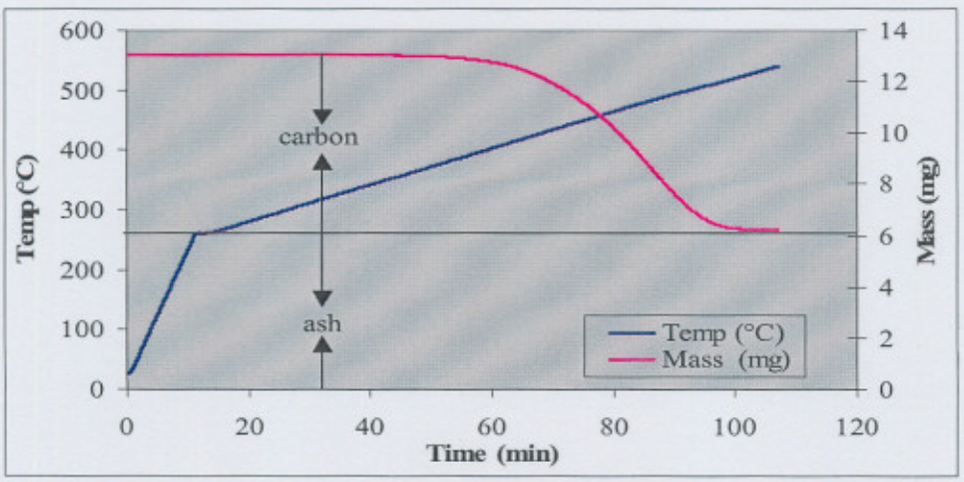

Figure3.16: Non-isothermal combustion of char A in oxygen

In Figure 3.16, the mass of the char sample and the temperature are given as a function of time. From the figure, the ash content can be calculated and was found to be 47 (±2) % by mass, which is in good agreement with the figures as presented in Table 2.2. From Figure 3.16, it can also be seen that the sample temperature is increasing linearly with time (constant heating rate).

The data from Figure 3.16 can be processed further and is plotted in a form of a thermogram as presented in Figure 3.17 and 3.18 for char A and B respectively. In these figures, the normalised amount of carbon (1-X) is given as a function of the reaction temperature for different heating rates. From these figures, it can be seen that the experiments with the lowest heating rates have the highest conversion at a specific temperature.

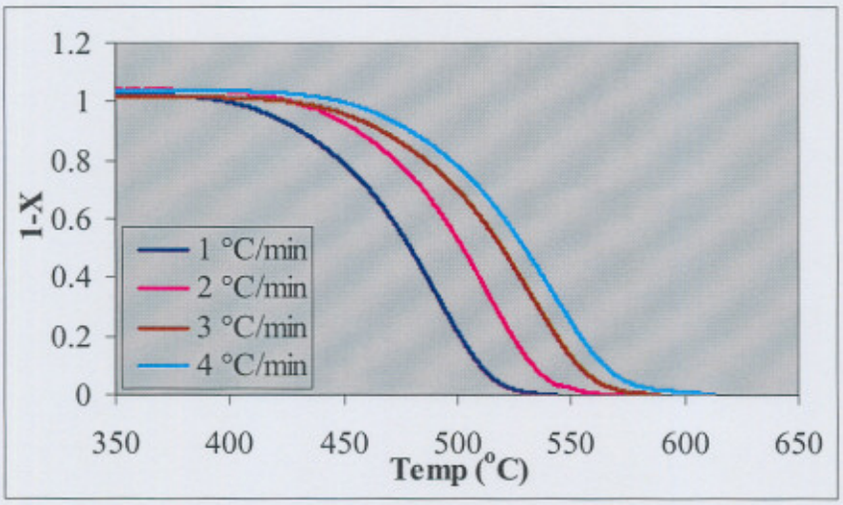

Figure 3.17: Non-isothermal combustion of char A in air

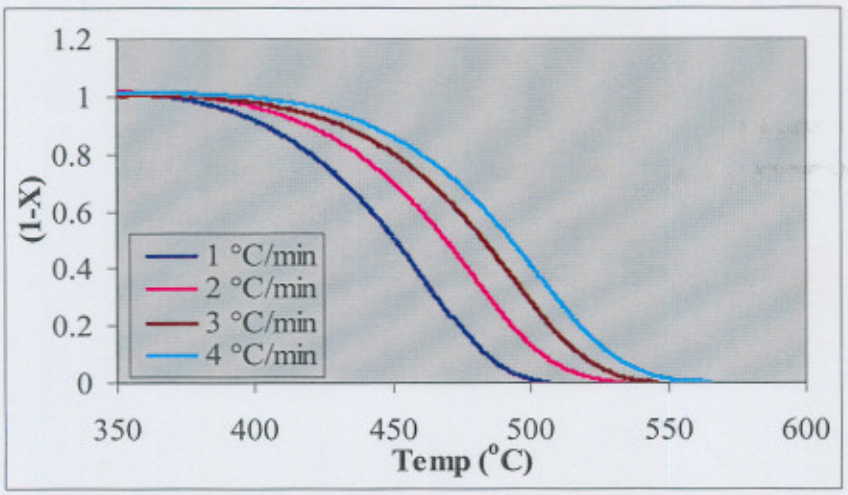

Figure 3.18: Non-isothermal combustion of char B in air

The same procedure was followed for other gas compositions and the results areshown in Appendix A.

3.6.3 Methods used for evaluation

The interpretation of the experimental results obtained under non-isothermal conditions is more complex than under isothermal condition, since the temperature is also changing while the conversion increases. Two methods have been used to evaluate the data:

- A method from literature, as developed by Flynn and Wall (1966)
- A newly designed two-step regression method (Everson *et al.*, 2003)

The conventional and the new method are discussed in Section 3.6.3.1 and3.6.3.2 respectively.

3.6.3.1 The method of Flynn and Wall

In the literature, two methods for the kinetic evaluation of non-isothermal reaction data are used. These two methods are the Flynn and Wall (1966) method, and the direct evaluation method (Russell *et al.*, 1998). In the Flynn and Wall method, the activation energy of the combustion reaction is obtained from non-isothermal experiments carried out at different heating rates. The direct evaluation method uses a single thermogramme to determine the different kinetic parameters. Since a large set of experiments have been carried out, the method of Flynn and Wall has been used in this study, and is explained in detail in this section.

The overall reaction rate of the char is assumed to be (with *f(X)* being any unspecified particle reaction model):

$$\frac{dX}{dt} = k_0 e^{\frac{-E}{RT}} P_{O_2}^n f(X) = \frac{3M_s}{\rho_s R_p} k_{so}' e^{\frac{-E}{RT}} P_{O_2} (1-X)^{\frac{2}{3}} \qquad [3.58]$$

If a constant heating rate (B) is applied, the temperature change is given as:

$$\frac{dT}{dt} = B \qquad [3.59]$$

Substituting Equation 3.59 into 3.58 results in:

$$\frac{dX}{dT} = \frac{1}{B} k_0 e^{\frac{-E}{RT}} P_{O_2}^n f(X) \qquad [3.60]$$

Integrating and rearranging results in:

$$F(X) = \frac{1}{B} k_0 {P_{O_2}}^n \int_{T_0}^{T} e^{\frac{E}{RT}} dT \qquad [3.61]$$

where:

$$F(X) = \int_0^X \frac{1}{f(X)} dX \qquad [3.62]$$

Equation 3.61 can be written as (Flynn and Wall, 1966)

$$F(X) = (\frac{ZE}{RB}) p(y) \qquad [3.63]$$

with:

$$Z = k_0 P_{O_2}{}^n \qquad [3.64]$$

also:

$$p(y) = \frac{\exp(-y)}{y} + \int_{y_0}^{y} (\frac{\exp(-y)}{y}) dy \qquad [3.65]$$

and:

$$y = \frac{E}{RT} \qquad [3.66]$$

The parameter *p(y)* can be approximated by the equation (Doyle, 1962):

$$\log[p(y)] = -2.315 - 0.457 \frac{E}{RT} \qquad [3.67]$$

This equation can be substituted to Equation 3.63 to obtain:

$$\log[F(X)] = \log[\frac{k_0 E}{R}] - \log B - 2.315 - 0.457 \frac{E}{RT} + n \log P_{O_2} \qquad [3.68]$$

Differentiation of the expression at a constant level of conversion will therefore lead to the following:

$$E = \frac{-R}{0.457} \frac{d \log B}{d(\frac{1}{T})} \qquad [3.69]$$

Thus, if a plot of the logarithm of the heating rate versus the inverse temperature for a specific conversion is constructed, the value of the activation energy can be obtained from the slope of the linear fit through the data. It has to be mentioned here, that the determination of the activation energy with this method is independent of the particle reaction model and that the activation energy is determined at different levels of conversion for different heating rates. Thus in order to obtain an accurate result many heating rates would be required. This is considered as a limitation of this method. Once the activation energy is known, the particle reaction model can be found using Equation 3.63. The plot of $F(X)$ versus $p(y)$ should have a linear relationship and can hence be used to find the appropriate particle reaction model. Successively, if $F(X)$ is known, the value of Z can be calculated from the slope of the plot between $F(X)$ and $p(y)$. The reaction order with respect to oxygen (n) and the pre-exponential factor (k_0) can now be determined from a plot of the logarithm of Z versus the logarithm of the oxygen partial pressure as can be derived from Equation 3.64.

3.6.3.2 Regression method

A newly developed method by (Everson *et al.*, 2003) is presented in this investigation, which uses the equations developed by Flynn and Wall (1966) together with a linear regression to evaluate the reaction rate model and the corresponding kinetic parameters. The term $p(y)$ is not approximated in a linear form (Doyle approximation) but is calculated numerically for each case in this method. In order to determine the activation energy a regression calculation is carried out using the logarithmic form of Equation 3.63:

$$\log(p(y)) = \log(B) - \log(\frac{ZE}{R}) + \log(F(X)) \qquad (3.70)$$

For a constant oxygen partial pressure and for any unspecified combustion model, a plot of the logarithm of the heating rate (B) against the logarithm of the parameter $p(y)$ for a certain activation energy (E) should have a slope of unity for all levels of carbon conversion. Consequently a regression procedure using different heating rates and oxygen partial pressures with results over a range of carbon conversions can be used with the activation energy as the unknown parameter. Thus, in contrast to the method developed by Flynn and Wall (1966), the activation energy is assumed to be independent of the degree of conversion of the carbon.

The evaluation of the reaction rate model and the corresponding reaction rate parameters can be obtained from a second regression calculation using Equation 3.63. With the activation energy determined from, (first regression) and with an assumed particle reaction model, the unknown parameter Z can be obtained by a regression procedure such that Equation 3.63 is satisfied. Experimental results at different heating rates, involving all carbon conversion levels and partial pressures of oxygen are used for this calculation. With the regressed values of the parameter Z at different partial pressures of oxygen, a plot of the logarithmic form of Equation 3.64 can be used to determine the parameters n and k_0 from the slope and intercept respectively.

3.6.4 Determination of kinetic parameters

In this section, the kinetic parameters are determined based on the reaction controlled shrinking unreacted core model. This model has been used to describe the char conversion mechanism, since it predicted the isothermal combustion experiments adequately (see Section 3.5.3). The kinetic parameters have been calculated both from the Flynn and Wall (Section 3.6.4.1) and the regression method (Section 3.6.4.2).

3.6.4.1 Method proposed by Flynn and Wall

Activation energy

A plot of the logarithm of the heating rate versus the reciprocal temperature at which a specific conversion is reached is presented in Figure 3.19 and 3.20 for char A and B respectively. Evaluations were carried out for carbon conversions ranging from 10 to 90% conversion with intervals of 10%.

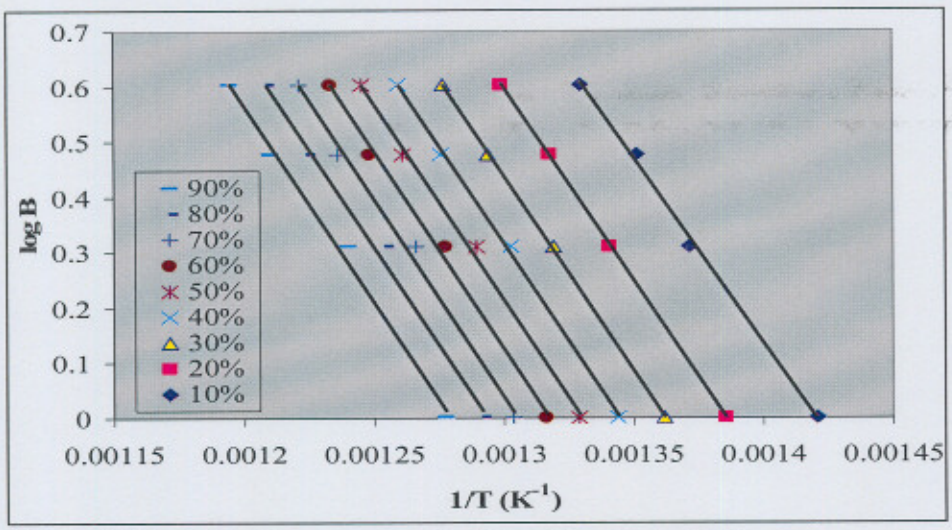

Figure 3.19: Activation energy calculation for char A in air

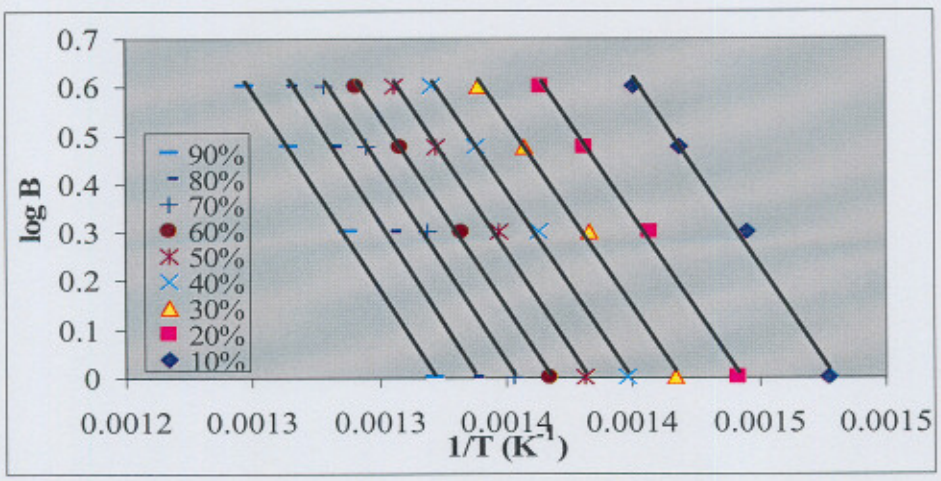

Figure 3.20: Activation energy calculation for char B in air

This process was carried out for different oxygen concentrations and the results are given in Appendix B. As given in Equation 3.69, the activation energy can now be determined from the slope of the various lines that are given in Figure 3.19 and 3.20 for char A and B respectively. In Table 3.4 and 3.5, the values for the activation energy as a function of conversion and oxygen fraction are presented. The activation energies of the char samples were based on the averaged values obtained from Table 3.4 and 3.5.

Table 3.4: Activation energies (kJ mol^{-1}) for char A as a function of conversion and oxygen fraction

Oxygen fraction (-) / Conversion	0.21	0.4	0.6	0.7	1
10%	123	120	127	125	126
20%	129	122	131	128	135
30%	131	125	132	125	137
40%	129	125	135	127	141
50%	131	127	136	131	141
60%	132	128	138	133	148
70%	130	129	139	135	142
80%	130	129	140	137	147
90%	130	130	141	140	158

Average E = 133 (±12) kJ mol^{-1}

Table 3.5: Activation energies (kJ mol^{-1}) for char B as a function of conversion and oxygen fraction

Oxygen fraction (-) / Conversion	0.21	0.4	0.6	0.7	1
10%	143	145	133	106	132
20%	142	147	135	126	135
30%	143	152	133	135	137
40%	144	154	135	137	139
50%	146	155	137	142	139
60%	145	159	139	145	141
70%	146	161	140	148	144
80%	149	165	140	151	144
90%	146	170	141	151	148

Average E = 143 (±15) kJ mol^{-1}

The obtained activation energies were compared to some literature reported values as shown in Table 3.6.

Table 3.6: Literature values for activation energy

Author	Char origin	Activation energy ($kJ\ mol^{-1}$)
Gopalakrishnan and Barthomew, (1996)	coal	109-134
Sorensen *et al.* (1994)	coal	130-133
Hecker *et al.* (1992)	coal	133
Floess *et al.* (1991)	coal	130
Park (1990)	Bituminous coal	80-125
Lizzio *et al.* (1988)	coal	126
Peek (1999)	coal	168
Suuberg *et al.* (1988)	Anthracite coal	131
Trangmar (1989)	coal	130-175
Khan (1987)	coal	130
Tsai and Scaroni (1987)	coal	125
Wells and Smoot (1987)	coal	134
Tseng and Edgar (1985)	Anthracite coal	137
Field (1969)	coal	126

In Table 3.6 it is shown that the activation energies reported for the combustion of coal chars ranges from 80 to 175 kJ mol^{-1}. The determined values for the high-ash coal chars are well in the region of the literature values, and the experimental error is about 10%.

Evaluation of the model

In this section, the parameters relevant to the reaction controlled shrinking unreacted-core model are determined. In fitting this model, plots of F(X) versus p(y), as defined in Equations 3.61 to 3.66, were constructed and a typical graphs are shown in Figure 3.21 and 3.22 for char A and B respectively. Other results are given in Appendix C for both chars.

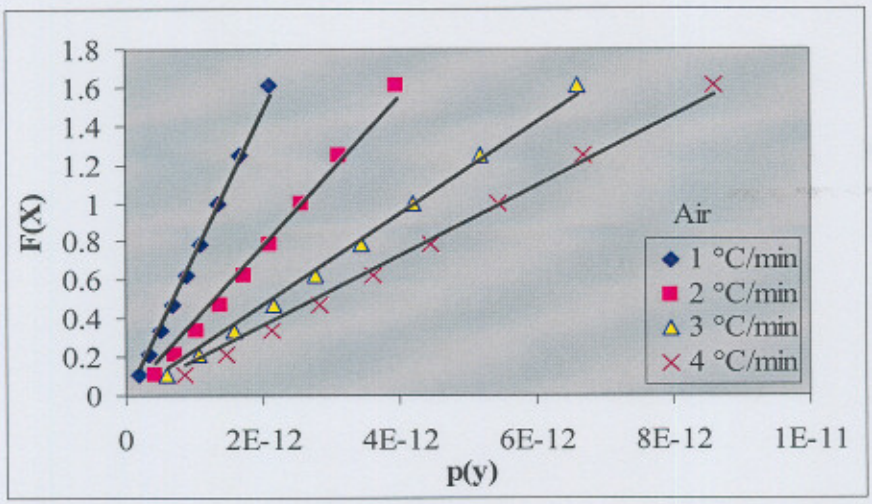

Figure 3.21: Reaction controlled SUCM for char A combustion in air

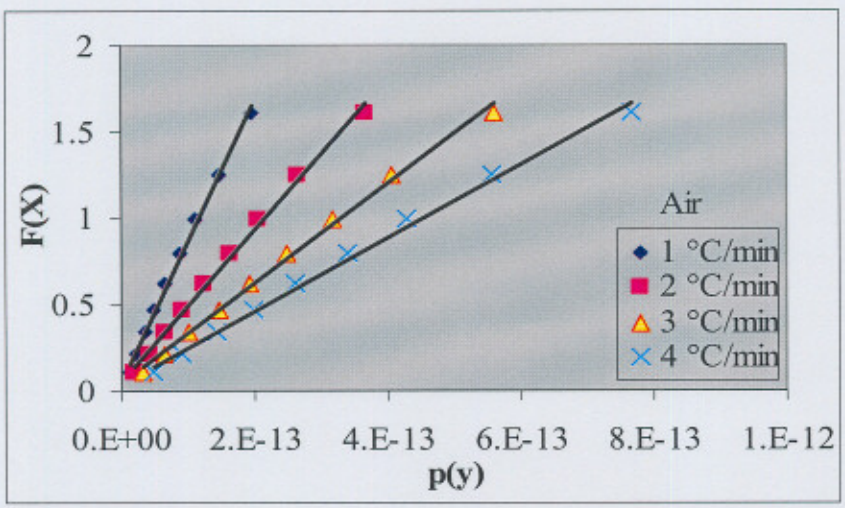

Figure 3.22: Reaction controlled SUCM for char B combustion in air

It is seen that the reaction controlled shrinking unreacted-core model gives good fits for non-isothermal char combustion, which confirms the experimental results from the isothermal study (see Section 3.5.3). In Table 3.7 and 3.8, the values of the slopes of all the plots similar to Figure 3.21 and 3.22 for different oxygen fraction and char type are given.

Table 3.7: Slopes (dimensionless) derived for the calculation of pre-exponential factor for char A

Oxygen fraction Heating rate (°C min^{-1})	0.21	0.4	0.6	0.7	1
1	$7.68 \cdot 10^{11}$	$1.58 \cdot 10^{12}$	$2.84 \cdot 10^{12}$	$3.44 \cdot 10^{12}$	$3.73 \cdot 10^{12}$
2	$4.22 \cdot 10^{11}$	$8.05 \cdot 10^{11}$	$1.44 \cdot 10^{12}$	$1.86 \cdot 10^{12}$	$2.30 \cdot 10^{12}$
3	$2.49 \cdot 10^{11}$	$5.25 \cdot 10^{11}$	$9.84 \cdot 10^{11}$	$1.30 \cdot 10^{12}$	$1.56 \cdot 10^{12}$
4	$1.94 \cdot 10^{11}$	$4.05 \cdot 10^{11}$	$7.90 \cdot 10^{11}$	$9.87 \cdot 10^{11}$	$1.25 \cdot 10^{12}$

Table 3.8: Slopes (dimensionless) derived for the calculation of pre-exponential factor for char B

Oxygen fraction Heating rate (°C min^{-1})	0.21	0.4	0.6	0.7	1
1	$8.00 \cdot 10^{12}$	$1.3 \cdot 10^{13}$	$2.04 \cdot 10^{13}$	$2.02 \cdot 10^{13}$	$2.95 \cdot 10^{13}$
2	$4.34 \cdot 10^{12}$	$7.01 \cdot 10^{12}$	$1.00 \cdot 10^{13}$	$1.23 \cdot 10^{13}$	$1.52 \cdot 10^{13}$
3	$2.86 \cdot 10^{12}$	$5.33 \cdot 10^{12}$	$6.56 \cdot 10^{12}$	$7.63 \cdot 10^{12}$	$1.14 \cdot 10^{13}$
4	$2.09 \cdot 10^{12}$	$4.11 \cdot 10^{12}$	$5.16 \cdot 10^{12}$	$5.81 \cdot 10^{12}$	$7.55 \cdot 10^{12}$

Since the activation energy is known, the values of Z can be calculated from the slopes, given in Table 3.7 and 3.8. These values are reported for a specific oxygen concentration and heating rate, Table 3.9 and 3.10 for char A and B respectively.

Table 3.9: Calculated values of Z (s^{-1}) for char A

Oxygen fraction Heating rate (°C min^{-1})	0.21	0.4	0.6	0.7	1
1	$7.98 \cdot 10^5$	$1.65 \cdot 10^6$	$2.96 \cdot 10^6$	$3.58 \cdot 10^6$	$3.88 \cdot 10^6$
2	$8.78 \cdot 10^5$	$1.67 \cdot 10^6$	$2.99 \cdot 10^6$	$3.87 \cdot 10^6$	$4.78 \cdot 10^6$
3	$7.76 \cdot 10^5$	$1.64 \cdot 10^6$	$3.07 \cdot 10^6$	$4.05 \cdot 10^6$	$4.85 \cdot 10^6$
4	$8.05 \cdot 10^5$	$1.68 \cdot 10^6$	$3.29 \cdot 10^6$	$4.11 \cdot 10^6$	$5.19 \cdot 10^6$
Average Z	$8.14 \cdot 10^5$	$1.66 \cdot 10^6$	$3.07 \cdot 10^6$	$3.90 \cdot 10^6$	$4.67 \cdot 10^6$
Error (±)	$8.85 \cdot 10^4$	$3.65 \cdot 10^4$	$2.98 \cdot 10^5$	$4.76 \cdot 10^5$	$1.12 \cdot 10^6$

Table 3.10: Calculated values of Z (s^{-1}) for char B

Oxygen fraction Heating rate (°C min^{-1})	0.21	0.4	0.6	0.7	1
1	$7.85 \cdot 10^6$	$1.29 \cdot 10^7$	$2.01 \cdot 10^7$	$1.98 \cdot 10^7$	$2.89 \cdot 10^7$
2	$8.52 \cdot 10^6$	$1.38 \cdot 10^7$	$1.97 \cdot 10^7$	$2.41 \cdot 10^7$	$2.97 \cdot 10^7$
3	$8.43 \cdot 10^6$	$1.57 \cdot 10^7$	$1.93 \cdot 10^7$	$2.25 \cdot 10^7$	$3.37 \cdot 10^7$
4	$8.22 \cdot 10^6$	$1.62 \cdot 10^7$	$2.02 \cdot 10^7$	$2.28 \cdot 10^7$	$2.96 \cdot 10^7$
Average Z	$8.25 \cdot 10^6$	$1.46 \cdot 10^7$	$1.98 \cdot 10^7$	$2.23 \cdot 10^7$	$3.05 \cdot 10^7$
Error (±)	$2.98 \cdot 10^5$	$1.56 \cdot 10^6$	$4.11 \cdot 10^5$	$1.81 \cdot 10^6$	$2.18 \cdot 10^6$

Evaluation of the partial pressure dependency

The reaction order with respect to oxygen (n) and the pre-exponential factor (k_0) are determined from a plot of the averaged values of $\ln Z$ versus $\ln(Po_2)$ as slope and intercept respectively. This relation is given in Figure 3.23 and the order of oxygen is determined as 1.1 and 0.83 for char A and B respectively. The pre-exponential factor is 14 s^{-1} $Pa^{-1.1}$ for char A and $2.5 \cdot 10^3$ s^{-1} $Pa^{-0.83}$ for char B as given in Table 3.11.

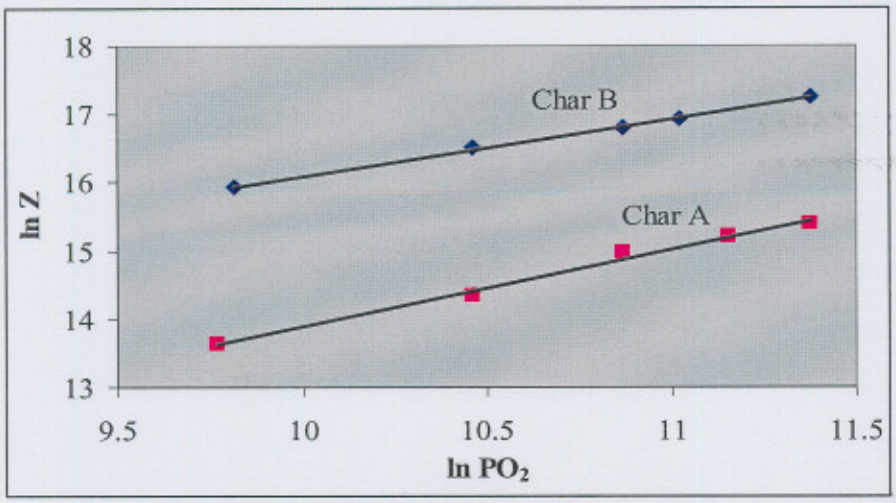

Figure 3.23: Estimation of pre-exponential factor and reaction order for both chars using Flynn and Wall method

A summary of averaged reaction rate parameters obtained for char A and B is given in the Table 3.11.

Table 3.11: Averaged kinetic parameters for the reaction controlled shrinking unreacted core model according to the Flynn and Wall method

Kinetic parameter	Char A	Char B
Activation energy, E	133 (± 12) kJ mol^{-1}	143 (± 15) kJ mol^{-1}
Reaction order in oxygen, n	1.12 (± 0.1)	0.83 (± 0.1)
Pre-exponential factor, k_o (from Eq. 3.58)	14* $s^{-1}Pa^{-1.12}$	$2.5\ 10^{3}$* $s^{-1}Pa^{-0.83}$
Pre-exponential factor, k'_{so} (from Eqs. 3.8 and 3.28)	26* mol $m^{-2}s^{-1}Pa^{-1.12}$	$1.8\ 10^{3}$* mol $m^{-2}s^{-1}Pa^{-0.83}$

**based on the average activation energy reported in row 2 of this table*

It can be seen from Table 3.11 that the reaction order with respect to oxygen is close to 1. The observed activation energy values do not differ significantly thus indicating similarities in both chars studied. The difference in the pre-exponential (k'_{so}, which takes into account the effect of the particle radius) factor could be attributed to the different

structures of the chars as reported in Section 2.8. It has to be said however, that the pre-exponential factor is very sensitive to the value of the activation energy.

Comparison of model results with experimental results

In order to validate the experimental results, the obtained reaction rate parameters from Table 3.11 were substituted into Equation 3.60, and the differential equation was solved numerically. Figure 3.24 and 3.25 show the comparison between the experimental thermogrammes and the predicted thermogrammes, for char A and B respectively.

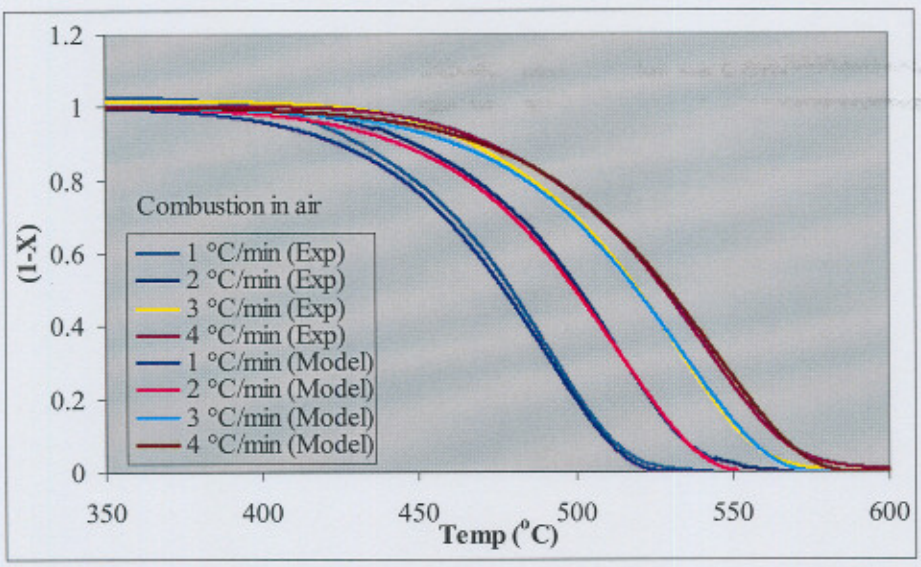

Figure 3.24: Prediction of the burnoff curve for char A in air

It is seen from Figure 3.24 and 3.25 that the model predicts the thermogrammes fairly well, especially between 10 and 90% conversion is a good agreement. At low (<10%) and high (>90%) there are some discrepancies between model and experiments. Although the experimental error for the determined activation energy is relatively large, the average activation energy, obtained with this method, does describe all thermogrammes well (see Appendix D)

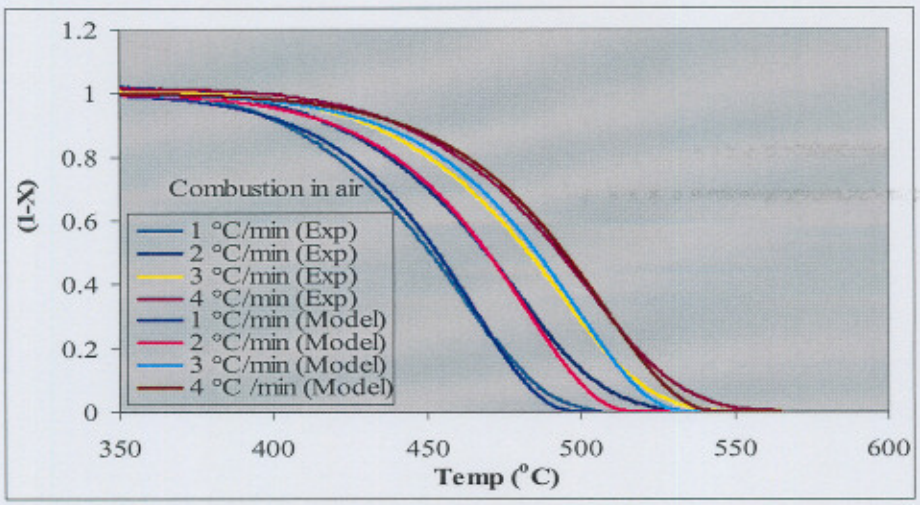

Figure 3.25: Prediction of burnoff curve for char B in air

3.6.4.2 Regression method

Using the regression method, a calculation was carried out using Equation 3.70 by regressing the activation energy to obtain a slope of unity when log B is plotted against log $p(y)$. This calculation involved all carbon conversions for different set of experiments at a certain partial pressure of oxygen (21%, 40%, 60%, 70% and 100%). Figure 3.26 and 3.27 show typical results for an air mixture consisting of 21% (mole) oxygen for nine different carbon conversion levels at a regressed value of 130 (±10) and 139 (±10) kJ/mol for char A and B respectively (the dotted lines represent slopes of unity). In contrast to the method of Flynn and Wall, the determined activation energy is not a function of the conversion. In Figure 3.26 and 3.27, the dotted lines represent the slopes of unity.

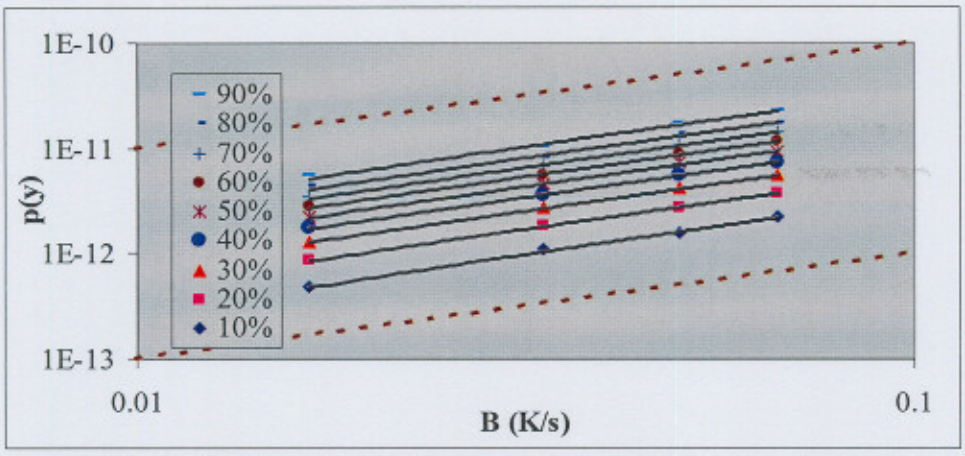

Figure 3.26: Evaluation of activation energy for char A in air using the regression method

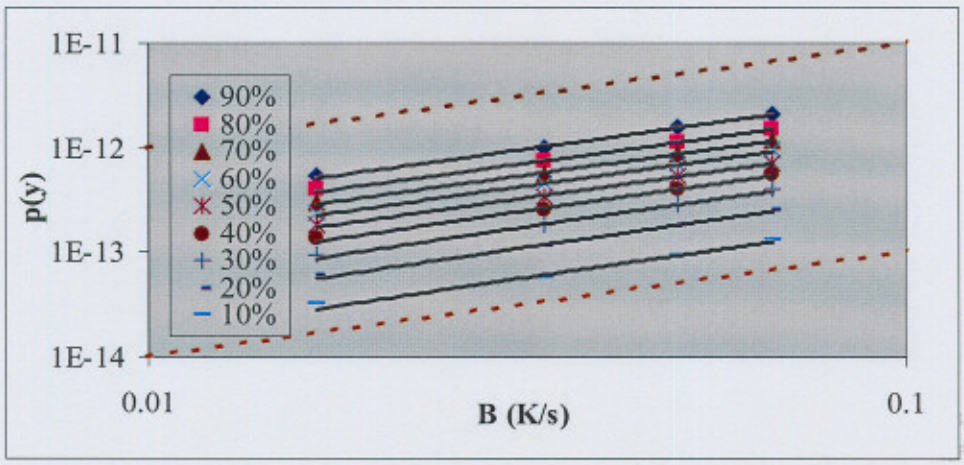

Figure 3.27: Evaluation of activation energy for char B in air using the regression method

Once the activation energy is determined, the parameter Z can be calculated for a specific combustion model ($F(X)$) using Equation 3.63. A second regression was done, involving the unknown variable Z (for each partial pressure of oxygen) and carried out in such a way that Equation 3.63 was satisfied for all carbon conversion levels and heating rates. The reaction controlled shrinking unreacted core model particle models fitted the results accurately, again confirming the isothermal results. The obtained values of Z for different oxygen fractions are presented in Table 3.12.

Table 3.12: Values of Z (s^{-1}) obtained from the regression method

Oxygen fraction	0.21	0.4	0.6	0.7	1
Char A	$3.00\ 10^5$	$6.30\ 10^5$	$1.19\ 10^6$	$1.53\ 10^6$	$1.97\ 10^6$
Char B	$3.26\ 10^6$	$6.01\ 10^6$	$7.79\ 10^6$	$8.86\ 10^6$	$1.24\ 10^7$

The parameters n and k_o are obtained from Equation 3.64 by plotting the natural logarithm of Z against the natural logarithm of the oxygen fraction as shown in Figure 3.28 for both chars.

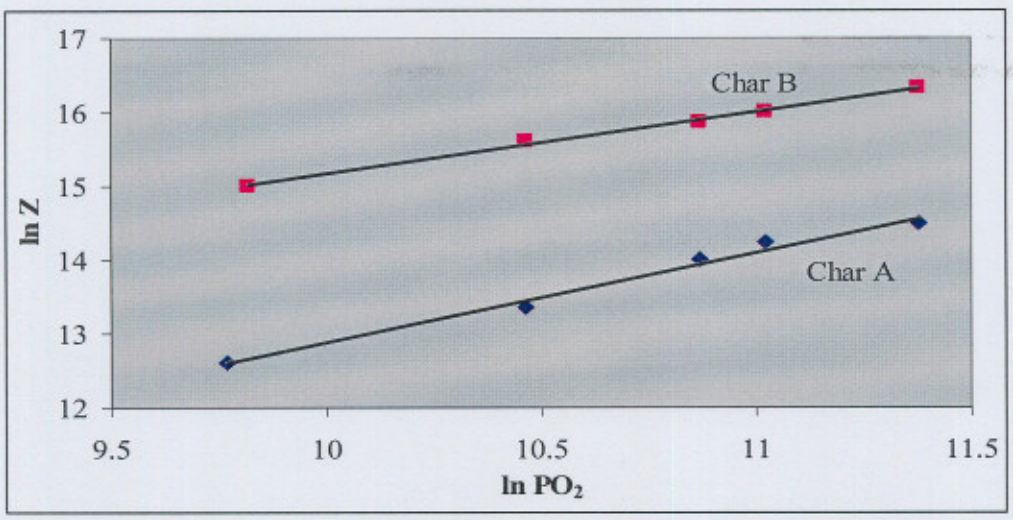

Figure 3.28: Evaluation of reaction order and pre-exponential factors for both chars using the regression method

A summary of results yielded by the regression method is shown below in Table 3.13.

Table 3.13: Summary of results from the regression method

Kinetic parameter	Char A	Char B
Activation energy, E	130 (± 10) kJ mol^{-1}	139 (± 10) kJ mol^{-1}
Reaction order, n	1.23 (± 0.1)	0.84 (± 0.1)
Pre-exponential factor, k_o (from Eq. 3.58)	1.9^{*} $s^{-1}Pa^{-1.23}$	$9.1\ 10^{2*}$ $s^{-1}Pa^{-0.84}$
Pre-exponential factor, k'_{so} (from Eq. 3.28)	3.5^{*} mol $m^{-2}s^{-1}Pa^{-1.23}$	$6.5\ 10^{2*}$ mol m^{-2} s^{-1} $Pa^{-0.84}$

**based on the average activation energy reported in row 2 of this table*

A parity plot of *BF(X)* against *(ZE/R)p(y)* (obtained from Equation 3.63) shows that the model can accurately describe the experimental results, as can be seen from Figure 3.29 and 3.30 for char A and B respectively.

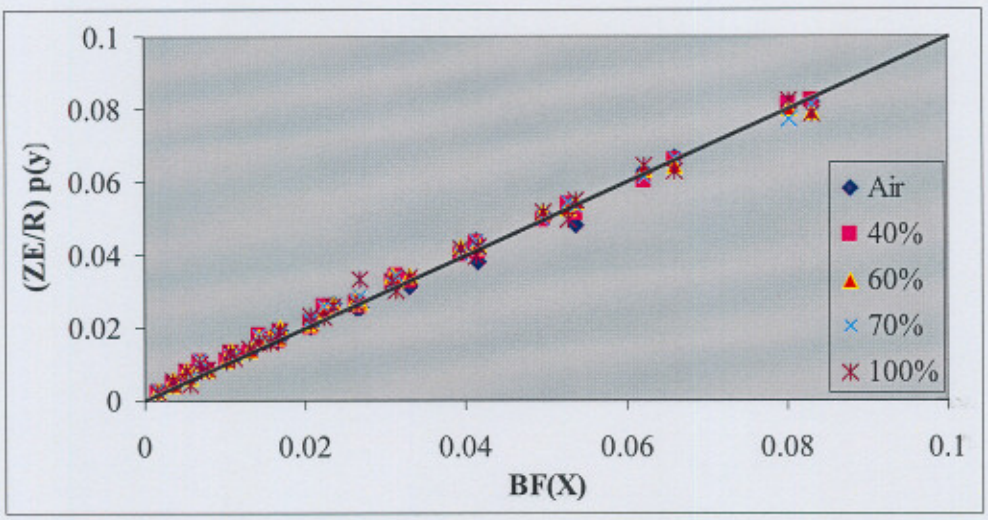

Figure 3.29: Model validation and parameter evaluation for char A using the regression method

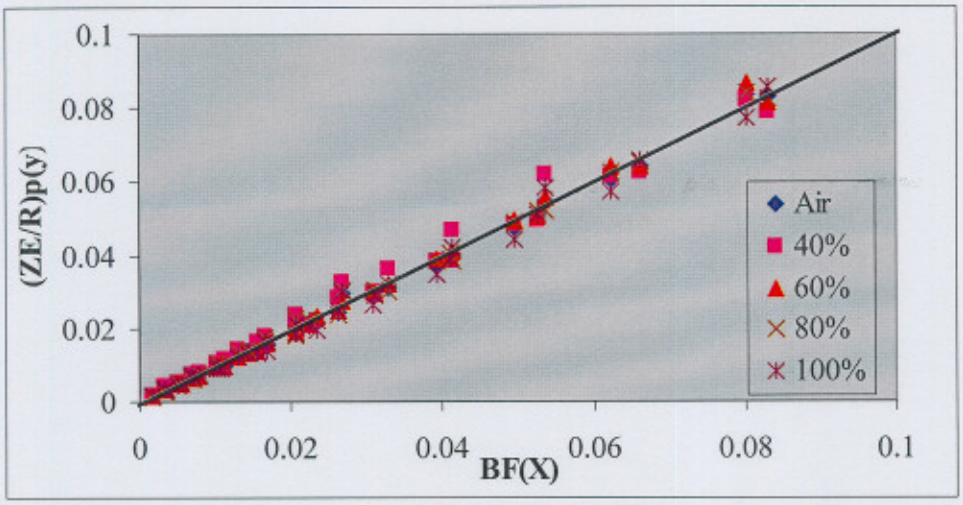

Figure 3.30: Model validation and parameter evaluation for char B using the regression method

In order to further validate the experimental results, the obtained regression kinetic parameters from Table 3.13 were substituted into Equation 3.61, and the differential equation was solved numerically. Figure 3.31 and 3.32 show the comparison between the experimental thermograms and the predicted thermograms, for char A and B respectively.

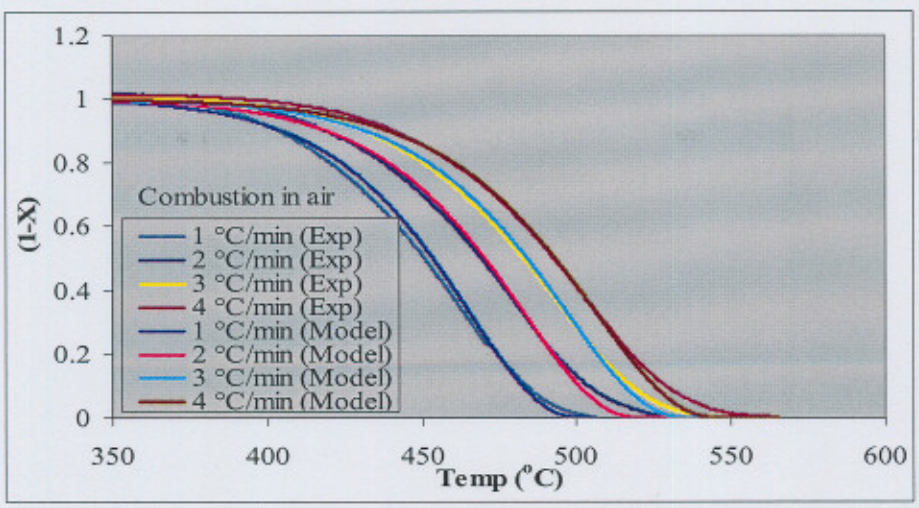

Figure 3.31: Burnoff curves (char A) from regression parameters

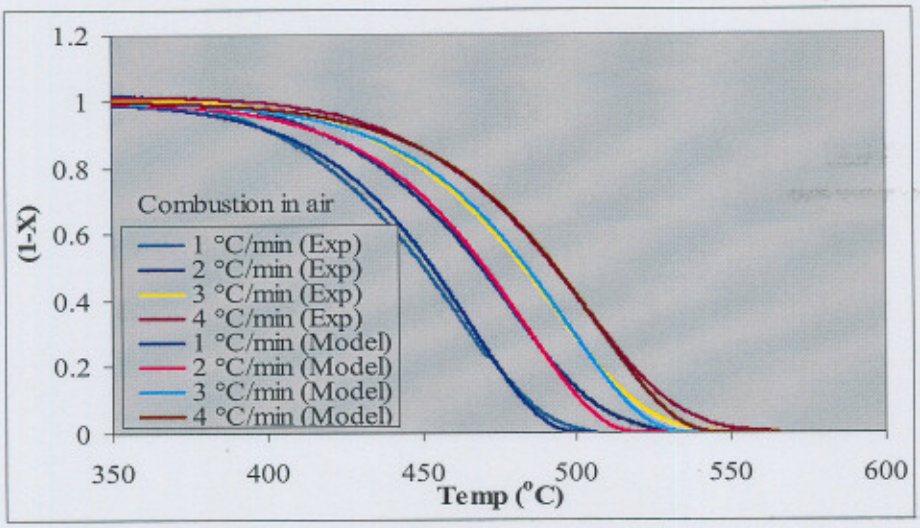

Figure 3.32: Burnoff curves (char B) from regression parameters

It is seen that the regression method also describes the experimental data fairly well. Further results at other oxygen concentrations are shown in Appendix E for char A and B respectively.

3.6.5 Comparison of methods

The purpose of this section is to provide a comparison of results obtained from the non-isothermal combustion of both chars using the Flynn and Wall and the regression method and to show the validity of the regression method by comparing results with isothermal results. Kinetic parameters such as activation, pre-exponential factor and the reaction order have been evaluated from both non-isothermal methods for both chars. A comparison of the results for both chars obtained from the two non-isothermal methods is presented in Table 3.14 and 3.15.

Table 3.14: Comparison for char A

Parameter	Flynn and Wall	Regression
Act. energy (E) (kJ mol^{-1})	133 (± 12)	130 (± 10)
Reaction order (n)	1.1 (± 0.1)	1.2 (± 0.1)
Pre-exp. Factor (k_o)	14 $s^{-1}.Pa^{-1.1}$	1.9 $s^{-1}Pa^{-1.2}$
Pre-exp. Factor (k_{so})	26 mol $m^{-2}s^{-1}Pa^{-1.12}$	3.5 mol $m^{-2}s^{-1}$ $Pa^{-1.23}$
Particle conversion model	Reaction controlled SUCM	Reaction controlled SUCM

Table 3.15: Comparison for char B

Parameter	Flynn and Wall	Regression
Act. energy (E) (kJ mol^{-1})	143 (± 15)	139 (± 10)
Reaction order (n)	0.83 (± 0.1)	0.84 (± 0.1)
Pre-exp. Factor (k_o)	$2.5\cdot10^{3}$ $s^{-1}.Pa^{-0.8}$	$9.1\cdot10^{2}$ $s^{-1}.Pa^{-0.8}$
Pre-exp. Factor ($k_{so}^{'}$)	$1.8\cdot10^{3}$ mol $m^{-2}s^{-1}Pa^{-0.83}$	$6.5\cdot10^{2}$ mol m^{-2} s^{-1} $Pa^{-0.84}$
Particle conversion model	Reaction controlled SUCM	Reaction controlled SUCM

It is seen from Table 3.14 and 3.15 that the reaction rate parameters obtained from both methods do agree well if the activation energy and reaction order of oxygen is considered. The difference in the determined values for the pre-exponential factor can be attributed to the exponential nature of the Arrhenius equation: a small change in activation energy results in a relatively large change in the pre-exponential factor. Both models predict the combustion of high ash chars accurately. The advantage of the regression model is that the activation energy is determined from all experiments, while the Flynn and Wall method only uses the experiments for a single oxygen fraction.
In order to predict the isothermal experimental data, the non-isothermal obtained kinetic parameters from Table 3.14 and 3.15 were substituted into Equation 3.27, and the differential equation was solved numerically. Figure 3.33 and 3.34 show the comparison between the experimental thermograms and the predicted thermograms, for char A and B respectively.

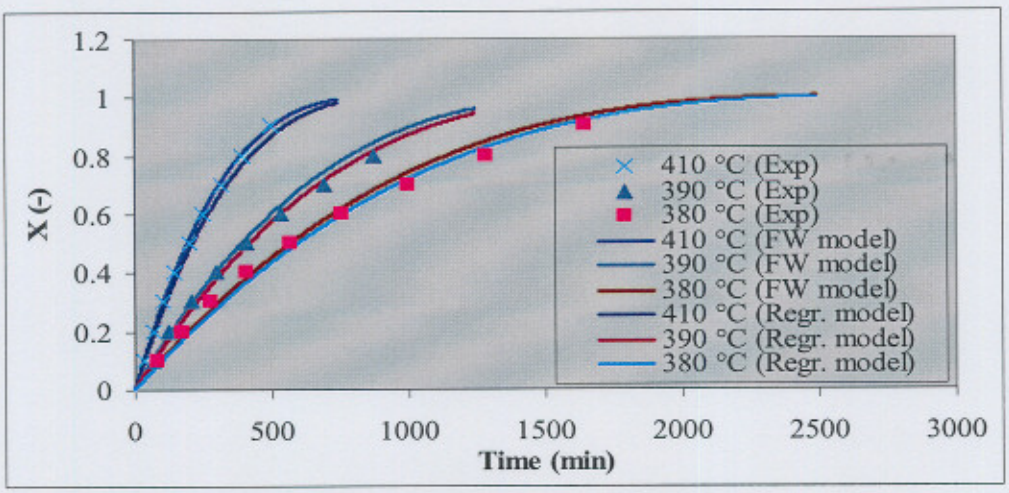

Figure 3.33: Prediction of isothermal burnoff curve (char A)

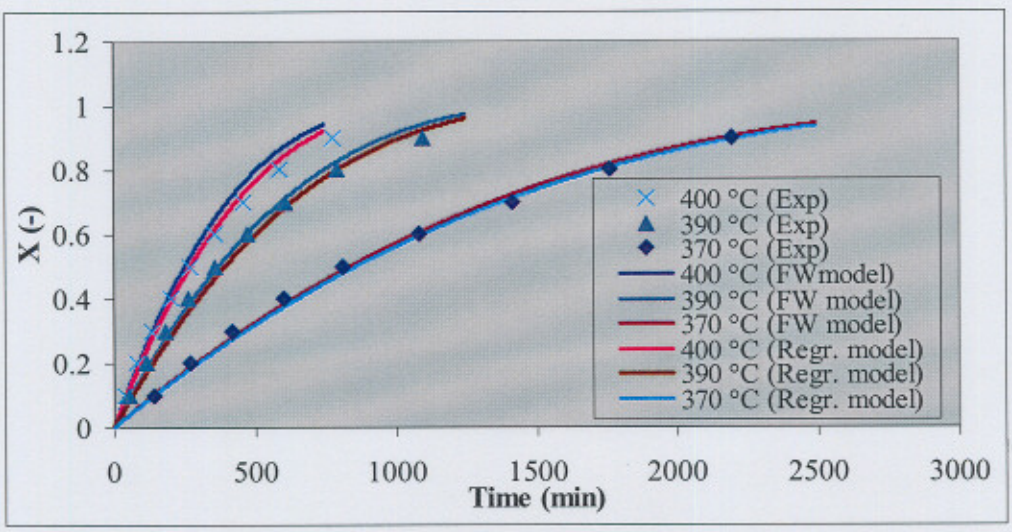

Figure 3.34: Prediction of isothermal burnoff curve (char B)

It is seen from Figure 3.33 and 3.34 that the non-isothermal kinetic parameters predict the isothermal thermograms reasonable well indicating the validity of the regression method.

3.7 CONCLUSIONS

It was possible to perform experiments, suitable for a kinetic study, involving the highly exothermic combustion reaction in a TGA even with high concentrations of oxygen. Experiments under isothermal conditions were confined to between 370 and 410 °C and non-isothermal experiments up to 560 °C. For the non-isothermal operation stability (no temperature runaway) was controlled by adjusting the heating rate and in certain cases with the oxygen concentration.

A systematic procedure was developed for the determination of the most suitable reaction overall rate model using experimental isothermal results. This procedure consisted essentially of a range of models, which included surface and volume reactions. Regarding the surface-based reactions, the well-known shrinking core model (unreacted core) was tested for the three possible rate-controlling mechanisms, namely gas film diffusion, diffusion through the ash layer and chemical reaction on the surface. For the volume based reactions, also based on the shrinking core model concept, a porous core with reaction and diffusion exists and the concept of the Thiele modulus is used to assess the relative significance of the controlling mechanisms. The limits of this model were tested which are (1) an impervious core model, equivalent to a shrinking unreacted model with surface reaction, and characterized by a large Thiele modulus, and (2) a very porous core model with reaction controlling (homogeneous model) characterized by a small Thiele modulus.

From the isothermal experiments, it was found that the shrinking core model with a rate controlling surface reaction was applicable for both chars examined at temperatures between 370 and 410 °C. Under the conditions adopted and with the exceedingly low porosities reported in Section 2.6, it is clear that the penetration of oxygen is negligible and that the combustion rate is determined by the surface intrinsic reaction rate and the available area. The limit of the volume-based model with a large Thiele modulus, which approximates the shrinking unreacted model, was also found to be applicable.

Two non-isothermal methods using linear heating rates were considered, namely a method proposed by Flynn and Wall (1966) and a new method developed for this study (Everson *et al.*, 2003). The main advantage of these methods is that a suitable (wide)

temperature range can be covered with a single experiment. The method of Flynn and Wall however was found to require a large number of experiments involving a large number of heating rates in order to get accurate results. The new method which is based on a two-step regression is capable of testing a reaction rate model requiring fewer and shorter time duration experiments and consists basically of non-linear regression procedures using all the results at different heating rates (temperatures) and carbon conversions. The disadvantage of this method is that it is confined to systems described by relatively simple kinetics and cannot be used to verify most of the models described above which were accomplished with an isothermal method. It is however suitable to test the shrinking unreacted core model with surface reaction.

The validity of the non-isothermal method was verified with the results obtained from the Flynn and Wall method and with isothermal results. It was found that the shrinking unreacted core model with surface reaction was applicable and all the relevant parameters were determined for the chars examined.

A full set of reaction rate parameters were obtained for the shrinking core model. Activation energies compare well with literature. The dependence on oxygen partial pressure (power rate dependence) was found close to unity, which is normally assumed by many researchers. The value of the pre-exponential factor, not readily available in the literature, has also been evaluated and for two different types of coal-chars and was found to be extremely sensitive relative to the value of the activation energy.

The activation energies for the two coal-chars do not differ much, which indicates an insignificant catalytic affect despite the different minerals composition (Section 2.7). Porosities for both chars are very small with the consequence that the shrinking core model with surface reaction is applicable to both. The pre-exponential factor and the dependence on partial pressure of oxygen are different which can possibly be attributed to the surface properties of the chars (Section 2.8).

NOMENCLATURE

a_o, a_1, a_3	constants in Table 3.1.	-
B	heating rate	$^oC\ s^{-1}$
C_A	concentration of oxygen in reacted core	moles m^{-3}
C'_A	concentration of oxygen in an ash layer	moles m^{-3}
C_{AO}	concentration of oxygen in gas phase	moles m^{-3}
C_s	concentration of carbon in reacted core	moles m^{-3}
C_{so}	initial concentration of carbon	moles m^{-3}
D_e	effective diffusuvity of oxygen in reacted core	$m^2\ s^{-1}$
D'_e	effective diffusuvity of oxygen in reacted core	$m^2\ s^{-1}$
E	activation energy	J $mole^{-1}$
$f(X)$	particle conversion model	-
$F(X)$	defined in Equation 3.62	-
k_g	mass transfer coefficient	mol $m^{-2}\ s^{-1} Pa^{-1}$
k_o	Pre-exponential factor	$s^{-1}\ Pa^{-n}$
k_s	reaction rate constant	m Pa^{-1}
k'_s	reaction rate constant	mol $m^{-2} s^{-1}\ Pa^{-n}$
k_s^{sv}	reaction rate constant	m^4 $moles^{-1}\ s^{-1}$
k'_{so}	Pre-exponential factor	mol $m^{-2}\ s^{-1}\ Pa^{-n}$
k_v	reaction rate constant	m^3 $moles^{-1}\ s^{-1}$
k'_v	reaction rate constant	s^{-1}
k'_{vO}	pre-exponential factor	s^{-1}
m_{ash}	mass of ash	mg
m_o	initial mass of char	mg
m_t	mass of char at time, t	mg
M_s	molar mass of carbon	kg mol^{-1}
n	reaction order with respect to oxygen	-

N_s	number of moles reacted	moles
P_A	partial pressure of oxygen in reacted core	Pa
P_{AO}	partial pressure of oxygen in gas phase	Pa
P_{O_2}	partial pressure of oxygen	Pa
$p(y)$	defined in Equation 3.65	-
r	radius of particle (spherical) at any time	m
R	universal gas constant	J mol^{-1} K^{-1}
r_A^s	rate of reaction for oxygen per unit area	moles m^{-2} s^{-1}
r_A^v	rate of reaction for oxygen per unit volume	moles m^{-3} s^{-1}
r_c	radius of shrinking unreacted core	m
r_m	radius of shrinking reacted core	m
r_o	reactivity rate	s^{-1}
R_p	initial particle radius	m
r_s^s	rate of reaction for carbon per unit area	moles.m^{-2} s^{-1}
r_s^v	rate of reaction for carbon per unit volume	moles m^{-3} s^{-1}
t	time	s
$t_{0.9}$	time for 90% conversion	s
t_1	duration of 1st period (SRCM)	s
t_2	duration of 2nd period (SRCM)	s
t_∞	time for complete conversion	s
T	temperature	°C
X	fractional conversion of carbon	-
Z	defined by Equation 3.64	s^{-1}

Greek Letters

α	constant in Table 3.1	-
β	power dependence in Table 3.1, ($\beta = 1$ or 2/3)	-
γ	defined in Equation 3.10 as $\gamma = \frac{r_c}{R_p}$	-
ε_o	constant in Table 3.1	-
ξ	dimensionless radius, at core	-
ξ_c	dimensionless radius, $\xi = \frac{r_c}{R_o}$	-
ξ_m	dimensionless shrinking core radius, $\xi_m = \frac{r_m}{R_o}$	-
$\xi_m^{0.9}$	dimensionless shrinking core radius at X = 0.9	-
ϕ	Thiele modulus, $\phi = R_p \sqrt{\frac{k_v C_{SO}}{D_{eA}}}$	-
$\phi^{0.9}$	Thiele modulus at X = 0.9.	-
ρ_S	density of carbon,	kg m^{-3}
τ	dimensionless time in Table 3.1	-
ψ	constant in Table 3.1	-

Abbreviations

SRCM	shrinking reacted core model
SUCM	shrinking unreacted core model
TGA	thermogravimetric analyser

REFERENCES

BARRIO, M. AND HUSTAD J.E. 2000, CO_2 gasification of birch char and the effect of CO inhibition on the calculation of chemical kinetics. In: Bridgewater AV editor. Proceedings of the conference: Progress in Thermochemical Biomass Conversion, Tyrol, Austria.

BHATIA, S.K. AND PERLMUTTER, D.D. 1980. A random pore model for fluid-solid reactions: Isothermal, kinetic control. *American Institute of Chemical Engineering Journal*, **26**(3): 79-385.

BISCHOFF, K.B. AND FROMENT, G.F. 1963, Chemical reactor analysis and design. *John Wiley and Sons*. 1st edt: 239-256.

COPE, R.F.1995. Effects of minerals on the oxidation rates of Beulah Zap lignite char, PhD dissertation, Brigham Young University.

CHORNET, E., BALDASANO, J.M. AND TARKI, H.T. 1979. Kinetic expressions for coal char-gas reactions. *Fuel*, **58**(5): 395-396.

DOYLE, C. D. 1962. Kinetic analysis of thermogravimetric data. *Journal of Applied Polymer Science*, **6**(15): 285-292.

ESSENHIGH, R. H. 1982. Fundamentals of coal combustion in Chemistry of Coal Utilization: Second Supplementary Volume. Elliot, M. A., *Ed. Wiley and Sons, Inc., New York*. Pp.1153-1313.

ESSENHIGH, R.H.1981, Fundamentals of coal combustion, Chemistry of coal utilization, 2nd suppl. Vol., M.A. Elliott (Ed), *Wiley-Interscience, New York.*

EVANS, D. G. AND HERMANN, J.A. 1970. The porosity of brown coal char. *Fuel*, **49**(2): 110-118.

EVERSON, R.C., NEOMAGUS, H.W.J.P. AND NJAPHA, D. 2003. Kinetics of combustion of coal-chars using a non-isothermal thermogravimetric method: A regression procedure for evaluation of rate equations and parameters. *Submitted to Fuel.*

FLYNN, J. H. AND WALL, L. A. 1966. A quick direct method for the determination of activation energies from thermogravimetric data. *Polymer Letters*, **4**: 323-328.

FIELD, M. A.1969. Rate of combustion of size-graded fractions of char from low-rank coal between 1200 K and 2000 K. *Combustion and Flame* **13**(3)**:** 237-252.

GARDNER, N.C., SAMUELS, E. AND WILKS, K. 1979. Modelling of coal combustion. *Advanced Chemistry Series*. **131**: 217-220.

GONENC, Z. S. 1990. Comparison of pyrolysis product distributions from captive sample techniques. *Fuel*, **69**(3): 383-390.

GROVES, S.J., WILLIAMSON, J. AND SANYAL, A. 1987. Determination of pyrite during pulverized coal combustion. *Fuel*, **66**(4): 461-466.

GUO, Y.C., CHAN, C.K. AND LAU, K.S. 2003. Numerical studies of pulverised coal combustion in a tabular coal combustor with slanted oxygen jet, *Fuel*, **82**(8): 893-907.

GURURAJAN, V. S., AGARWAL, P. K. AND AGNEW, J. B. 1992. Mathematical modelling of fluidised bed coal gasifiers. *Trans ICHemE*, **70**: 211-238.

HABERMEHL, D., ORYWAL, F. AND BEYER, H. D. 1981. Plastic properties of coal, in Chemistry of coal utilisation: Second Supplementary Volume. Elliot, M. A., *Ed. Wiley and Sons, Inc., New York.* Pp 317-424.

HASHIMOTO, K., MIURA, K. AND UEDA, T. 1986. Correlation of gasification rates of various coals measured by rapid heating method in steam atmosphere at relatively low temperatures. *Fuel*, **65**(11): 1516-1523.

HILL, M. AND FOTT, P. 1993. Kinetics of gasification of Czech brown coals. *Fuel*. **72**(4): 525-529.

HOWARD, J. 1982. Fundamentals of coal pyrolysis and hydropyrolysis, in Chemistry of coal utilization: 2nd Supplementary Volume. Elliot, A. E., *Ed. Wiley and Sons*, Inc.pp 665-784.

HURT, R.H. AND MITCHELL, R.E. 1992. On the combustion of heterogeneous char particle population, "*24th symposium (International) on combustion*". The combustion institute, Pittsburgh, PA, 1233.

ISHIDA, M. AND WEN, C.Y.1968, Comparison of kinetic and diffusional models for solid-gas reactions., *AICHE*, **14**(2): 311-317.

JENKINS, R. G., NANDI, S. P. AND WALKER, P. L. 1973. Reactivity of heat-treated coals in air at 500°C. *Fuel*, **52**(10): 288-293.

JOHNSON, J. L. 1979. Kinetics of bituminous coal char gasification with gases containing steam and hydrogen. *Advances in Chemistry*, **137**: 145-178.

KHAN, M. R. 1987. Significance of coal surface area for appraising the reactivity of low-and high temperature chars. *Fuel,* **66**(12): 1626-1634.

KUNIO, Y. AND KUNII, D. 1969. Basic studies on fluidised beds. *Journal of Chemical Engineering*, **2**: 170-174.

LAINE, N.R., VASTOLA, F.J. AND WALKER, P.L. 1964. The importance of active surface area in the carbon-oxygen reaction. *Journal of Physical Chemistry*, **67**: 2030-2033.

LAURENDEAU, N.M. 1978. Heterogeneous kinetics of coal char gasification and combustion. *Progress in Energy and Combustion Science*, **4**(4): 221-270.

LEVENSPIEL, O. 1972. Chemical Reaction Engineering, 2nd Edition. *Wiley and Sons, Inc., New York*. 838p.

LILIEDAHL, T. AND SJOSTROM, K. 1997. Modelling of char-gas reaction kinetics. *Fuel*, **76**(1): 29-37.

LIZZIO, A.A., PIOTROWSKI, A, RADOVIC, L.R. 1988. Effect of oxygen chemisorption on char gasification reactivity profiles obtained by thermogravimetric analysis. *Fuel*, **67**(12): 1691-1695.

LORENZ, H., CARREA, E., TAMURA, M. AND HAAS, J. 2000. The role of char surface structure development in pulverized fuel combustion. *Fuel*, **79**(10): 1161-1172.

MAHAJAN, O. P., YARZAB, R. AND WALKER, P. L. 1978. Unification of coal-char gasification reaction mechanisms. *Fuel*, **57**(10): 643-646.

MIURA, K., HASHIMOTO, K. AND SILVESTON, P. L. 1989. Factors affecting the reactivity of coal char during gasification, and indices representing reactivity. *Fuel*, **68**(11): 1461-1475.

MEIJER, R. 1992. Kinetics and mechanism of the alkali-catalysed gasification of carbon. Thesis. University of Amsterdam, The Netherlands.

MONSON, C.R., GERMANE, G.J., BLACKHAM, A.U. AND SMOOT, L.D. 1995. Char oxidation at elevated pressure, *Combustion and Flame*, **100**(4): 669-683.

MOORS, J. H. J., BANIN, V. E., HAAS, J. H. P., WEBER, R. AND VEEFKIND, A. 1999. Prediction and validation of burnout curves for Gottelborn char using reaction kinetics determined in shock tube experiments. *Fuel*, **78**(1): 25-29.

MUHLEN, H. J, VAN HEEK, K. H. AND JUNTGEN, H. 1985. Kinetic studies of steam gasification of char in the presence of H_2, CO_2 and CO. *Fuel*, **64**(7): 944-949.

NSAKALA, N., ESSENHIGH, R. H. AND WALKER, P.L. 1977. Studies on coal reactivity: Kinetics of lignite pyrolysis in nitrogen at 808 °C. *Combustion Science Technology*, **16**: 153-163.

OLIVELLA, M.A. AND HERAS de LAS, F.X.C. 2002, Study of the reactivities of chars from sulfur rich Spanish coals, *Thermochimica Acta*, **385**(1-2): 171-175.

PEEK, W. H. 2000. M-Eng Thesis. The determination of the kinetics of combustion of coal chars using isothermal and non-isothermal thermogravimetric methods. University of Potchefstroom.

QUEROL, X., FERNANDE'Z, J.L. AND SOLER, A.L. 1994. Trace elements in coal and their behaviour during combustion in a large power station. *Fuel*, **74**(3): 331-343.

READE, W. 1996. An improved method for predicting high-temperature char oxidation rates, M.S. Thesis, Brigham Young University.

RUSSELL, N. V., BEELEY, T. J., MAN, C. K., GIBBINS, J. R. AND WILLIAMSON, J. 1998. Development of TG measurements of intrinsic char combustion reactivity for industrial and research purposes. *Fuel Processing Technology*, **57**(2): 113-130.

RUSSEL, N.V., GIBBINS, J. R. AND WILLIAMSON, J. 1999. Structural ordering in high temperature coal chars and effect on reactivity. *Fuel*, **78**(7): 803-807.

SERIO, M. A., SOLOMON, P. R. AND SUURBERG, E. M. 1987. International Conference on Coal Science. *Elsevier*, Amsterdam. 597p.

SIMONS, G.A. 1980. The unified coal-char reaction. *Fuel*, **59**(2): 143-144.

SMITH, I.W. 1982. The combustion of coal char: A review, *11th symposium(International) on combustion*, The Combustion Institute, Pittsburgh, PA, 1045.

SMITH, K.L., SMOOT, L.D., FLETCHER, T.H. AND PUGMIRE, R.J. 1994. The structure and reaction processes of coal, *Plenum Press, New York.*

SMOOT, L.D. AND SMITH, P.J. 1985. Coal combustion and gasification, *Plenum Press, New York and London.*

SORENSEN, L.H. 1994. Fuel reactivity as a function of temperature, pressure and conversion, Ph.D. thesis, Riso National Laboratory, Denmark.

SORENSEN, L.H., GJERNES, E., JESSEN, T. AND FJELLERUP, J. 1996. Determination of reactivity parameters of model carbons, cokes and flame-chars. *Fuel*, **75**(1): 31-38.

SUURBERG, E.M., WOJTOWICZ, M. AND CALO, J.M. 1988. Reaction order for low temperature oxidation of carbon, *22nd symposium (International) on combustion*, The Combustion Institute, Pittsburgh, PA, 79.

TAKARADA, T., TAMAI, Y. AND TOMITA, A. 1985. Reactivities of 34 coals under steam gasification. *Fuel*, **64**(10): 1438-1442.

TOMECZEK, J. AND GIL, S. 2003. Volatiles release and porosity evolution during high pressure coal pyrolysis. *Fuel*, **82**: 285-292.

TSAI, S. C. 1982. Fundamentals of Coal Beneficiation and Utilization. *Elsevier*, Amsterdam. 292p.

TSAI, C. Y. AND SCARONI, A. W. 1987. Co-carbonization of a solvent refined coal with selected coal types-I. Thermoplsticity and optical texture development. *Carbon,* **22**(2): 206-207.

TSENG, H. P. AND EDGAR, T. F. 1985. Combustion behaviour of bituminous and anthracite coal char between 425 and 900 °C. *Fuel* **64**(3): 373-379.

WALKER, P. L. 1977. The scientific base of coal gasification. *Industrial Heating*, **44**(11): 16-20.

WALKER, P. L., RUSINKO, F. AND AUSTIN, L. G. 1959. Advances in Catalysis. Eley, O. D., Selwood, P. W. and Weisz, P. B., Eds. *Academic Press, Inc. New York and London.* Pp134-221.

WELLS, W. F. AND SMOOT, L. D. 1987. Particle size dependence of coal char reactivity. *Combustion and Flame*, **68**(1): 81-83.

WICKE, E. 1955. Contributions to the Combustion Mechanism of Carbon. Procured 5th Symposium (Int.) Combustion. Reinhold Publishing Corp., New York. Pp 245-252.

WEN, C. Y. 1968. Coal conversion reaction engineering. *Industrial Engineering Chemistry*, **60**: 34-43.

CHAPTER 4

GASIFICATION REACTION KINETICS

4.1 INTRODUCTION

In this chapter, the reaction kinetics of gasification of two high ash chars is presented. Preliminary experiments have been conducted non-isothermally in order to study the different reactions that take place in the gasification process. Also, the reaction kinetics, gasification reactions have been studied isothermally with mixtures of CO_2/N_2, CO_2/CO, H_2O/N_2, H_2O/H_2 and $CO_2/CO/H_2O/H_2$ at atmospheric pressure and temperatures between 800 and 950 ^oC.

In Section 4.2, the relevant literature on gasification reactions is given as well as the different gasification models are reviewed. In Section 4.3, different reaction rate equations concerning the models used are given. The experimental procedure of gasification is presented in Section 4.4 and the results and discussion are given in Section 4.5. Finally, the conclusions are presented in Section 4.6.

4.2 LITERATURE SURVEY

4.2.1 Introduction

In this section, a literature study on the most important char gasification reactions, relevant to a commercial gasification process, is presented. Different intrinsic reaction and particle conversion models used in modelling gasification reaction are discussed.

4.2.2 Gasification reactions

The most important char gasification reactions occurring in a gasifier are (Gururajan *et al.*, 1992):

$$C + \delta O_2 \rightarrow 2(1-\delta)CO + (2\delta - 1)CO_2 \qquad [4.1]$$

$$C + H_2O \rightarrow CO + H_2 \qquad [4.2]$$

$$C + CO_2 \rightarrow 2CO \qquad [4.3]$$

$$C + 2H_2 \rightarrow CH_4 \qquad [4.4]$$

$$CO + H_2O \Leftrightarrow CO_2 + H_2 \qquad [4.5]$$

where δ is a stoichiometric factor with values in the range of 0.5 to 1. Reactions 4.1 and 4.4 are exothermic and they provide the necessary heat for the endothermic reactions 4.2 and 4.3, and reaction 4.4 only takes place at high pressures (Muhlen, 1985). A more detailed description of the gasification with CO_2 and steam is given in Section 4.3.2.1 and 4.3.2.2 respectively. Reaction 4.5 is the water gas shift reaction occurring in the gas phase.

4.2.3 Factors affecting the reaction rates of coal chars

The factors affecting the reaction rate during combustion have been presented in Section 3.2.3 and are very similar to those affecting the gasification rates. Char gasification is considered a first order reaction, both for CO_2 and steam when working at pressures

below atmospheric pressure (Molina and Mondragon, 1998). For pressures above atmospheric, the reaction order approaches zero. In gasification, the formation of CO and H_2 has been reported to result in a retarding effect (Molina and Mondragon, 1998). Gasification experiments are usually studied at high temperatures because of the nature of reactions involved. Reactions carried out at high temperatures might result in diffusive restrictions and in order to avoid this, the particle size is usually chosen small enough. The particle size where diffusion can be neglected depends on the type of coal. Kovacik *et al.* (1991), found diffusion restrictions for bituminous and subbituminous coals at 900 °C and particle size above 105 μm. Matsui *et al.*, 1987 did not find diffusion restrictions when working with subbituminous coal of 710 μm particles.

Many investigators such as Miura *et al.* (1989), Takarada *et al.* (1985) and van Heek and Muhlen (1985) have reported that, in general, the intrinsic gasification rate of low ash chars (carbon content > 80%) is relatively low and is correlated with the coal rank and parameters such as carbon content. On the other hand, the gasification rate of high ash chars (carbon content < 80%) is relatively high due to the catalytic activity of mineral constituents such as Ca, K and Na and they do not show any trend with the coal rank parameters. Several investigators examined the catalytic effect of coal minerals. Hashimoto *et al.,* (1986) indicated that reactivity tended to increase with an increase of Na, Ca and K contained in the char.

4.2.4 Gasification models

Different forms of char conversion models have been proposed for steam and CO_2 gasification. Dutta *et al.* (1977) investigated coal char gasification in carbon dioxide and found that the reaction can be represented by a homogeneous model with reaction orders of unity for both gas and solids. Golovina (1980) investigated char gasification in carbon dioxide, at high temperatures and pressures, and concluded that the reaction is first order in CO_2 at atmosphere pressure. Kwon *et al.*, (1988) studied the kinetics of char carbon dioxide gasification taking into account the effects of particle size, gas concentration etc. and reported that the overall reaction is chemically controlled and can be represented by a shrinking core model. Osafune and Marsh (1988) have reported that for gasification of

char in carbon dioxide in the temperature range 867-1287 °C, the experimental data also followed a shrinking core model. Kovacik *et al.* (1991) studied char gasification by carbon dioxide in a fixed bed reactor. The experimental data was found to follow the shrinking core model. Shufen and Ruizheng (1994) studied lignite char gasification in CO_2, H_2 and H_2O mixtures under pressure. They found that the shrinking core model represented the reaction both for steam and carbon dioxide. Standish and Tanjung, (1988) reported that for gasification of wood char particles in CO_2, the reaction could be represented by the shrinking core model. Bhat *et al.* (2000) studied the reaction kinetics of rice husks in a thermogravimetric balance at temperatures between 750 and 900 °C. The data was analysed based on the shrinking core models.

Some researchers Plante and Chornet (1988); DeGroot and Shafizadeh (1984) have studied gasification kinetics without including the effect of the product gases. Although these measurements may be useful (for example, to rank the coals according to their reactivity or to examine the catalytic effect of inorganic salts), they cannot be used to estimate the gasification in synthesis gas mixtures.

The reactions 4.2 and 4.3 (as given in Section 4.2.2) are the typical gasification reactions, and most researchers have focussed on one of the reactions taking into account the inhibitive effect of product gases (e.g. Johnson, 1981 and Goyal *et al.*, 1989). Kinetic rate expressions derived from mechanistic considerations Johnson (1981) and Smith (1982) clearly show that the reaction products CO and H_2 inhibit the rate of reaction. Other experimental investigations Goyal *et al.*, (1989) and Muhlen *et al.*, (1985) have also confirmed the strong inhibitive effect of the reaction products.

The combination of the two reactions (reaction 4.2 and 4.3) and the influence of the product gases on the reaction rate have only received attention from a few authors (Bliek, 1984; Goyal *et al.*, 1989 and Johnson, 1981). Johnson (1981) correlated the gasification rates of American bituminous coal chars measured over a wide range of pressures (0.1 – 7.0 MPa) and temperatures (800 – 1100 °C) in atmospheres containing varying amounts of CO, CO_2, H_2, H_2O and CH_4. Johnson's empirical correlations account for the effect of inhibitive effect of products on reaction rates. Bliek, (1984) developed Langmuir Hinshelwood type rate expressions for the intrinsic reaction rates of chars (prepared from semi-anthracite and brown coals) in CO/CO_2, H_2/H_2O and synthesis gas mixtures in

temperature range of 677-927 °C at atmospheric pressure. Bliek (1984) found that the reaction rate in synthesis gas mixtures is well approximated by the sum of the individual rates in C/CO_2 and H_2/H_2O mixtures. Goyal *et al.* (1989) measured the rate of gasification of a Western Kentucky bituminous coal char, prepared in a laboratory and from a pilot scale gasifier, in steam, steam-hydrogen and synthesis gas mixtures in the temperature range of 927 - 1027 °C and in the pressure range of 0.4-2.8 MPa. They found that over the reaction conditions investigated, pressure had little influence on the reaction rate.

4.3 FUNDAMENTAL REACTION RATE EQUATIONS

4.3.1 Introduction

This section describes the relevant theory with respect to the modelling of char gasification. In describing the chemical reaction kinetics, the power rate law equation has been criticised for inadequately predicting rates over a wide range of experimental conditions, especially for high-pressure char gasification models. Fundamental studies show that gasification processes consist of film diffusion, adsorption, surface reaction and desorption. It is generally thought that in order to model the effects of total and partial pressure over a broad temperature range, a detailed fundamental modelling approach is required, and the Langmuir-Hinshelwood (LH) type of expressions are recommended in the case of gasification (Essenhigh, 1988; Essenhigh, 1991 and Banin *et al.*, 1997). The advantage of the LH kinetics is that it includes the physical interaction between carbon and reactants and therefore provides a more fundamental basis for modelling char gasification rates at elevated pressures. In the following sections, the LH models are applied to CO_2 gasification, steam gasification and the combined CO_2 and steam gasification in the Sections 4.3.2.1, 4.3.2.2 and 4.3.2.3 respectively.

4.3.2 Langmuir-Hinshelwood rate equations

4.3.2.1 Carbon dioxide gasification mechanism and rate equations

According to Gadsby *et al.* (1948), the elemental steps in the gasification reaction of carbon with CO_2 are expressed as follows:

$$C + CO_2 \rightarrow C(O) + CO \qquad [4.6]$$

$$C + CO \Leftrightarrow C(CO) \qquad [4.7]$$

$$C(O) \rightarrow CO \qquad [4.8]$$

Reif (1952) and Ergun (1956) proposed a mechanism based on an oxygen exchange mechanism:

$$C + CO_2 \Leftrightarrow C(O) + CO \qquad [4.9]$$

$$C(O) \rightarrow CO \qquad [4.10]$$

In both mechanisms, the rate of carbon gasification is adversely influenced by the presence of the product CO. It is generally accepted that the kinetics of gasification of carbonaceous materials with carbon dioxide below 1027 °C are governed by a LH type of expression (Wigmans, 1982). A lot of research has been dedicated to elucidate the reaction mechanism of the CO_2-carbon reaction. Several authors (e.g. Walker *et al.*, 1959, Laurendeau, 1978, Johnson, 1979 and Kapteijn *et al.*, 1992) have studied the CO_2- carbon reaction and found that the rate of gasification of carbon by CO_2 in the presence of CO at atmospheric and moderate pressures, with surface reaction controlling the reaction rate, is best described by an equation of the following form:

$$\frac{dX}{dt} = \frac{k_r K_{CO_2} P_{CO_2}}{1 + K_{CO_2} P_{CO_2} + K_{CO} P_{CO}} f(X) \qquad [4.11]$$

where *f(X)* is the particle conversion model, the model that describes the relative conversion rate, as conversion progresses.

With,

$$\frac{dX}{dt}\frac{1}{f(X)} = r \qquad [4.12]$$

Equation 4.11 can be rewritten as:

$$r = \frac{k_r K_{CO_2} P_{CO_2}}{1 + K_{CO_2} P_{CO_2} + K_{CO} P_{CO}} \qquad [4.13]$$

After integration, Equation 4.12 gives,

$$rt = F(X) \qquad [4.14]$$

where *F(X)* is defined in Section 3.2.4.

In the absence of CO, Equation 4.13 reduces to:

$$r = \frac{k_r K_{CO_2} P_{CO_2}}{1 + K_{CO_2} P_{CO_2}} \qquad [4.15]$$

Equation 4.15 can be linearised to:

$$\frac{r}{P_{CO_2}} = -rK_{CO_2} + k_r K_{CO_2} \qquad [4.16]$$

Since the experiments are carried out isothermally, r can be obtained from the slope of $F(X)$ as a function of time (see Equation 4.14). Using Equation 4.16, the values for K_{CO_2} and k_r can be determined from a plot of $\frac{r}{P_{CO_2}}$ versus r from slope and intercept respectively.

The temperature dependence of the reaction and the adsorption constant are given by the Arrhenius (Equation 4.17) and the Van't Hoff (Equation 4.18) relation respectively:

$$k_r = k_0 e^{\frac{-E}{RT}} \qquad [4.17]$$

$$K = K_0 e^{\frac{-\Delta H}{RT}} \qquad [4.18]$$

4.3.2.2 Steam gasification mechanism and rate equations

The reaction mechanism of carbon with steam at low pressures can be written as follows (Huttinger and Merdes, 1992):

$$C + H_2O \Leftrightarrow C(O) + H_2 \qquad [4.19]$$

$$C(O) \rightarrow CO \qquad [4.20]$$

$$C + H_2 \Leftrightarrow C(H)_2 \qquad [4.21]$$

$$C + \frac{1}{2}H_2 \Leftrightarrow C(H) \qquad [4.22]$$

If the steam-hydrogen follows a LH mechanism, a surface reaction controlling rate equation can be expressed as:

$$r = \frac{k_r K_{H_2O} P_{H_2O}}{1 + K_{H_2O} P_{H_2O} + K_{H_2} P_{H_2}} \qquad [4.23]$$

In the absence of H_2 Equation 4.23 reduces to:

$$r = \frac{k_r K_{H_2O} P_{H_2O}}{1 + K_{H_2O} P_{H_2O}} \qquad [4.24]$$

Equation 4.24 can be presented in a linear form as:

$$\frac{r}{P_{H_2O}} = -rK_{H_2O} + k_r K_{H_2O} \qquad [4.25]$$

The parameters corresponding to steam gasification can be calculated similar to CO_2 gasification (Section 4.3.2.1).

4.3.2.3 Overall reaction rates of char with product gases

The rate of gasification of char is significantly influenced by the surface adsorption and desorption reaction of CO_2 and H_2O. These reactions may take place on a common site or two independent sites (Bliek, 1984). In such mixtures, the homogeneous water gas shift reaction (Equation 4.5) can take place, resulting in composition changes. It is often assumed that the gas phase water gas shift reaction is fast as compared to the heterogeneous gasification reactions. Therefore the composition of the mixture fed to the TGA equipment was chosen at the equilibrium composition at the gasification temperatures employed. The equilibrium constant, K_{eq} is a function of the gas concentrations and temperature, and can be expressed as:

$$K_{eq} = \frac{[CO_2][H_2]}{[CO][H_2O]} \qquad [4.26]$$

where the equilibrium constant, K_{eq}, can be calculated with (Yan *et al.*, 1998):

$$K_{eq} = \exp(-3.7774 + \frac{4118.6}{T}) \qquad [4.27]$$

If the carbon-steam and carbon-CO_2 adsorption reaction proceed at a common active site the overall rate with surface reaction controlled for gasification can be expressed as (Ergun and Mentser, 1965):

$$r = \frac{[k_{r_{CO_2}} K_{CO_2} P_{CO_2} + k_{r_{H_2O}} K_{H_2O} P_{H_2O}]}{1 + K_{CO_2} P_{CO_2} + K_{CO} P_{CO} + K_{H_2O} P_{H_2O} + K_{H_2} P_{H_2}} \qquad [4.28]$$

When CO_2 and steam adsorb on two separate and independent active sites, the overall rate with surface reaction control is considered to be additive (Bliek, 1984):

$$r = [\frac{k_{r_{CO_2}} K_{CO_2} P_{CO_2}}{1 + K_{CO_2} P_{CO_2} + K_{CO} P_{CO}} + \frac{k_{r_{H_2O}} K_{H_2O} P_{H_2O}}{1 + K_{H_2O} P_{H_2O} + K_{H_2} P_{H_2}}] \qquad [4.29]$$

4.4 EXPERIMENTAL

4.4.1 Introduction

In this section, the equipment used in the gasification experiments is described. The procedures used for char preparation and char gasification with CO_2 and steam is also presented. The same chars were used as reported on in Chapter 2 and been used for the combustion experiments.

4.4.2 Description of the experimental apparatus

All gasification experiments were carried out using the 951 horizontal TGA presented in Section 3.4.1. In the case of steam gasification the feed gas was introduced via two temperature controlled saturators. The vapour temperature in the saturators was carefully monitored and its reading was correlated to the percentage moisture. The feed line from

the last saturator to the TGA was insulated and kept at 125 °C to prevent condensation. Since gasification experiments were performed at higher temperatures, nitrogen was first used to attain the reaction conditions before the introduction of the steam or CO_2 mixture. In the case of steam gasification the steam concentration was varied from 10% to 20% because of the saturation limitations whereas in the case of CO_2 gasification it was possible to use pure CO_2. All CO_2 and steam gasification experiments were conducted isothermally except preliminary experiments in Section 4.5.2.

4.4.3 Char preparation

Similar to the combustion experiments (Section 3.3), the coal samples were converted to char before each experiment. The char preparation was carried out according to the following procedure:

1. The sample temperature is equilibrated at 30 °C in a nitrogen atmosphere.
2. The sample is heated at a constant rate of 50 °C/min to 900 °C.
3. The sample is held isothermally at 900 °C for 60 minutes.
4. The sample is cooled down to 30 °C.

4.4.4 Char gasification

The following method was employed in all isothermal gasification experiments:

1. The sample temperature is equilibrated to 30 °C.
2. The sample is heated with nitrogen at constant heating rate of 50 °C/min to the reaction temperature
3. At constant temperature, the reactive gases are introduced into the TGA, and the temperature is kept constant.
4. The sample is cooled down to room temperature after the conversion is complete.

4.4.5 Char properties

The properties of chars used in this investigation are given in Chapter 2.

4.5 RESULTS AND DISCUSSION

4.5.1 Introduction

The gasification results of the two coal chars are presented in this section. First, the different gas-char reactions have been studied, and the most important reactions (reaction with CO_2 and steam) have been investigated for both char A and B. Finally, the simultaneous gasification with CO_2 and steam is presented in Section 4.5.8.

4.5.2 Reactivities of different gases

In a gasifier, the gases that are present in significant quantities are CO_2, H_2O, CO and H_2 and are studied in this investigation. In order to determine the most relevant gasification reactions, the reaction of char with the different gases is given in Figure 4.1. In this figure, the conversion of the char is given as a function of time, under non-isothermal conditions (a ramp of 1 °C/min was applied, starting at 250 °C) for the different gases.

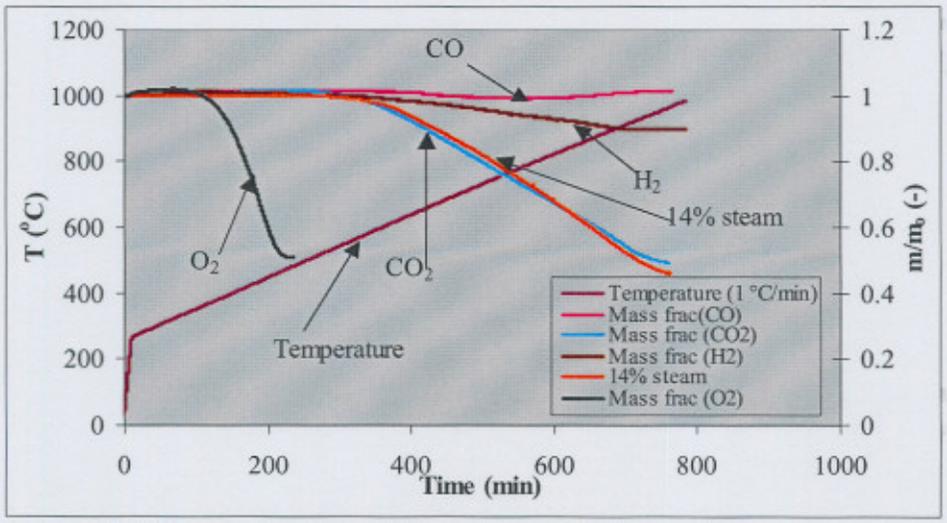

Figure 4.1: Char gasification with various gasifying agents

From this figure, it can be seen that the combustion reaction is much faster than the gasification reactions and that the char reacts much faster with CO_2 and H_2O than with CO and H_2. Several authors e.g. Weeda (1995) and Bliek (1984) have observed the same sequence in reactivity. From these experiments, it can be concluded that the reaction with CO_2 and H_2O are the most important reactions, and will therefore be studied in more detail in the following two sections.

4.5.3 Reaction of chars with carbon dioxide

In this section the experimental results obtained for char gasification with carbon dioxide are presented for char A and B. The focus is placed on CO_2 gasification under isothermal conditions between 800 and 950 °C.

4.5.3.1 Experimental results

Figure 4.2 shows a typical 20% CO_2 gasification data derived isothermally at 900 °C. From this figure it can be concluded that the ash content is 47 (±2) %, which agrees well with the ash content given in Table 2.2, showing that all carbon has reacted in the gasification experiments.

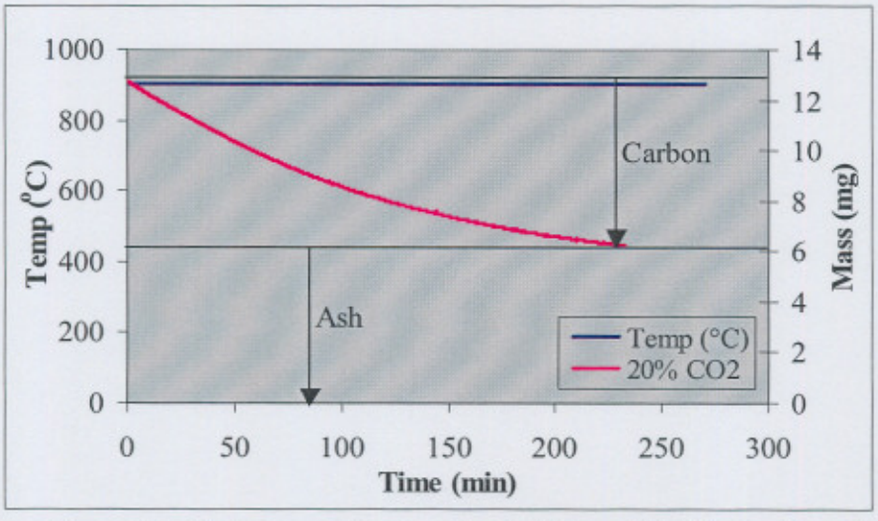

Figure 4.2: Typical raw data for char A CO_2 gasification at 900 °C

The data obtained from Figure 4.2 can be processed further and the extent of carbon conversion can be calculated, similar to the combustion experiments, as presented in Section 3.5. A plot of the carbon conversion as a function of time for different fractions of CO_2 is given in Figure 4.3 and 4.4 for char A and B respectively. (The figures for different temperatures is given in Appendix F)

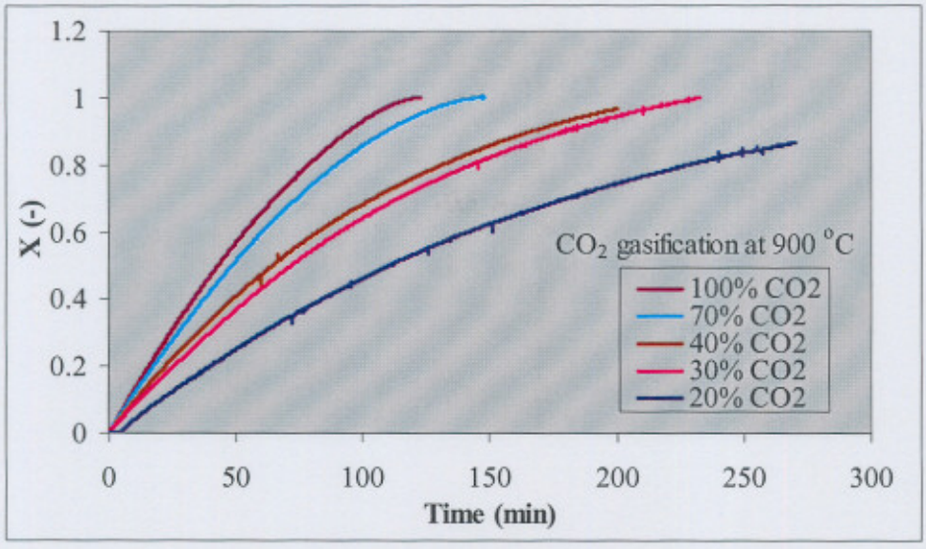

Figure 4.3: Conversion rate as a function of time at 900 °C (char A)

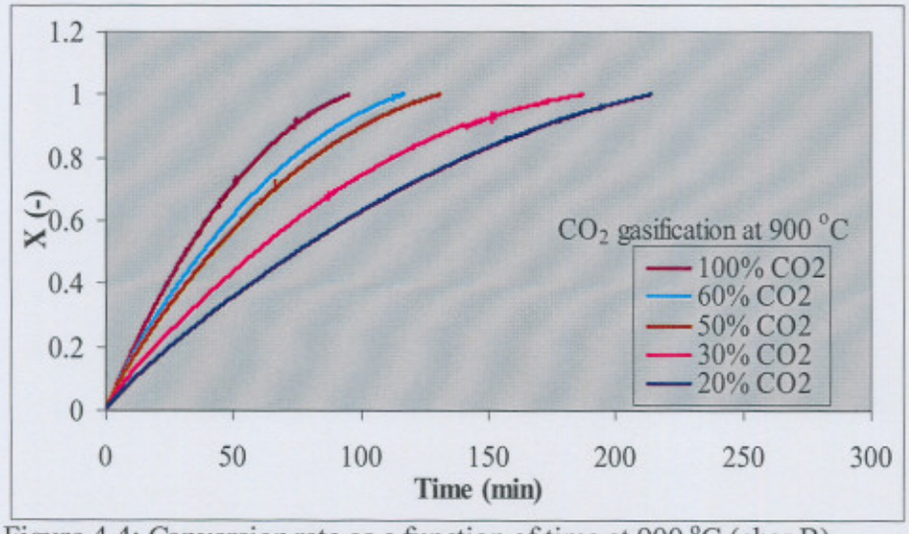

Figure 4.4: Conversion rate as a function of time at 900 °C (char B)

Evaluation of particle conversion model

The experimental data were normalised to 90% conversion, and are given in Figure 4.5 and 4.6 for char A and B respectively together with the different conversion models, as presented in Section 3.3. Confirming both the isothermal and non-isothermal combustion (Section 3.5 and 3.6), the reaction controlled shrinking unreacted-core model fitted the experiments the best. The same conclusion could be drawn for char B, as shown in Figure 4.6. Further results of experimental data against the reaction controlled SUCM at different temperatures are presented in Appendix G. The applicability of this model is attributed to the low porosity of char particles involved in this investigation.

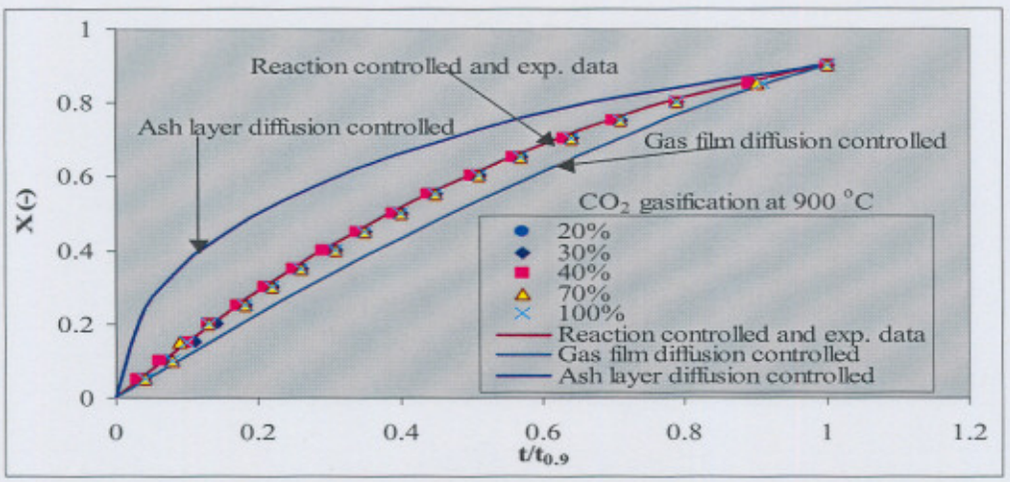

Figure 4.5: Conversion models for char A gasification at 900 °C

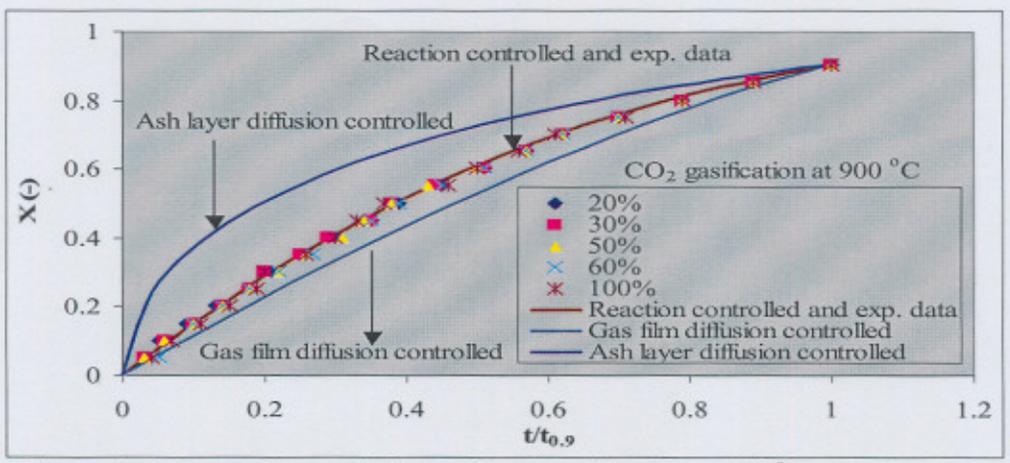

Figure 4.6: Conversion models for char B gasification at 900°C

Determination of LH-parameters

For the surface reaction controlled SUCM, the experimental data could be plotted according to Equation 4.14, as given in Figure 4.7 and 4.8 for char A and B respectively.

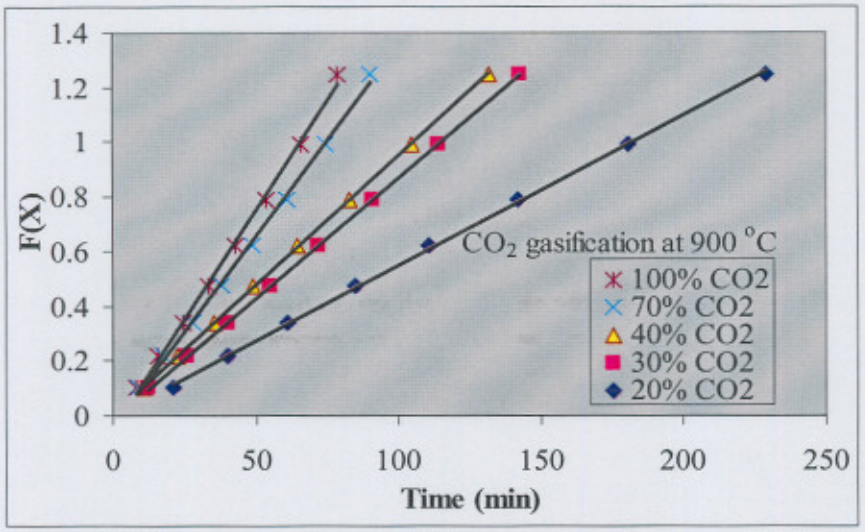

Figure 4.7: Char conversion model for char A gasification at 900 °C

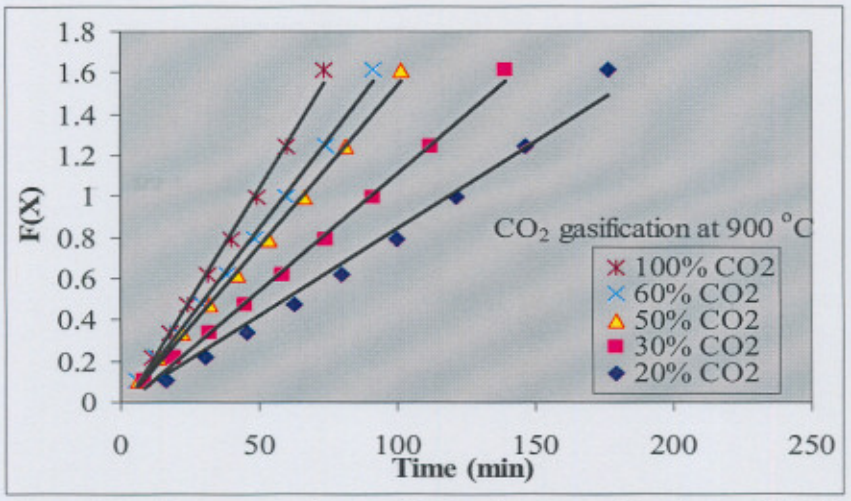

Figure 4.8: Char conversion model for char B gasification at 900 °C

This model was found to agree under all experimental conditions evaluated for both chars (see Appendix H). The slopes derived from the fitting of Equation 4.14 are presented in Table 4.1 and 4.2 for char A and B respectively.

Table 4.1: Values derived from the slopes (s^{-1}) of *F(X)* against time for char A

CO_2 fraction (-) Temperature (°C)	0.2	0.3	0.4	0.5	0.6	0.7	1
800	$1.08\ 10^{-4}$	$1.48\ 10^{-4}$	$1.72\ 10^{-4}$	-	$2.42\ 10^{-4}$	-	$2.82\ 10^{-4}$
850	$1.68\ 10^{-4}$	$3.32\ 10^{-4}$	$3.55\ 10^{-4}$	-	-	$3.85\ 10^{-4}$	$4.68\ 10^{-4}$
900	$6.00\ 10^{-5}$	$8.33\ 10^{-5}$	$1.00\ 10^{-4}$	-	-	$1.35\ 10^{-4}$	$1.57\ 10^{-4}$
950	$4.67\ 10^{-5}$	-	-	$6.00\ 10^{-5}$	$7.33\ 10^{-5}$	$9.50\ 10^{-5}$	$1.15\ 10^{-4}$

Table 4.2: Values derived from the slopes (s^{-1}) of *F(X)* against time for char B

CO_2 fraction (-) Temperature (°C)	0.2	0.3	0.4	0.5	0.6	0.7	1
800	$6.33\ 10^{-5}$	-	-	$1.02\ 10^{-4}$	$1.18\ 10^{-4}$	-	$1.35\ 10^{-4}$
850	-	$1.17\ 10^{-4}$	$1.38\ 10^{-4}$	-	$1.63\ 10^{-4}$	$1.85\ 10^{-4}$	$1.95\ 10^{-4}$
900	$1.45\ 10^{-4}$	$1.82\ 10^{-4}$	-	$2.50\ 10^{-4}$	$2.77\ 10^{-4}$	-	$3.47\ 10^{-4}$
950	-	$3.82\ 10^{-4}$	$4.60\ 10^{-4}$	$5.23\ 10^{-4}$	$6.02\ 10^{-4}$	-	$7.50\ 10^{-4}$

In order to obtain the reaction and adsorption constants, the slopes presented in Table 4.1 and 4.2 were linearised according to Equation 4.16 and given in Figure 4.9.

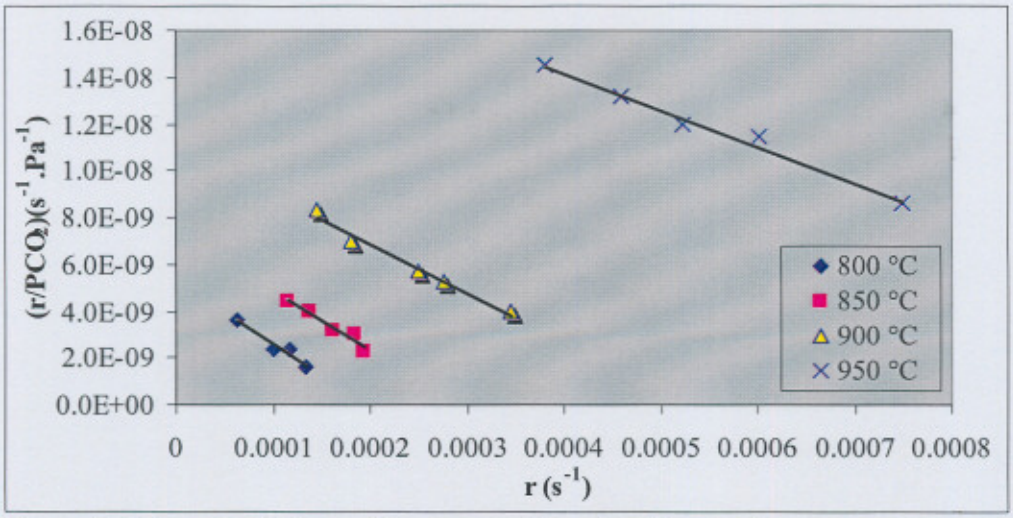

Figure 4.9: Linearised form of the Langmuir results for char A

The results fit the Langmuir equation well at all temperatures studied. The kinetic constants were derived from the plots of Figure 4.9 (char A given as an example) as

previously described in Section 4.3.2.1. Table 4.3 and 4.4 summarizes the kinetic constants obtained for both chars during CO_2 gasification.

Table 4.3: Kinetic constants for carbon dioxide gasification (char A)

Temp (°C)	$k_r K_{CO_2}$ ($s^{-1}.Pa^{-1}$)	K_{CO_2} (Pa^{-1})	k_r (s^{-1})
800	$3.47 \cdot 10^{-9}$	$1.85 \cdot 10^{-5}$	$1.88 \cdot 10^{-4}$
850	$4.55 \cdot 10^{-9}$	$1.74 \cdot 10^{-5}$	$2.62 \cdot 10^{-4}$
900	$8.04 \cdot 10^{-9}$	$1.72 \cdot 10^{-5}$	$4.69 \cdot 10^{-4}$
950	$1.21 \cdot 10^{-8}$	$1.46 \cdot 10^{-5}$	$8.31 \cdot 10^{-4}$

Table 4.4: Kinetic constants for carbon dioxide gasification (char B)

Temp (°C)	$k_r K_{CO_2}$ ($s^{-1}.Pa^{-1}$)	K_{CO_2} (Pa^{-1})	k_r (s^{-1})
800	$5.31 \cdot 10^{-9}$	$2.74 \cdot 10^{-5}$	$1.94 \cdot 10^{-4}$
850	$7.48 \cdot 10^{-9}$	$2.58 \cdot 10^{-5}$	$2.89 \cdot 10^{-4}$
900	$1.10 \cdot 10^{-8}$	$2.05 \cdot 10^{-5}$	$5.34 \cdot 10^{-4}$
950	$2.04 \cdot 10^{-8}$	$1.56 \cdot 10^{-5}$	$1.31 \cdot 10^{-3}$

It is observed from both tables, that the reaction rate constant (k_r) increases and the CO_2 adsorption constant (K_{CO_2}) decreases with increasing temperature.

The activation energy associated with k_r was calculated according to Equation 4.17, and is given in Figure 4.10 for char A and B respectively.

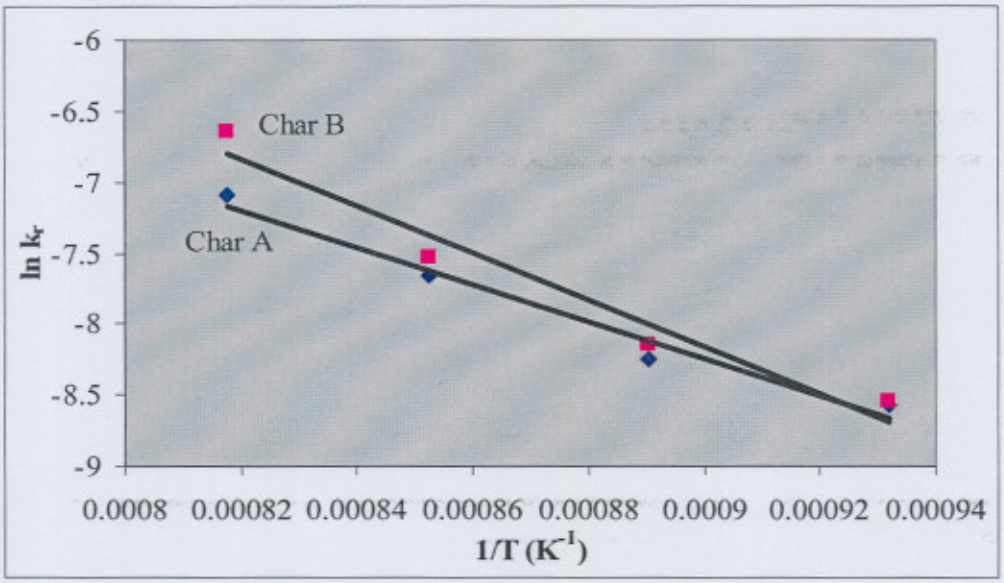

Figure 4.10: Determination of activation energy for both chars

From this figure, the activation energies could be calculated and are given in Table 4.5, together with several values that were found in the open literature.

Table 4.5: Activation energy values reported from literature

Reference	**Char origin**	**E (activation energy) kJ/mol**
This investigation	Char A	109
This investigation	Char B	136
Ye *et al*, (1998)	Coal	91*
Sinag *et al.*, (2003)	Coal	128-146*
Marquez *et al.*, (2002)	Coal	176-248*
Fu, W.B. Wang, Q, (2001)	Coal	245*

**based on a power law reaction rate*

It is seen that the activation energy varies widely; nevertheless the calculated activation energy values falls within range of the literature reported values.

The pre-exponential factors were computed from the intercepts of Figure 4.10 using the linearised form of Equation 4.17 and are given in Table 4.6.

Table 4.6: Averaged kinetic parameters for carbon dioxide gasification

Kinetic parameter	Char A	Char B
Activation energy, E	109 (±11) kJ mol^{-1}	136 (±12) kJ mol^{-1}
Pre-exponential factor, k_o (from Eq. 4.17)	3.6 10^1 s^{-1}	8.2 10^2 s^{-1}

based on the average activation energy reported in row 2 of this table

The adsorption enthalpy for gasification with CO_2 was calculated from Equation 4.18. Figure 4.11 shows a plot used to determine the adsorption enthalpy for both chars.

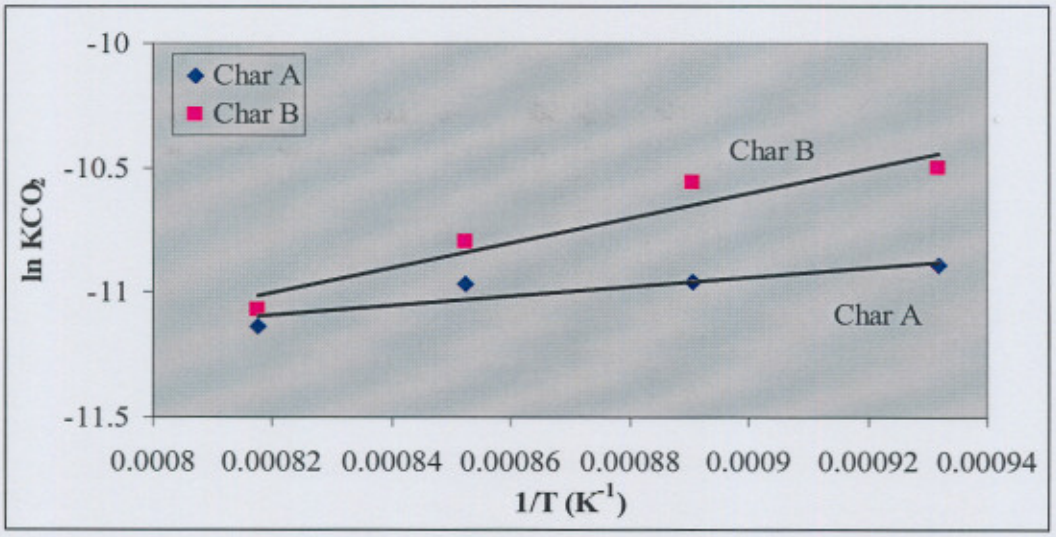

Figure 4.11: Determination of adsorption enthalpy for CO_2 gasification

The enthalpy of adsorption was determined to be 16 kJ/mol and 41 kJ/mol for char A and char B respectively. The values of adsorption constants are scarcely published in literature. Mugge *et al.*, (2001) found 23 kJ/mol for activated carbon. The differences in values of the heat of adsorption and the activation energy could be attributed to the different nature and composition of the char (see Section 2.8).

In order to predict the burnoff curves the calculated kinetic constants were fitted into the Langmuir rate (Equation 4.15). Figure 4.12 and 4.13 show a comparison between the experimental data and the calculated results from the Langmuir-Hinshelwood rate model.

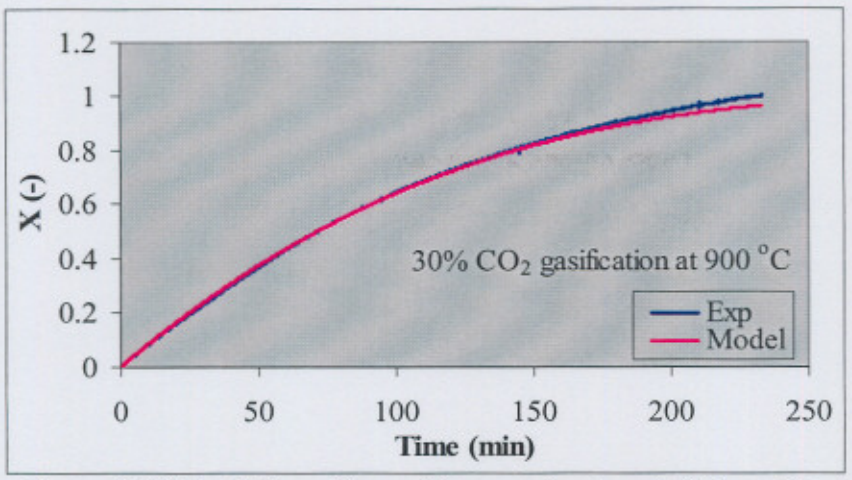

Figure 4.12: Prediction of burnoff curves for char A CO_2 gasification

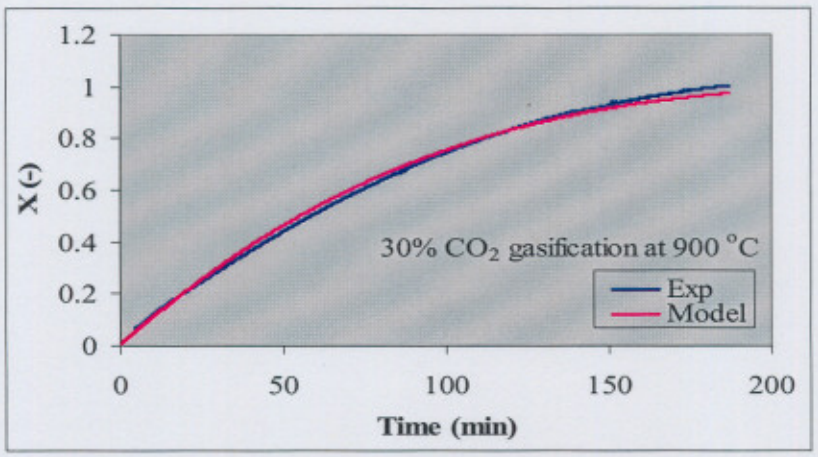

Figure 4.13: Prediction of burnoff curves for char B CO_2 gasification

It is seen that that the model gives a good prediction of the experimental data for both chars. The model showed consistency under different experimental conditions; see Appendix I for the other results of both chars.

4.5.4 Carbon dioxide/Carbon monoxide mixture

In this section the results obtained from the CO_2/CO gasification are presented. Since the carbon monoxide is the product of the CO_2-char reaction it is important to study its effect during gasification. To account for the carbon monoxide effects experiments were conducted with fractions of CO in the feed stream. These results were compared to those obtained without CO as seen in Figure 4.14. Because of the inhibition effect of carbon monoxide, experiments were conducted at 900 and 950 °C.

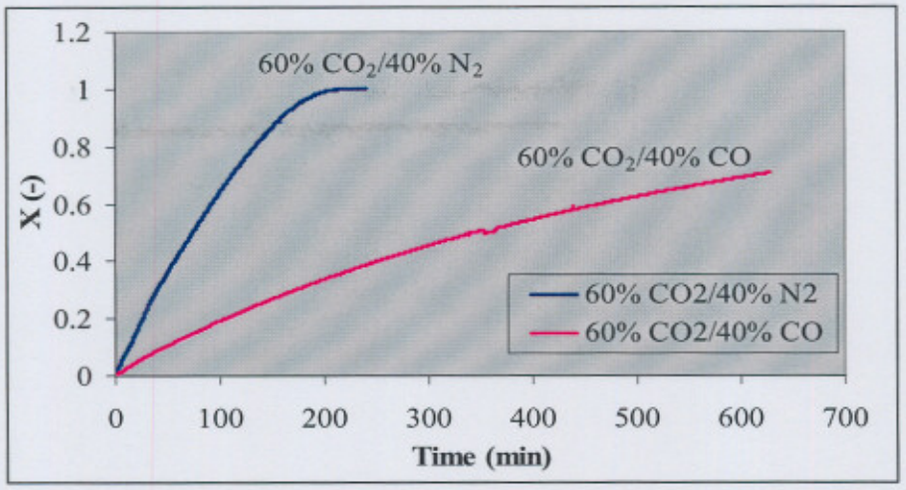

Figure 4.14: Inhibition effect of CO during CO_2 gasification at 900 °C

The effect of CO inhibition is clearly seen in Figure 4.14. The maximum conversion is difficult to attain at lower temperatures because of the nature of reaction. For this reason the experiments where CO is concerned were only carried out at 900 and 950 °C. With all the CO_2 associated kinetic constants calculated (Section 4.5.3), the adsorption constant associated with CO was calculated from Equation 4.13. Table 4.7 shows the adsorption parameters obtained for CO_2/CO gasification for char Aand B respectively.

Table 4.7Adsorption parameters for carbon monoxide for both chars

Temperature (°C)	K_{CO} (Pa^{-1}) for char A	K_{CO} (Pa^{-1}) for char B
900	$1.0\ 10^{-4}$	$2.6\ 10^{-4}$
950	$1.9\ 10^{-5}$	$1.4\ 10^{-4}$

It is seen that the adsorption is high at 900 °C compared to 950 °C indicating stronger inhibition at lower temperatures.

4.5.5 Steam/Nitrogen mixture

Another important reaction that takes place in the gasifier is the reaction between steam and carbon (Equation 4.2). In this section, the reaction kinetics of this reaction is presented together with the effect of product gas. Experiments were carried out temperatures between 800 and 950 °C with feed mixtures varying from 10 to 20% steam.

4.5.5.1 Experimental results

Figure 4.15 shows the relationship between temperature, time and mass fraction obtained during a typical steam gasification experiment.

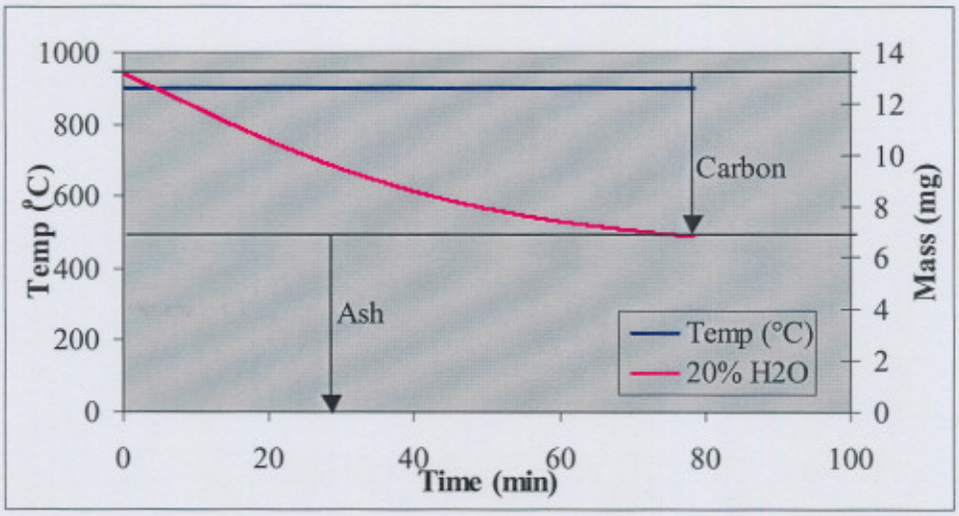

Figure 4.15: Typical steam gasification at 900 °C

From this figure and the other experiments, it could be concluded that, similar to the CO_2 experiments, the ash content was 48 (±3)%. The data was normalised to the carbon only, and the conversion of the carbon as a function of time is given in Figure 4.16 and 4.17 for char A and B respectively. Other experimental results obtained at different temperatures are presented in Appendix J.

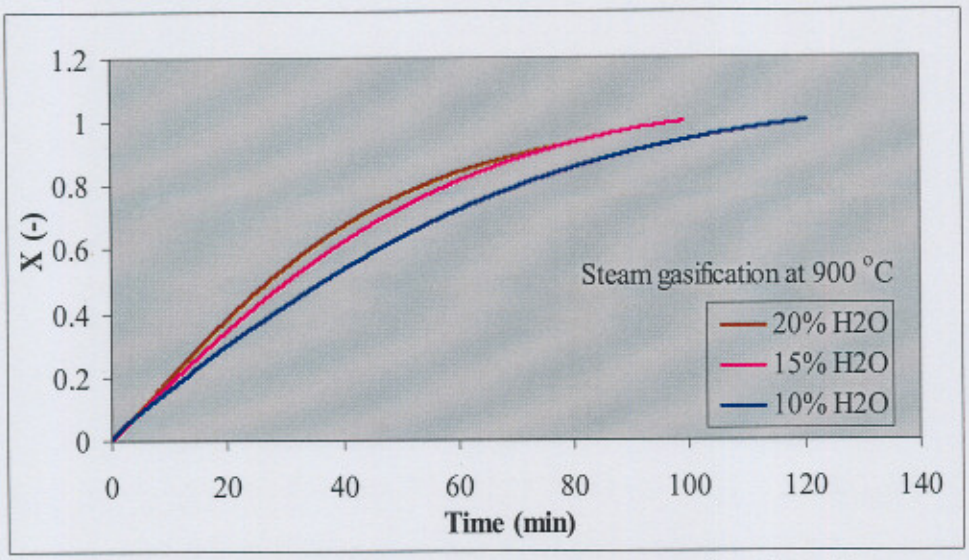

Figure 4.16: Conversion rate as function of time at 900 °C (char A)

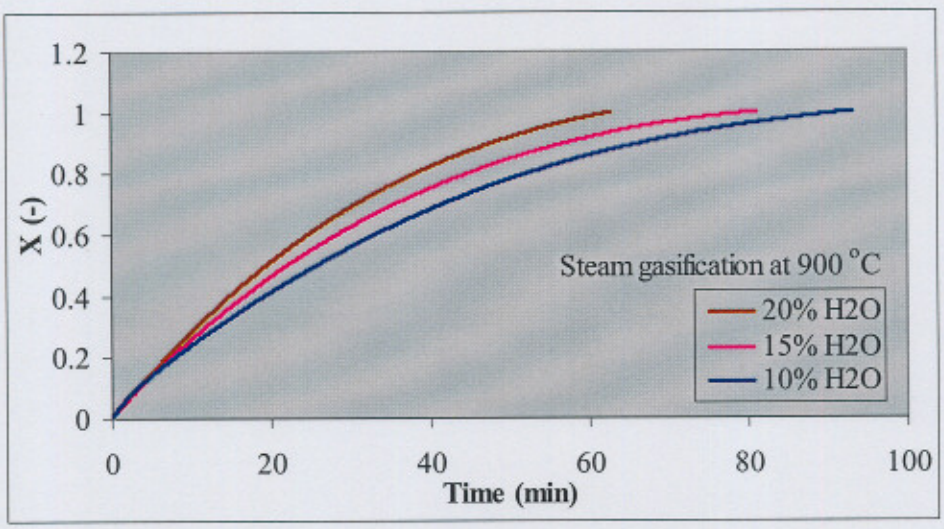

Figure 4.17: Conversion rate as function of time at 900 °C (char B)

From both figures, it can be concluded that the conversion rate increases with an increase in steam concentration.

Evaluation of particle conversion model

A comparative study on different shrinking unreacted core models was conducted for both chars. In this case, plots of the conversion as a function of the dimensionless time as given in Equation 3.26 were constructed for the different forms of the shrinking unreacted core model, and are given in Figure 4.18.

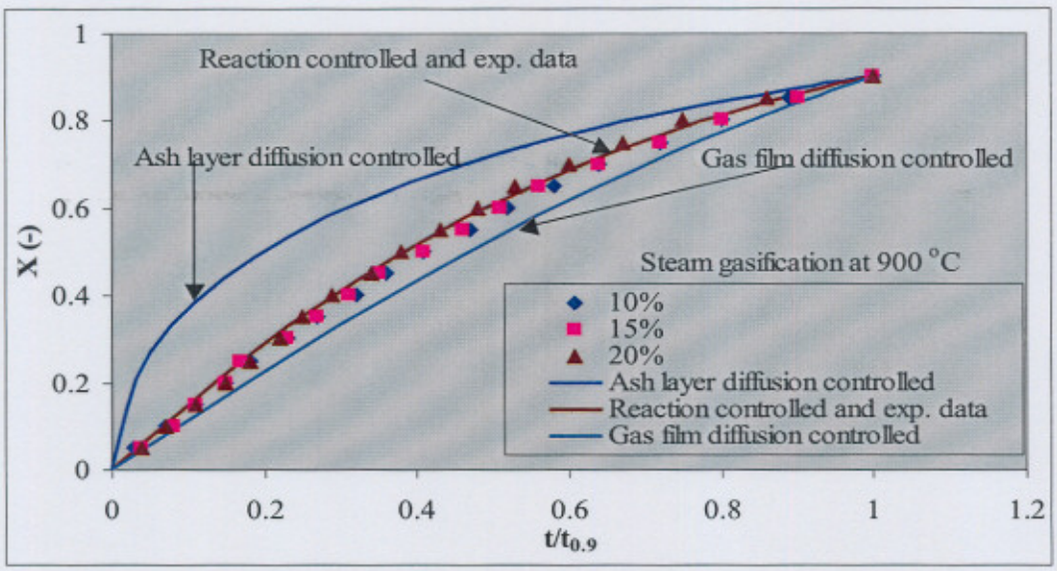

Figure 4.18: Conversion models for char A gasification in steam at 900 °C

It is seen from this figure, that the reaction controlled shrinking unreacted core model describes the experimental data well. This is consistent with CO_2 gasification and combustion results indicating the validity of the reaction controlled shrinking unreacted core model. A similar plot was also constructed for char B as well; see Figure 4.19 and also Appendix K for results at different temperatures.

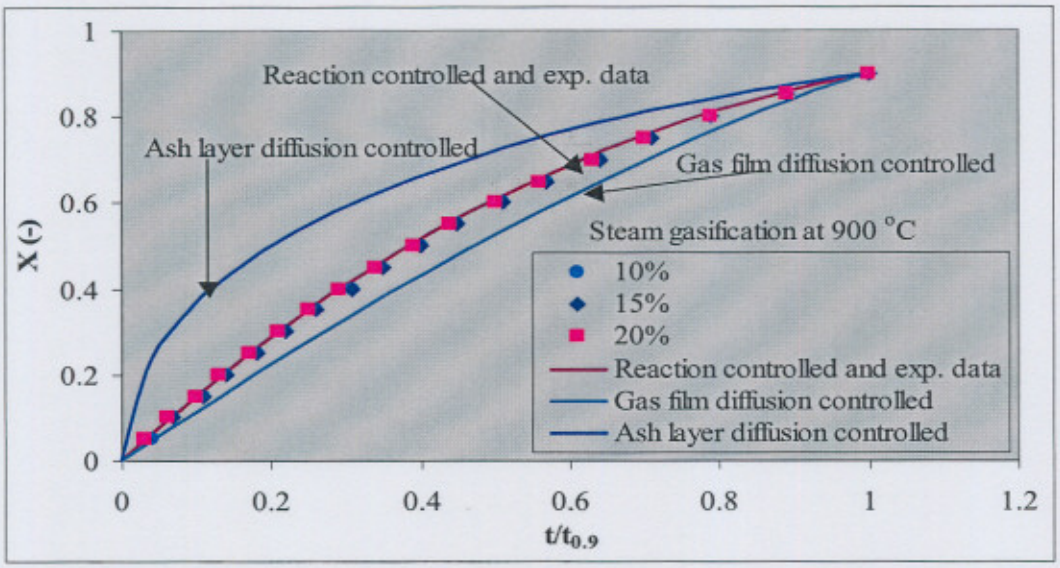

Figure 4.19: Conversion models for char B gasification in steam at 900 °C

Determination of Langmuir-Hinshelwood parameters

In order to determine the reaction kinetic constants plots of the reaction controlled shrinking unreacted core model as a function of time were constructed using Equation 4.14; see Figure 4.20 and 4.21 for char A and B respectively.

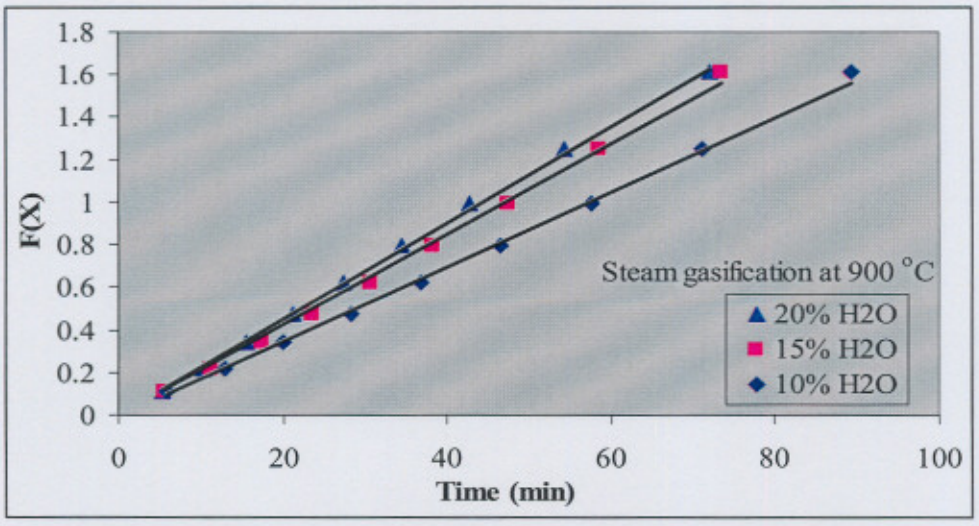

Figure 4.20: Unreacted-core shrinking model for char A steam gasification

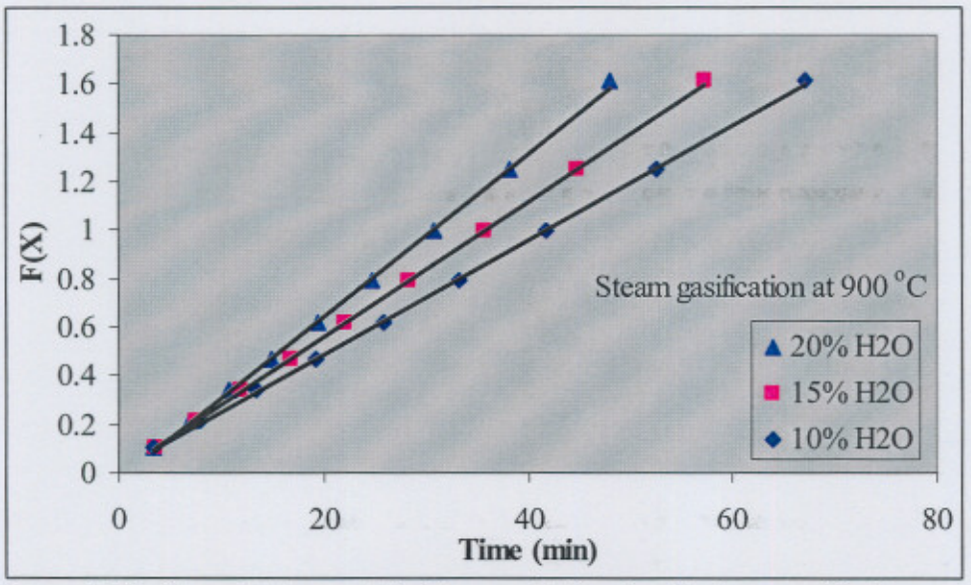

Figure 4.21: Unreacted-core shrinking model for char B steam gasification

Similar plots were also obtained for different temperatures and the results are given in Appendix L. The slopes derived from Equation 4.14 are presented in Table 4.8 and 4.9 for char A and B respectively.

Table 4.8: Slopes (s^{-1}) derived for char A steam gasification

Steam concentration Temperature (°C)	0.10	0.15	0.20
800	$5.33\ 10^{-5}$	$6.00\ 10^{-5}$	$6.67\ 10^{-5}$
850	$1.30\ 10^{-4}$	$1.60\ 10^{-4}$	$1.78\ 10^{-4}$
900	$3.00\ 10^{-4}$	$3.68\ 10^{-4}$	$4.25\ 10^{-4}$
950	$5.88\ 10^{-4}$	$7.45\ 10^{-4}$	$8.67\ 10^{-4}$

Table 4.9: Slopes (s^{-1}) derived for char B steam gasification

Steam concentration Temperature (°C)	0.10	0.15	0.20
800	$7.83\ 10^{-5}$	$8.67\ 10^{-5}$	$9.67\ 10^{-5}$
850	$1.62\ 10^{-4}$	$1.98\ 10^{-4}$	$2.21\ 10^{-4}$
900	$3.92\ 10^{-4}$	$4.65\ 10^{-4}$	$5.55\ 10^{-4}$
950	$7.63\ 10^{-4}$	$9.70\ 10^{-4}$	$1.20\ 10^{-4}$

A linearised Langmuir plot for steam gasification (Equation 4.25) was used to calculate adsorption constant parameters, see Figure 4.22, although limited points were used the results are acceptable for the purpose of this investigation

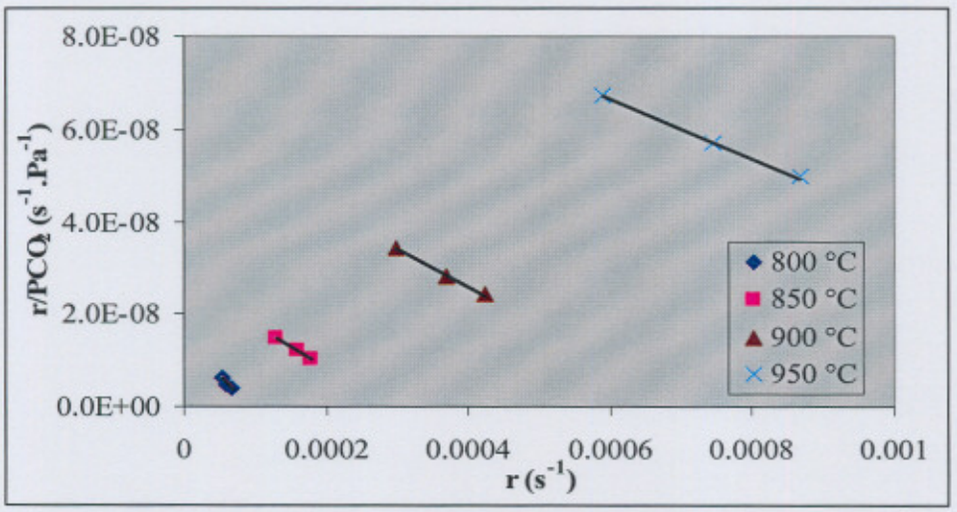

Figure 4.22: Linearised Langmuir-Hinshelwood plot for char A at 900 °C

The results presented in Table 4.8 and 4.9 were used to calculate the adsorption constants as previously described in Section 4.3.2.1. The kinetic parameters for both chars are summarised in Table 4.10 and 4.11 for char A and B respectively.

Table 4.10: Kinetic parameters for char A steam gasification

Temp (°C)	$k_r K_{H_2O}$ ($s^{-1}.Pa^{-1}$)	K_{H_2O} (Pa^{-1})	k_r (s^{-1})
800	$1.51\ 10^{-8}$	$1.71\ 10^{-4}$	$8.81\ 10^{-5}$
850	$2.74\ 10^{-8}$	$9.58\ 10^{-5}$	$2.86\ 10^{-4}$
900	$5.82\ 10^{-8}$	$8.04\ 10^{-5}$	$7.24\ 10^{-4}$
950	$1.05\ 10^{-7}$	$6.38\ 10^{-5}$	$1.64\ 10^{-3}$

Table 4.11: Kinetic parameters for char B steam gasification

Temp (°C)	$k_r K_{H_2O}$ ($s^{-1}.Pa^{-1}$)	K_{H_2O} (Pa^{-1})	k_r (s^{-1})
800	$2.71\ 10^{-8}$	$1.57\ 10^{-4}$	$1.73\ 10^{-4}$
850	$3.48\ 10^{-8}$	$1.05\ 10^{-4}$	$3.33\ 10^{-4}$
900	$5.82\ 10^{-8}$	$8.50\ 10^{-5}$	$6.85\ 10^{-4}$
950	$1.10\ 10^{-7}$	$3.50\ 10^{-5}$	$3.14\ 10^{-3}$

The activation energy was calculated from Equation 4.17 using the k_r associated values presented in Table 4.10 and 4.11. Figure 4.23 shows an Arrhenius plots for both chars in steam.

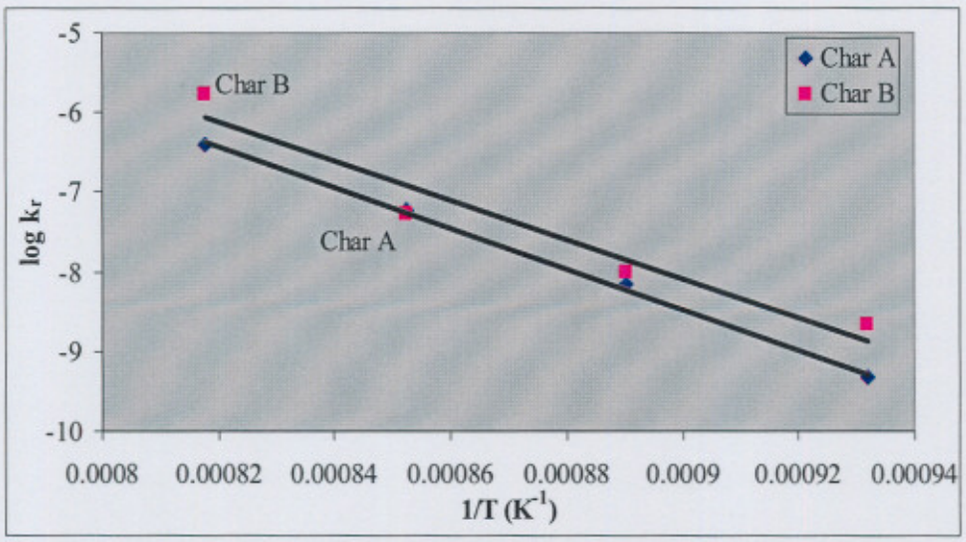

Figure 4.23: Activation Energy calculation for char A and B in steam

The activation energy determined for both chars compared well with each other. These values were also compared with literature reported figures; see Table 4.12.

Table 4.12: Values of activation energies for steam gasification

Reference	**Char origin**	**E (Activation Energy) kJ/mol**
This investigation (char A)	Coal	209
This investigation (char B)	Coal	215
Muhlen *et al.* (1985)	Coal	153
Liliedahl *et al.* (1997)	Coal	121
Ye *et al.* (1997)	Coal	131
Wen. (1968)	Coal	209
Weeda *et al.* (1993)	Coal	183
Ma *et al.* (1992)	Coal	163
Bliek. (1984)	Coal	168

all results based on the LH model

It is seen that the literature reported, activation energies vary between 121 and 209 kJ mol^{-1}. The experimentally found activation energies lie in the upper range of reported values of Table 4.12, and even relatively high compared to other chars. A possible reason could be due to greater fractions of carbon existing in their mineral-free state as shown by the CCSEM results in Chapter 2. The values of the pre-exponential factors were calculated from the intercepts of Figure 4.23 using the linearised form of Equation 4.17. The averaged kinetic parameters for both chars are summarised in Table 4.13.

Table 4.13: Values of pre-exponential factor for steam gasification

Kinetic parameter	Char A	Char B
Activation energy, E	209 (± 12) kJ mol^{-1}	215 (± 12) kJ mol^{-1}
Pre-exponential factor, k_0 (from Eq. 4.17)	$2.0 \cdot 10^{6*}$ s^{-1}	$1.2 \cdot 10^{6*}$ s^{-1}

**based on the average activation energy reported in row 2 of this table*

The adsorption enthalpy for char gasification in the presence of steam was also calculated from Equation 4.18. Figure 4.24 shows a plot used to compute the adsorption enthalpies for both chars.

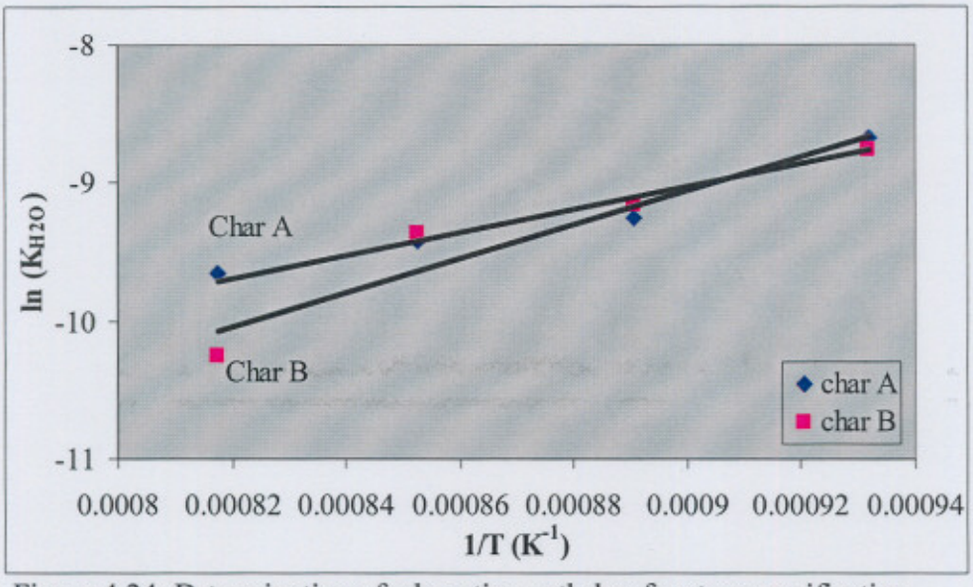

Figure 4.24: Determination of adsorption enthalpy for steam gasification

The adsorption enthalpy for char A was determined at 69 kJ/mol and that of char B at 97 kJ/mol. It is noted here, that the adsorption enthalpies for steam are higher than those of carbon dioxide indicating more surface coverage. This is an explanation for the higher reaction rate of steam gasification compared to CO_2 gasification. The difference in the adsorption enthalpy could possibly be attributed to the different surface nature of the chars (see Section 2.8). After evaluating all the kinetic parameters it was possible to predict the burnoff curves by fitting the kinetic parameters into Equation 4.24. Figure 4.25 and 4.26 shows the burnoff behaviours for char A and B respectively.

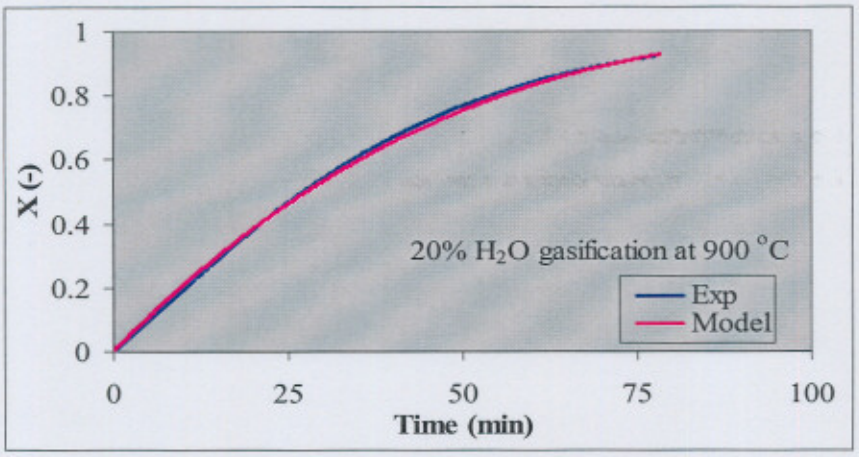

Figure 4.25: Burnoff behaviour for H_2O/N_2 (char A) at 900 °C

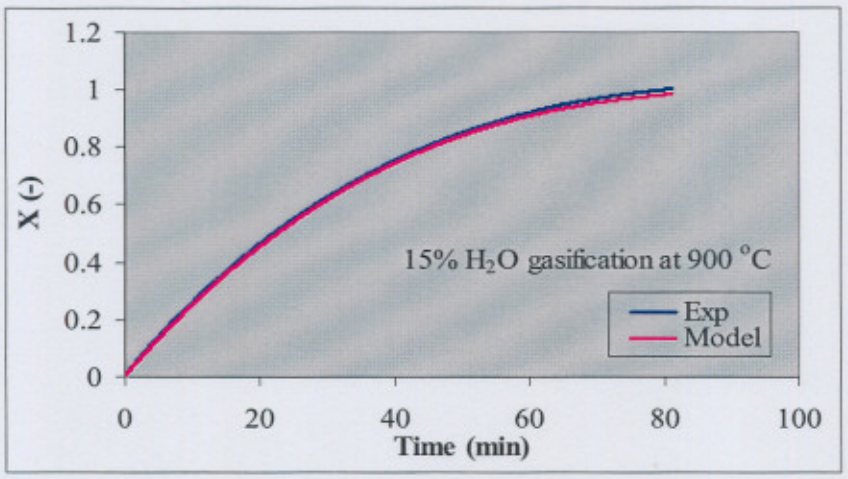

Figure 4.26: Burnoff behaviour for H_2O/N_2 (char B) at 900 °C

These plots showed consistency under all experimental conditions evaluated, more results are shown in Appendix M.

4.5.6 Steam/Hydrogen mixture

In order to account for the effect of hydrogen during steam gasification, hydrogen was added in the feed gas. Figure 4.27 shows a comparison of the conversion-time plots in the absence and the presence of hydrogen. It is seen that the presence of hydrogen in the feed gas inhibits the reaction rate. Several investigators (e.g. Muhlen *et al.* (1985), Whitty

(1997), Meijer *et al.* (1992)) have also observed the same behaviour of hydrogen during steam gasification.

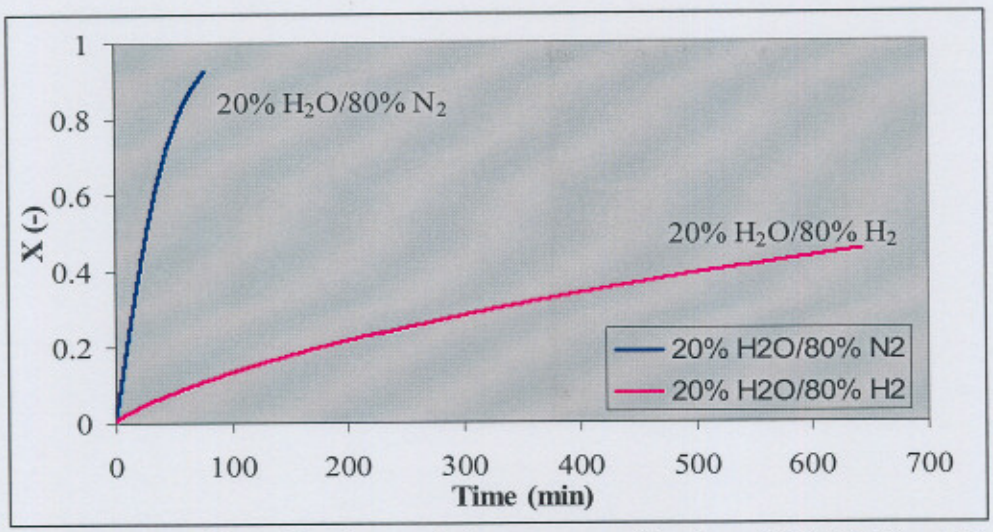

Figure 4.27: Effect of hydrogen during steam gasification at 900 °C (char A)

With all the H_2O associated kinetics calculated (Section 4.5.5), the adsorption constants associated with H_2 were calculated using Equation 4.23. Table 4.14 shows the kinetics derived for H_2O/H_2 gasification for char A and B respectively. Experiments involving hydrogen were carried out at 900 and 950 °C because of the strong inhibition effect.

Table 4.14: Adsorption parameters of hydrogen for both chars

Temperature (°C)	K_{H_2} (Pa^{-1}) for char A	K_{H_2} (Pa^{-1}) for char B
900	$9.36\ 10^{-4}$	$7.58\ 10^{-4}$
950	$4.07\ 10^{-4}$	$4.23\ 10^{-4}$

It is seen that the adsorption is high at 900 °C than at 950 °C indicating the strong inhibition of H_2 at lower temperatures.

4.5.7 ($CO_2/CO/H_2/H_2O$) Mixtures

To investigate whether the reactions of carbon with CO_2 and carbon with steam proceed on similar or different carbon sites, experiments were carried out in mixtures of $H_2O/H_2/CO/CO_2$ at water gas shift equilibrium conditions. The equilibrium conditions were chosen in order to avoid changes in composition that may arise due to water gas shift reaction. Table 4.15 shows the equilibrium compositions at different temperatures employed during experimentation.

Table 4.15: Water gas shift reaction conditions

T (°C)	CO_2 (%vol)	H_2 (%vol)	H_2O (%vol)	CO (%vol)
900	18.0	29.0	20.0	33.0
950	33.4	13.3	20.0	33.3

The rate of gasification of carbons in synthesis gas mixtures is predominantly governed by the interaction of the reactions of the CO_2/CO and H_2O/H_2. It was possible to predict the overall reaction mechanism for both chars under synthetic gas mixtures since all the kinetic constants were obtained from CO_2-CO and H_2O-H_2 experiments. Figure 4.28 is a plot of the experimental curve against predicted mechanisms for mixtures of $CO_2/CO/H_2O/H_2$.

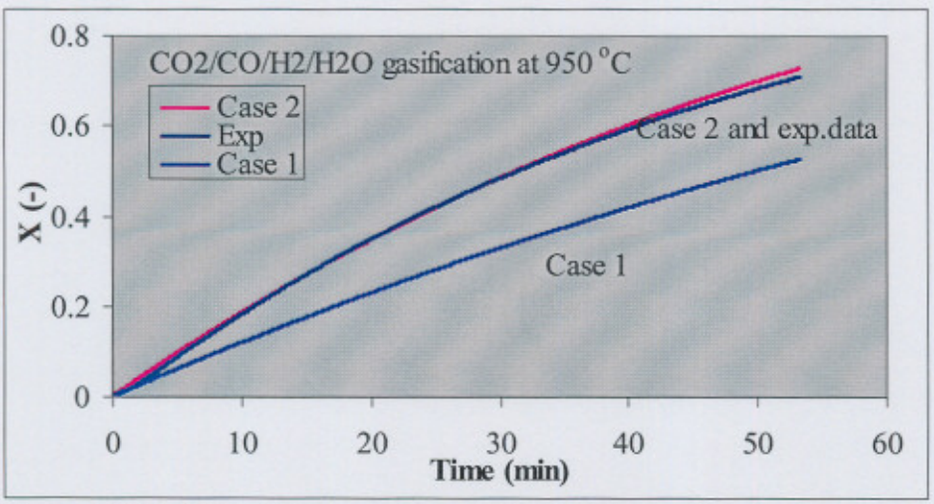

Figure 4.28: Char gasification under synthetic mixtures for char A

Case 1 as seen in Figure 4.28 refers to a situation whereby the char-CO_2 and the char-steam occur on the same sites (Equation 4.28). This situation is described as competitive adsorption. It is seen that case 1 does not describe the experimental data as obtained from the mixture of $CO_2/CO/H_2/H_2O$. Case 2 is a fit based on the assumption that the char-CO_2 and char-steam reactions take place on different carbon sites (Equation 4.29). Case 2 describes the experimental data better than case 1. This means that carbon-CO_2 and carbon-steam proceed at different carbon sites. Ergun and Mentser (1965) found case 1 to be applicable to the chars they studied. The results obtained in this investigation agree well with those obtained by (Bliek, 1984).

4.5.8 Comparison of reactions with carbon dioxide and steam

It was further possible to compare the experimental burnoff curves for CO_2 gasification of both chars under identical conditions. Figure 4.29 is a plot of conversion against time for char A and B respectively.

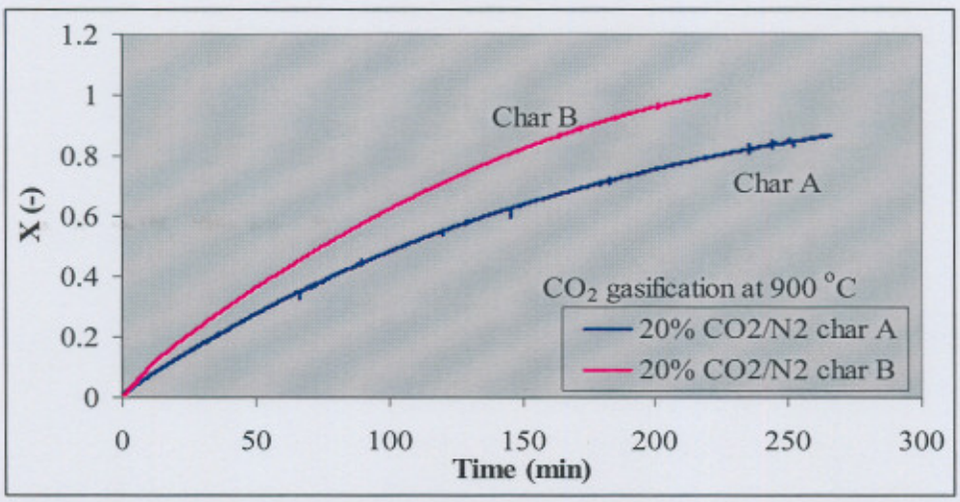

Figure 4.29: CO_2 gasification for char A and char B at 900 °C

It is seen that char B reacts faster than char A under CO_2 atmosphere. With regard to steam gasification, char B was also found to be more reactive than char A under the same experimental conditions. Figure 4.30 is a plot of char A against char B both at 20% steam

concentration. The difference in reactivity is due to the difference in adsorption enthalpy and particles size of the chars.

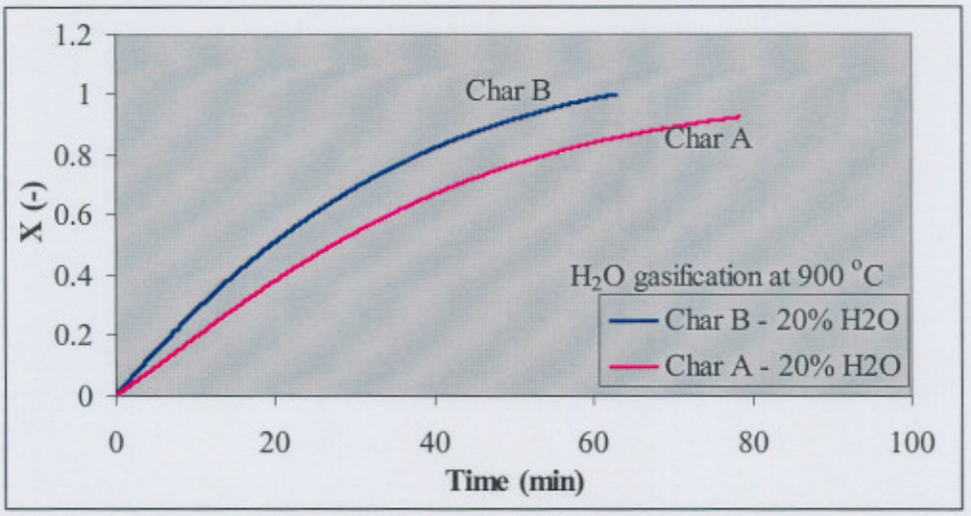

Figure 4.30: Steam gasification for char A and char B at 900 °C

4.5.9 Discussion of results with respect to characteristics

The shrinking unreacted core reaction model with surface reaction has been found valid for both chars investigated under CO_2 and steam gasification. This is consistent with the combustion results presented in Chapter 3. The shrinking unreacted reaction model is motivated by the fact that both chars have a non-porous structure resulting in negligible gas penetration into the core of the particle.

The activation energies for both chars under CO_2 and steam gasification were found to match each other. These values compare well to literature reported values. This is an indication that the kinetics of both chars studied in this investigation were not affected by the difference in total mineral matter. This is in agreement with the results obtained from the CCSEM where it was shown that greater fractions of chars occur with no mineral association.

The steam gasification showed higher reactivities than CO_2 gasification indicating that steam gasification results to more char converted in the gasifier. This is supported by the fact that higher values of adsorption enthalpies were obtained for steam gasification (see Table 4.16).

Table 4.16: Adsorption enthalpies for steam and carbon dioxide

Reactant	ΔH (kJ/mol) Char A	ΔH (kJ/mol) Char B
Carbon dioxide	16	41
Steam	69	97

4.6 CONCLUSIONS

The gasification of high ash chars was successfully studied at temperatures between 800 and 950 °C under isothermal conditions using an atmospheric thermogravimetric analyser. All experiments with, carbon dioxide and steam/nitrogen (maximum 20%), carbon monoxide and hydrogen were carried out to completion under constant temperatures.

It was established from non-isothermal experiments within a temperature range up to 800 °C that carbon dioxide and steam/nitrogen (14%) are the most reactive amongst the gases involved in gasification. Carbon monoxide and hydrogen only have significant reactivity at very high temperatures and pressures. The reaction rates for gasification involving carbon dioxide and stream/nitrogen were found to be lower than the corresponding combustion reaction rates involving oxygen. Steam is more reactive than carbon dioxide and this can be attributed to weak hydrogen bonds forming water molecules compared to the double bonds forming the carbon dioxide molecules. For binary mixtures of carbon dioxide/carbon monoxide and steam/hydrogen, it was found that the carbon monoxide and hydrogen respectively have a retarding affect on the reaction rates.

Different forms of the shrinking core model were investigated, with isothermal results, and the shrinking core model with a controlling surface reaction was shown to be the most applicable in the presence a typical gasification gas mixture. The validity of this model can be attributed to the core having an exceptional low porosity (Section 2.6) and consequently negligible penetration of the gases at the temperatures between 800 and 950 °C. This result is in agreement with results obtained for combustion.

It has been found that the gasification reaction rates (intrinsic) can be adequately described by Langmuir-Hinshelwood type rate equations and that established equations have been validated according to reliable data processing procedures.

In the case of carbon dioxide/carbon monoxide and steam/hydrogen gasification the inhibiting effect of the carbon monoxide and hydrogen respectively, have been included in the overall reaction rate equation.

The activation energies for both chars investigated was found to agree with some values published in the literature. In the case of carbon dioxide gasification, the activation energies were determined to be 109 and 136 kJ/mol for char A and B respectively. The activation energies obtained for steam gasification were determined to be 209 kJ/mol and 215 kJ/mol for char A and B respectively. The kinetics evaluated was also verified by successfully predicting the experimental burnoff results.

The adsorption enthalpies for steam gasification (69 kJ/mol for char A and 97 kJ/mol for char B) were found to be higher than those of carbon dioxide gasification (16 kJ/mol for char A and 41 kJ/mol for char B). The high values of adsorption enthalpies were attributed to higher reactivities observed for steam gasification compared to carbon dioxide gasification.

Experiments were done and models evaluated for a multicomponent gasification mixture consisting of a feed mixture of $CO/CO_2/H_2/H_2O$. Reaction parameters determined with results from the binary mixtures were used to predict results and it was found that the overall rate is best described with the assumption that the important reactions proceed on separate sites.

NOMENCLATURE

E	activation energy	$J.mol^{-1}$
$f(X)$	particle conversion model	-
$F(X)$	defined in 4.13	-
ΔH	enthalpy of adsorption	$J.mol^{-1}$
k_o	pre-exponential factor	s^{-1}
k_r	reaction rate constant	s^{-1}
K_{eq}	equilibrium constant for the water gas shift reaction	-
K_{CO_2}	adsorption constant for CO_2	Pa^{-1}
K_{CO}	adsorption constant for CO	Pa^{-1}
K_{H_2O}	adsorption constant for H_2O	Pa^{-1}
K_{H_2}	adsorption constant for H_2	Pa^{-1}
P_{CO_2}	partial pressure of CO_2	Pa
P_{H_2}	partial pressure of H_2	Pa
P_{H_2O}	partial pressure of H_2O	Pa
r	rate of reaction	s^{-1}
R	universal gas constant	$J.mol^{-1}.K^{-1}$
t	time	s
T	temperature	°C
X	conversion	-

Greek Letters

δ	stoichiometric coefficient	-

Abbreviations

SRCM	shrinking reacted core model
SUCM	shrinking unreacted core model
TGA	thermogravimetric analyser

REFERENCES

BANIN, V. E., MOORS, R. AND VEEFKIND, B. 1997. Kinetic study of high-pressure coal char combustion: Experiments and modelling. *Fuel* **76**(10): 945-949.

BARRIO, M., GOBEL, B., RISNES, H., HENRIKSON, U., HUSTAD, J. E. AND SORENSON, L. H. 2000. Steam gasification of wood char and the effect of hydrogen inhibition on the chemical kinetics. Nordic Seminar on the Thermochemical Conversion of Solid Fuels. Chamers University of Technology, Sweden.

BARRIO, M. AND HUSTAD J.E. 2000, CO_2 gasification of birch char and the effect of CO inhibition on the calculation of chemical kinetics. In: Bridgewater AV editor. Proceedings of the conference: Progress in Thermochemical Biomass Conversion, Tyrol, Austria.

BHAT, A., BHEEMARASETTI, R. J. V. AND RAO, R. T. 2001. Kinetics of rice husk char gasification. *Energy Conversion and Management* **42**: 2061-2069.

BLIEK, A. 1984. Mathematical modelling of a cocurrent fixed bed coal gasifier. PhD Thesis, University of Twente, The Netherlands.

DE GROOT, W. F. AND SHAFIZADEH, F. 1984. Kinetics of gasification of Douglas Fir and cottonweed chars by carbon dioxide. *Fuel* **63**(2): 210-216.

DUTTA S, WEN C.Y AND BELT R.J.J. 1977. Reactivity of coal and char. 1. Carbon dioxide atmosphere. *Ind Eng Chem Process*, **16**(1): 20-30.

ERGUN, S. AND MENTSER, M. 1965. Reaction of carbon with carbon dioxide and steam. *Chemistry and Physics of Carbon* **1**: 203-263.

ERGUN, S. 1956. Kinetics of the reaction of carbon dioxide with carbon. *J. Phys. Chem.* **60**: 480-485.

ESSENHIGH, R. H. 1988. An integration path for the carbon-oxygen reaction with internal reaction. *22nd symposium (International) on Combustion;* The combustion institute, Pittsburgh, PA, **22**: 89-96.

ESSENHIGH, R. H. 1991. Rate equation for the carbon-oxygen reaction: An evaluation of the Langmuir adsorption isotherm at atmospheric pressure. *Energy and Fuels* **5**: 41-48.

FU, W.B. AND WANG, Q.H. 2001. A general relationship between the kinetic parameters for the gasification of coal chars with CO_2 and coal type. *Fuel Processing Technology*, **72**: 63-77.

GADSBY, J., LONG, F., SLEIGHTON, P. AND SYKES, K. W. 1948. The mechanism of the carbon-carbon dioxide reactions. *Proc. Roy. Soc., (London)* **A193**: 357p.

GOLOVINA, E.S. 1980. The gasification of carbon by carbon dioxide at high temperatures and pressures. *Carbon*, **18**(3): 197-201

GOYAL, A., ZABRANSKY, R. F. AND REHMAT, A. 1989. Gasification kinetics of Western Kentucky bituminous coal char. *Industrial Engineering Chemistry*, **28**: 1767-1778.

GURURAJAN, V.S., ARGAWAL, P.K. AND AGNEW, J.B. 1992. Mathematical modelling of fluidised bed coal gasifiers. *Trans ICHemE*, **70**: 211-238.

HEMATI, M. AND LAGUERIE, C. 1988. Determination of the kinetics of the wood sawdust steam gasification of charcoal in a thermobalance, *Entropie*, **142**: 29-40.

HUTTINGER, K.J. AND MERDES, W.F. 1992. The carbon-steam reaction at elevated pressure:formations of product gases and hydrogen inhibitions, *Carbon*, **30**(6): 883-894.

JOHNSON, J. L. 1979. Kinetics of bituminous coal char gasification with gases containing steam and hydrogen. *Advances in Chemistry*, **137**: 145-178.

JOHNSON, J. L. 1981. In Chemistry of Coal Utilisation, Second Supp. Volume (Ed. M. A. Elliott), pp 1491-1598 (Willey Inter. Science, New York).

KAPTEIJN, F. AND MOULIJN, J. A. 1992. Transient kinetic techniques for detailed insight in gas solid reactions. *Energy and Fue*l, **6**: 494-497.

KOVACIK, C. CHAMBERS, A. AND OZUM, B. 1991. Gasification kinetics of two Alberta coal chars. *Can. J. Chem. Eng.*, **69**: 811-815.

KWON, T.W., KIM, S.D. AND FUNG, D.P.C. 1988. Reaction kinetics of char-CO_2 gasification. *Fuel*, **67**(4): 530-535.

LAURENDEAU, N. M. 1978. Heterogeneous kinetics of coal char gasification and combustion. *Prog. Energy Combust. Sci.*, **4**: 221-270.

LILIEDAHL, T. AND SJOSTROM, K. 1997. Modelling of char-gas reaction kinetics. Fuel, **76**(1): 29-37.

MA, Z., ZHANG, C., ZHU, Z. AND SUN, E. 1992. A study on the intrinsic kinetics of gasification of Jincheng coal char. *Fuel Processing Technology*, **31**(1): 69-76.

MATSUI. I, KOJIMA, T., KUNII, D. AND FURUSAWA, T. 1987. Study of char gasification by carbon dioxide. 2. Continuous gasification in fluidised bed. *American Chemical Society*, **26**(1): 95-100.

MARQUEZ, F.M., CORDERO, T., MIRASOL, J.R. AND RODR'IGUEZ, J.J. 2002. CO_2 and steam gasification of a grapefruit skin char. *Fuel*, **81**: 423-429.

MEIJER, R. 1992. Kinetics and mechanism of the alkali-catalysed gasification of carbon. Thesis. University of Amsterdam.

MIURA, K., HASHIMOTO, K. AND SILVESTON, P. L. 1989. Factors affecting the reactivity of coal char during gasification, and indices representing reactivity. *Fuel*, **68**(11): 1461-1475.

MOLINA, A. AND MONDRAG'ON, F. 1998. Reactivity of coal gasification with steam and CO_2. Fuel, **77**(15): 1831-1839.

MUGGE, J., BOSCH, H. AND REITH, T. 2001. Measuring and modelling gas adsorption kinetics in single porous particles. *Chemical Engineering Science*. **56**: 5351-5360.

MUHLEN, H. J, VAN HEEK, K. H. AND JUNTGEN, H. 1985. Kinetic studies of steam gasification of char in the presence of H_2, CO_2 and CO. *Fuel*, **64**(7): 944-949.

OLLERO, P., SERRERA, R., ARJONA, R. AND ALCANTARILLA, S. 2002. Diffusional effects in TGA gasification experiments for kinetic determination. *Fuel*, **30**(1): 1-12.

OSAFUME, K. AND MARSH, H. 1988. Gasification kinetics of coal chars in carbon dioxide. *Fuel*, **67**(3): 384-388.

PLANTE, P., ROY, C. AND CHORNRT, E. 1988. CO_2 gasification of wood charcoals derived from vacuum and atmospheric pyrolysis, *The Canadian Journal of Chemical Engineering*, **66**: 307-312.

REIF, A. E. 1952. The mechanism of carbon dioxide-carbon reaction. *Journal of Physical Chemistry*, **60**: 785-792.

SINAG, A., SINEK, K., TEKES, A.T., MISIRLIOGLU, Z., CANEL, M. AND WANG, L. 2003. Study on CO2 gasification reactivity of chars obtained from Soma-Isiklar lignite (Turkey) at various coking temperatures. *Chemical Engineering and Processing*, **42**: 1027-1031.

SHUFEN, L. AND RUIZHENG, S. 1994. Kinetic studies of lignite char pressurised gasification with CO_2, H_2 and steam. *Fuel*, **69**(9): 413-416.
SMITH, I.W., 1982. The combustion of coal char: A review, *11th Symposium (International) on combustion*, The Combustion Institute, Pittsburgh, PA, 1045.

STANDISH, N. AND TANJUNG, A.F.A., 1988. Gasification of single wood charcoal particles in CO_2. *Fuel*, **67**(5): 666-672.

TAKARADA, T., TAMAI, Y. AND TOMITA, A. 1985. Reactivities of 34 coals under steam gasification. *Fuel*, **64**(10): 1438-1442.

WALKER, P. L., RUSINKO, F. AND AUSTIN, L. G. 1959. Advances in Catalyses. Eley, O. D., Selwood, P. W. and Weisz, P. B., Eds. Academic Press, Inc. New York and London. Pp 134-221.

WEEDA, M., ABCOUWER, H. H., KAPTEIJN, F. AND MOULIJN, J. A. 1993. Steam gasification kinetics and burn-off behaviour for a bituminous coal derived char in the presence of H_2. *Elsevier Science Publishers* , **93**: 235-241.

WEEDA, M. 1995. Kinetics of coal gasification under industrial conditions. PhD Thesis, University of Amsterdam.

WIGMANS, T. 1982. Catalytic gasification of carbon, a mechanistic study. PhD Thesis, University of Amsterdam.

WHITTY, K. J. 1997. Pyrolysis and gasification behaviour of black liquor under pressurised conditions, Academic Dissertation, Report 97-3, *Abo Akademi*, Department of Chemical Engineering.

YAN, H. M., HENDREICH, C. AND ZHANG, D. K. 1998. Effect of combustion product distribution coefficient on the modelling of fluidised bed coal gasifiers. *Autralian Chemical Engineering Conference. CHEMECA'98.*

YE, D. P., AGNEW, J. B. AND ZHANG, D. K. 1998. Gasification of a South Australian low-rank coal with carbon dioxide and steam: kinetics and reactivity studies. *Fuel*, **77**(11): 1209-1219.

CHAPTER 5

GENERAL CONCLUSIONS AND RECOMMENDATIONS

5.1 GENERAL CONCLUSIONS

A detailed characterisation of two chars, used in this study, revealed that the ash content is exceptionally high and was found to be 48 % and 67% for char A and B respectively. The average particle size of char A is 70 μm and that of char B was 20 μm. Both chars have very low porosities (< 5%) and can be regarded as impervious. The mineral content of the ash shows large contents of calcium and sulphur and to a lesser extent in iron compared to other South African coals. Microscopic inspection of the chars show that the char particles are a collection of mainly carbon rich particles (< 10% minerals) and mineral rich particles (<10% carbon), This was more pronounced for char A than for char B.

The combustion of the high-ash chars was studied up to 560 ˚C at atmospheric condition and agreed with a surface reaction controlled shrinking unreacted core model, which was both concluded from isothermal and non-isothermal experiments. The relevant reaction kinetic parameters associated with this model were derived from non-isothermal experiments and quantified using a conventional and a newly developed non-isothermal method. The new method is based on a two-step regression and is capable of testing a reaction rate model requiring fewer experiments with shorter time durations. A full set of reaction rate parameters were obtained for the shrinking core model. Activation energies compared well with literature and the difference between the two chars was small, which indicates an insignificant catalytic affect despite the different minerals composition. The dependence on oxygen partial pressure was found to differ only slightly from unity. The values of the pre-exponential factor were also determined and differ for the two chars examined. This could be attributed to the different surface properties of both chars.

The reaction with steam and carbon dioxide were the most important reactions in the gasification of the two chars. These, relative slow gasification reactions, were studied

between 800 and 950 °C at atmospheric conditions and could also be modelled with a surface reaction controlled shrinking unreacted core model. Langmuir-Hinshelwood type of reaction rate equations described both reactions effectively. The carbon dioxide and steam gasification rate decreased in the presence of the products carbon monoxide and hydrogen respectively. The activation energies for both chars did not differ significantly and were higher for steam gasification than for carbon dioxide gasification, again indicating the insignificant effect that the minerals in the ash have on the reaction rate of the chars. The adsorption enthalpies for steam gasification were found higher than those of carbon dioxide gasification and can possibly explain the higher reaction rate in steam gasification. Heats of reaction are different for different chars and depend on the nature of sites and its population. If both gasification reactions occur simultaneously in the presence of both reactants and products, the overall rate is best described with the assumption that the important reactions proceed on separate sites.

5.2 RECOMMENDATIONS

In this investigation, a thorough characterisation and reaction kinetic study has been carried out for two chars with high ash contents. In order to establish any uniqueness of high ash chars, it is recommended that more char samples of different ash contents must be characterised as this will provide useful information on the reactivity (pre-exponential factor, activation energy, heat of adsorption) of the char in relation to the ash content and mineral composition of the char. A detailed, microscopic, characterisation of the carbon surface, again in relation with the most important reaction kinetic rate parameters is also recommended.

Further, it is proposed that the combustion and gasification experiments are carried out with larger char particles in order to simulate the conditions in a fluidised bed gasifier better. To account for the effect of internal- and external diffusion, more pronounced for larger particles, it is also recommended to study these aspects.

Since the reaction model and associated parameters have been determined in this investigation, it is important to test the validity of these reaction kinetic rate expressions with experiments on pilot plant scale. Ultimately, the determined reaction kinetic rate expressions should be incorporated into a reactor model including heat balances, hydrodynamics and other important factors, needed for the design of a fluidised bed reactor with a high ash coal as a feed stock.

APPENDIX A

RESULTS OF THE NON-ISOTHERMAL COMBUSTION EXPERIMENTS

A.1 Introduction

In this appendix the results of the non-isothermal experiments are presented. Only two chars were evaluated: char A and char B. Heating rates were varied from 1 °C/min to 4 °C/min. The different heating rates were also combined with five different oxygen fractions in the feed stream: 21%, 40%, 60%, 70% and 100% oxygen. First, all the results for char A will be shown and will be followed by char B results under identical conditions.

A.2 Non-isothermal combustion of Char A

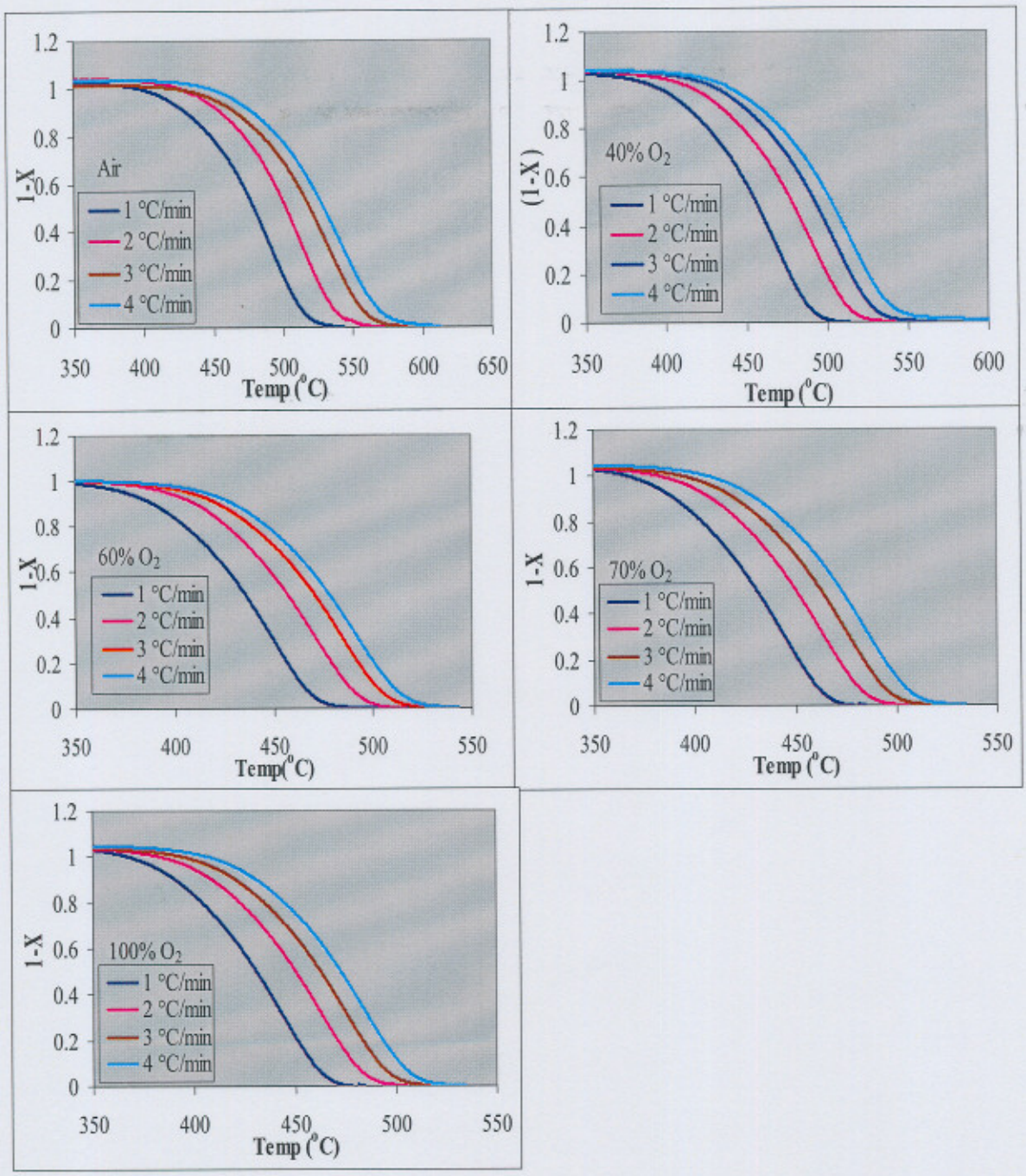

A.3 Non-isothermal combustion of Char B

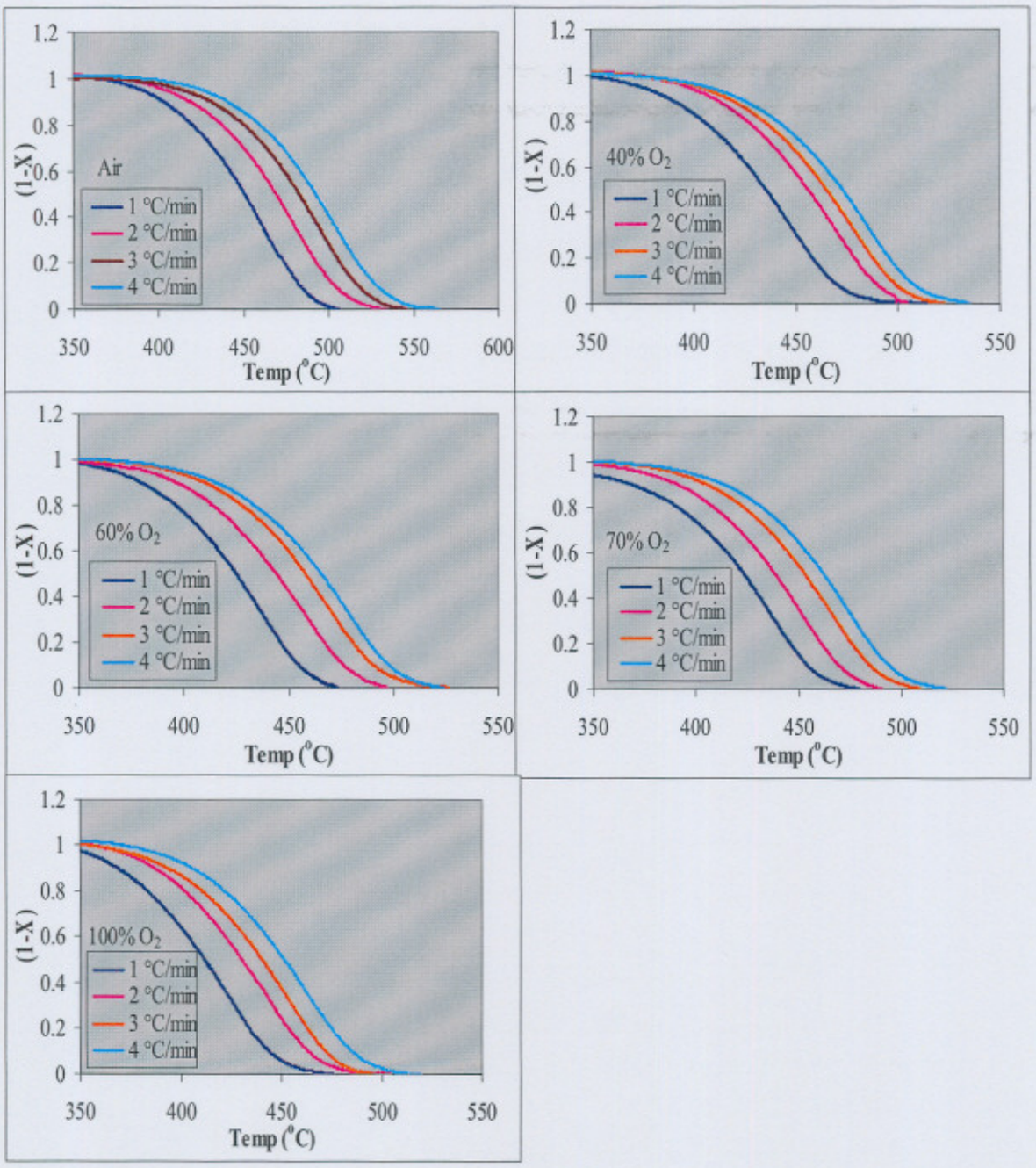

APPENDIX B

EVALUATION OF ACTIVATION ENERGY FROM NON-ISOTHERMAL DATA-METHOD OF FLYNN AND WALL

B.1 Introduction

In this appendix the results of the activation energy calculations by the method of Flynn and Wall are presented. This method uses non-isothermal data for all the evaluations. The data obtained from both chars is presented here. Evaluations were conducted between 1 ^{o}C/min and 4 ^{o}C/min. For each char studied five figures were obtained since five different partial pressures were studied.

On each figure there is a series of linear data fits, the slope of which provides the value of the activation energy through easy manipulation, as was described in Chapter 3. Linear fits are done for data at corresponding conversion levels, obtained from experiments at different heating rates. A wide range of experimental conditions is therefore covered by a single evaluation.

B.1 Non-isothermal combustion of char A

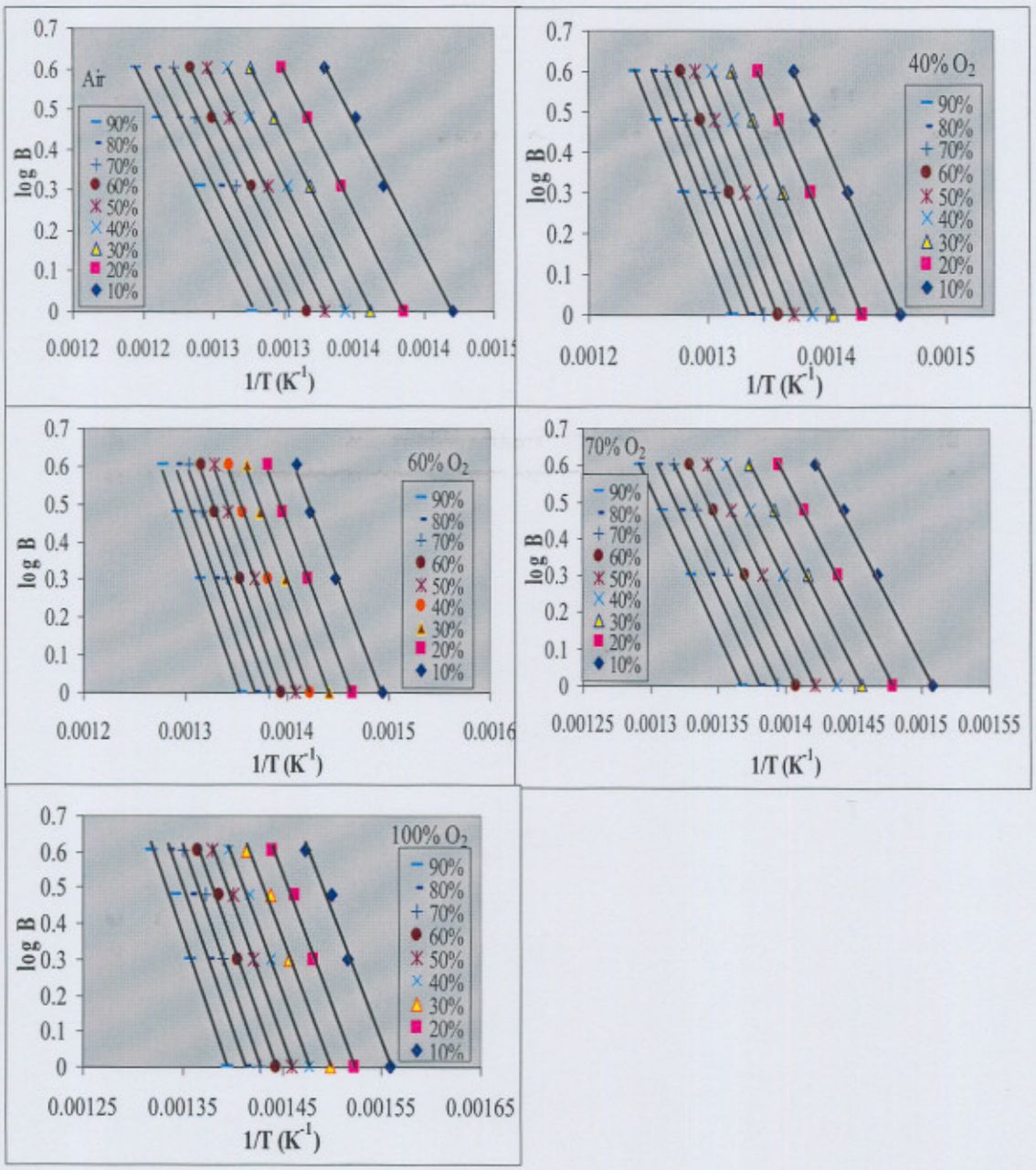

B.2 Non-isothermal combustion of char B

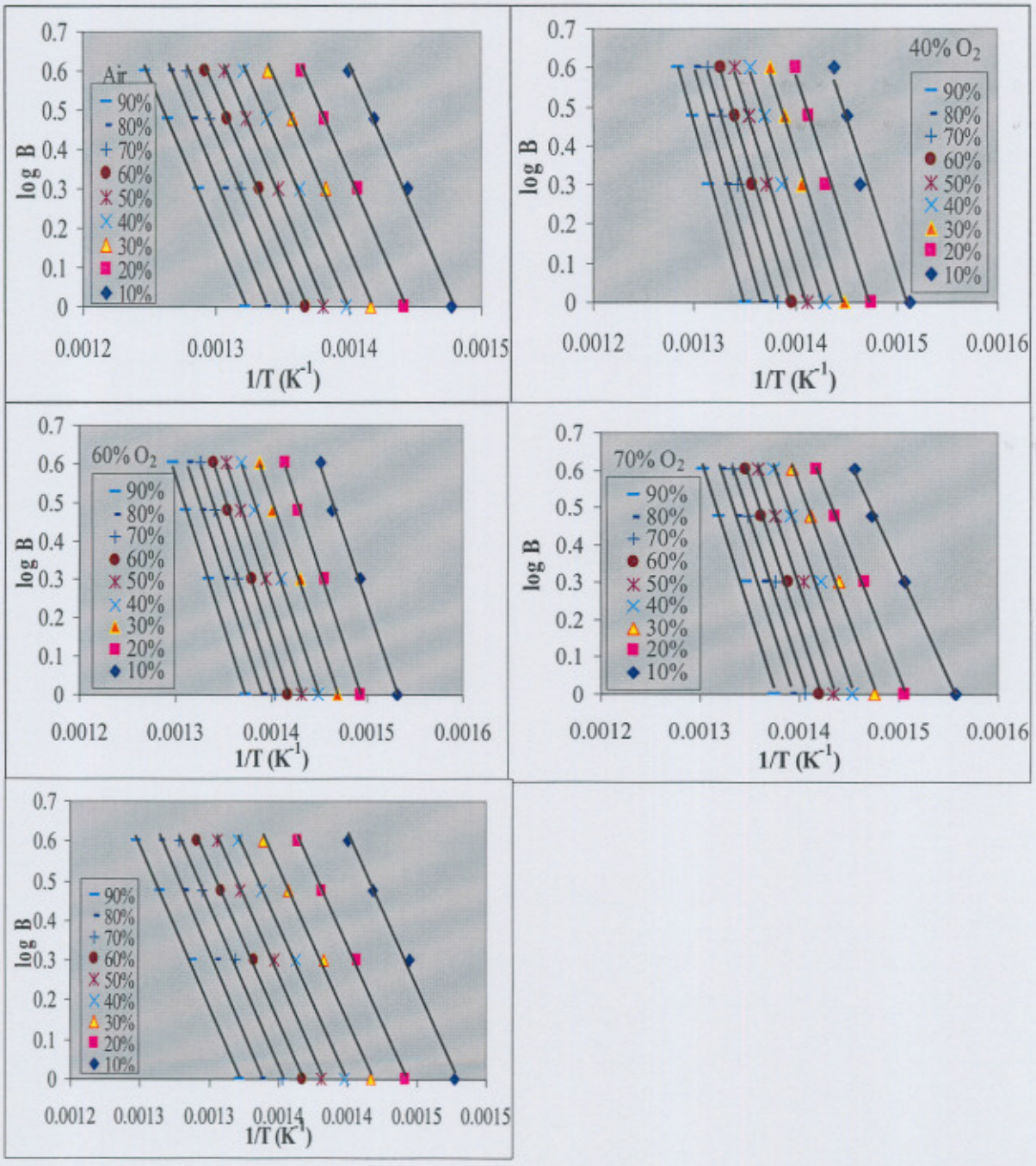

APPENDIX C

EVALUATION OF THE CONVERSION MODEL

C.1 Introduction

In this non-isothermal work the function F(X) representing the char conversion behaviour is fitted against p(y) which is a function of activation energy. The F(X) values were obtained from the reaction controlled shrinking unreacted-core model. The results are displayed for five oxygen partial pressures evaluated.

Each oxygen partial pressure consists of a presentation with four lines representing different heating rates used. First, the experiments of char A are shown and char B experiments follows them.

C.2 Reaction model evaluations for char A

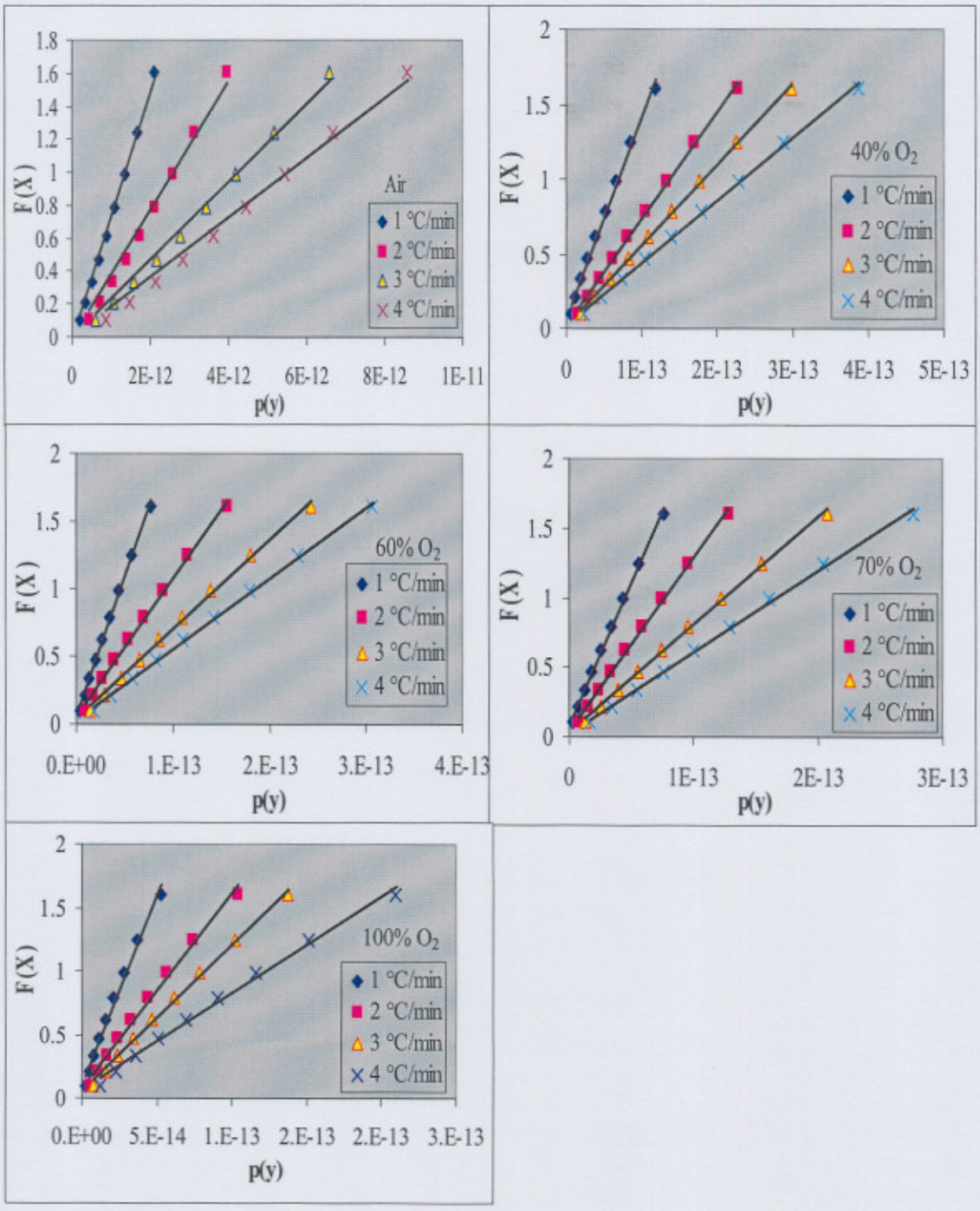

C.3 Reaction model evaluations for char B

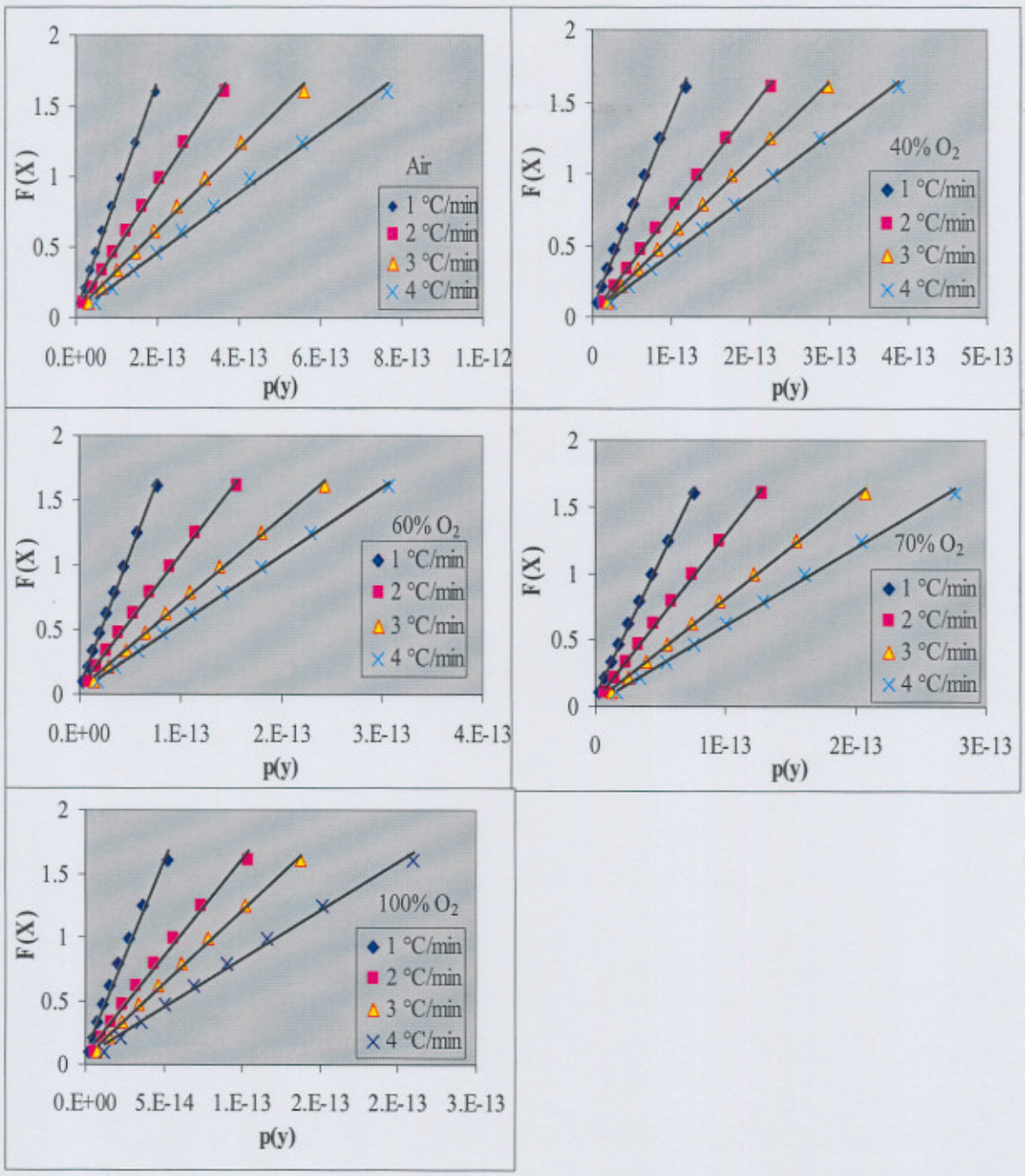

APPENDIX D

EVALUATION OF THE OVERALL KINETIC RATE EQUATION FROM NON-ISOTHERMAL DATA

D.1 Introduction

In this appendix the char experimental data is plotted against the calculated data from the model evaluated. In this way the correctness and the validity of the model can be assessed. Experiments were conducted for 21%, 40%, 60%, 70% and 100% oxygen between 1 K/min and 4 K/min. For each oxygen concentration a plot of (1-X) versus temperature at different heating rates is constructed.

First the burnoff behaviour for char A is shown for all conditions evaluated and then char B results follows. For all results shown the shrinking unreacted-core reaction model was used.

D.2 Burnoff behaviour for char A

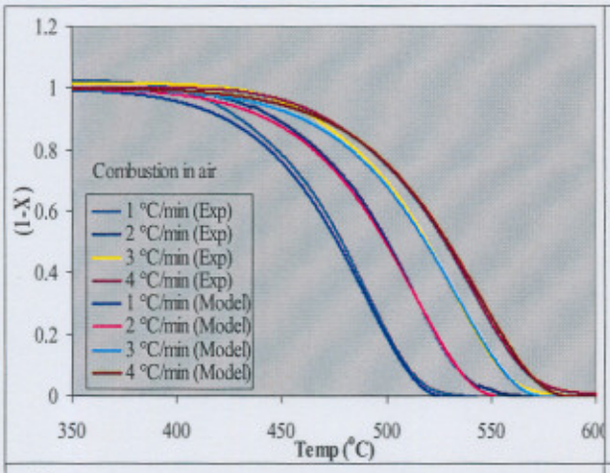

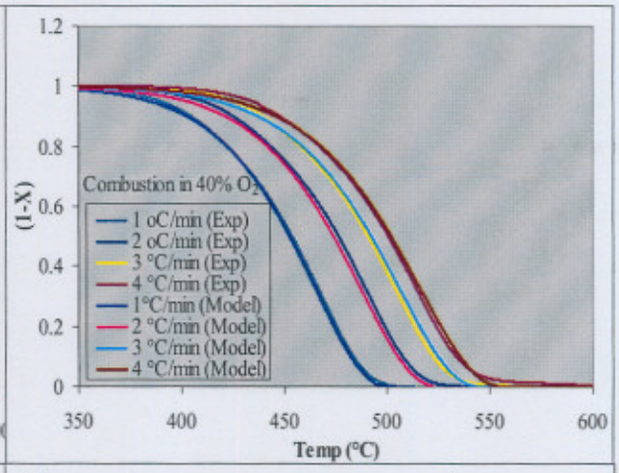

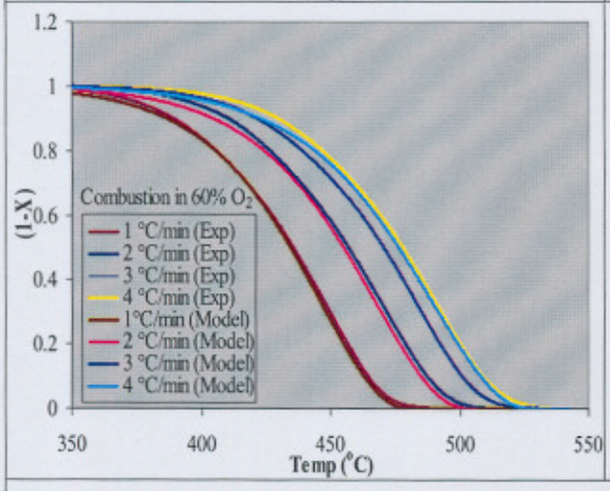

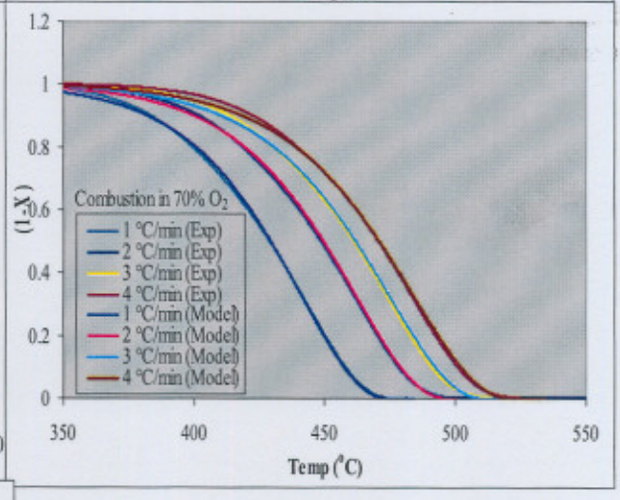

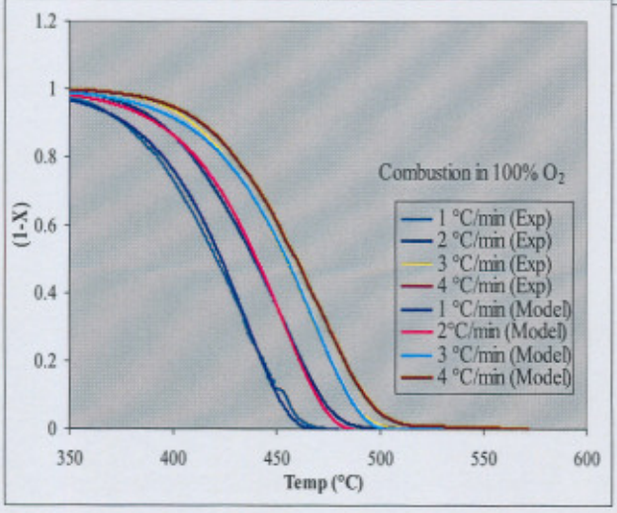

D.3 Burnoff behaviour for char B

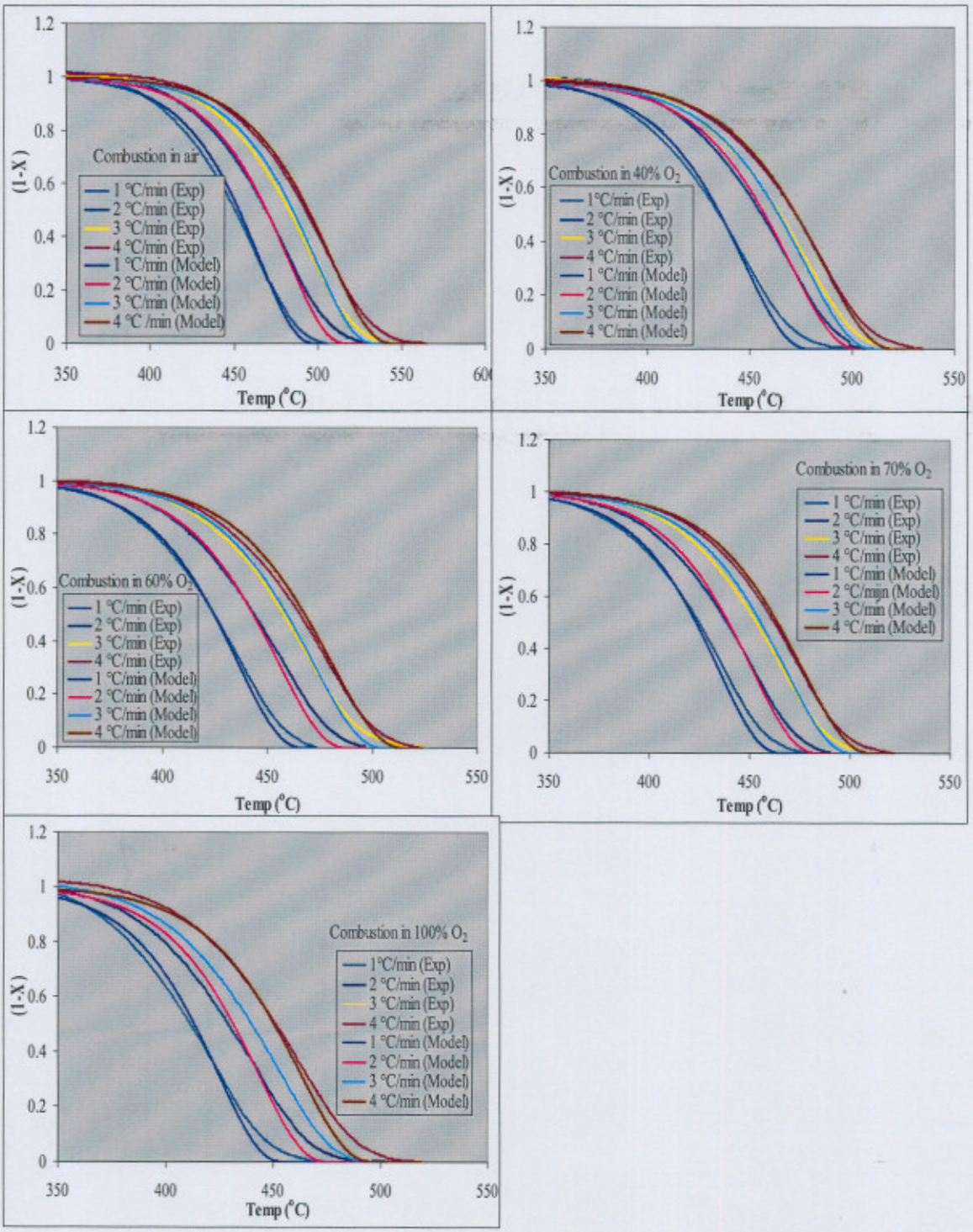

APPENDIX E

EVALUATION OF THE OVERALL KINETIC RATE EQUATION FROM NON-ISOTHERMAL REGRESSION DATA

E.1 Introduction

In this appendix, the char experimental data is plotted against the calculated data from the regression model evaluated. In this way the correctness and the validity of the model can be assessed. Experiments were conducted for 21%, 40%, 60%, 70% and 100% oxygen between 1 K/min and 4 K/min. For each oxygen concentration a plot of (1-X) versus temperature at different heating rates is constructed.

First the burnoff behaviour for char A is shown for all conditions evaluated and then char B results follows. For all results shown the shrinking unreacted-core reaction model was used.

E.2 Burnoff behaviour for char A

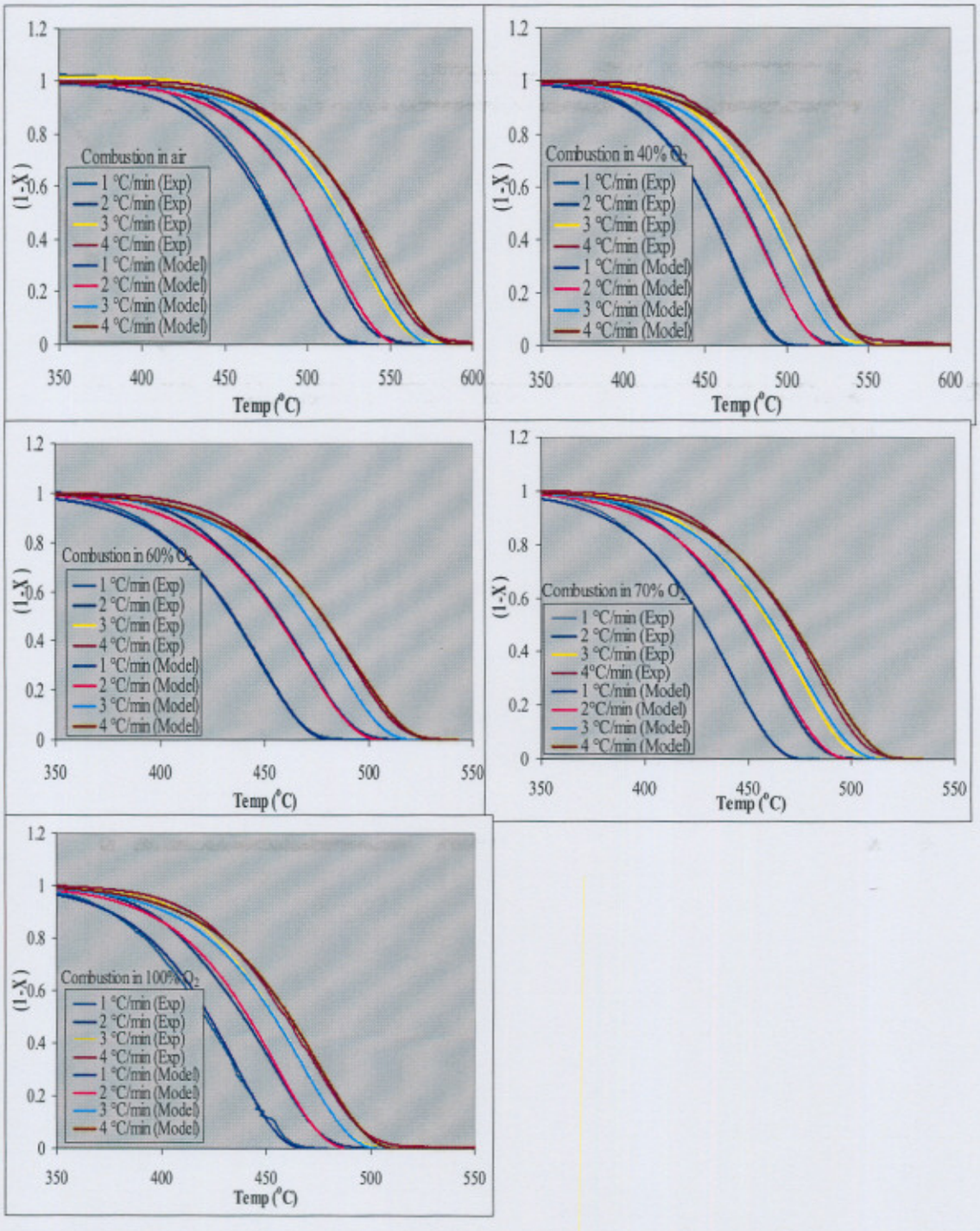

E.3 Burnoff behaviour for char B

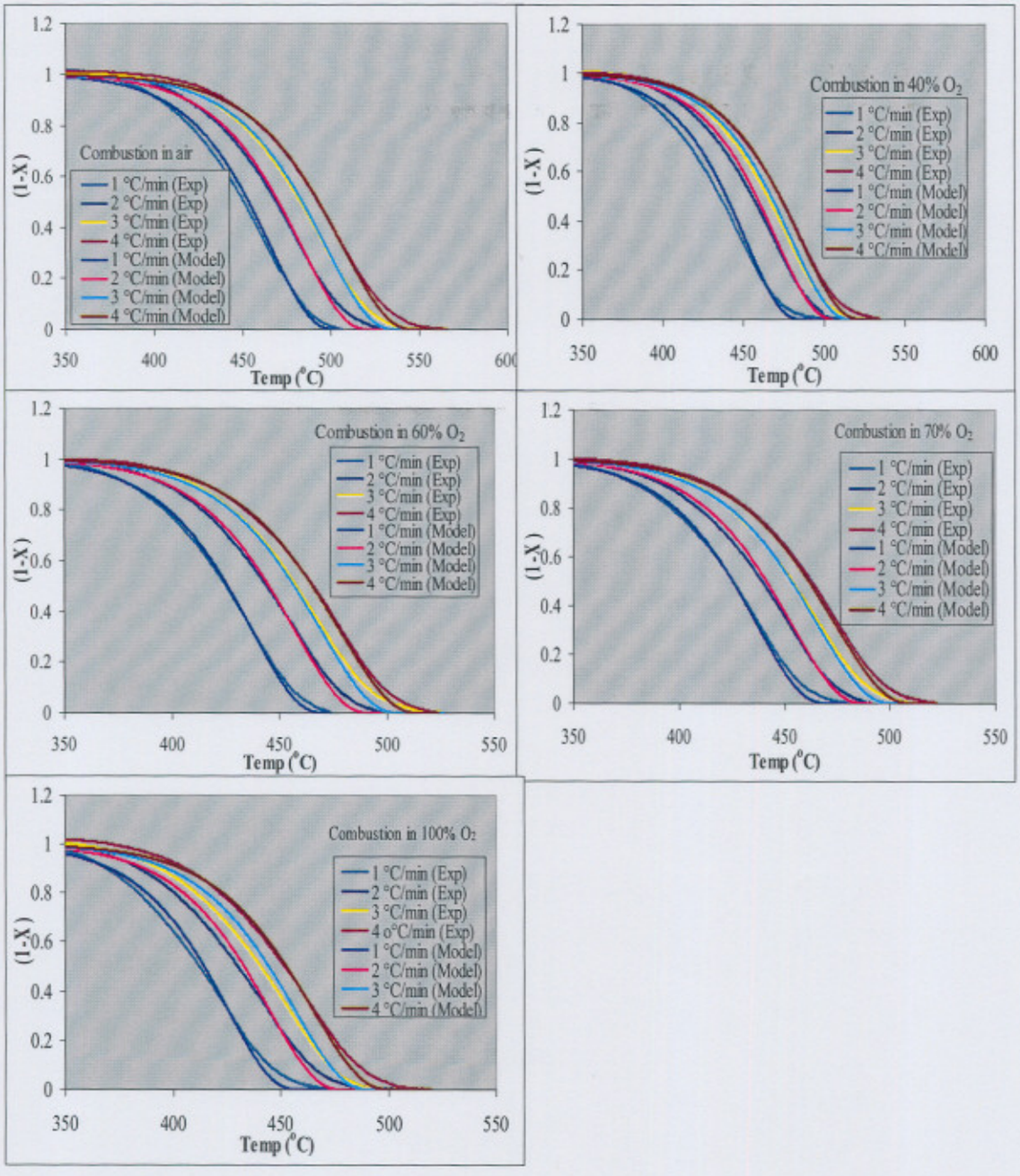

APPENDIX F

CHAR CONVERSION BEHAVIOR UNDER CARBON DIOXIDE GASIFICATION

F.1 Introduction

In this appendix all the results from the isothermal CO_2 gasification are presented in the form of plots of conversion against time for various process temperatures. Experiments were conducted for both char A and char B. All experiments were performed at temperatures between 800^0C and 950^0C at various CO_2 concentrations. In this appendix results obtained from both chars are presented.

F.2 Burnoff curves for char A CO_2 gasification

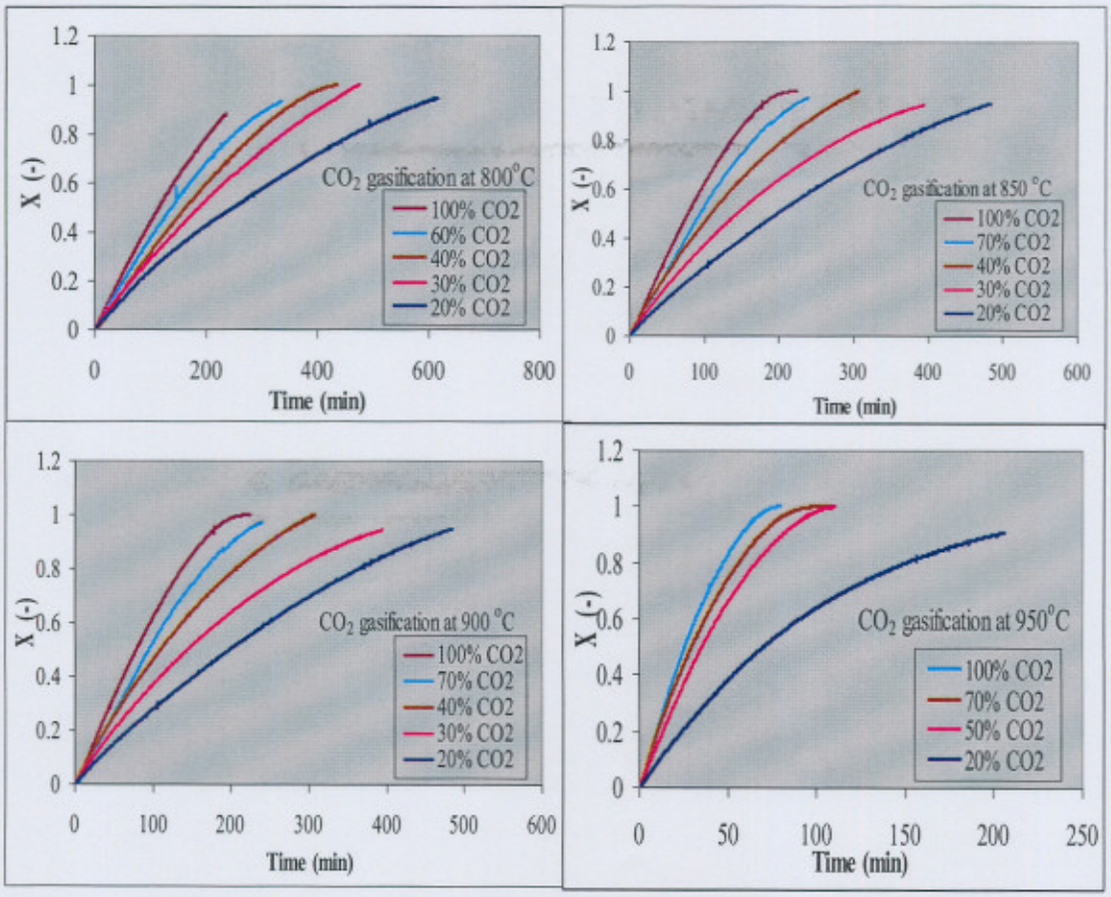

F.3 Burnoff curves for char B CO_2 gasification

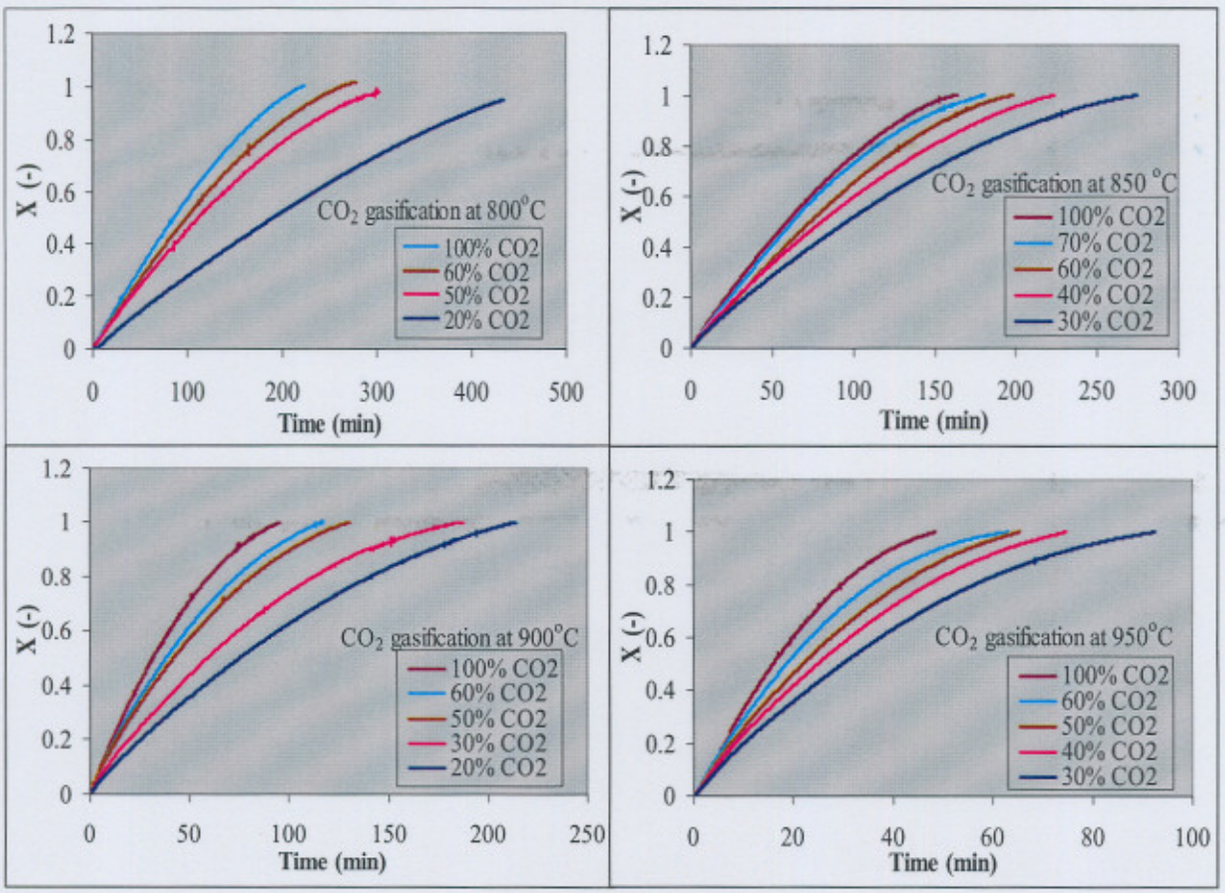

APPENDIX G

VALIDATION OF THE SHRINKING UNREACTED-CORE REACTION MODEL FOR CARBON DIOXIDE GASIFICATION

G.1 Introduction

In this appendix the shrinking unreacted-core reaction model is validated. This is done by plotting the experimental data of conversion as a function of dimensionless time on the same set of axis with the conversion-dimensionless time data based on the unreacted-core shrinking model.

Plots were constructed for all CO_2 concentrations at different temperatures used. In the first part of this appendix char A results are given followed by char B results.

G.2 Model validation for char A CO_2 gasification

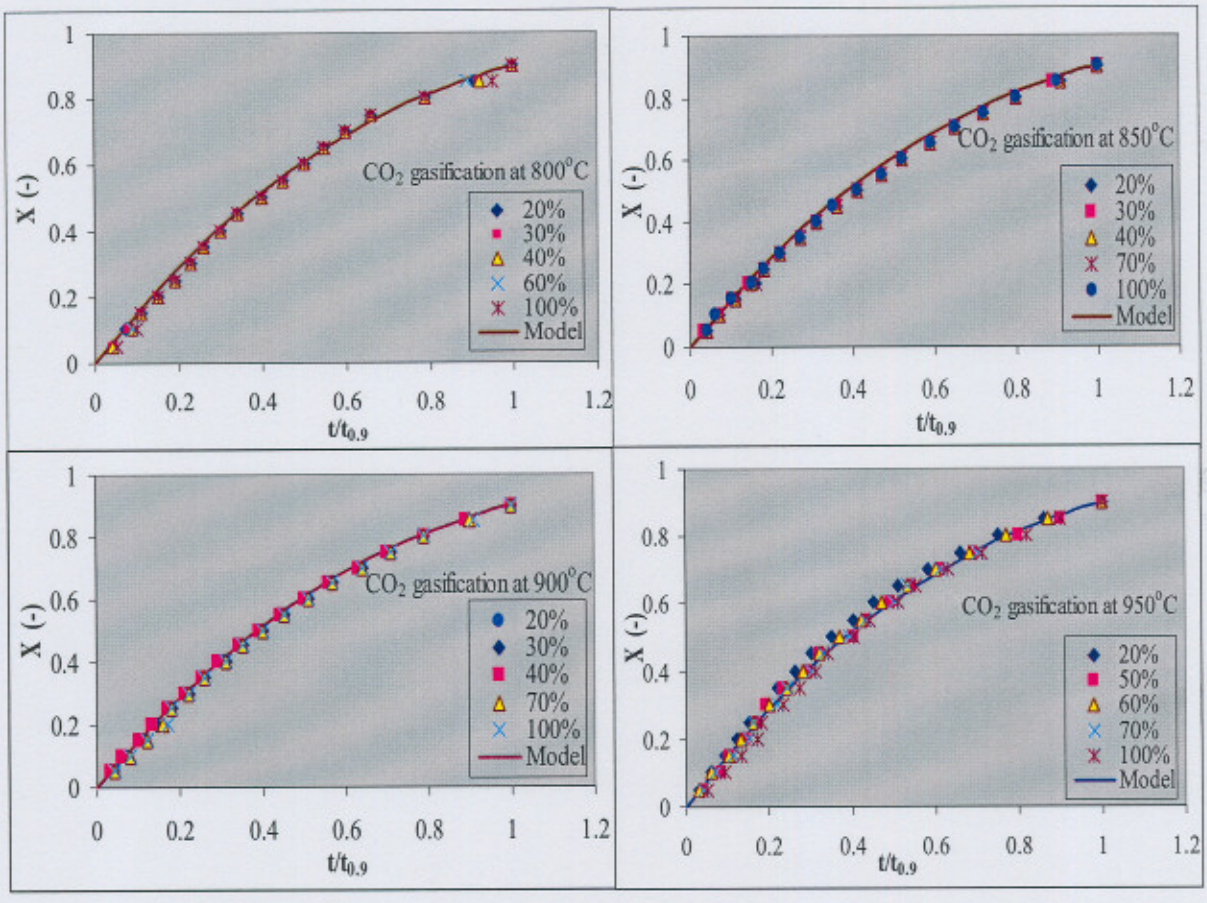

G.3 Model validation for char B CO_2 gasification

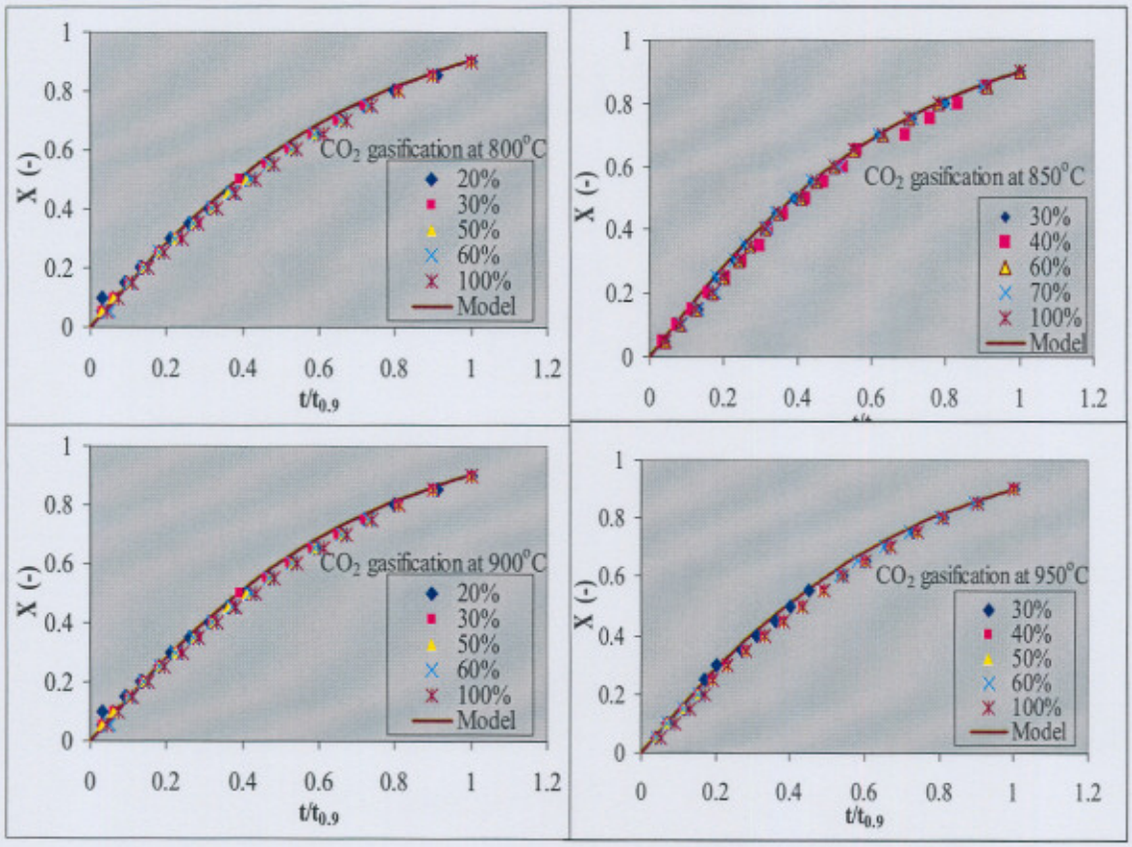

APPENDIX H

THE SHRINKING UNREACTED-CORE REACTION MODEL FOR CARBON DIOXIDE GASIFICATION

H.1 Introduction

In this appendix the char conversion model plots are presented. The char conversion model used is the shrinking unreacted-core reaction model. Experiments are presented for char A and char B at temperatures between 800 °C and 950 °C. All experiments were conducted at CO_2 concentrations between 20% to 100% CO_2.

H.2 Char A conversion model for CO_2 gasification

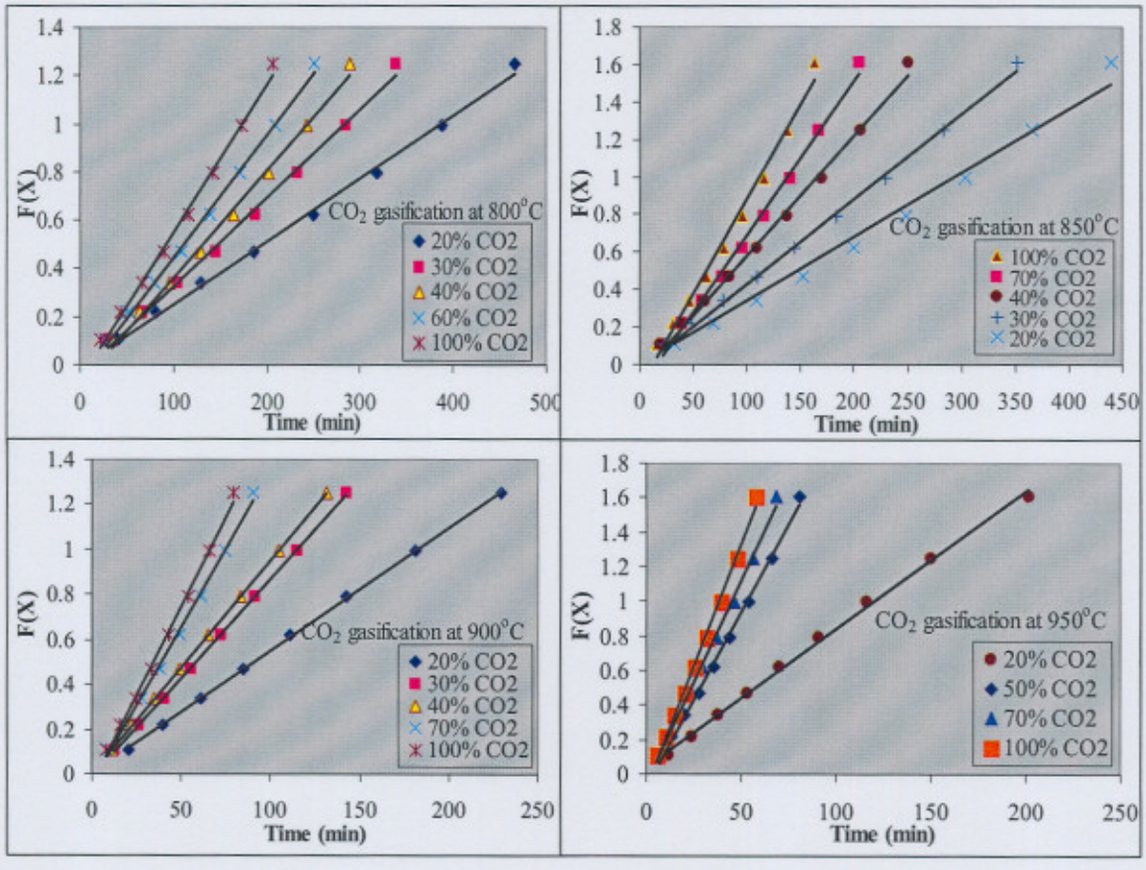

H.3 Char B conversion model for CO_2 gasification

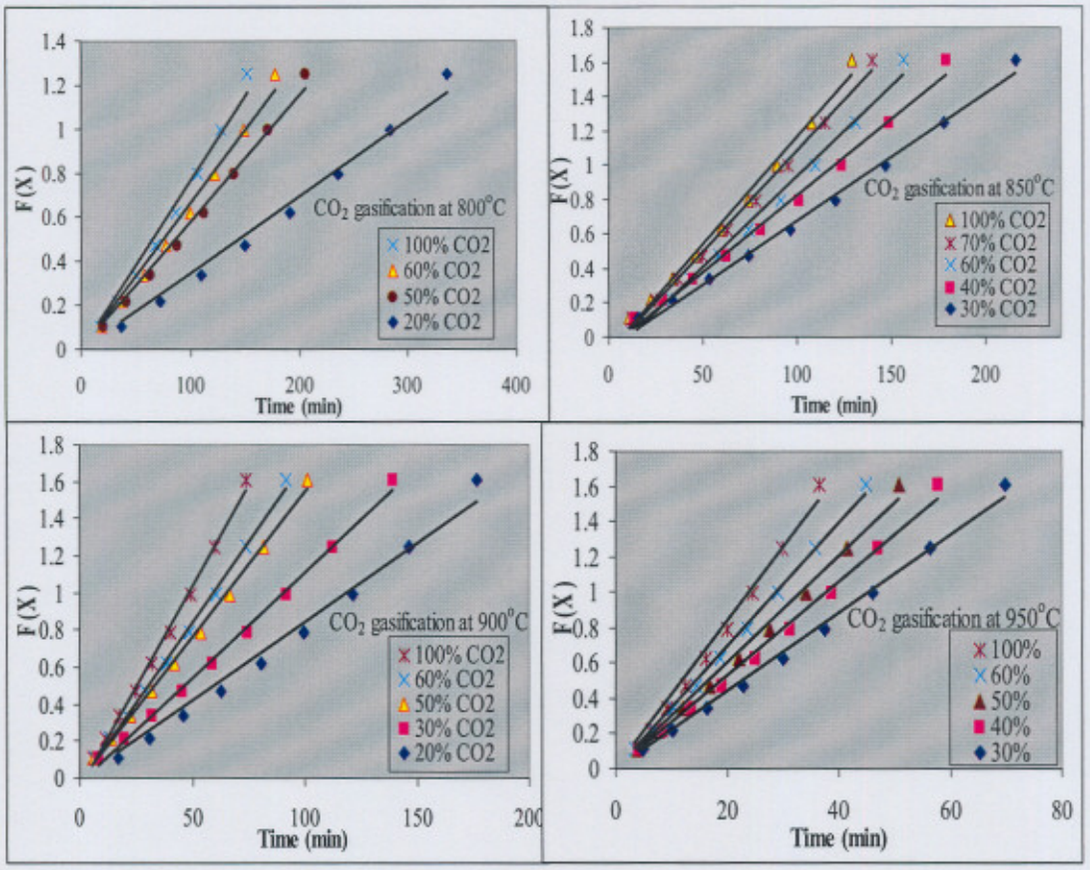

APPENDIX I

VALIDATION OF CARBON DIOXIDE GASIFICATION KINETICS

I.1 Introduction

In this appendix all the obtained kinetic parameters were fitted into the derived Langmuir-Hinshelwood model. This was done in order to predict accuracy of the kinetic parameters calculated. For each experiment conducted a plot of X versus time is plotted using the experimental data that is then fitted against the data predicted by the model.

Plots were constructed for temperature points between 800°C and 950°C at CO_2 concentrations ranging from 20% to 100% CO_2. Char A results are presented first and are followed by char B results.

I.2 Burnoff curves for char A CO_2 gasification at 800 °C

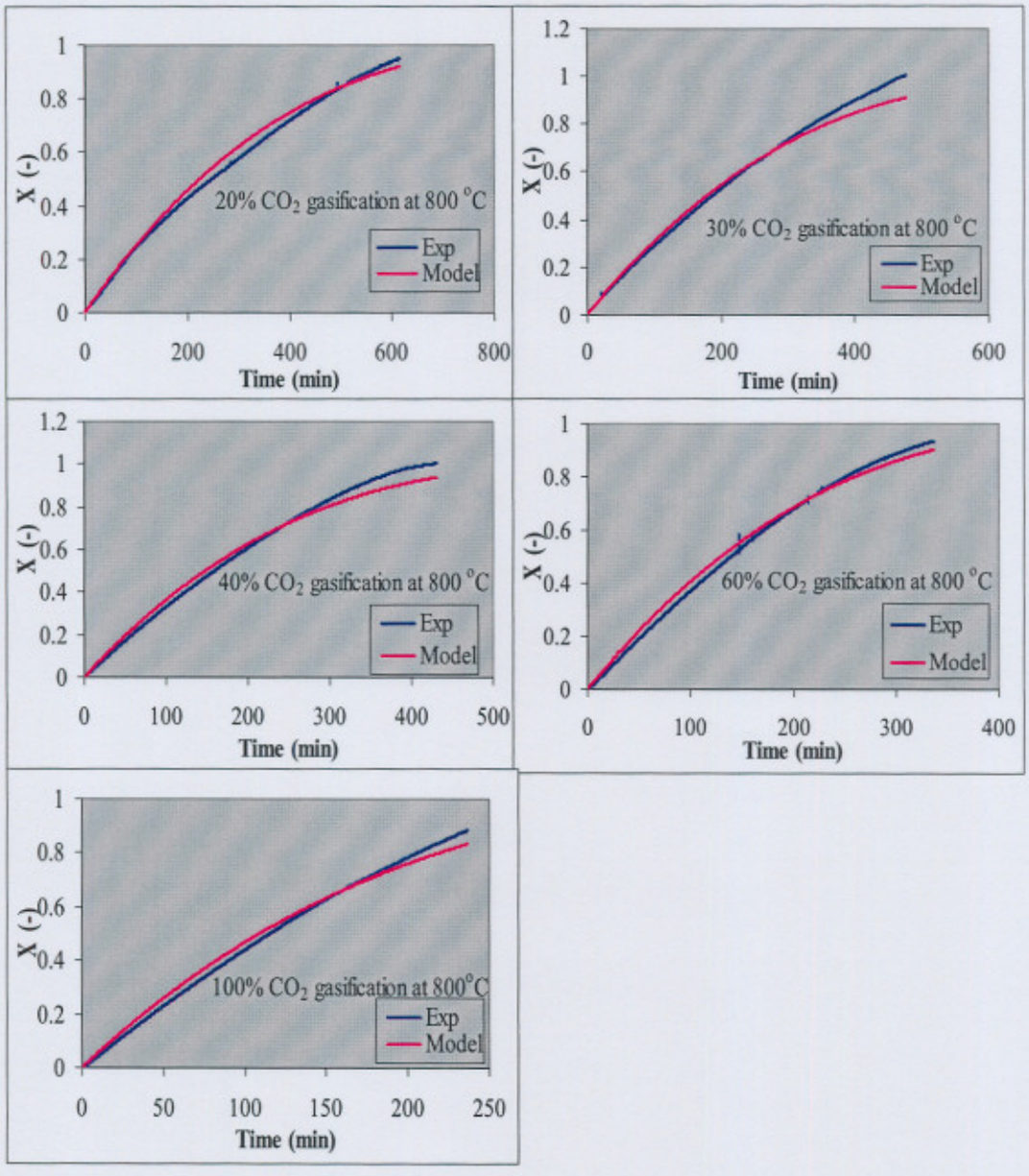

I.3 Burnoff curves for char A CO_2 gasification at 850 °C

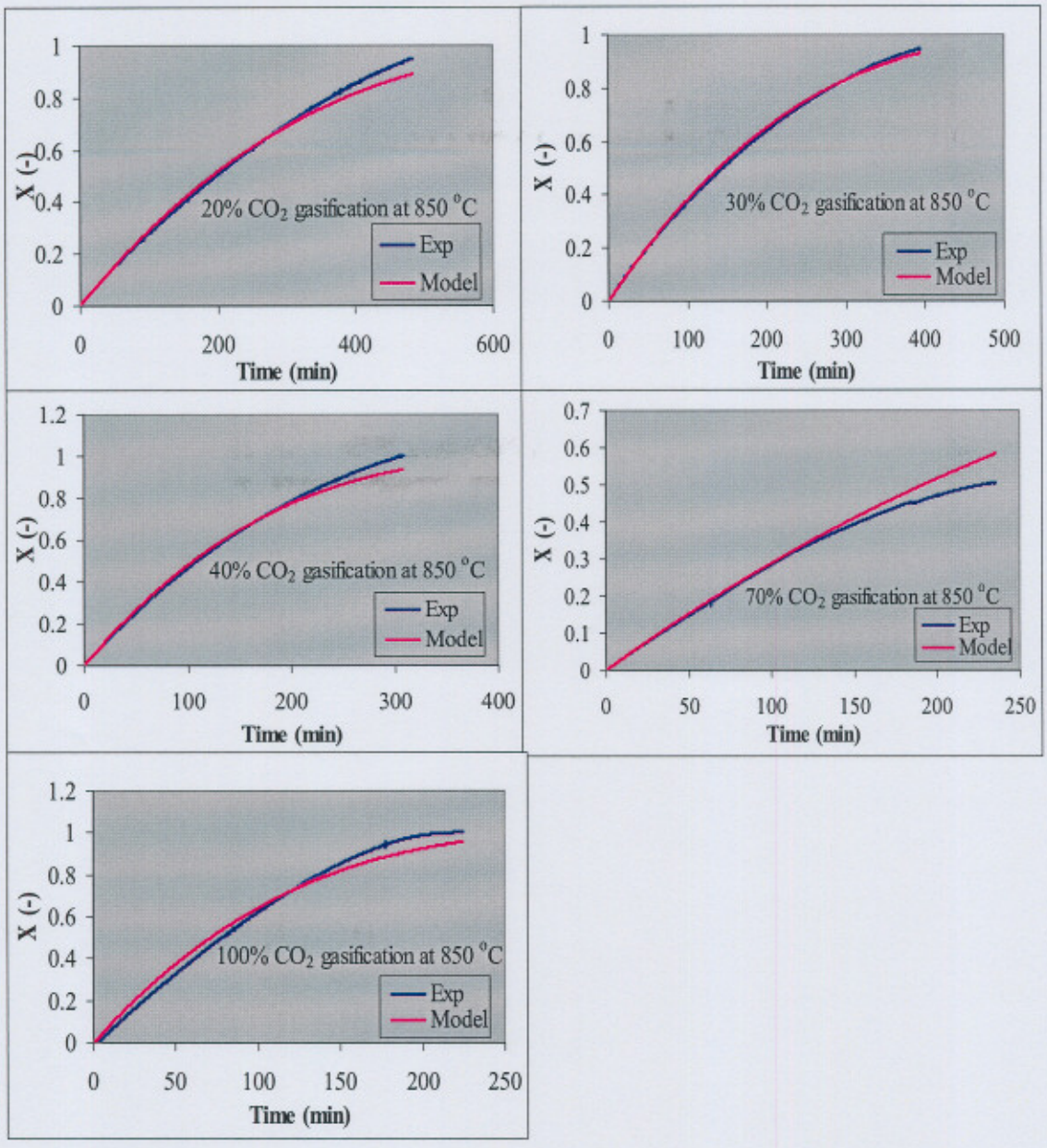

I.4 Burnoff curves for char A CO_2 gasification at 900 °C

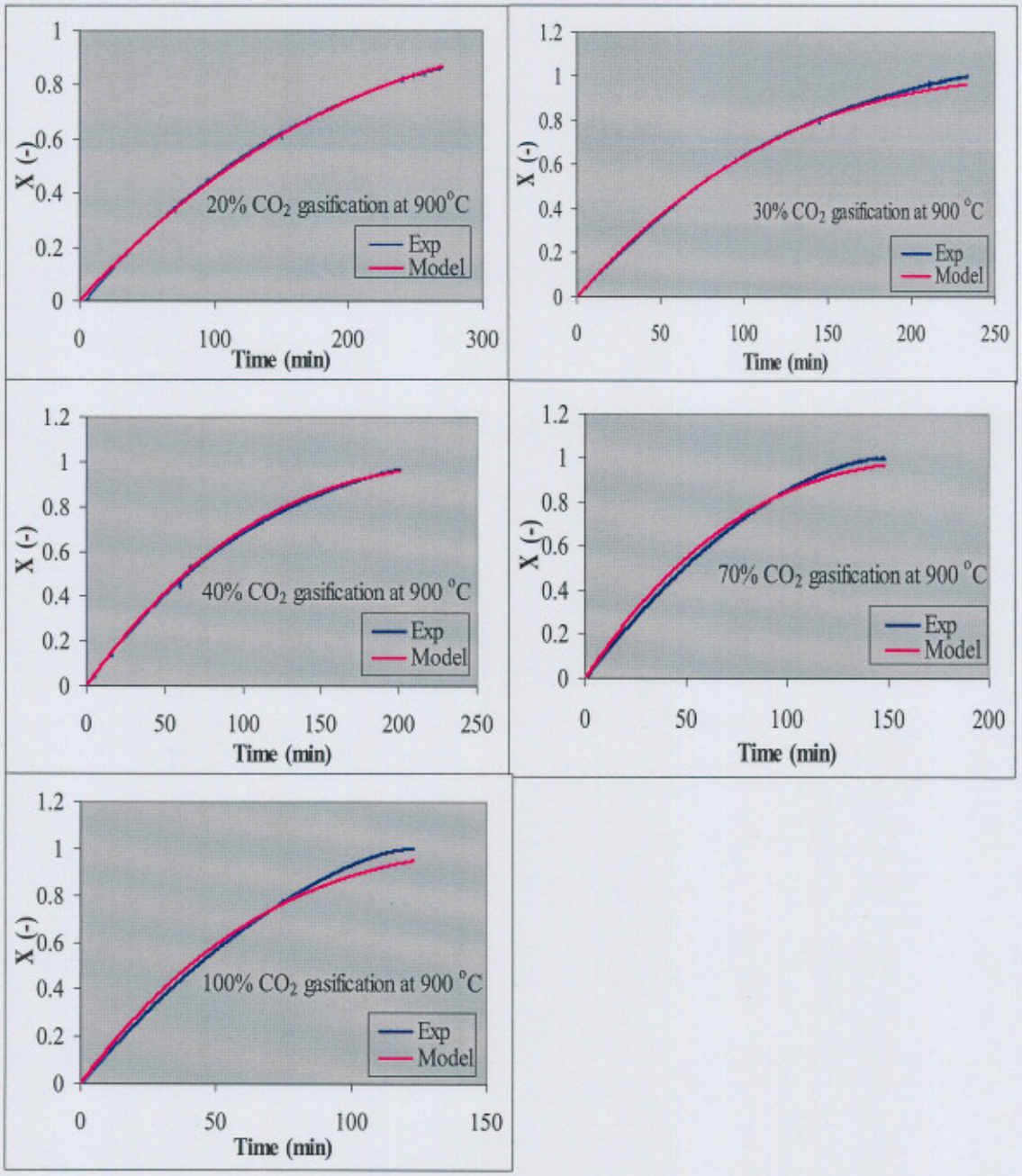

I.5 Burnoff curves for char A CO_2 gasification at 950 °C

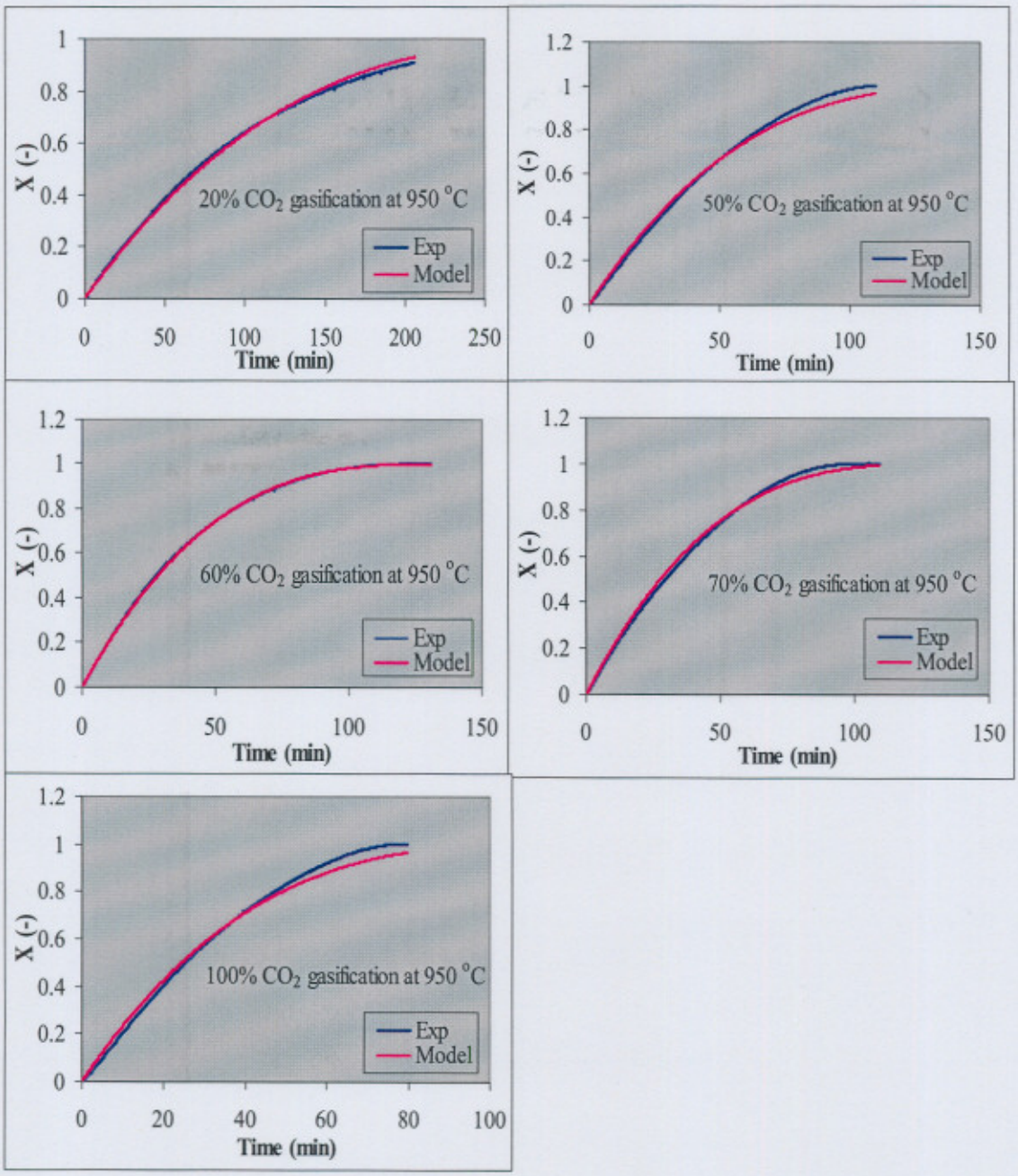

I.6 Burnoff curves for char B CO_2 gasification at 800 °C

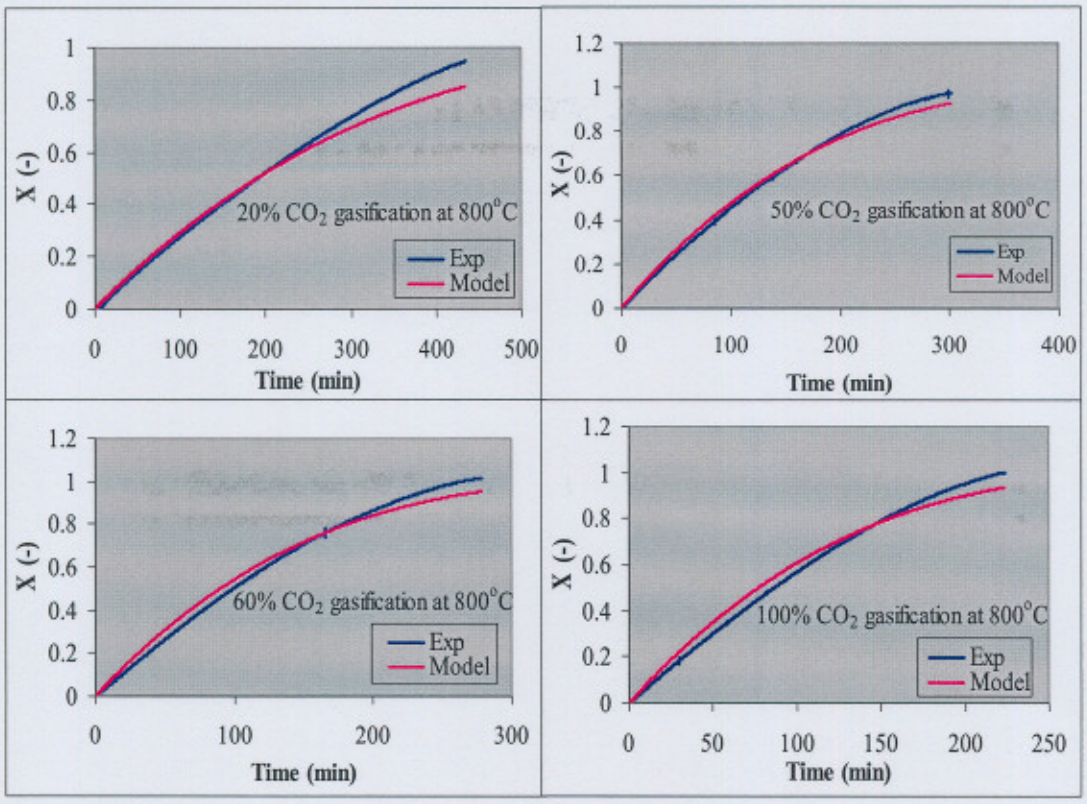

I.7 Burnoff curves for char B CO_2 gasification at 850 °C

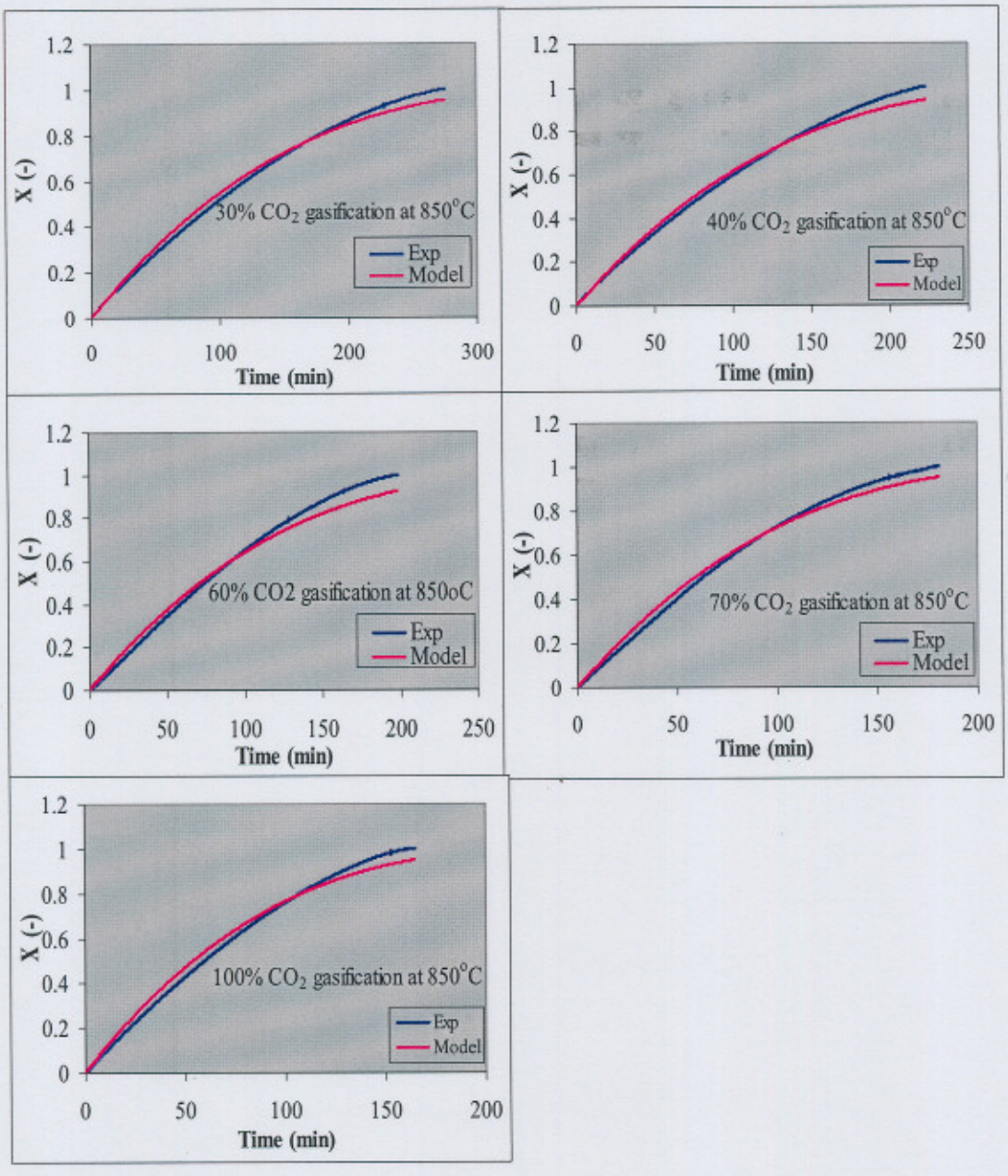

I.8 Burnoff curves for char B CO_2 gasification at 900 °C

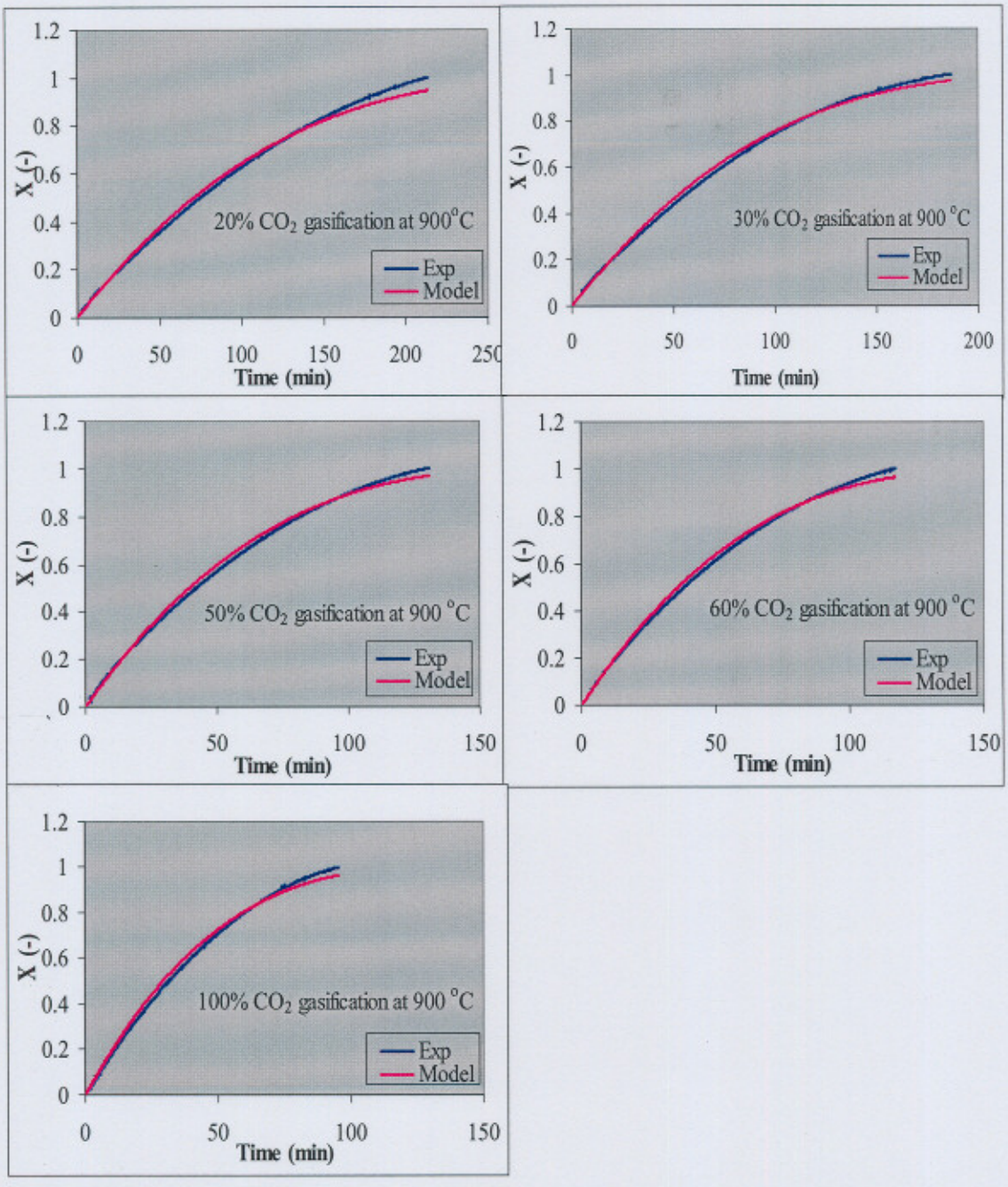

I.9 Burnoff curves for char B CO_2 gasification at 950 °C

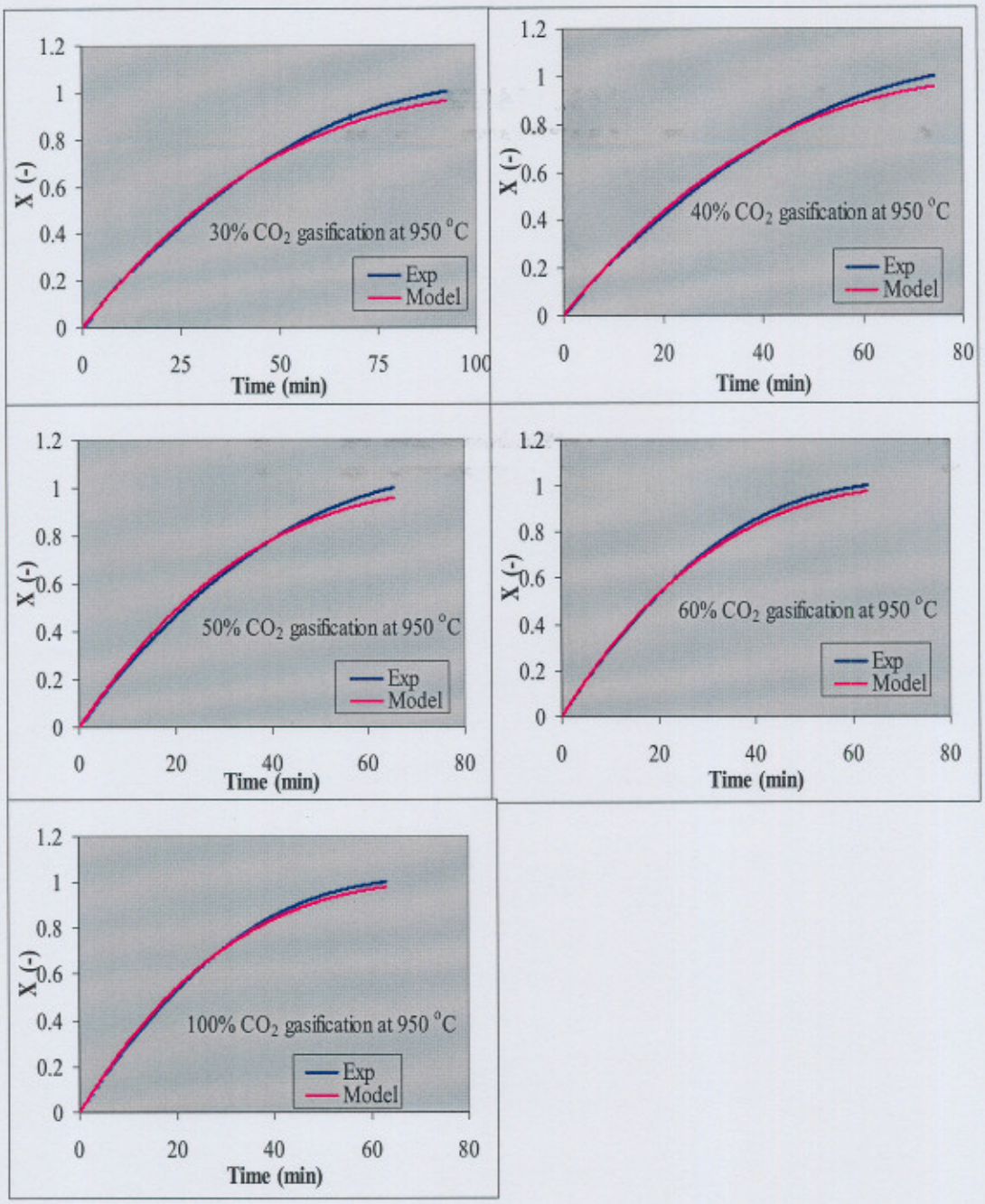

APPENDIX J

BURNOFF CURVES FOR STEAM GASIFICATION

J.1 Introduction

In this appendix the conversion as a function of time results for steam gasification are shown. Experiments were conducted between 800 °C and 950 °C for both chars investigated. The steam concentration was varied between 10% and 20% because of the limitations of the instrument.

J.2 Burnoff curves for char A steam gasification

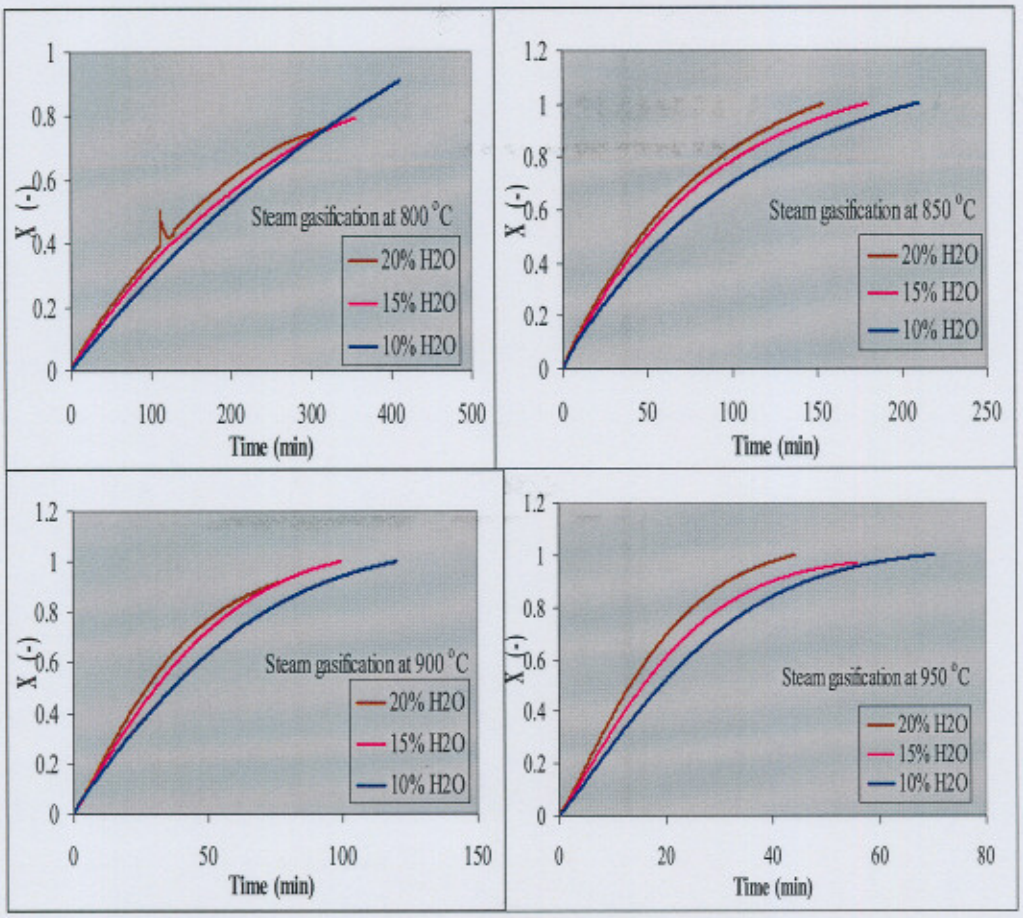

J.3 Burnoff curves for char B steam gasification

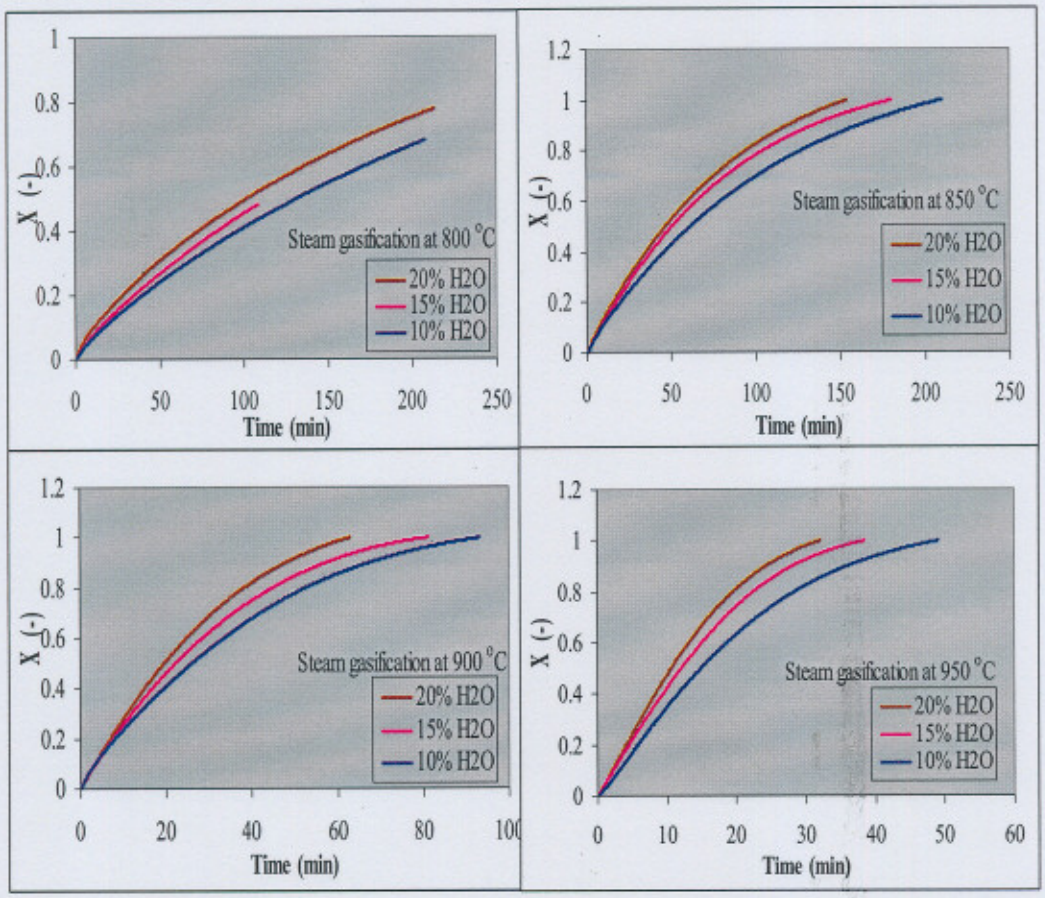

APPENDIX K

VALIDATION OF THE SHRINKING UNREACTED-CORE REACTION MODEL FOR STEAM GASIFICATION

K.1 Introduction

In this appendix the reaction controlled SUCM is validated. This is done by plotting the experimental data of conversion as a function of dimensionless time on the same set of axis with the conversion-dimensionless time data based on the reaction controlled shrinking unreacted core model.

Plots were constructed for all steam concentrations at different temperatures used. In the first part of this appendix char A results are given followed by char B results.

K.2 Model validation for char A steam gasification

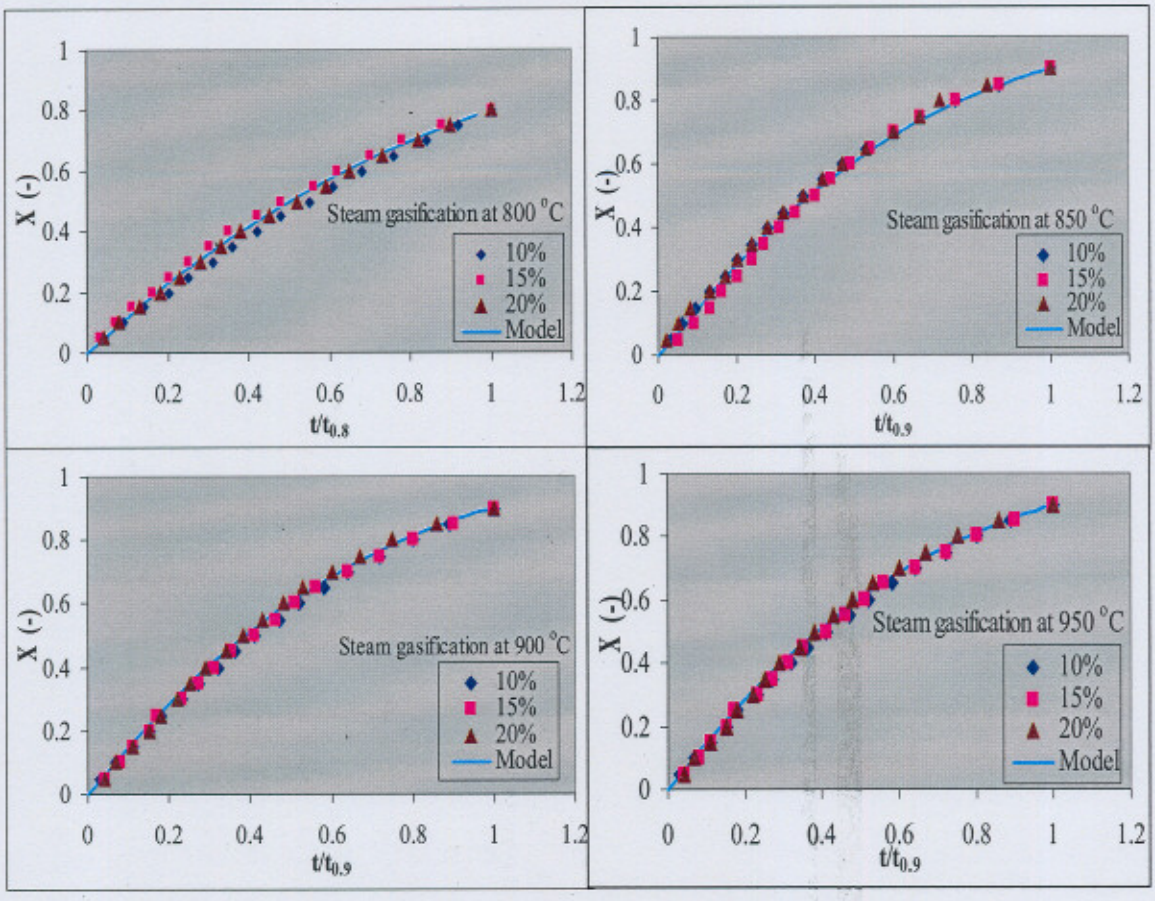

K.3 Model validation for char B steam gasification

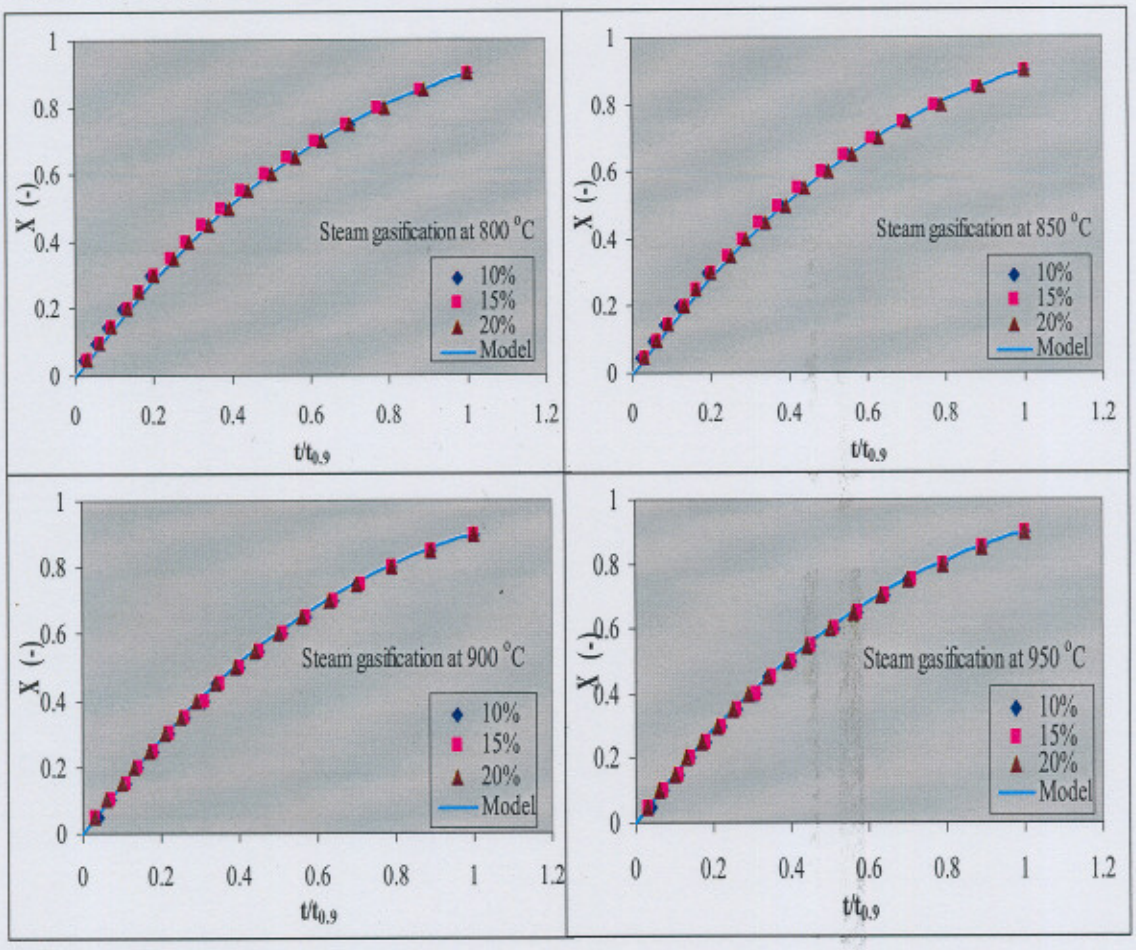

APPENDIX L

THE REACTION CONTROLLED SHRINKING UNREACTED CORE MODEL FOR STEAM GASIFICATION

L.1 Introduction

In this appendix the char conversion model plot as a function time is presented. The char conversion model used is the reaction controlled SUCM. Experiments are presented for char A and char B at temperatures between 800 °C and 950 °C. All experiments were conducted at steam concentrations between 10% to 20%. Char A results are given first and are followed by char B results respectively.

L.2 Char A conversion model for steam gasification

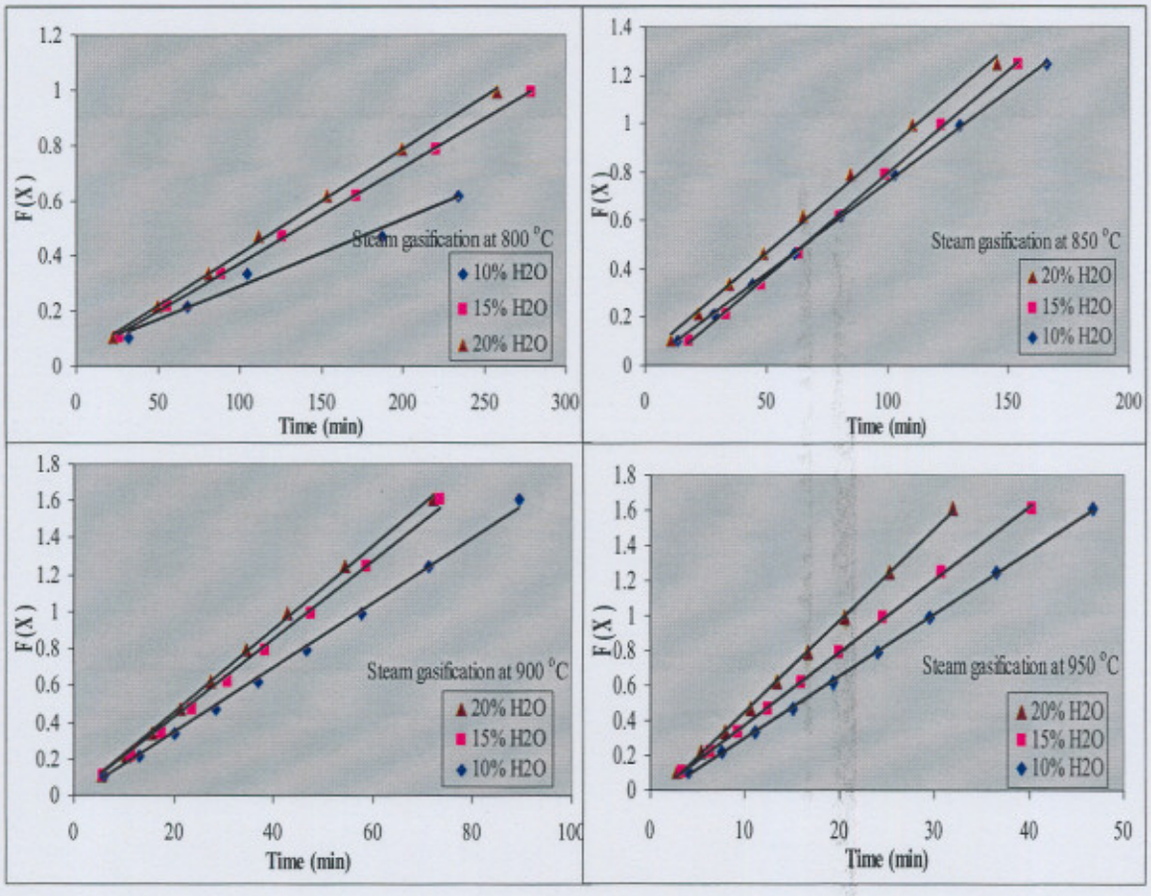

L.3 Char B conversion model for steam gasification

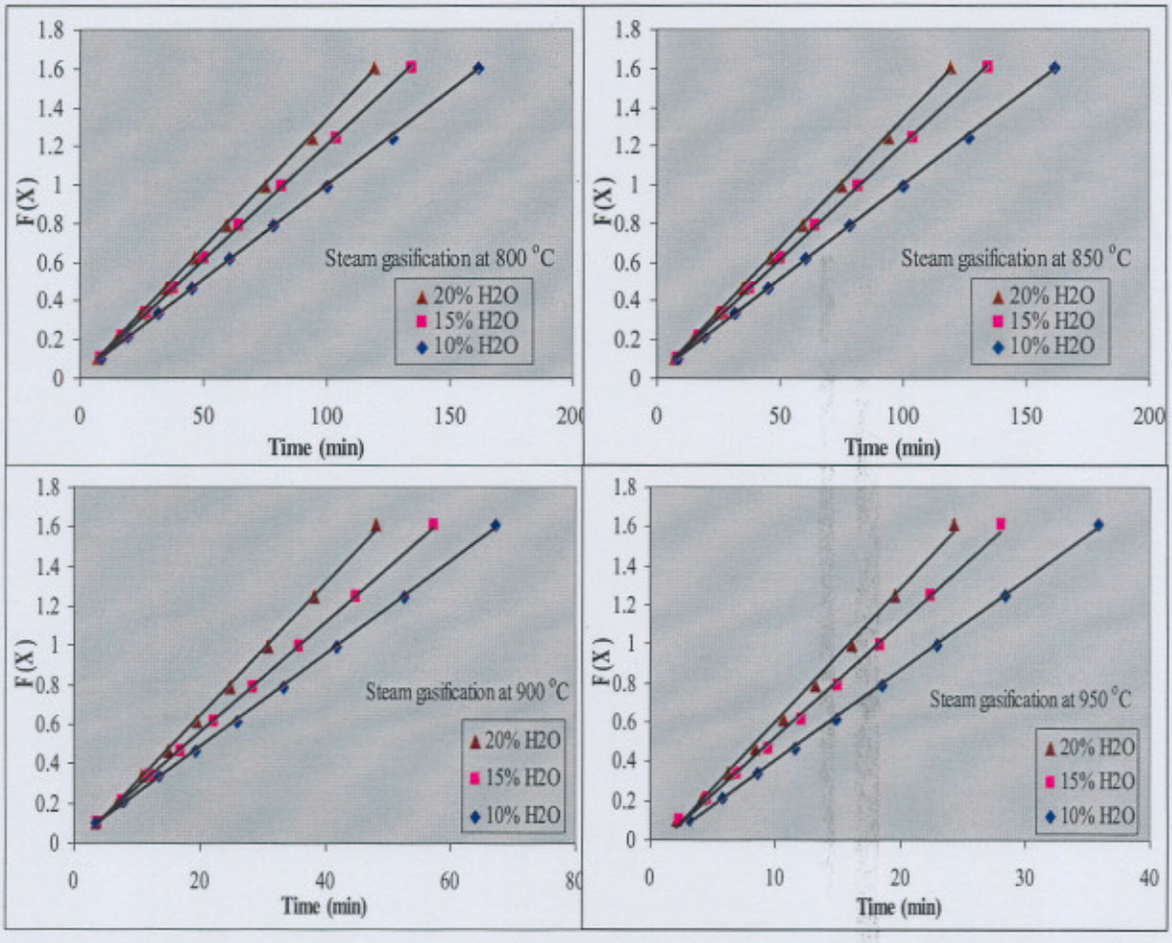

APPENDIX M

VALIDATION OF STEAM GASIFICATION KINETICS

M.1 Introduction

In this appendix all the obtained kinetic parameters were fitted into the derived Langmuir-Hinshelwood model. This was done in order to predict validity of the kinetic parameters calculated. For each experiment conducted a plot of X versus time is plotted using the experimental data that is then fitted against the data predicted by the model.

Plots were constructed for temperature points between 800 °C and 950 °C at steam concentrations ranging from 10% to 20%. Char A results are presented first and are followed by char B results.

M.2 Burnoff curves for char A steam gasification at 800 °C

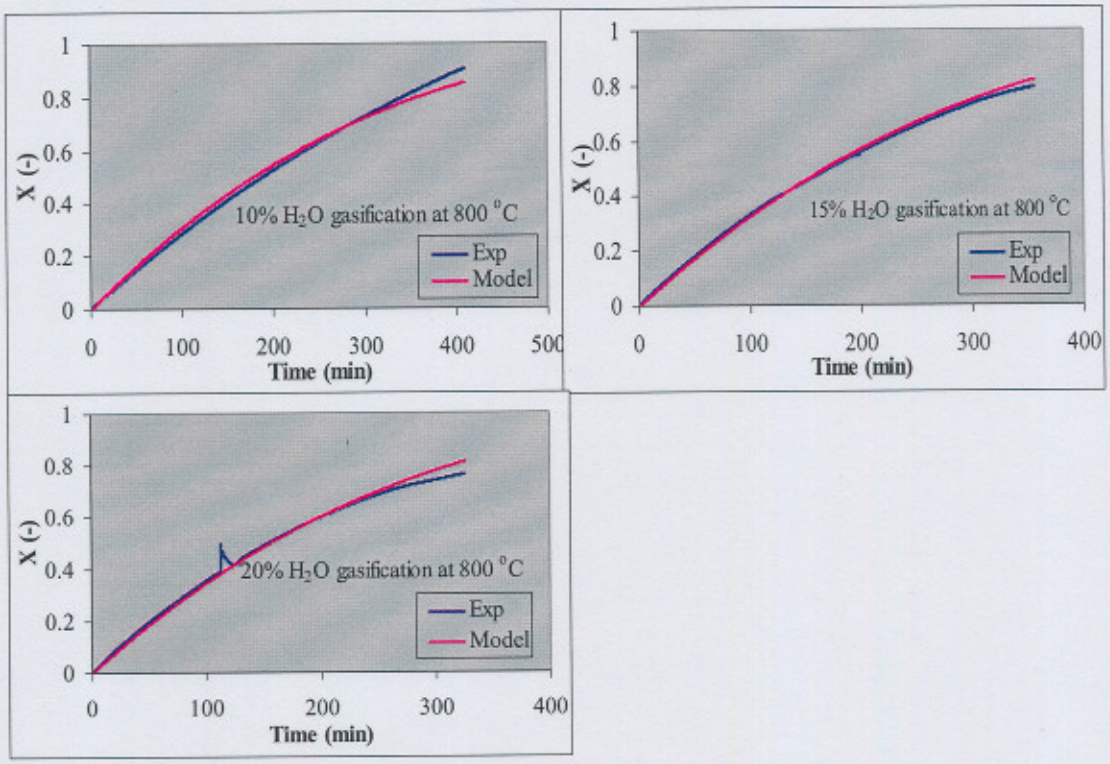

M.3 Burnoff curves for char A steam gasification at 850 °C

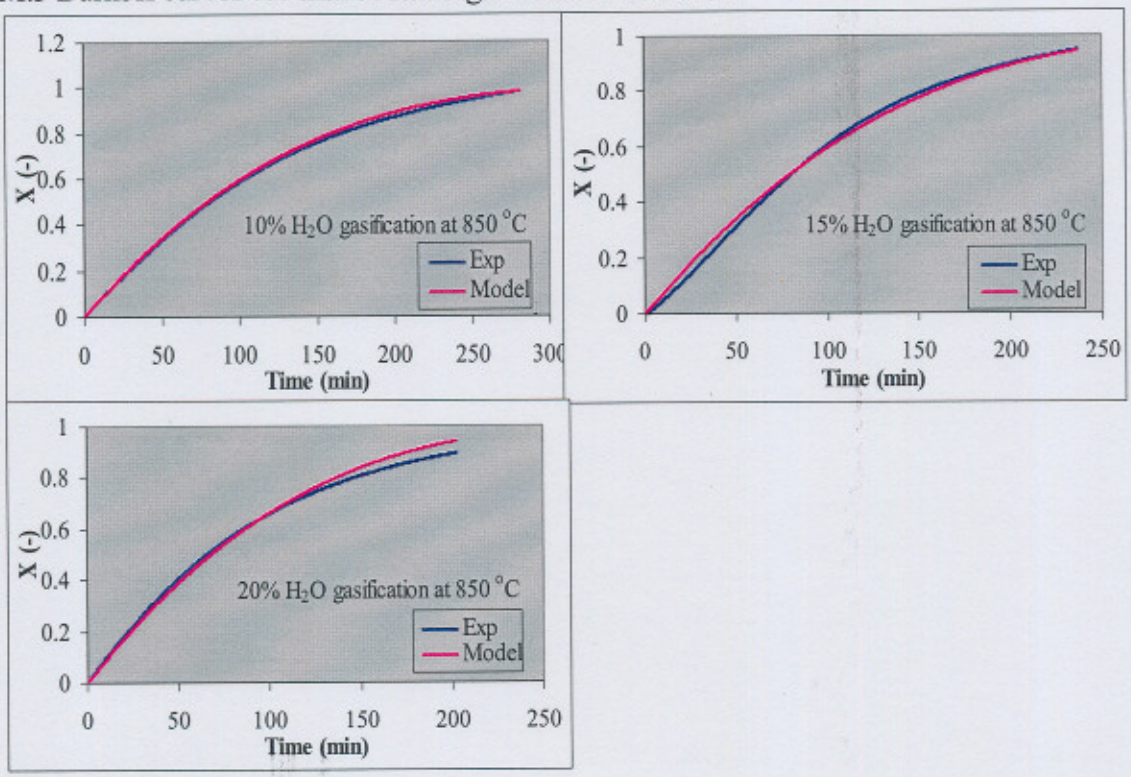

M.4 Burnoff curves for char A steam gasification at 900 °C

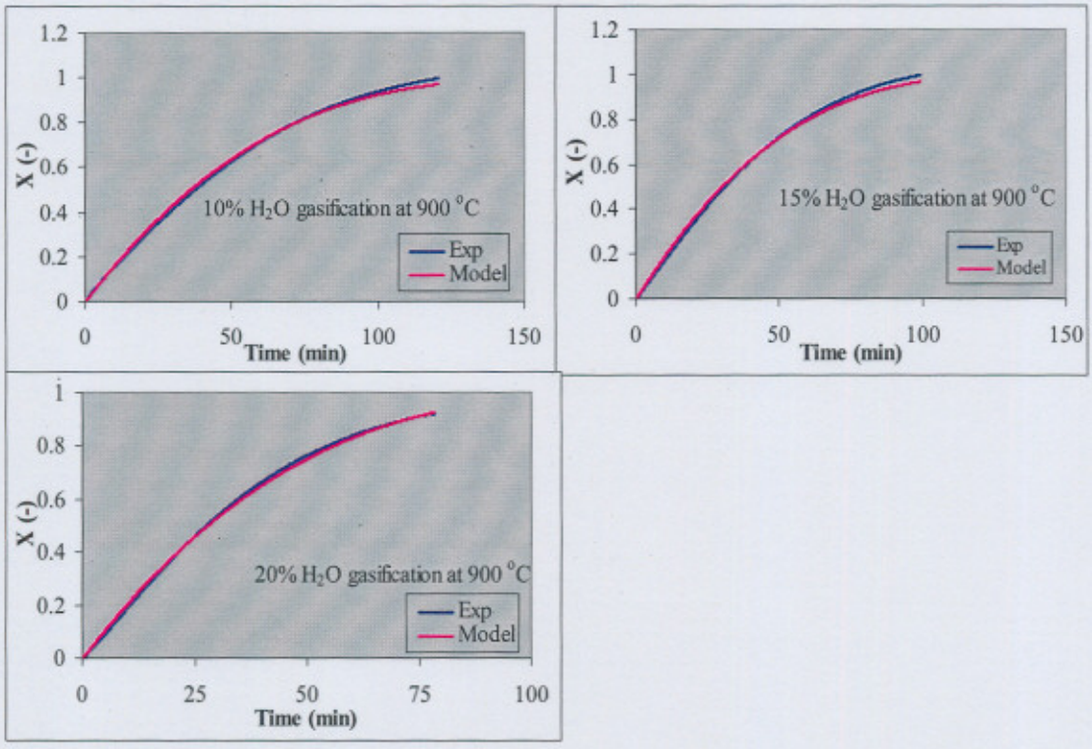

M.5 Burnoff curves for char A steam gasification at 950 °C

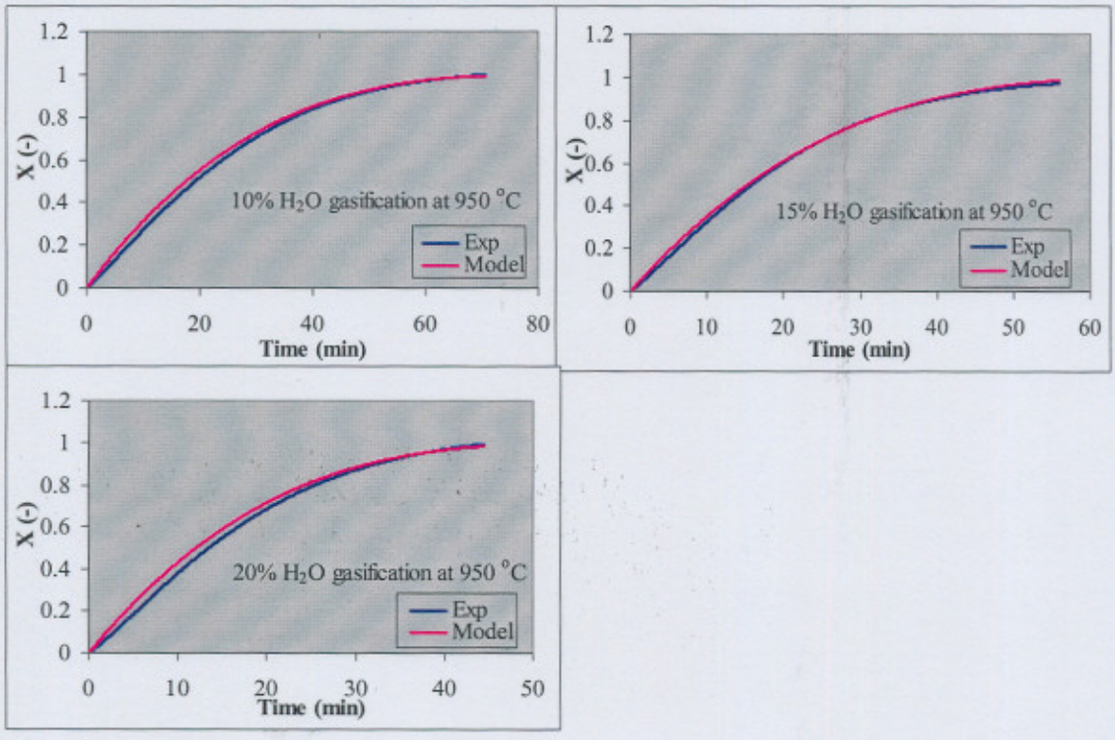

M.6 Burnoff curves for char B steam gasification at 800 °C

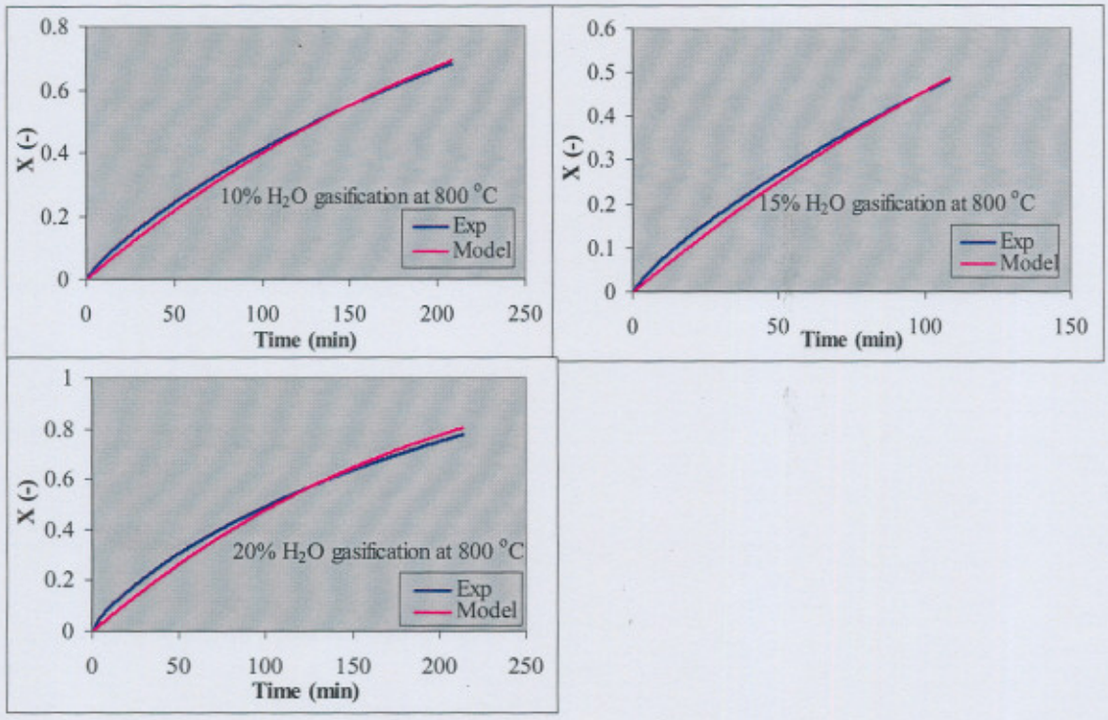

M.7 Burnoff curves for char B steam gasification at 850 °C

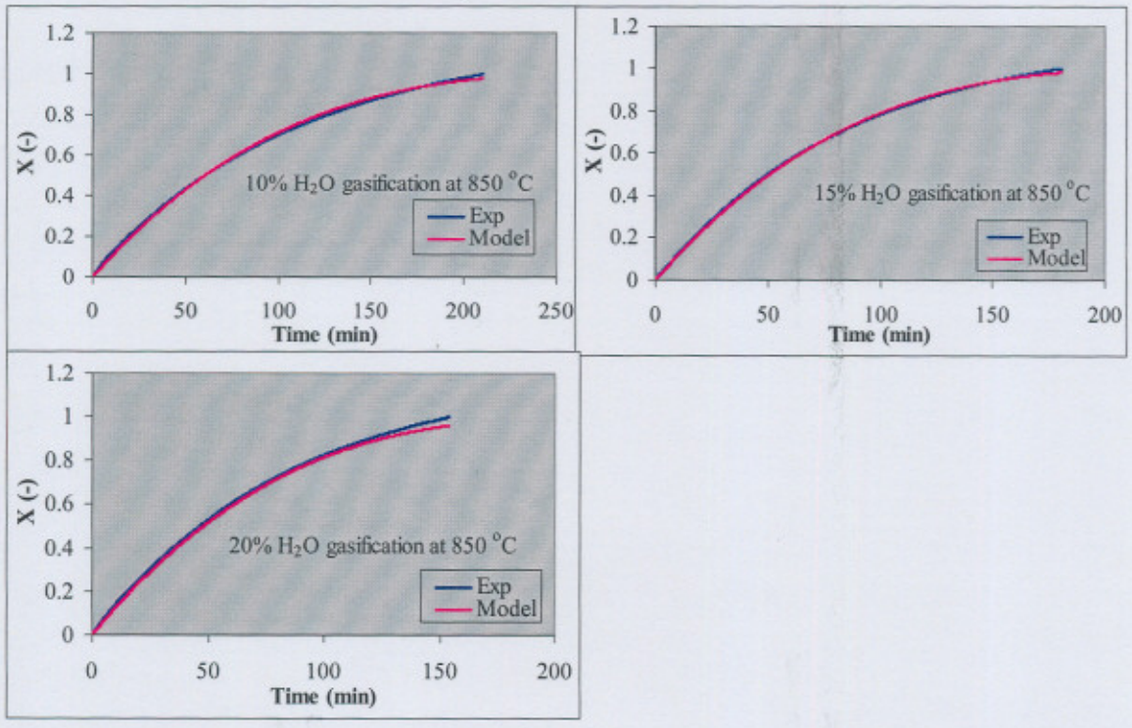

M.8 Burnoff curves for char B steam gasification at 900 °C

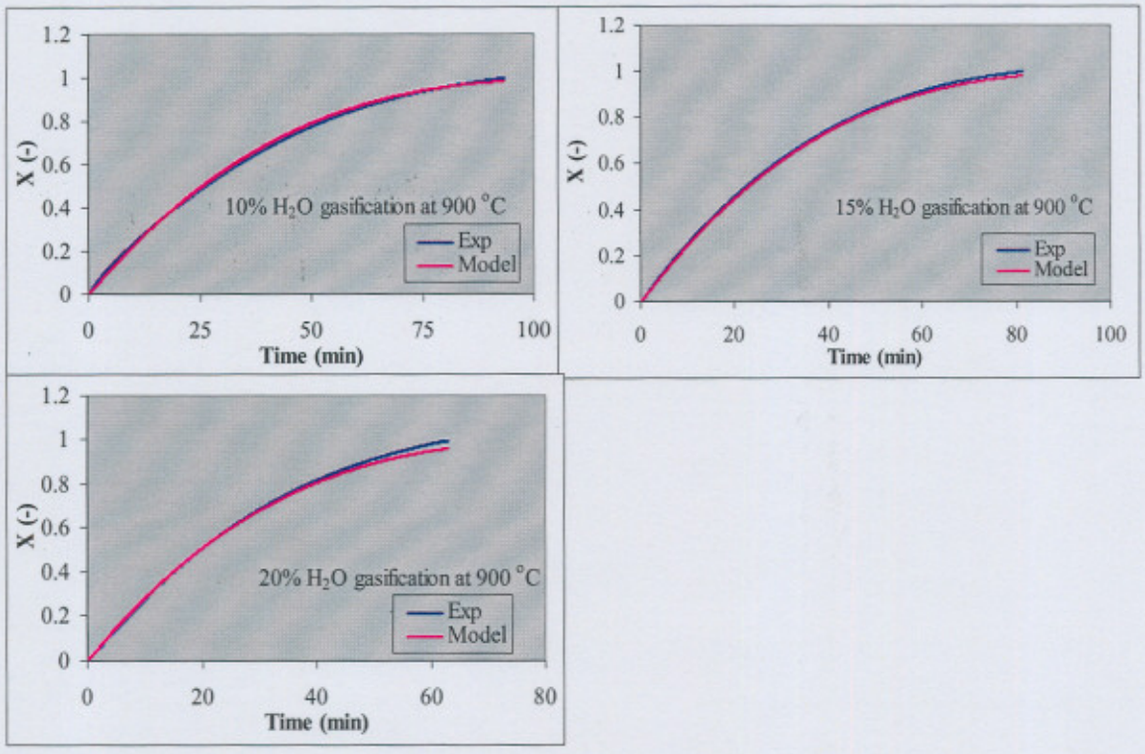

M.9 Burnoff curves for char B steam gasification at 950 °C